RCA Review

December 1970 Volume 31 No. 4

RG 174-252

GIFT OF

Lohnes and Culver

TO THE

BROADCAST PIONEERS LIBRARY

1771 N STREET, N.W., WASHINGTON, D. C. 20036

10/13/88

RCA Review, published quarterly in March, June, September and December by RCA Research and Engineering, RCA Corporation, Princeton, New Jersey 08540. Entered as second class matter July 3, 1950 under the Act of March 3, 1879. Second-class postage paid at Princeton, New Jersey, and at additional mailing offices. Effective Jan. 1, 1971, subscription rates as follows: United States and Canada: one year $6.00, two years $10.50, three years $13.50; in other countries, one year $6.40, two years $11.30, three years $14.70. Single copies up to five years old $3.00.

LOHNES AND CULVER

JAN 22 1971

GML____ RHC__✓__ FDV____

RCA Review

A technical journal published quarterly by RCA Research and Engineering in cooperation with the subsidiaries and divisions of RCA.

Chemical Vapor Phase Deposition of Electronic Materials

607 **Foreword**
L. R. Weisberg and G. W. Cullen, **Guest Editors**

Semiconductors

613 Low-Temperature Vapor Growth of Homoepitaxial Silicon
D. Richman, Y. S. Chiang, and P. H. Robinson

620 Heteroepitaxial Growth of Germanium and Silicon on Insulating Substrates
D. J. Dumin, P. H. Robinson, G. W. Cullen, and G. E. Gottlieb

635 Vapor-Phase Growth of Several III-V Compound Semiconductors
J. J. Tietjen, R. E. Enstrom, and D. Richman

647 The Preparation of Ternary and Quaternary Compounds by Vapor Phase Growth
B. J. Curtis, F. P. Emmenegger, and R. Nitsche

662 Vapor Growth of (II-VI)-(III-V) Quaternary Alloys and Their Properties
W. M. Yim, J. P. Dismukes, and H. Kressel

680 Vapor Deposition of Semiconducting Mononitrides of Scandium, Yttrium, and the Rare Earth Elements
J. P. Dismukes, W. M. Yim, J. J. Tietjen, and R. E. Novak

692 Vapor Phase Growth of Magnetic Semiconducting Spinels
H. L. Pinch and L. Ekstrom

Superconductors

702 Compounds and Alloys for Superconducting Applications
R. E. Enstrom, J. J. Hanak, and G. W. Cullen

Insulators

715 Deposition and Properties of Silicon Dioxide and Silicate Films Prepared by Low-Temperature Oxidation of Hydrides
W. Kern and A. W. Fisher

728 Vapor Deposition and Characterization of Metal Oxide Thin Films for Electronic Applications
C. C. Wang, K. H. Zaininger, and M. T. Duffy

742 Preparation, Properties, and Applications of Chemically Vapor Deposited Silicon Nitride Films
M. T. Duffy and W. Kern

754 Chemical Vapor Deposition of Aluminum Oxide Films from Organo-Aluminum Compounds
M. T. Duffy and W. Kern

771 Interface Properties of Chemically Deposited Silica Films on Gallium Arsenide
W. Kern and J. P. White

786 Technical Papers

788 Patents

790 Authors

798 Index to Volume 31, 1970

December 1970 Volume 31 No. 4

RCA Corporation

Robert W. Sarnoff Chairman of the Board and President
Elmer W. Engstrom Chairman of the Executive Committee of the Board

Editorial Advisory Board

Chairman, J. A. Rajchman RCA Laboratories
E. D. Becken RCA Global Communications
G. H. Brown RCA Patents and Licensing
G. D. Cody RCA Laboratories
A. L. Conrad RCA Services
H. L. Cooke, RCA Research and Engineering
A. N. Goldsmith Honorary Vice President, RCA
N. L. Gordon RCA Laboratories
G. B. Herzog RCA Laboratories
J. Hillier RCA Research and Engineering
E. O. Johnson RCA Solid-State Division
H. W. Leverenz RCA Patents and Licensing
D. S. McCoy RCA Laboratories
L. S. Nergaard RCA Laboratories
H. F. Olson RCA Laboratories
K. H. Powers RCA Laboratories
P. Rappaport RCA Laboratories
F. D. Rosi RCA Laboratories
L. A. Shotliff RCA International Licensing
T. O. Stanley RCA Laboratories
J. J. Tietjen RCA Laboratories
W. M. Webster RCA Laboratories
L. R. Weisberg RCA Laboratories

Secretary, Charles C. Foster RCA Research and Engineering

Editor Ralph F. Ciafone

Associate Editors

W. A. Chisholm RCA Limited
D. B. Dobson Aerospace System Division
M. G. Gander RCA Service Company
J. Gold Graphic Systems Division
T. G. Greene Missile and Surface Radar Division
W. O. Hadlock RCA Research and Engineering
W. A. Howard National Broadcasting System
C. Hoyt Consumer Electronic Systems Division
C. A. Meyer RCA Electronic Components
M. G. Pietz Defense Engineering
D. R. Pratt Commercial Electronic Systems Division
C. W. Sall RCA Laboratories
I. M. Seideman Astro-Electronics Division

© RCA Corporation 1970 All Rights Reserved Printed in USA

Foreword

In the decade of the 1950's, growth of materials from the melt was the main preparation technique in the electronics industry. Advances such as the control and elimination of edge dislocations were achieved, an understanding of the growth of alloys was developed, and the technique of dendritic growth was tamed and harnessed.

Despite these impressive achievements, just a few years later in the decade of the 60's, the technique of chemical vapor phase deposition (CVD) became pre-eminent, and has continued to grow in importance. Its use has been extended from the realm of materials preparation to device fabrication. In this technique, chemicals in a vapor state serve as the source of materials deposited either in the amorphous or crystalline form on a variety of substrates. The present dominance of CVD is the result of a number of unique advantages that it offers, which can often make the difference between success or failure in a given application. These unique advantages are:

[a] Growth of a material can occur at temperatures hundreds of degrees below its melting point. This can have at least four beneficial effects:

1. During synthesis of very high melting point materials, technological problems involved in the use of high-temperature crucibles, high-power generators, and high-temperature insulation are greatly reduced.
2. Contamination from the surroundings due to impurity diffusion or to reactions at high temperature with the containers is minimized.
3. Diffusion of impurities and host atoms within the growing material is greatly diminished.
4. High pressures often employed to suppress decomposition of materials are avoided.

[b] Compositions represented by interior portions of a phase diagram can be directly synthesized without crossing phase boundaries. This is especially important for materials with peritectic phase structures or that melt incongruently.

[c] Problems due to the distribution coefficient of impurity or host atoms are eliminated. This allows materials to be prepared with a greater degree of homogeneity. Furthermore, alloys can be grown at relatively high growth rates without encountering constitutional supercooling.

[d] In the growth of alloys, local inhomogeneities can often be reduced, since it is easier to thoroughly mix gases than liquids.

[e] More precise control of geometry, dopant distribution, and alloy composition can be achieved. Dopants can be abruptly added to or removed from the gaseous stream wherever desired, and the alloy composition can be suddenly changed. Growth rates can be low enough to achieve submicron thickness dimensions.

[f] High-vacuum systems required for evaporative processes can be avoided. Often the vacuum is utilized essentially to maintain purity, but the impurity content of the carrier gases now available is as low as that of a high-vacuum ambient.

The purpose of this issue of *RCA Review* is to demonstrate the broad impact chemical vapor phase deposition (CVD) has had on the electronics industry. Brought together in this issue is a review of the research employing CVD from one of the many organizations active in the field, RCA Laboratories. Despite such widespread activity, we believe that the important role that CVD has played is not necessarily appreciated unless one can conveniently focus on the results, as is done in this issue. In this respect, Table 1 summarizes how the above advantages of CVD apply to each of the specific materials described in this issue.

A key feature demonstrated by the papers is the enormous versatility of the use of CVD. Note that the issue covers the gamut from exploratory research to device application, including integrated-circuit fabrication. The subjects include the full range of amorphous coatings, to highly polycrystalline films, to highly perfect single-crystal layers. Materials deposited include elements, compounds and mixtures, and binary, ternary, and quaternary alloys. And, as indicated in the table of contents, the materials cover a wide range of electronic behavior,

Table 1—Summary of Advantages of CVD for Materials Described in Subsequent Papers

Material Synthesized	Capability Provided by the Use of the CVD Process	Application
Homo- and heteroepitaxial silicon and germanium thin films	reproducible control of the doping level and film thickness film growth at low temperatures to minimize reaction between the growing film and the substrate materials	high speed integrated circuitry
Homoepitaxial III-V films	ability to form abrupt grown-in horizontal junctions; control of the doping level and film thickness film growth at low temperatures to minimize dissociation preparation of compositions not obtainable by melt processes due to constitutional supercooling	high temperature transistors and rectifiers, EL diodes, injection lasers, transferred electron oscillators and amplifiers, photoemitters
Ternary and quaternary chalcogenides and oxides; metal-phosphorus sulfur compounds	compounds can be produced which cannot be synthesized by melt processes due to incongruent melting or high dissociation pressure at the melting point	exploratory: the alloys have been prepared for the evaluation of basic properties
(II-VI)-(III-V) quaternary alloys	the capabilities provided by the CVD process are similar to those cited for growth of the III-V compounds	exploratory: the alloys have been prepared for the evaluation of basic properties

(continued next page)

Table 1—(continued)

Material Synthesized	Capability Provided by the Use of the CVD Process	Application
Mononitrides of Sc, Y, and the rare earth elements	good control of stoichiometry and purity as compared to other methods previously used for the preparation of these materials epitaxial growth may be realized good control of film thickness and geometry	possible application as photoemitters, EL diodes and transistors if control of doping can be achieved
Chromium chalcogenide spinels	achievement of epitaxial growth control of purity control of film thickness	applications are contingent on the achievement of junctions by controlled doping
Niobium stannide	achievement of single phase material control of composition and "doping" control of the film thickness and geometry preparation of single crystals of a peritectic melting material	superconducting magnets, flux concentrators, radiation shielding, power transmission
Silicon oxide, aluminum oxide, transition metal oxides and silicon nitride	low temperature deposition, of particular importance in maintaining the properties of underlying semiconductor structures control of film composition, crystallinity and thickness	gate insulators of MOS transistors dielectric component of radiation hardened devices storage medium of MNOS memory devices

and include conductors,* semiconductors, and insulators, besides magnetically and optically active compounds.

Yet another feature of CVD demonstrated in these papers is its remarkable ability to easily combine materials of different types in a single structure. For example, the III-V compounds can be epitaxially grown on heteroepitaxial silicon on sapphire, or the two materials can be individually heteroepitaxially deposited on various areas of a single insulating substrate wafer. The II-VI compounds, and various (II-VI)-(III-V) alloy combinations may soon be included in such epitaxially grown layered structures. Vapor-deposited aluminum oxide has been combined with epitaxially deposited silicon on sapphire for radiation-resistant metal–oxide–semiconductor transistor structures. Layered structures of vapor-deposited discrete dielectrics on heteroepitaxially grown silicon are also being investigated. As the capability for the chemical vapor growth of new materials is developed, these materials are quickly teamed with existing CVD technology to provide materials combinations that cannot be synthesized by other methods.

Table 2—Contents of *RCA Review* December 1963 Special Issue on Epitaxial Growth

"Foreword," by H. W. Laverenz

"The Etching of Germanium Substrates in Gaseous Hydrogen Chloride," by J. A. Amick, E. A. Roth, and H. Gossenberger

"Chemical Polishing of Silicon with Anhydrous Hydrogen Chloride," by G. A. Lang and T. Stavish

"The Growth of Germanium Epitaxial Layers by the Pyrolysis of Germane," by E. A. Roth, H. Gossenberger, and J. A. Amick

"Epitaxial Deposition of Silicon by Thermal Decomposition of Silane," by S. R. Bhola and A. Mayer

"Epitaxial Deposition of Silicon and Germanium Layers by Chloride Reduction," by E. F. Cave and B. R. Czorny

"Vapor-Phase Synthesis and Epitaxial Growth of Gallium Arsenide," by N. Goldsmith and W. Oshinsky

"The Growth of Single-Crystal Gallium Arsenide Layers on Germanium and Metallic Substrates," by J. A. Amick

"Transport of Gallium Arsenide by a Close-Spaced Technique," by P. H. Robinson

"Epitaxial Growth of GaAs Using Water Vapor" by G. E. Gottlieb and J. F. Corboy

"Gas Phase Equilibria in the System GaAs-I_2," by D. Richman

"Epitaxial Growth from the Liquid State and Its Application to the Fabrication of Tunnel and Laser Diodes," by H. Nelson

* A recent paper representing RCA Research on the use of the CVD process for metals that is not included in this issue is, "Vapor-Deposited Tungsten as a Metallization and Interconnection Material for Silicon Devices," by J. M. Shaw and J. A. Amick (*RCA Review*, June 1970).

For simplicity, these papers cover research using CVD carried out only during the past six years at RCA. While these papers are predominantly of a review nature (nearly 200 scientific publications from RCA are referenced), many new results are included to ensure that the information presented is up to date. This issue also serves to update the December 1963 issue of RCA Review on epitaxial growth and closely related topics. In an effort to provide continuity between these two issues, the table of contents of the December 1963 RCA Review is provided in Table 2.

In conclusion, we hope that the collection of these papers in a single volume will serve to provide insight into, and appreciation for, the versatility and power of a materials preparation technique that has had an important impact on both materials and device research in the electronics industry.

L. R. Weisberg

G. W. Cullen

Low-Temperature Vapor Growth of Homoepitaxial Silicon

D. Richman, Y. S. Chiang, and P. H. Robinson
RCA Laboratories, Princeton, N. J.

Abstract—The use of silane in either hydrogen or helium carrier gas to achieve low-temperature homoepitaxial deposition of device-quality silicon is reviewed. Although temperatures as low as 800°C have been reached in the silane-in-helium system, optimum temperatures appear to be 900°C for silane in helium and 1050°C for silane in hydrogen. At 900°C, single-crystal films were successfully grown with a growth rate of 3 μm/min using silane in helium. Examination by capacitance-voltage techniques has shown that very abrupt junctions can be grown in either system at these low temperatures.

Introduction

If a high growth rate could be maintained in a low-temperature silicon deposition process, one would benefit from the slower diffusion rates coupled with the minimized impurity contamination. In the past few years, we have been exploring such processes using silane as the source of silicon. This paper reviews the work done in these Laboratories to develop low-temperature deposition systems using either hydrogen[1-3] or helium[4-6] as the carrier gas.

The choice of helium as a substitute for the more commonly used hydrogen was based upon the conclusion[7] that the low-temperature rate-limiting step in the vacuum epitaxial deposition of silicon from silane was the rate of removal of hydrogen from the growing surface. Assuming the correctness of this postulate, an inert carrier gas other than hydrogen should be used when decomposing silane in a flowing system if high growth rates at low temperature are to be obtained. The substitution of helium for hydrogen has led to a significant lowering of the homoepitaxial growth temperature of silicon. Helium has also been used successfully in the deposition of single-crystal silicon layers on both sapphire and spinel.

Concurrent with the work on silane in helium, studies of homo- and heteroepitaxial growth from silane in hydrogen were in progress. We consider here only homoepitaxy; heteroepitaxy is treated in an accom-

panying paper.[8] This work has explored the temperature range over which highly perfect single-crystal silicon can be deposited, and also what factors are important in controlling the impurity concentration profiles in the deposited layers. In the following sections, the experimental growth methods and some results are reviewed.

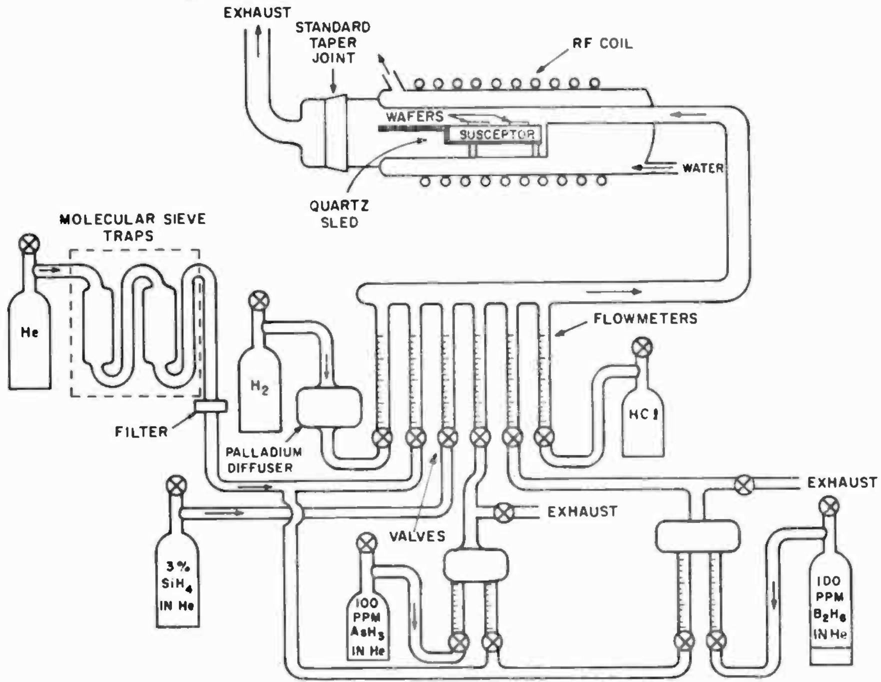

Fig. 1—Schematic diagram of the silane-in-helium growth system.

Experimental

Silane in Helium

A schematic of the growth system used for the silane-in-helium deposition is shown in Fig. 1. Accurate control of the gas composition and flow rates is achieved by the array of precision gas flowmeters. A key feature of this work is the design of the reaction chamber, which is also shown schematically in Fig. 1. The stepped water-cooled chamber is used so that the gas sees a uniform cross section throughout the reaction zone, thereby reducing the possibility of turbulent flow in the gas stream passing over the substrates, and also to prevent preheating

of the gas stream and premature decomposition of the silane. It was felt that a streamlined cooled flow would reduce the amount of homogeneous gas phase decomposition of the silane and so reduce the amount of amorphorus or polycrystalline silicon "raining" down upon the growing surface. Eliminating unwanted reactions such as this is crucial for obtaining device-quality epitaxial layers, and was one of the reasons that hydrogen was originally chosen as the standard carrier gas for silane deposition systems. The full details of substrate preparation and growth procedures have been given in previous publications.[4-6]

Silane in Hydrogen

The growth chamber used for studying the deposition of silicon from silane in hydrogen is shown in Fig. 2. Note that in contrast to the

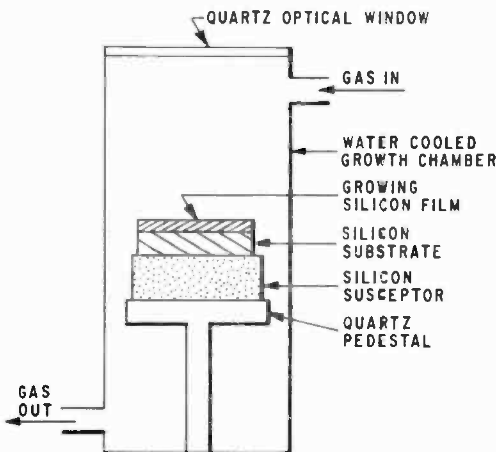

Fig. 2—Schematic diagram of the growth chamber used for silane-in-hydrogen deposition.

silane-in-helium work a vertical geometry is used in this case. This geometry is possible for silane in hydrogen, because the high hydrogen concentration suppresses the homogeneous gas phase decomposition of the silane. Another difference in the two deposition systems is the choice of susceptor used to couple with the rf power source. The helium system utilizes a silicon-carbide-coated graphite block machined to closely fit the opening in the deposition chamber. The hydrogen system, which employs a smaller reaction tube, utilizes a high-purity silicon susceptor having a low resistivity core for easy induction at low temperatures. Such a susceptor minimizes the possibility of contamina-

tion of the growing layers by the susceptor. The details of the experimental procedure have been published previously.[1-3]

Results

Silane in Helium

With the silane-in-helium technique, single-crystal epitaxial layers have been obtained at temperatures as low as 800°C and growth rates as high as 0.5 μm/min. At 900°C, growth rates for single crystals as high as 3.0 μm/min have been obtained.[6] One of the most important factors found to influence the lowest temperature at which single-crystal growth could be obtained was the surface treatment of the substrate.[6] Thus the layers with the fewest stacking faults and the lowest epitaxial temperature were obtained on surfaces that had been HCl etched in situ immediately prior to growth. Surfaces exposed to flouride ion required heating above 950°C[6] before epitaxy could be obtained. Similarly, heating in hydrogen alone resulted in more faulted layers than those obtained with HCl etching.

A second factor limiting the quality of the layers obtained in the helium system is the presence of trace amount of oxygen. At the low temperatures of growth used (< 1000°C), oxygen that reaches the substrate surface is not removed, since SiO is not volatile at these temperatures. The growth morphology has been shown to be a function of the oxygen content of the gas.[5] As the oxygen content of the gas is reduced, the growth changes from island growth to layered growth with a stepped surface, to, in the purest case, a mirror-smooth, featureless surface.

Doping experiments using arsine and diborane have shown[5] that both n- and p-type doping over several orders of magnitude are possible. Only a little information on device structures is available. Examination of the abruptness of the junction in p+-on-n structures grown at 900°C was studied by measuring the *C-V* characteristics of mesa structures etched in the grown layers. The slope of ½ obtained from log *C* versus log *V* plot indicates that, indeed, abrupt junctions were obtained.

The minority-carrier lifetime in silicon deposited at 900°C has also been determined. A p+-p-n+ structure was grown and 17-mil-diameter diodes were formed by etching using low-temperature oxide deposition for masking. Fig. 3 shows a typical curve of the forward-bias *I-V* characteristics obtained for these diodes. From the zero bias current (I_o) and the carrier concentration of the p-type layers, the lifetime

could be calculated using

$$\tau = \frac{en_i}{2I_o} Ad, \quad [1]$$

where n_i is the intrinsic carrier concentration, e is the electronic charge, A is the area of the diode, and d is the width of the depletion region. The lifetime for the diode illustrated was found to be 1 μsec.

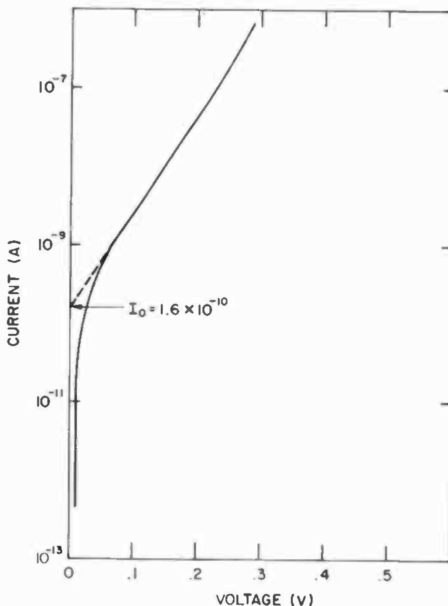

Fig. 3—Current-voltage relationship under forward bias of a diode fabricated from a p+-p-n+ growth in the silane-in-helium deposition system.

Silane in Hydrogen

The silane-in-hydrogen system has been used principally for the deposition of silicon on insulating substrates. However, some work has been done to establish the applicability of such a system to the growth of highly perfect, abrupt-junction structures required for avalanche diodes. The high current densities developed in these devices during operation lead to premature burn out if any defects or precipitates are present. Using the silane-in-hydrogen system it was found that silicon grown in the temperature range 1050 to 1150°C had the requisite

crystal perfection. The second problem, that of junction abruptness, could be met if the back surface of the substrate was coated with SiO_2 to prevent autodoping.[9] Fig. 4 shows the doping profiles obtained for three n-p+ structures grown on n+ substrates in the silane-in-hydrogen system. The constancy of the doping is noteworthy as is the abruptness of the junction.

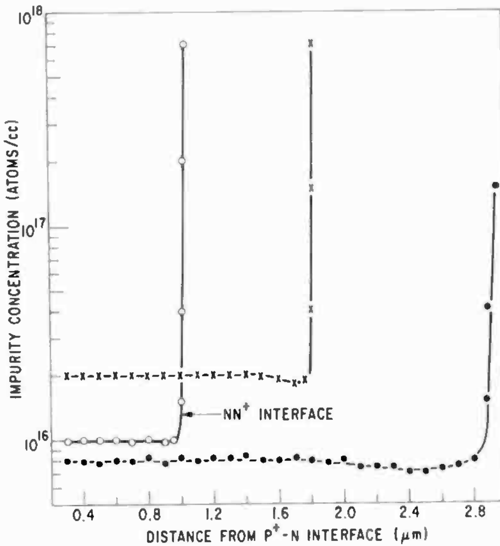

Fig. 4—Concentration-distance profiles for three n+-n layer structures grown in the silane-in-hydrogen deposition system.

Conclusions

The homoepitaxial deposition of silicon from silane can be carried out in either a hydrogen or helium environment. Substitution of helium for hydrogen allows the epitaxial growth temperature to be lowered below 1000°C to temperatures as low as 800°C. Key factors in determining the quality of the epitaxial layers grown at low temperatures are the purity of the gases employed and the treatment of the silicon substrate immediately prior to deposition. Silane deposition appears to be especially well suited to the preparation of layered structures where abrupt changes in concentration are important. More work remains to be done to fully evaluate the potential of low-temperature deposition for device fabrication.

Acknowledgments

The authors would like to thank J. Assour for helpful discussions and measurements of the concentration–distance profiles, and G. W. Looney and R. O. Wance for their technical assistance.

References

[1] S. R. Bhola and A. Mayer, "Epitaxial Deposition of Silicon by Thermal Decomposition of Silane," **RCA Review**, Vol. 24, p. 511, Dec. 1963.

[2] C. W. Mueller and P. H. Robinson, "Grown-Film Silicon Transistors on Sapphire," **Proc. IEEE**, Vol. 52, p. 1487, Dec. 1964.

[3] P. H. Robinson and C. W. Mueller, "Deposition of Silicon Upon Sapphire Substrates," **Trans. AIME**, Vol. 236, p. 268, March 1966.

[4] D. Richman and R. H. Arlett, "Low-Temperature Epitaxial Growth of Single Crystalline Silicon from Silane," **Jour. Electrochem. Soc.**, Vol. 116, p. 872 (1969).

[5] D. Richman, **Semiconductor Silicon**, R. R. Haberecht and E. L. Kern, Eds., The Electrochemical Society, N.Y., N.Y. (1969).

[6] Y. S. Chiang and D. Richman, to be published in Trans. AIME.

[7] B. A. Joyce and R. R. Bradley, "Epitaxial Growth of Silicon from the Pyrolysis of Monosilane on Silicon Substrates," **Jour. Electrochem. Soc.**, Vol. 110, p. 1235 (1963).

[8] D. J. Dumin, P. H. Robinson, and G. W. Cullen (this issue).

[9] D. C. Bupta and R. Yee, "Silicon Epitaxial Layers with Abrupt Interface Impurity Profiles," **Jour. Electrochem. Soc.**, Vol. 116, p. 1561 (1969).

Heteroepitaxial Growth of Germanium and Silicon on Insulating Substrates*

D. J. Dumin, P. H. Robinson, G. W. Cullen, and G. E. Gottlieb

RCA Laboratories, Princeton, N.J.

Abstract—The growth and electrical properties of germanium and silicon on insulator substrates is reviewed, and aspects of research carried out at RCA are described in some detail. It is shown that the electrical properties of the films are very sensitive functions of the growth parameters, such as growth temperature, growth rate, and substrate material and orientation. The initial nucleating layer is particularly important, and examples of the effect of this layer on properties of germanium and silicon films are given. The current state-of-the-art properties of 1-2 μm thick films are reviewed. Examples of the uses of these films in the fabrication of individual MOS and bipolar transistors and in the fabrication of MOS integrated circuits are given.

Introduction

Thin films of silicon and germanium have recently become available as single crystals grown on oxide substrates.[1] The two substrates used most have been sapphire (Al_2O_3)[2] and spinel ($MgO\text{-}nAl_2O_3$).[3] The main advantage of these films for circuit applications is that they provide isolation between active and passive elements and a low internal device capacitance. Accordingly, high-speed integrated circuits have been fabricated with these films.[4]

In order to intelligently utilize these thin semiconductor layers, it has been necessary to extensively study the electrical properties of the films. The salient electrical properties of the films and some examples of their uses in device and circuit applications are described, and the more important aspects of this work are summarized in tabular form with appropriate references to the literature.

* This work was supported in part by the Naval Electronics Systems Command under Contract #N00039-68-C-2512 and the USAF Avionics Laboratories under Contract #F33615-68-C-1368 and by RCA Laboratories.

Film Growth

The films were grown in both vertical and horizontal, water cooled, rf heater reaction chambers, using either silicon, silicon carbide, or pyrolytic-carbon-coated graphite susceptors. The carrier gasses were either palladium-diffused hydrogen or dry helium. The films were grown via pyrolysis of SiH_4 or GeH_4 and H_2 or helium mixtures, and doping was accomplished by addition of PH_3, B_2H_6, or AsH_3 to the gas stream during growth.[5] The film thicknesses were monitored during growth using an infrared interference technique.[6]

The quality of the semiconducting film was strongly dependent on the surface preparation of the oxide substrate. The wafers were mechanically polished and, as such, contained a work damaged surface. Various chemical etches to remove this work damaged layer were studied, and it was found that prefiring of the substrate in H_2 or SiH_4 at temperatures as high as 1500°C produced a good single-crystal surface upon which to grow the films. In general, about 15 minutes in H_2 at 1300°C was suitable for preparation of the sapphire substrates and 1200°C for 5 minutes in H_2 was suitable for the spinel substrates.

A typical growth cycle consisted of chemical cleaning of the wafers to remove any organic compounds from the surface. The wafer was then prefired in H_2, after which the wafer temperature was lowered to the growth temperature and growth commenced when SiH_4 or GeH_4 was added to the gas stream. The desired n- or p-type dopants were added at this time. The wafers were then cooled and either used for electrical measurements or used in device or circuit fabrication. The changes in the electrical properties due to the post-firing of the films in various ambients was studied.

Epitaxial growth of (100) silicon and germanium was observed on either $(1\bar{1}02)$ sapphire or (100) spinel, while the (111) films were obtained on (0001) sapphire and (111) spinel.[7]

Growth rates were typically between 0.1 μm/min and 10 μm/min. Growth temperatures have been varied from 500°C to 950°C for germanium and 800°C to 1300°C for silicon.

Electrical Characteristics

The semiconductor layers were characterized electrically by measuring the Hall mobility and carrier concentration as a function of various processing parameters. The minority-carrier lifetime and the temperature dependence of the mobility and carrier concentration were measured. The results of these measurements are described below for both germanium and silicon.

A. Germanium Films

The characterization of the germanium films has been simplified to a considerable extent by the fact that defects in the germanium films act as shallow acceptors with activation energy of the order of 0.05 eV above the valence band edge.[8] This fortuitous circumstance allows the measurement of the hole concentration to act as a rough guide of crystal quality, with, in general, the higher-quality films having a lower hole concentration, and incidentally, also a higher Hall mobility.

Initially, the germanium films grown on sapphire and spinel tended to have both high hole concentrations and relatively low mobilities.[9] As the films became thicker the electrical properties improved; however, the films were all heavily doped p-type and high hole concentration precluded the possibility of controllably doping the films with either p-type or n-type impurities. The measured hole concentration was linked to the defect structure in the films. It proved to be impossible to grow germanium films directly on sapphire or spinel at growth temperatures in excess of 700°C, since the films tended to agglomerate at the higher growth temperatures. Similar problems have arisen in the growth of germanium on calcium floride.[10]

To overcome this chemical bonding problem, it was decided to try growing a thin silicon layer between the germanium and the substrate.[11]

In Fig. 1 the measured values of Hall mobility and hole concentration have been plotted as a function of growth temperature for 2-μm-thick germanium films grown on a 0.1-μm-thick layer of silicon grown on $(\bar{1}102)$ sapphire. The silicon was grown at about 1125°C, which proved to be nearly optimum for production of the thin undercoating layer. The use of the silicon undercoating allowed the germanium to be grown at temperatures as high as 900°C. The Hall mobility of undoped 2-μm-thick films increased by a factor of 7 compared to films grown without the silicon undercoating and the carrier concentration dropped. It was found that the impurity-caused acceptor levels in the films were less than $3 \times 10^{15}/\text{cm}^3$. Thus all of the data described in Fig. 1 was dominated by the defect acceptor, and further improvements in the electrical properties of the germanium films may be obtained if further improvements in growth techniques are forthcoming.

The low defect-acceptor concentration obtained in films grown at 850°C with the silicon undercoating allowed the production of p-type and n-type films with controlled carrier concentrations from $10^{16}/\text{cm}^3$ to $10^{19}/\text{cm}^3$. Previously, control of carrier concentration below $10^{17}/\text{cm}^3$ was difficult, if not impossible.

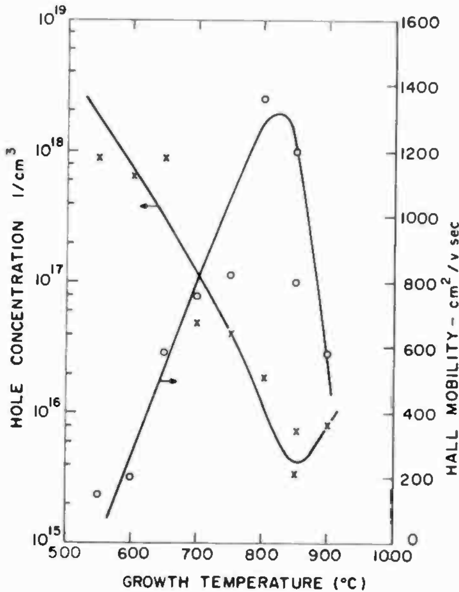

Fig. 1—Carrier concentration and Hall mobility of 2-μm p-type germanium films.

The Hall mobilities of p-type and n-type films as a function of carrier concentration are shown in Fig. 2 and Fig. 3, respectively, for films grown on 0.1-μm Si grown on ($\bar{1}102$) sapphire. The p-type films were obtained via addition of B_2H_6-H_2 mixtures to the gas stream during

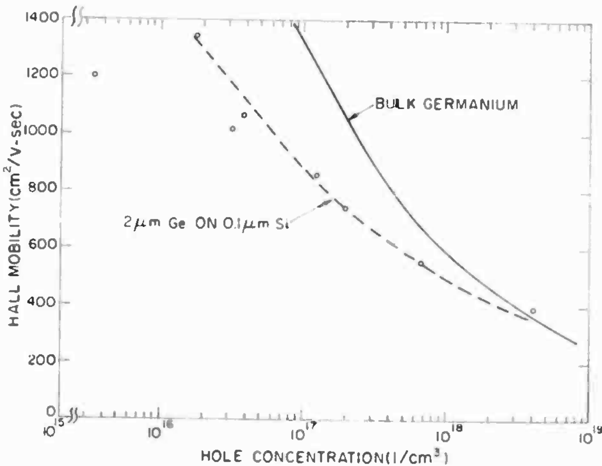

Fig. 2—Hall mobility versus hole concentration in 2-μm p-type germanium films grown on 0.1 μm of silicon on sapphire.

growth, while the n-type films were grown by using PH_3-H_2 mixtures added to the gas stream. At all carrier concentrations the Hall mobilities were less than obtained in bulk germanium, but at carrier concentrations in excess of $10^{17}/cm^3$ for p-type films, and $10^{18}/cm^3$ for n-type films, the difference between film and bulk mobilities was not large. The most lightly doped film shown in Fig. 4 was grown with no B_2H_6 added and, as such, represents the quality of the undoped germanium films. Measurements of the temperature dependence of the carrier concentration in lightly doped and undoped p-type films has resulted in an activation energy of 0.08 eV for the defect-caused acceptor in these films.[12]

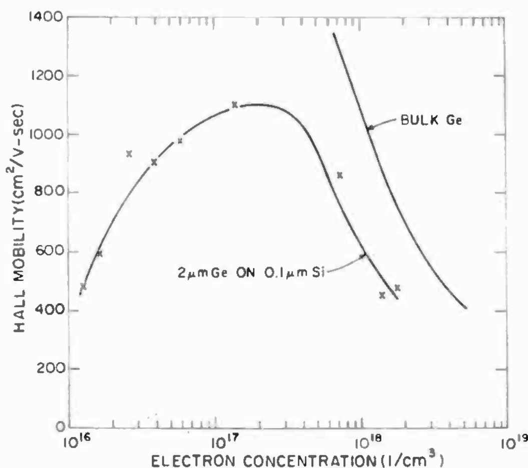

Fig. 3—Hall mobility versus electron concentration in 2-μm n-type germanium films.

In the n-type films described in Fig. 3, it is seen that the Hall mobilities started to drop as the carrier concentration dropped below $10^{17}/cm^3$. This drop in Hall mobility at the lower carrier concentrations was due to compensation of the films by the defect acceptor. In thinner films the defect-acceptor compensation was more severe since the defect density rose as the Si-Ge interface was approached. In several of the 2-μm-thick n-type films grown with carrier concentrations of $10^{17}/cm^3$ or less, a layer of p-type germanium was detected near the germanium–silicon interface. Thus, the measured values of the electrical properties of the films were the values integrated over the films thickness and, as such, included the defect-acceptor compensation and possibly over-compensation near the germanium–silicon interface. The present lower limit on the defect-accepetor concentration (low $10^{15}/cm^3$) placed the lower limit

of $10^{16}/cm^3$ on the electron concentration in the 2-μm-thick germanium films.

B. Silicon Films

The electrical characteristics of the silicon films were found to be heavily dependent on the growth parameters. High growth temperatures and low growth rates tended to introduce more aluminum from the substrates into the films, while low growth temperatures and higher growth rates lead to an increased density of defects. Thus it was necessary to extensively measure the electrical properties of the films grown under various growth conditions in order to determine the optimum growth temperatures and growth rates. The object of these measurements was to determine methods of producing films with both high mobilities and controlled carrier concentrations.

Examples of the variation in carrier concentration and Hall mobility as a function of growth temperature are shown in Figs. 4 and 5. These data were taken on films of various thicknesses grown on $(1\bar{1}02)$ and (0001) sapphire and (111) spinel.[2,3] In Fig. 4 it is seen that as the growth temperature increased, the hole concentration increased. The dopant in these films was aluminum and was introduced via the hydrogen and/or silicon reduction of the oxide substrate.[13] It is significant that the films grown on spinel were doped over an order of magnitude less than the films grown on either orientation of sapphire.[14] The Hall mobilities of all of the films described in Fig. 5 show the same general variation with changes in the growth temperatures. At low growth temperatures and high growth temperatures, the mobilities dropped. At some intermediate growth temperature, films with the highest mobility were obtained. Both the optimum growth temperature and the maximum mobilities obtained at that temperature varied according to the substrate material and the substrate orientation. The (111) silicon films grown on the (111) spinel had the highest mobilities with values in excess of 300 cm^2/V sec being representative. The 2-μm-thick (100) films grown on the $(1\bar{1}02)$ sapphire orientation had higher mobilities than the 2-μm-thick (111) films grown on the (0001) sapphire, while the thicker films grown on the (0001) sapphire had higher mobilities than the thicker films grown on the $(1\bar{1}02)$ sapphire. In general, all of the thicker films had higher mobilities than the thinner films due to improvements in the crystal structure of the thicker films and less aluminum autodoping in the surface layers of the thicker films.

Measurements have been made of the Hall mobility and carrier concentration as a function of film thickness in p- and n-type films grown

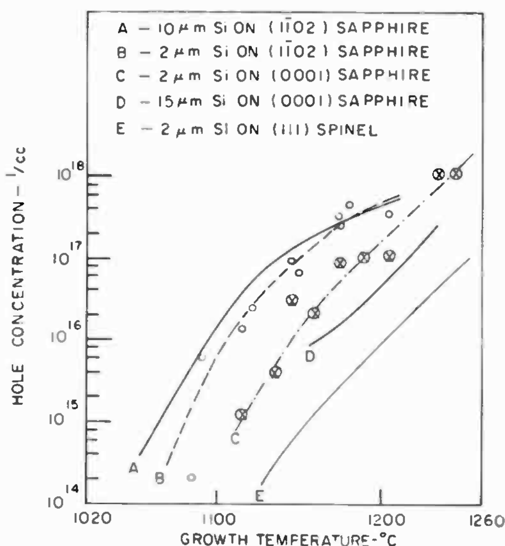

Fig. 4—Hole concentration versus growth temperature of p-type silicon films grown on sapphire and spinel.

on (1̄102) sapphire[15] and p-type films grown on (111) spinel.[16] The Hall mobility and the carrier concentration dropped as the films were made thinner. The drop in Hall mobility has been attributed to increased scattering of the carriers by crystalline imperfections in the

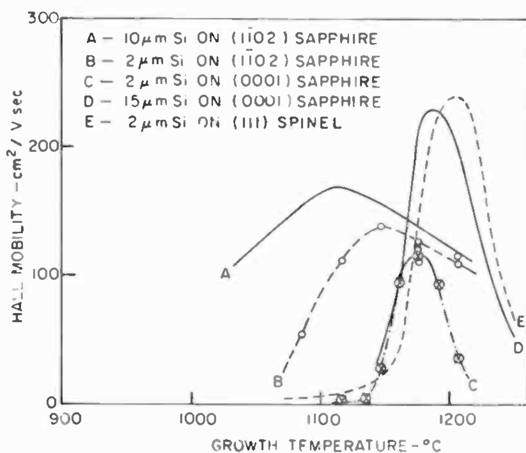

Fig. 5—Hall mobility versus growth temperature of p-type silicon films grown on sapphire and spinel.

films. The dislocation density in these films has been shown to increase as the films were made thinner.[2] The drop in carrier concentration in the thinner films was attributed to compensation of the majority carriers by deep donor and acceptor levels introduced by defects in the films. This donor–acceptor pair has been shown to have energy levels in silicon-on-sapphire films of 0.3 eV above the valence band edge and 0.25 eV below the conduction band edge,[17] respectively. These levels account for the high-resistivity films that are often obtained at growth temperatures below 1000°C, by pinning the Fermi level near mid-gap. The density of these levels can be decreased by up to two orders of magnitude by oxidizing the films in dry O_2 with 1% HCl at 1200°C, which suggests that the levels are possibly related to defect-impurity interactions, although the impurity species has not yet been identified.[17]

The minority-carrier lifetime was measured in silicon-on-sapphire films as a function of film thickness, and it was shown that the minority-carrier lifetime increased with increasing film thickness.[18] The silicon–sapphire interface acted as a fast recombination surface, and minority carriers reaching this interface had lifetimes less than 0.1 nsec. However, lifetimes as high as 1-10 nsec were measured on thicker films 5-15 μm from this interface.

One of the contributing factors to the fall-off in mobilities observed in films grown at lower growth temperatures was donor compensation. The SiH_4-H_2 mixtures used to grow these films contained unwanted donor impurities, and these impurities were most effective in acting as compensating centers in the less heavily doped films grown at the lower temperatures. In fact, it proved possible to grow n-type films using the sources of SiH_4-H_2 used to grow the films described in Fig. 4 and 5 simply by raising the growth rate by a factor of 5. Using the higher growth rate, the total time at high temperature was significantly reduced, as was the aluminum autodoping.

To demonstrate the effects of growth rate on electrical properties of the silicon-on-sapphire films, a series of very thin films, 0.15 μm thick, were grown on $(1\bar{1}02)$ sapphire at 1150°C. The films were all p-type and doped $2\text{-}5 \times 10^{17}/cm^3$. The Hall mobility versus growth rate is shown in Table 1 for these films. As can be seen, the Hall mobility increased as the growth rate increased up to a growth rate of 10 μm/min. At higher growth rates the Hall mobility dropped. Similar measurements made on films grown at different temperatures, have shown that the optimum growth rate tended to drop as the growth temperature dropped.

Using current state-of-the-art technology for growing thin silicon films on sapphire and spinel, the Hall mobilities versus carrier concen-

Table 1—Hall Mobilities of 0.15-μm-thick Films Grown on (1$\bar{1}$02) Sapphire at 1150°C

Growth rate (μm/min)	Hall mobility (cm²/V-sec)
0.7	40
1.5	59
4.0	68
10	100
15	61

trations shown in Figs. 6 and 7 for p-type and n-type films are representative. The Hall mobilities of both p-type and n-type films are seen to drop at the higher carrier concentrations due to the increased ionized impurity scattering. As the carrier concentrations were decreased, the Hall mobilities in the best p-type films remained relatively close to bulk values, while the mobilities in n-type films saturated at about 60% of bulk values. For carrier concentration in the 10^{13}-10^{15}/cm³ range, the mobilities dropped, probably due to compensation by both shallow donors and acceptors and by the dominance of the deep donor–acceptor pair that became more important as the carrier concentration was reduced.[16] In general the films grown on (111) spinel have had somewhat higher mobilities than the films grown on (1$\bar{1}$02) sapphire. This may be due to the reduced autodoping found in the films grown on spinel, but is probably also associated with improved crystal structure in the films grown on (111) spinel. In general, the films grown on (100) spinel and (0001) sapphire have had lower mobilities than those in Figs. 6 and 7.

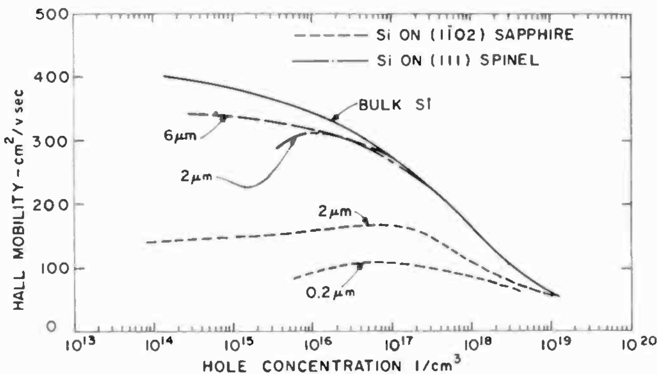

Fig. 6—Hall mobility versus hole concentration in silicon films.

One of the side effects of the autodoping problem relates to changes that can occur in the electrical properties of the films during post-growth heat treatments. From the viewpoint of device processing, it would be highly desirable if the film properties did not change during device fabrication. The typical types of thermal cycling that can occur during device processing include heating of the wafers in hydrogen, helium, or various oxidizing ambients. From the growth studies it was found that heating of the films in hydrogen increased the hole concentration due to the hydrogen reduction of the subtrate releasing aluminum into the film.[13] Accompanying the release of aluminum was the release of oxygen and in the case of spinel, magnesium. The importance of the oxygen and magnesium in altering the electrical properties is still under study, since excessive amounts of oxygen have been seen to lower Hall mobilities.[19]

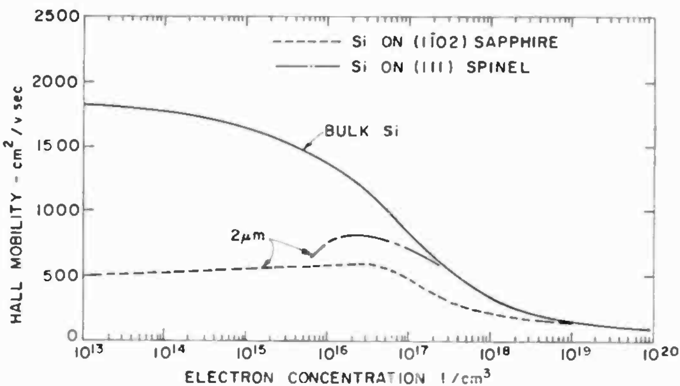

Fig. 7—Hall mobility versus electron concentration in silicon films.

Post-firing of the films in helium or other inert ambients has had little effect on the electrical properties of the films. Post-firing of the films in oxidizing ambients, however, altered the film properties significantly. In bulk silicon, oxidation is known to remove p-type impurities from the wafer and to push the n-type impurities back into the wafer.[20] This same effect occurs in the thin films,[13] but is accentuated by the limited number of impurities found in the films. Both the relatively high diffusivity of aluminum and the tendancy for aluminum to segregate in an oxide result in the rapid loss of aluminum from the films upon oxidation. The loss of aluminum thus lowered the acceptor concentration of as-grown films after thermal oxidation. In addition to the loss of aluminum, oxygen entered the films during oxidation

and introduced scattering centers that could lower the Hall mobilities.[19] Thus, from a practical point of view, it is desirable to use the substrate material that introduces the minimum autodoping and to grow the films at the lowest temperature consistent with the production of high-mobility films.[21]

A growth system that utilizes SiH_4 in He has been used to grow silicon-on-silicon at growth rates up to 3.1 μm/min at temperatures as low as 900°C.[22] This system has been used to grow silicon-on-sapphire and spinel, and while much work remains to be done to determine the electrical properties of films grown with He as the carrier gas, the preliminary results look encouraging. Hall mobilities of 330 cm²/V-sec have ben obtained on p-type films grown on (111) spinel, and n-type mobilities of 660 cm²/V-sec on $(1\bar{1}23)$ sapphire and 530 cm/²V-sec on (111) spinel have been measured.[23]

Due to the differences in the coefficients of thermal expansion of the film and the substrate, the composite structure became deformed upon cooling from the growth temperature. Measurements of the film and substrate deformation have been used to calculate the compressive stresses in the films, and values of stress of the order of 10^9-10^{10} dynes/cm² have been found, independent of film thickness.[24] The possibility of stress-related effects on the electrical properties of the films has been considered as one possible explanation of why it has proved relatively easy to obtain p-type films with bulk values of mobilities, while n-type films have consistently had lower mobilities relative to bulk values.[25]

Device Applications

The silicon films grown on sapphire have found the greatest number of uses in fabrication of both MOS transistors and integrated circuits.[26] The first reported MOS transistors on silicon on sapphire had values of $g_m = 4000$ μmho for channel lengths of 7.5 μm.[27] These transistors had very low source–drain capacitances, in addition to having negligable isolation capacitance.[28] Both p-channel and n-channel MOS transistors have been fabricated.

The development of the depletion transistor in silicon on sapphire[29] has led to complementary MOS integrated circuits. The first reported circuit was a memory cell with read–write cycle of 7.5 nsec.[4] This circuit contained 10 transistors/bit on a 400 mil² area. Both enhancement and depletion transistors were used. More complicated integrated circuits have been fabricated, with a high-speed associative memory[30] and a 50-stage dynamic shift register[31] being good examples.

The 50-stage shift register shown in Fig. 8 contained 420 transistors on a 70 × 100 mil substrate and has been operated in excess of 90 MHz.

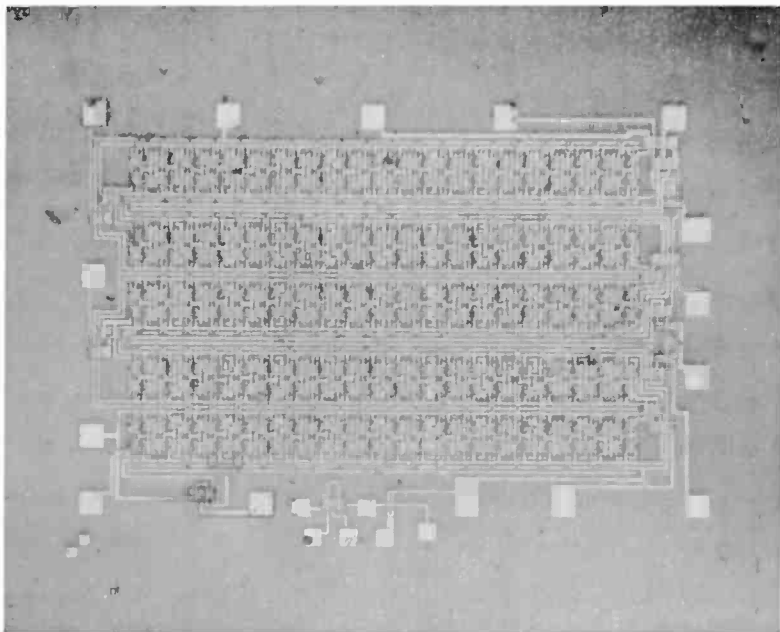

Fig. 8—Photograph of a 50-stage dynamic shift register fabricated in silicon on sapphire. This shift register has been operated at 90 Mhz.

Application of the thin silicon films to bipolar transistor fabrication and to bipolar circuitry has been very difficult. It has been observed that the lateral diffusion of dopants in silicon-on-sapphire films proceeded at a rate comparable to that in bulk silicon, while diffusion of dopants in a direction normal to the sapphire surface was a factor of 2 to 5 times faster than in bulk silicon.[23] The high density of growth imperfections has resulted in spikey diffusion fronts for both phosphorus and boron diffusions. The minority-carrier lifetime is also low in these films; however, it does increase approximately linearly as the films become thicker,[18] and lifetimes in the range of 1-12 nsec have typically been obtained.[32]

In spite of these problems, double-diffused p-n-p transistors with gains of 4-8 have been fabricated,[33] although yields have been low. An alternative approach to the double-diffused bipolar transistor has

been the fabrication of an all-epitaxial n-p-n bipolar structure.[34] The junction definition that has been obtained is very sharp, and interdiffusion of dopants was kept to a minimum by growing the silicon film at a growth rate of 2-3 μm/min. Base widths of 0.5 to 1 μm have been obtained. An HCl gettering treatment has also been developed,[35] and measurements indicate that bipolar transistors with a base width of 0.7 μm and minority carrier lifetime of 15 nsec have had current gains in excess of 20. Cutoff frequencies of the order of 500 MHz have been measured.

Summary

To summarize the characteristics of heteroepitaxial germanium and silicon the following list has been compiled. This list, with references indicating where details can be found, highlights the more significant features of RCA research in this field.

(1) Measurement of thermally induced plastic deformation and stress in the range 10^9–10^{10} dynes/cm^2 in the films.[24]

(2) Identification of aluminum as the major p-type dopant and association of the autodoping problem with H_2 and Si reduction of the substrate.[12-14]

(3) Effects of post-firing of the films in H_2, He, and O_2 and particularly the removel of p-type dopants from the films upon thermal oxidation.[2, 3, 19, 21]

(4) Effects of the changes in the growth parameters on the electrical properties of the films, particularly changes in mobility and carrier concentration with growth rate, growth temperature, substrate orientation and substrate material.[1-3, 11]

(5) The use of infrared interferences scheme to monitor, *in situ,* the film thickness while growing the film.[6]

(6) Demonstration that silicon grown on magnesium aluminate spinel contains less aluminum than silicon grown on sapphire.[14, 16, 32]

(7) Use of stoichiometric spinel to avoid thermal-mechanical instabilities found in aluminia-rich spinel.[14, 3]

(8) Determination of electrical properties (mobility, carrier concentration, minority-carrier lifetime, and deep-level density) as a function of film thickness.[2, 9, 15-18]

(9) The variation of electrical properties as a function of carrier concentration.[2, 21]

(10) Variation of electrical and optical properties as a function of

defect structure and the identification of the deep donor–acceptor pair caused by defects in the films.[15, 17]

(11) The importance of the nucleation of the initial layer on the electrical properties of subsequent layers and the use of a thin undercoating of silicon to significantly improve the electrical properties of the germanium films.[2, 11, 12]

(12) Reproducible growth of high-mobility 1-2 μm-thick germanium films doped in the low $10^{15}/cm^3$ range.[11, 12]

(13) The fabrication of MOS transistors in silicon on sapphire.[27]

(14) Development of complementary MOS transistor circuit fabricated in silicon on sapphire.[4]

(15) Fabrication of high-speed medium-scale integrated MOS circuits in silicon-on-sapphire.[30, 31]

Acknowledgments

The authors are extremely indebted to C. W. Mueller for his many suggestions and his constant guidance of this work. The many contributions of E. C. Ross, C. C. Wang, R. S. Silver, and K. H. Zaininger are gratefully acknowledged. Much of the data presented in this paper was taken with the assistance of R. O. Wance, J. Corboy, and F. Dougherty.

References:

[1] D. J. Dumin "Epitaxial Growth of Germanium on Single Crystal Spinel," **Jour. Electrochem. Soc.,** Vol. 114 p. 749, (1967); C. W. Mueller and P. H. Robinson, "Grown-Film Silicon Transistors on Sapphire," **Proc. IEEE,** Vol. 52, p. 1487 (1964); H. M. Manasevit and W. I. Simpson, "Single Crystal Silicon on a Sapphire Substrate," **Jour. Appl. Phys.,** Vol. 35, p. 1349 (1964).

[2] D. J. Dumin, "Electrical Properties of Silicon Films Grown Epitaxially on Sapphire," **Jour. Appl. Phys.,** Vol. 38, p. 1909 (1967); D. J. Dumin and P. H. Robinson, "Carrier Transport in Thin Silicon Films," **Jour. Appl. Phys.,** Vol. 39, p. 2759 (1968); P. B. Hart, et al, "Electrical Properties of Epitaxial Silicon Films on α-alumina," **Brit. Jour. Appl. Phys.,** Vol. 18, p. 1389, (1967).

[3] P. H. Robinson and D. J. Dumin, "The Deposition of Silicon on Single-Crystal Spinel Substrates," **Jour. Electrochem. Soc.,** Vol. 115, p. 75 (1968); G. W. Cullen, G. E. Gottlieb, C. C. Wang, and K. H. Zaininger, "Epitaxial Growth and Properties of Silicon on Alumina-Rich Single-Crystal Spinel," **Jour. Electrochem. Soc.,** Vol. 116, p. 1444 (1969); C. C. Wang, G. E. Gottlieb, G. W. Cullen, S. H. McFarlane, and K. H. Zaininger, "Heteroepitaxy of Silicon on Stoichiometric Spinel," **Trans. Met. Soc. of AIME,** Vol. 245, p. 441 (1969); H. Schlotterer, "Mechanical and Electrical Properties of Epitaxial Silicon Films on Spinel," **Solid-State Electronics,** Vol. 10, p. 947 (1968).

[4] J. F. Allison, J. R. Burns, and F. P. Heiman, "Silicon-on-Sapphire Complementary MOS Memory Cells," **IEEE Jour. Solid-State Circuits,** Vol. SC-2, p. 208 (1967).

[5] P. H. Robinson and C. W. Mueller, "The Deposition of Silicon-on-Sapphire Substrates," **Trans. AIME,** Vol. 236, p. 268 (1966).

[6] D. J. Dumin, "Measurement of Film Thickness Using Infrared Interference," **Rev. Sci. Instr.,** Vol. 38, p. 1107 (1967).

[7] H. M. Manasevit, et. al., "Heteroepitaxial Silicon-Aluminum Oxide Interface—Pt. I," **Trans. Met. Soc., AIME,** Vol. 233, p. 540 (1965).

[8] R. P. Ruth, J. C. Marinace, and W. C. Dunlap, "Vapor Deposited Single Crystal Germanium," **Jour. Appl. Phys.**, Vol. 31, p. 995, (1960).
[9] D. J. Dumin, "Epitaxial Growth of Germanium on Single Crystal Spinel," **Jour. Electrochem. Soc.**, Vol. 114, p. 749 (1967).
[10] B. W. Sloope and C. O. Tiller, "Electrical Properties of Epitaxial Ge Films Deposited on (111) CaF_2 Substrates," **Jour. Appl. Phys.**, Vol. 38, p. 140 (1967).
[11] D. J. Dumin, "Growth and Properties of Thin Germanium Films," **Jour. Electrochem. Soc.**, Vol. 117, p. 95 (1970).
[12] D. J. Dumin, "Acceptor States Due to Defects in Thin Germanium Films," **Jour. Vac. Sci. and Tech.**, Vol. 6, p. 498 (1969).
[13] D. J. Dumin and P. H. Robinson, "Autodoping of Silicon Films Grown Epitaxially on Sapphire," **Jour. Electrochem. Soc.**, Vol. 113, p. 469 (1966).
[14] P. H. Robinson and D. J. Dumin, "The Deposition of Silicon on Single-Crystal Spinel Substrates," **Jour. Electrochem Soc.**, Vol. 115, p. 75 (1968).
[15] D. J. Dumin and P. H. Robinson, "Electrically and Optically Active Defects in Silicon-on-Sapphire Films," **Jour. Crystal Growth**, Vol. 3, p. 214 (1968).
[16] G. W. Cullen, G. E. Gottlieb, C. C. Wang, and K. H. Zaininger, "Epitaxial Growth and Properties of Silicon on Alumina-Rich Single Crystal Spinel," **Jour. Electrochem. Soc.**, Vol. 116, p. 1444 (1969).
[17] D. J. Dumin, "Deep Levels Within the Forbidden Gap of Silicon-on-Sapphire Films," **Solid-State Electronics**, Vol. 13, p. 415 (1970).
[18] D. J. Dumin and R. S. Silver, Diffused Diodes in Silicon-on-Saphire," **Solid-State Electronics**, Vol. 11, p. 353 (1968).
[19] E. C. Ross and G. Warfield, "Effects of Oxidation on Electrical Characteristics of Silicon-on-Sapphire Films," **Jour. Appl. Phys.**, Vol. 40, p. 2339 (1969).
[20] A. S. Grove, et al, "Redistribution of Acceptor and Donor Impurities During Thermal Oxidation of Silicon," **Jour. Appl. Phys.**, Vol. 35, p. 2695 (1964).
[21] G. W. Cullen, G. E. Gottlieb, C. C. Wang, "The Epitaxial Growth of Silicon on Sapphire and Spinel Substrates: Suppression of Changes in the Film Properties During Device Processing," **RCA Review**, Vol. 31, p. 355, June 1970.
[22] D. Richman and R. H. Arlett, "Low Temperature Epitaxial Growth of Single Crystalline Silicon From Silane," **Jour. Electrochem. Soc.**, Vol. 116, p. 872 (1969); D. Richman, Y. S. Chiang, and P. H. Robinson "Low-Temperature Vapor Growth of Homoepitaxial Silicon," **RCA Review**, p. 613, Dec. 1970 (this issue).
[23] Y. S. Chiang and D. Richman, Private communication.
[24] D. J. Dumin, "Deformation of and Stress in Epitaxial Silicon Films on Single Crystal Sapphire," **Jour. Appl. Phys.**, Vol. 36, p. 2700 (1965).
[25] H. Schlotterer, "Mechanical and Electrical Properties of Epitaxial Silicon Films on Spinel," **Solid State Electronics**, Vol. 11, p. 947 (1968).
[26] J. F. Allison, D. J. Dumin, F. P. Heiman, C. W. Mueller and P. H. Robinson, "Thin Film Silicon; Preparation, Properties, and Device Applications," **Proc. IEEE**, Vol. 57, p. 1490 (1969).
[27] C. W. Mueller and P. H. Robinson, "Grown-Film Silicon Transistors on Sapphire," **Proc. IEEE**, Vol. 52, p. 1487 (1964).
[28] E. C. Ross and C. W. Mueller, "Extremely Low Capacitance Silicon Film MOS Transistors," **IEEE Trans. Electron Devices**, Vol. ED-13, p. 379 (1966).
[29] F. P. Heiman, "Thin-Film Silicon-on-Sapphire Deep-Depletion MOS Transistors," **IEEE Trans. Electron Devices**, Vol. ED-13, p. 855 (1966); S. R. Hofstein, "An Analysis of Deep Depletion Thin Film MOS Transistors," **IEEE Trans. Electron Devices**, Vol. ED-13, p. 846 (1966).
[30] J. R. Burns and J. H. Scott, "Silicon-on-Sapphire Complementary MOS Circuits for High Speed Association Memory," presented at 1969 Fall Joint Computer Conference, Las Vegas, Nevada, Nov. 18-20, 1969.
[31] J. R. Burns, J. Meyer, and J. Scott, "High Speed Silicon-on-Sapphire 50 Stage Shift Register," **Digest of Papers ISSCC**, Philadelphia (Feb. 1970).
[32] F. P. Heiman, "On the Determination of Minority Carrier Lifetime from the Transient Response of an MOS Capacitor," **IEEE Trans. Electron Devices**, Vol. ED-14, p. 781 (1967).
[33] D. J. Dumin and A. Kokkas, Private communication, 1965.
[34] F. P. Heiman and P. H. Robinson, "Silicon-on-Sapphire Epitaxial Bipolar Transistors," **Solid State Electronics**, Vol. 11, p. 411 (1968).
[35] F. P. Heiman and P. H. Robinson, to be published, **Jour. Electrochem. Soc.** (1970).

Vapor-Phase Growth of Several III-V Compound Semiconductors*

J. J. Tietjen, R. E. Enstrom, and D. Richman
RCA Laboratories, Princeton, N. J.

Abstract—A review is presented of the vapor-phase growth method that has been developed at RCA Laboratories for the synthesis of a broad spectrum of III-V compounds. The predominant feature of this technique is the use of gases as the source chemicals, thereby providing improved control of the chemical composition, homogeneity, crystalline perfection, and impurity concentrations and distributions of the epitaxial layers. As a result, a number of notable advances have been made with respect to the material properties and device utilization of several III-V compounds.

1. Introduction

III-V compound semiconductors and their alloys cover a wide range of electrical and optical properties that make them potentially useful for a variety of practical applications. These include electro-optic and microwave devices, high-temperature applications, and electron-emitting phenomena. Unfortunately, the synthesis of these materials is frequently complicated by the combination of high melting temperatures and dissociation pressures, and large concentration differences between the isothermal liquidus and solidus in the phase diagrams of these alloy systems. However, many of the difficulties associated with these complications are minimized when vapor-phase crystal-growth methods are employed, primarily because of the low growth temperatures that are possible with this technique. In addition, vapor-phase growth facilitates preparing these compounds in thin-layer geometries, which is often essential for optimum use in device structures.

* The research reported herein was made possible by the support of the Advanced Research Projects Agency under Order Number 1034 through the U.S. Army Electronics Command, Ft. Monmouth, New Jersey 07703, under Contract No. DAAB-07-69-C-0145, and by the National Aeronautics and Space Administration, Electronics Research Center, under Contract No. NAS 12-538.

for the sake of brevity and clarity, only the more important properties will be summarized in this paper. The various materials are cataloged below, with an appropriate description of their properties. The references included with the headings provide direction to a more detailed description of these materials.

3.1 GaAs,[1,6] GaP,[11,18] and $GaAs_{1-x}P_x$[1] Alloys

This group of compounds encompasses energy gaps in the range of about 1.4 to 2.2 eV at room temperature and, therefore, involves optical transitions extending from the near infrared to the middle of the visible spectrum. The energy gaps are direct for values of x up to about 0.45 and are indirect for higher values of x. These materials can be prepared in thicknesses ranging from about 0.5 micron to 1 mm, at growth rates in the range of from 0.5 to greater than 10 microns/min on GaAs substrates, including dielectric materials such as sapphire and spinel.

Undoped samples of GaAs have been prepared with net electron concentrations as low as $9 \times 10^{13}/cm^3$ and mobilities as high as 8700 cm^2/V-sec and 108,000 cm^2/V-sec at room temperature and 77°K, respectively. All of these compounds can be readily synthesized with net electron concentrations, at room temperature, of less than $5 \times 10^{15}/cm^3$. Also, these materials can all be easily doped with donor or acceptor impurities to increase the carrier concentrations into the 10^{18} and $10^{19}/cm^3$ range, respectively, without seriously degrading their crystalline quality. It is noteworthy that $GaAs_{1-x}P_x$ alloys prepared by this growth technique were the first to show the proper dependence of the electron mobility on alloy composition, which provided strong evidence for the now-accepted fact that alloy scattering does not dominate in III-V alloy systems.[19]

3.2 InAs, InP, and $InAs_{1-x}P_x$ Alloys[2]

These materials are all direct-bandgap semiconductors, and cover the range of about 0.35 to 1.3 eV, at room temperature. Typical growth rates for these compounds range from 0.25 to 0.5 micron/min, with the lower rates corresponding to InP and InP-rich alloys. With such growth rates, layers having a thickness as low as about 0.2 micron to as high as 150 microns, depending on alloy composition, can be prepared. To date, these materials have been prepared on InAs, InP, and GaAs substrates.

Typical electron carrier concentrations for undoped layers are in

the range of 5×10^{15} to $1 \times 10^{16}/cm^3$. In general, the electron mobilities of these materials are equivalent to or exceed the highest values reported. Both n- and p-type doping has been achieved to provide carrier concentrations as high as the $10^{19}/cm^3$ range while maintaining good crystalline quality.

3.3 GaSb and $GaAs_{1-x}Sb_x$ Alloys

This growth technique has permitted the vapor-phase growth of $GaAs_{1-x}Sb_x$ across the entire alloy series for the first time. These compounds have direct transitions across their energy gaps that cover the range of approximately 0.7 to 1.4 eV, at room temperature. Because of the low melting point of many of these materials, relatively low growth temperatures are necessary. This restricts the partial pressure of antimony in the growth system to a low value, and results in low growth rates. Typical growth rates for these materials are about 0.2 micron/min, with layer thicknesses normally restricted to the range of about 0.2 to 25 microns, for growth on GaAs substrates.

As-grown layers of these compounds are usually p-type with hole concentrations in the low $10^{16}/cm^3$ range. The hole mobilities for GaAs-rich alloys are high, comparable to the highest values reported for unalloyed p-type GaAs. As a result of the strain introduced into GaSb-rich alloys due to the lattice and thermal expansion mismatch with the GaAs substrates, the mobilities of these materials are slightly lower than those reported for melt-grown alloys. This problem of strain could be alleviated by using GaSb substrates or by slow compositional grading between the substrate and the alloy layer.

3.4 GaN[4, 20]

GaN prepared by this method has provided the first single-crystal material suitable for good electrical and optical evaluation of this compound. GaN has a direct energy gap, at room temperature, of about 3.5 eV.[20] Normal growth rates are about 0.5 micron/min and, therefore, layers having thicknesses up to about 150 microns are easily prepared.

Undoped crystals have a very high inherent electron concentration, usually about $10^{19}/cm^3$, which is probably due to a high density of nitrogen vacancies. Although conducting p-type samples have been prepared, they are extremely difficult to reproduce, and the samples have been electrically inhomogeneous.

3.5 $Ga_{1-x}In_xAs$[21] and $Ga_{1-x}In_xP$[22] Alloys

$Ga_{1-x}In_xAs$ and $Ga_{1-x}In_xP$ alloys have energy gaps that cover the range 0.35 to 1.4 eV and 1.3 to 2.2 eV, respectively. The $Ga_{1-x}In_xAs$ alloys have a direct energy gap over the entire composition range. Similarly, InP is direct but the $Ga_{1-x}In_xP$ alloys become indirect above about 2.1 eV. The alloy composition is varied for both alloys principally by adjusting the HCl flow ratio to the indium and gallium metal sources. In addition, for the $Ga_{1-x}In_xP$ alloys, the composition is a function of the growth temperature. $Ga_{1-x}In_xAs$ alloys can be prepared by depositing pure GaAs or InAs initially on GaAs or InAs substrates, respectively, which are readily available, and then grading to the final alloy composition to achieve a layer having a low imperfection density and a minimum of strain. A similar procedure can be used for the $Ga_{1-x}In_xP$ alloys by using GaP or InP substrates. However, since GaP and InP substrates have not been readily available, GaAs substrates have also been used, but because of the lattice parameter and thermal expansion mismatches between the epitaxial layer and the substrate, these alloy layers are not as perfect. Donor carrier concentrations as low as $5 \times 10^{14}/cm^3$ have been achieved for undoped $Ga_{1-x}In_xAs$ alloys, and both alloy systems can be doped n- and p-type over the broad range required for device applications.

3.6 AlAs,[23] AlP,[14] AlN, and $Ga_{1-x}Al_xAs$

AlAs, AlP, and AlN are indirect-gap compounds with forbidden energy gaps of 2.16, 2.43, and about 4.0 eV, respectively; the latter value has not been well established as yet. GaAs is direct, and the crossover point to indirect gap $Ga_{1-x}Al_xAs$ alloy has been found to occur at 1.89 eV, which corresponds to a composition of about 27% AlAs.[24] Unlike gallium and indium chlorides, the aluminum chlorides produced by the reaction of HCl with the aluminum metal source have been found to attack the quartz deposition tube, but this can be prevented by using a protective liner of Al_2O_3 or carbon. AlAs and AlP have nearly the same lattice parameters as GaAs and GaP, respectively, thus making the latter materials useful as substrates to attain single-crystal deposits. Further, the constancy of the lattice parameter makes the $Ga_{1-x}Al_xAs$ alloy system of great interest since the attainment of low strain, large-bandgap epitaxial layers is more readily achieved than in systems where grading is required. Undoped AlAs layers with donor concentrations as low as $3 \times 10^{17}/cm^3$ and room temperature mobilities as high as 280 cm^2/V-sec have been achieved; these represent the best

properties reported so far. In addition, AlAs prepared by this method is sufficiently stable in normal ambients so that it can be processed into device structures, such as p-n junctions,[25] by conventional methods. Previously, AlAs had been considered to be too hygroscopic to permit such device utilization. The enhanced stability of these AlAs layers may be related to improved crystalline perfection and/or higher purity. For undoped AlP, carrier concentrations and room temperature mobilities are typically $1 \times 10^{18}/cm^3$ and 80 cm^2/V-sec, respectively.

4. Device Applications

The most notable accomplishment of this crystal-growth method has been the success with which it has been applied to the preparation of device structures. This has involved a broad range of materials and structures, and has accommodated the fabrication of several outstanding devices. The more important devices are listed below with a summary of their properties. The references cited provide direction to a more complete description of the devices and their characteristics.

4.1 Varactor Diodes[5]

Over 1000 p^+-n-n^+ varactor diode structures were incorporated in complete microwave devices, and provided the highest combination of reverse breakdown voltages and cutoff frequencies ever reported. Breakdown voltages in excess of −50 V are easily achieved, with cutoff frequencies above 150 GHz at −6 V bias.

4.2 Electroluminescent Diodes[7, 26–29]

Complex n^+-n-p-p^+ structures have been studied in $GaAs_{1-x}P_x$ in order to optimize the device parameters of visible electroluminescent diodes. These structures not only involved several changes in dopant type and concentration, but also subtle manipulation of the gross composition of the alloys involved. As a result of this study, diodes emitting in the red region of the spectrum can be reproducibly prepared having brightness values slightly above 30 ft-L at 1 A/cm^2, which is within a factor of 3 of the highest value reported to date.

4.3 Injection Lasers[8, 30, 31]

Abrupt p-n junction structures prepared in $GaAs_{1-x}P_x$ alloys resulted in the first room-temperature injection lasers operating in the visible region of the spectrum. In fact, these diodes have provided operation

at the shortest wavelength ever reported for a room-temperature injection laser, 6750 Å.

4.4 High-Temperature Rectifiers[9, 17]

High-power rectifiers capable of operating at temperatures above 300°C have been fabricated from both GaAs and $GaAs_{1-x}P_x$ alloy multilayer structures consisting of as many as six different layers. To achieve high reverse-bias breakdown voltages and high forward currents, the electron concentration had to be reduced to $<1 \times 10^{15}/cm^3$, and microplasma-free p-n junctions as large as 0.175 inch had to be prepared. The latter was particularly troublesome since the probability of encountering crystal defects, which cause microplasmas increases with the p-n junction area. Rectifiers fabricated from these wafers have attained reverse-bias voltages as high as 475 volts for a 0.050-inch-diameter and 250 volts for a 0.175-inch-diameter mesa p-n junction. Further, the 0.175-inch diode passed 50 A in the forward direction at 25°C before and after cycling to 300°C.

4.5 High-Temperature Transistors[10]

GaAs n-p-n and $GaAs_{1-x}P_x$ p-n-p structures with base layers as thin as 1 micron have been used for the fabrication of transistors. So far the GaAs n-p-n structures have given the best results and room-temperature current gains as high as 40 have been achieved. Transistor action has been demonstrated to temperatures as high as 300°C, and at this temperature the I-V characteristics are stable. Minority hole and electron lifetimes in GaAs and $GaAs_{1-x}P_x$ p-n junctions are about 10 and 5 nsec, respectively, for $x < 0.3$.

4.6 Transferred-Electron Oscillators and Amplifiers[6, 32–45]

A wide variety of oscillators and amplifiers have been prepared from GaAs and $GaAs_{1-x}P_x$ having outstanding electrical properties, as shown in Table 1. These devices operate in the frequency range of 1 to 40 GHz. Except for coplanar devices, n^+-n-n^+ layer structures have been used and the thickness of the n-layer, which determines the frequency of operation, has ranged from 2 to 100 microns.

4.7 Electro-Optic Modulators[11]

By using a technique of rapid vapor-phase growth, GaP crystals doped with Fe to provide high resistivity were prepared with thicknesses

suitable for transmitting collimated light beams. These crystals were used to demonstrate electro-optic modulation of visible radiation. However, the utility of these crystals was limited because of problems related to slight crystalline strain and isolated electrical shorting paths.

Table 1—Characteristics of Transferred-Electron Oscillators and Amplifiers Prepared by Vapor-Phase Growth

Oscillators	Freq. (GHz)	Mode	Power (Watts)	Efficiency (%)
High power, GaAs	1	pulsed	120	32
High power, $GaAs_{0.8}P_{0.2}$	3	pulsed	200	27
CW operation	9	cw	0.7	3
Series operation of 2 devices	8	pulsed	3.4	28
Hybrid operation	8	pulsed	19.1	22
Coplanar (n on semi-insulating GaAs)	1	pulsed	125	5
LSA operation	15	pulsed	3.5	8
Amplifiers				
Stabilized, super-	4-8	pulsed	2	6
critical GaAs with	4-8	cw	1	3
$nL > 10^{12}$ cm^{-2}	8-12	cw	1	3

4.8 Secondary-Emission Dynodes[12]

Highly doped p-type polycrystalline layers of GaP deposited on metallic substrates were optimized for use as negative-electron-affinity secondary emitters. These layers have provided revolutionary results as dynodes in commercial photomultiplier tubes. Among the most important results are the ability to discriminate between single and multiple photoelectronic events, increased speed of response, and lower dark currents.

4.9 Photocathodes[13, 21, 46]

Single-crystal GaAs, $GaAs_{1-x}P_x$, $Ga_{1-x}In_xAs$, $GaAs_{1-x}Sb_x$, and $InAs_{1-x}P_x$ alloys heavily doped with acceptor impurities have been prepared for use as negative-electron-affinity photocathodes in photomultiplier and image tubes. The bandgap of the alloy determines its spectral response. Thus $GaAs_{1-x}P_x$ alloys with a bandgap of about 1.7 eV have been used to detect ultraviolet and visible radiation up to about 7500 Å with a quantum yield about four times higher than the standard S-10 photocathode surface normally used for this wavelength region. Alloys in the other three systems have been prepared with bandgaps of about 1 eV,

and have been used to extend the response out to 12,000 Å. So far the $Ga_{1-x}In_xAs$ system has given the best results, with a quantum yield, at 10,000 Å, of more than 10 times that obtainable with the conventional S-1 photocathode. The $GaAs_{1-x}P_x$ alloy photocathode has been incorporated into commercial photomultiplier tubes with outstanding results.

5. Conclusions

A versatile vapor-phase growth method has been developed that permits the preparation of virtually all III-V compounds and their alloys in a compatible manner. The quality of the material produced by this technique is, in general, equivalent to or in advance of the state of the art of other methods used for the synthesis of III-V compounds.

The crystal-growth method has been extended to accommodate the preparation of device structures, and has resulted in the formulation of a number of novel devices having excellent properties.

References:

[1] J. J. Tietjen and J. A. Amick, "The Preparation and Properties of Vapor-Deposited Epitaxial $GaAs_{1-x}P_x$," **Jour. Electrochem. Soc.**, Vol. 113, p. 724-729 (1966).

[2] J. J. Tietjen, H. P. Maruska, and R. B. Clough, "The Preparation and Properties of Vapor-Deposited Epitaxial $InAs_{1-x}P_x$ Using Arsine and Phosphine," **Jour. Electrochem. Soc.**, Vol. 116, p. 492 (1969).

[3] R. B. Clough and J. J. Tietjen, "Vapor-Phase Growth of Epitaxial $GaAs_{1-x}Sb_x$ Alloys Using Arsine and Stibine," **Trans. Met. Soc. of AIME,** Vol. 245 p. 583 (1969).

[4] H. P. Maruska and J. J. Tietjen, "The Preparation and Properties of Vapor-Deposited Single-Crystalline GaN," **Applied Phys. Ltrs.**, Vol. 15, p. 327 (1969).

[5] J. J. Tietjen, G. Kupsky, and H. Gossenberger, "Vapor Phase Growth of Gallium Arsenide Microwave Diodes," **Solid State Electronics,** Vol. 9, p. 1049 (1966).

[6] R. E. Enstrom and C. C. Peterson, "Vapor Phase Growth and Properties of GaAs Gunn Devices," **Met. Soc. of AIME,** Vol. 239 p. 413 (1967).

[7] C. J. Nuese, J. J. Tietjen, J. J. Gannon, and H. F. Gossenberger "Optimization of Electroluminescent Efficiencies for Vapor-Growth $GaAs_{1-x}P_x$ Diodes," **Jour. Electrochem. Soc.**, Vol. 116, p. 248 (1969).

[8] J. J. Tietjen, J. I. Pankove, I. J. Hegyi, and H. Nelson, "Vapor-Phase Growth of $GaAs_{1-x}P_x$ Room-Temperature Injection Lasers," **Trans. Met. Soc. of AIME,** Vol. 239, p. 385 (1967).

[9] R. E. Enstrom, H. Kressel and L. Krassner, **High Temperature Power Rectifiers of $GaAs_{1-x}P_{-x}$, Semiconductors and Semimetals,** Vol. 6, R. K. Willardson and A. C. Beer, editors, in press.

[10] J. P. Dismukes, R. H. Dean and C. J. Nuese, "Development of GaAs and $GaAs_{1-x}P_x$ Thin-Film Bipolar Transistors," Final Report, Contract No. NAS 12-2091, Electronics Research Center, Cambridge, Mass., 1969; also C. J. Nuese and R. H. Dean, Quarterly Report No. 4, August 1970.

[11] D. Richman and J. J. Tietjen, "Rapid Vapor Phase Growth of High-Resistivity GaP for Electro-Optic Modulators," **Trans. Met. Soc. of AIME,** Vol. 239, p. 418 (1967).

[12] R. E. Simon, A. H. Sommer, J. J. Tietjen, and B. F. Williams, "New High-Gain Dynode for Photomultipliers," **Appl. Phys. Ltrs.**, Vol. 13, p. 355 (1968).

[13] R. E. Simon, A. H. Sommer, J. J. Tietjen, and B. F. Williams, "$GaAs_{1-x}P_x$ as a New High-Quantum-Yield Photoemissive Material for the Visible Spectrum," **Appl. Phys. Ltrs.**, Vol. 15, p. 43 (1969).

[14] D. Richman, "Vapor Phase Growth and Properties of Aluminum Phosphide," **Jour. Electrochem. Soc.**, Vol. 115, p. 945 (1968).

[15] W. M. Yim, "Solid Solutions in the Pseudobinary (III-V)-(II-VI) Systems and Their Optical Energy Gaps," **Jour. Appl. Phys.**, Vol. 40, p. 2617 (1969).

[16] J. P. Dismukes, W. M. Yim, J. J. Tietjen, and R. E. Novak, "Vapor Deposition of Semiconducting Mononitrides of Sc, Y, and the Rare-Earth Elements," **RCA Review**, Vol. 31, p. 680, Dec. 1970 (this issue).

[17] R. E. Enstrom and J. R. Appert, "Vapor Phase Growth of Large-Area Microplasma-Free P-N Junctions in GaAs and $GaAs_{1-x}P_x$," **Int. Symp. on GaAs**, Inst. of Physics and the Physical Society, p. 213 (1968).

[18] B. Curtis and R. Sussman, to be published.

[19] J. J. Tietjen and L. R. Weisberg, "Electron Mobility in $GaAs_{1-x}P_x$ Alloys," **Applied Phys. Letters**, Vol. 7, p. 261 (1965).

[20] J. I. Pankove, H. P. Maruska, and J. E. Berkeyheiser, "Optical Properties of GaN," to be published.

[21] R. E. Enstrom, D. Richman, J. Appert, D. G. Fisher, A. H. Sommer, and B. F. Williams, "Vapor Growth of $Ga_{1-x}In_xAs$ Alloys for Infra-Red Photocathode Applications," The Third International Symposium of Gallium Arsenide and Related Compounds, Oct. 5-7, 1970, Aachen, Germany; to be published in proceedings of conference.

[22] D. Richman, C. J. Nuese, and R. Clough, "Preparation and Properties of $In_xGa_{1-x}P$ Alloys," to be presented at the Metallurgical Society of AIME, Conf. on Preparation and Properties of Electronic and Magnetic Materials for Computers, Aug. 30—Sept. 2, 1970, New York, N. Y.; to be published in proceedings of conference.

[23] M. Ettenberg, A. G. Sigai, S. Gilbert, and A. Dreeben, "The Vapor Growth and Properties of AlAs," to be published.

[24] M. Yim, "Direct and Indirect Optical Energy Gaps of AlAs," to be published.

[25] C. J. Nuese, A. G. Sigai, M. Ettenberg, J. J. Gannon, and S. L. Gilbert, "The Preparation of Visible-Light-Emitting P-N Junctions in AlAs," to be published in **Appl. Phys. Letters**, July 1970.

[26] C. J. Nuese, J. J. Tietjen, J. J. Gannon and H. F. Gossenberger, "Electroluminescence of Vapor-Grown GaAs and $GaAs_{1-x}P_x$ Diodes," **Trans. Met. Soc. of AIME**. Vol. 242, p. 400 (1968).

[27] H. P. Maruska and J. I. Pankove, "Efficiency of $GaAs_{1-x}P_x$ Electroluminescent Diodes," **Solid State Electronics**, Vol. 10, p. 917 (1967).

[28] C. J. Nuese, H. Schade, and D. Herrick, "Efficiency Degradation of $GaAs_{1-x}P_x$ Electroluminescent Diodes Due to High-Energy Electron Irradiation," **Trans. AIME**, March 1970.

[29] H. Schade, C. J. Nuese, and D. Herrick, "Defect Centers in $GaAs_{1-x}P_x$ Electroluminescent Diodes Due to High-Energy Electron Irradiation," submitted to **Jour. Appl. Phys.**

[30] J. I. Pankove, H. Nelson, J. J. Tietjen, I. J. Hegyi, and H. P. Maruska, "$GaAs_{1-x}P_x$ Injection Lasers," **RCA Review**, Vol. 28, p. 560 (1969).

[31] J. J. Tietjen and S. Ochs, "Improved Performance of $GaAs_{1-x}P_x$ Laser Diodes," **Proc. IEEE** (Correspondence), Vol. 53, p. 180 (1965).

[32] L. E. Norton, R. E. Enstrom, and I. J. Hegyi, "High-Power 1-GHz Coplanar Gunn Effect Oscillators," **IEEE Trans. Electron** Dev., p. 142 (1968).

[33] B. E. Berson, R. E. Enstrom and J. F. Reynolds, "100 Watt L-Band Transferred-Electron Oscillators for Transponder Applications," **NEREM Record**, Vol. 10, p. 94 (1968).

[34] T. E. Walsh, B. S. Perlman and R. E. Enstrom, "Stabilized Supercritical Transferred Electron Amplifiers," **IEEE Jour. Solid State Circuits**, Vol. SC-4, p. 375, (1969).

[35] J. F. Reynolds, B. E. Berson, and R. E. Enstrom, "High Efficiency Transferred Electron Oscillators," **Proc. IEEE**, Vol. 57, p. 1692, (1969).

[36] R. E. Enstrom, J. F. Reynolds, and B. E. Berson, "Vapor Growth of Multilayer GaAs Structures for Series Operation of Transferred-Electron Oscillators," **Electronics Letters**, Vol. 5, p. 714 (1969).

[37] S. Y. Narayan, R. E. Enstrom and A. R. Gobat, "High Power CW Transferred Electron Oscillators," **Electronics Letters**, Vol. 6, p. 17 (1970).

[38] B. E. Berson, R. E. Enstrom and J. F. Reynolds, "High Power L- and S-Band Transferred Electron Oscillators," **RCA Review**, Vol. 31, p. 20, March 1970.

[39] B. E. Berson and S. Y. Narayan, "L-Band Epitaxial Gunn Oscillators," **Proc. IEEE** (Letters), Vol. 55, No. 6, p. 1078 (1967).

[40] B. E. Berson and S. Y. Narayan, "High Peak Power Epitaxial GaAs Oscillators," **IEEE Trans. Electron Devices**, Vol. Ed-14, p. 610 (1967).

[41] S. Y. Narayan, B. E. Berson and J. F. Reynolds, "Pulsed Epitaxial GaAs Gunn Oscillators," **NEREM Record,** Nov. 1967.

[42] A. E. Hahn and A. Matzelle, "CW Three-Terminal GaAs Oscillators," **IEEE Trans. Electron Devices**, Vol. Ed-14, p. 403 (1967).

[43] S. Y. Narayan and A. R. Gobat, "High Bias Voltage Operation of Epitaxial Gallium Arsenide Transferred Electron Oscillators," **Electronics Letters,** Vol. 4, p. 504 (1968).

[44] F. P. Califano, "Frequency Modulation of Three-Terminal Gunn Devices by Optical Means," **Electronics Letters,** Vol. 4, p. 411 (1968).

[45] M. C. Steele, F. P. Califano, and R. D. Larrabee, "High Efficiency Series Operation of Gunn Devices," **Electronics Letters,** Vol. 5.

[46] R. E. Enstrom and B. F. Williams, "Preparation and Properties of Vapor Grown $Ga_{1-x}In_xAs$ Alloy Photocathodes," Conf. on Photoelectric and Secondary Electron Emission, Aug. 27-28, 1969, University of Minnesota, Minneapolis, Minnesota.

The Preparation of Ternary and Quaternary Compounds by Vapor-Phase Growth

B. J. Curtis, F. P. Emmenegger,* and R. Nitsche†

Laboratories RCA Ltd., Zurich, Switzerland

Abstract—The application of the vapor-phase growth technique to the preparation and crystal growth of ternary and quaternary compounds is described. The size of the crystals obtained is in most cases sufficient to enable good physical characterization of the material to be made, with the reservation that incorporation of the transport agent may affect some properties.

1. Introduction

During the last 10 years the technique of crystal growth from the vapor phase has been applied to many problems. It is a powerful tool in the search for new compounds, particularly when the closed-tube transport method is employed.[1] In addition it can be used for phase analysis[1] in which a mixture consisting of several phases can be fractionated into spatially separated, individual, macroscopic single crystals that can then be studied by x-ray and other chemical and physical methods. Often a vapor-growth technique is the only available method by which the material in question can be synthesized even in polycrystalline form. This applies particularly to ternary and quaternary compounds that melt incongruently or that have inconveniently high equilibrium dissociation pressures at their melting points due to one or more volatile components. A further advantage of this method as applied to exploratory work is the relative simplicity of the apparatus. For the closed-tube technique, all that is required is a vacuum system, a means for loading the transport agent into the ampoule, the necessary silica ware to enable a sealed, evacuated ampoule to be prepared, and a furnace with two independently controllable zones capable of reaching temperatures around 1100°C. The apparatus required

* Present address University of Fribourg, Switzerland.

† Present address Institut für Kristallographie, Universität Freiburg i. Br., Germany.

for open-flow systems is a little more complicated since a gas-supply system is required together with the reactor and associated furnaces.

One disadvantage of chemical transport reactions is that some of the transport agent may be incorporated in the crystal. An iodine content of 2×10^{18} atoms/cm^3 was found by radiotracer methods in CdS crystals grown by iodine transport in a closed tube.[2] The possibility must not be overlooked that the incorporation of transport agent may have some influence on the physical properties of crystals grown by chemical transport.

This paper is a review of the way in which vapor-phase growth has been used to study ternary and quaternary compounds from the point of view of both their crystal chemistry and a number of their properties of interest to the solid state physicist. Four types of material are discussed: ternary chalcogenides, quaternary chalcogenides, ternary oxides, and ternary phosphides.

2. Preparation and Properties of Ternary and Quaternary Compounds Grown in Sealed Ampoules

Most of the work reviewed in this paper has been carried out in sealed silica ampoules with a transport agent (usually HCl, I_2, Br_2 or Cl_2) in a furnace with two independently controllable zones. The principle of the method, described in detail by Schäfer,[1] involves vaporizing the solid by forming volatile chemical intermediates and reacting back the resulting gas mixture at a different temperature, utilizing the temperature dependence of the chemical equilibrium. The enthalpy change for all the transport reactions utilized in this work is positive, which means that transport always occurs from a hotter to a cooler region. It is a very interesting fact that it is possible to prepare many stoichiometric ternary and quaternary compounds by chemical transport reactions. In most cases the partial pressures of the metal halogenides in the gas phase are rather different (e.g., compare the boiling points $Cu_2I_2 = 1290°C$, $SnI_2 = 717°C$, $SnI_4 = 364°C$, $CdI_2 = 796°C$; these must all be present in the gas phase during the formation of Cu_2CdSnS_4). Stoichiometric compounds can also be formed even when the source material deviates widely from the stoichiometric composition. This indicates that the free energy of formation of many complex compounds is larger than the sum of the free energies of the components.

The starting materials and a transport agent that is involatile at room temperature (e.g., NH_4I) can be loaded directly into the silica ampoule, which is then evacuated and sealed off. When volatile transport agents such as HCl, HBr, Br_2, I_2, or Cl_2 are used, they are con-

tained in small, break-seal capsules that are handled in the system shown in Fig. 1. The apparatus is first evacuated and flamed, if required, to remove absorbed water vapor. It is then sealed off at the neck (2 in Fig. 1), the break seal of ampoule (H) is broken by the magnetic hammer (M) and the transport agent is condensed in the reaction ampoule (T) by liquid nitrogen. The reaction ampoule is then sealed off at point 3 in Fig. 1. Alternatively, the transport agent can be filled into a known volume in the gas-handling system. Because of the constant vapor pressure over liquid Cl_2 (or HCl), the amount of Cl_2 contained in the dosage volume is independent of how full the tank is. The transport agent can be condensed into the reaction ampoule before sealing off.

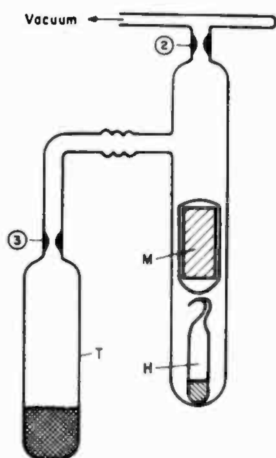

Fig. 1—Apparatus for loading a volatile transport agent into the transport ampoule.

The sealed ampoule is 15-20 mm in diameter and 100-180 mm long. The concentration of transport agent is in the range of 0.03 to 0.2 millimoles/cm^3. After sealing, the ampoule is placed in the two-zone furnace (temperature difference ranging from 50° to 150°C) and reacted for several days. In many cases the compounds can be synthesized from their constituent elements or mixtures of binary compounds by pre-reaction aided by close-range transport. When one or more components are volatile (e.g., P, S or As), part of the ampoule is allowed to extend out of the furnace during the synthesis step to hold the ampoule pressure within reasonable limits. Before crystal growth is started, the ampoule is heated under a reverse temperature gradient

to that necessary for transport. In this way, spurious nuclei are removed from the growth region of the ampoule; this increases the chance of obtaining good-sized crystals.

2.1 Ternary Chalcogenides

A large number of ternary chalcogenides have been prepared.[3-5] These are listed in Table 1 together with some physical properties and the conditions used for crystal growth.

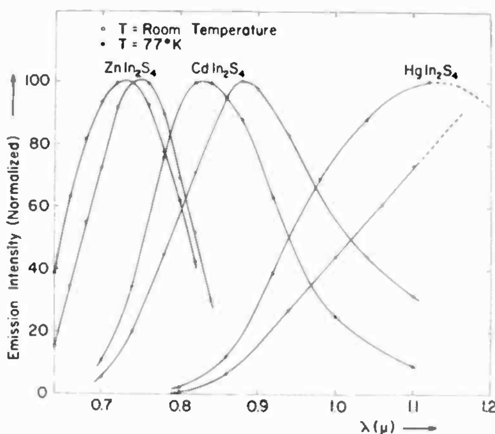

Fig. 2—Fluorescence spectra of $ZnIn_2S_4$, $CdIn_2S_4$ and $HgIn_2S_4$ under UV excitation (λ = 3660 Å)

The mechanism of the transport reaction can be illustrated with compounds of the type $A^{II}B^{III}_2X^{VI}_4$. If the starting material is a mixture of powdered AS and B_2S_3, transport occurs as follows:

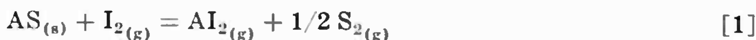

$$AS_{(s)} + I_{2(g)} = AI_{2(g)} + 1/2\ S_{2(g)} \quad [1]$$

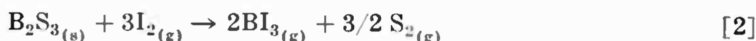

$$B_2S_{3(s)} + 3I_{2(g)} \rightarrow 2BI_{3(g)} + 3/2\ S_{2(g)} \quad [2]$$

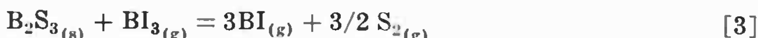

$$B_2S_{3(s)} + BI_{3(g)} = 3BI_{(g)} + 3/2\ S_{2(g)} \quad [3]$$

When the binary sulfides are re-formed in the cooler zone of the ampoule (by displacement of the equilibrium of Reactions [1] and [3] to the left) they react to form the ternary compound.

It can be seen from Table 1 and from Figs. 2 and 3 that several of the $A^{II}\ B_2^{III}\ X_4^{IV}$ and $Cd_4SiX_6^{VI}$ (X = S or Se; A = Zn, Cd, Hg; B = Ga, In) are photoconductors and/or phosphors when excited by 3660 Å UV

Table 1—Ternary Chalcogenides Prepared by Vapor-Phase Growth

Crystal	Shape	Maximum Dimensions (mm)	Structure	Agent	T_1 (°C)	T_2 (°C)	Color	Special Properties
$ZnGa_2S_4$	Polyhedra	0.5 × 0.5 × 0.5	S^2_4 or D^{11}_{2d}	I	1100	1000	white	
$CdGa_2S_4$	Columns	2 × 2 × 8	S^2_4	I	650	600	yellow	
$HgGa_2S_4$	Needles	10 × 0.3 × 0.3	S^2_4	I	1100	1000	yellow	phosphor
$ZnGa_2Se_4$	Polyhedra	4 × 4 × 4	S^2_4 or D^{11}_{2d}	I	1100	1000	orange red	phosphor
$CdGa_2Se_4$	Columns	1 × 1 × 6	S^2_4	I	950	750	orange red	phosphor
$HgGa_2Se_4$	Needles	10 × 0.5 × 0.5	S^2_4	I	760	700	black	phosphor
$ZnIn_2S_4$	Plates	10 × 10 × 0.1	C^5_{3v}	I	750	700	yellow	p-c,* phosphor
$CdIn_2S_4$	Octahedra	8 × 8 × 8	Spinel	I	850	750	red	p-c,* phosphor
$HgIn_2S_4$	Octahedra	3 × 3 × 3	Spinel	I	950	650	black	p-c,* phosphor
$ZnIn_2Se_4$	Columns	1 × 1 × 8	S^2_4	I	700	650	dark red	phosphor
$CdIn_2Se_4$	Columns	1 × 1 × 8	D^1_{2d}	I	650	600	black	phosphor
$HgIn_2Se_4$	Columns	6 × 2 × 2	S^2_4	I	750	700	black	phosphor
$MnIn_2S_4$	Octahedra	3 × 3 × 3	Spinel	I	1100	1000	red	
$CoIn_2S_4$	Polyhedra	2 × 2 × 2	Spinel	I	850	800	black	
$CoCr_2S_4$	Polyhedra	1 × 1 × 1	Spinel	NH_4Cl	1150	1000	black	
Fe_2GeS_4	Needles	5 × 1 × 0.1	Olivine Type	I	1050	1000	black	
Mn_2GeS_4	Needles	20 × 1 × 1	Olivine Type	I	850	800	yellow	
Mn_2SiS_4	Columns	3 × 1 × 1	Olivine Type	I	830	780	yellow	
Cu_3NbS_4	Cubes	2	Sulvanite-Type	I	850	750	orange	electro-optic
Cu_3NbSe_4	Plates	3 × 3 × 1	Sulvanite-Type	I	850	750	red	electro-optic
Cu_3TaS_4	Cubes	2	Sulvanite-Type	I	850	750	yellow	electro-optic
Cu_3TaSe_4	Plates	5 × 5 × 2	Sulvanite-Type	I	850	800	orange-red	electro-optic
Cu_2GeS_3	Needles	10 × 2 × 0.1	Zincblende with superstructure	I	750	700	yellow	
Cd_4GeS_6	Polyhedra	5 × 5 × 5	$C2/_c$	I	750	700	light yellow	
Cd_4GeSe_6	Polyhedra	3 × 3 × 3	$C2/_c$	I	750	700	yellow	
Cd_4SiS_6	Polyhedra	10 × 5 × 6	$C2/_c$	I	830	800	yellow	p-c,* phosphor
Cd_4SiSe_6	Polyhedra	2 × 2 × 2	$C2/_c$	I	830	800	black	photoconducting

* p-c = photoconducting.

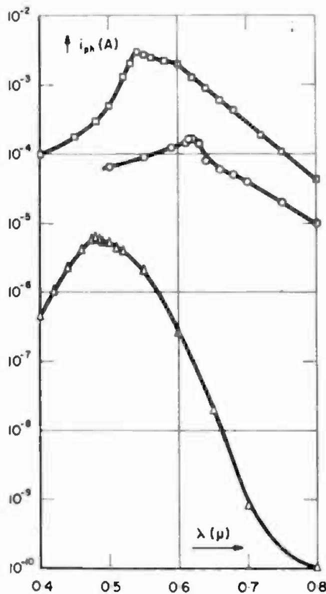

Fig. 3—Photocurrent versus wavelength
△ $ZnIn_2S_4$ ($E = 1000$ V/cm)
□ $CdIn_2S_4$ ($E = 120$ V/cm)
○ $HgIn_2S_4$ ($E = 300$ V/cm)

radiation[6-10] although their fluorescent properties are inferior to those of the standard ZnS-based phosphors. The luminescence and photoconductive properties of a few compounds of the $A^{II}\ B_2^{III}\ X_4^{IV}$ compounds can usually be approximated by the arithmetic mean of the bandgaps of the binary components. This is illustrated in Table 2.

Table 2—The Relationship of Ternary Chalcogenide Band Gap to That of the Constituent Binary Compounds.

	measured		calculated	measured
ZnS In_2S_3	3.65 2.0	$ZnIn_2S_4$	2.8	2.9
CdS In_2S_3	2.45 2.0	$CdIn_2S_4$	2.25	2.3
HgS In_2S_3	2.0 2.0	$HgIn_2S_4$	2.0	2.0
ZnSe In_2Se_3	2.6 1.2	$ZnIn_2Se_4$	1.9	1.8
CdSe In_2Se_3	1.8 1.2	$CdIn_2Se_4$	1.5	1.7

Compounds with the sulvanite structure, which have the formula Cu_3MX_4 ($M = Nb$ or Ta, $X = S$ or Se), exhibit a moderate electro-optic effect;[11] $r_{41} = 1 \times 10^{-10}$ cm/V ($ZnS = 2 \times 10^{-10}$ cm/V) and $n_o^3 r_{41} = 21 \times 10^{-10}$ cm/V (n_o = refractive index) compared to 27 $\times 10^{-10}$ cm/V for ZnS. The system Cu-Nb-S is also interesting in that iodine transport of mixtures ranging in composition from Cu_2S to NbS_2 (initial mixtures of composition $(1\text{-}m)\,Cu_2S + m\,Nb_2S_4$) yielded single crystals of five different ternary phases.[12] The phases obtained are shown (projected onto the Cu-Nb line) in Fig. 4. Definite compounds

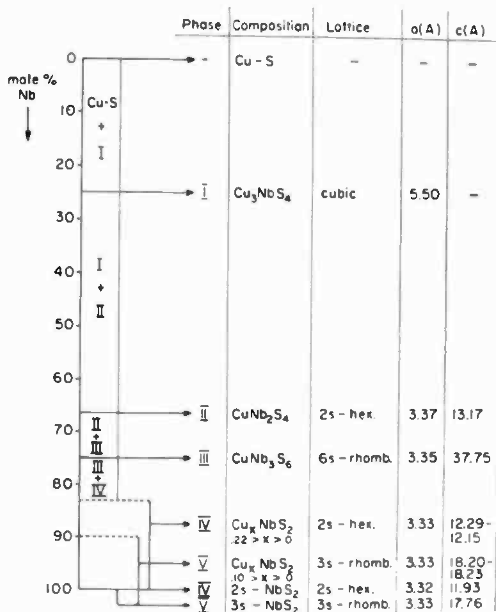

Fig. 4—Phases in the Cu-Nb-S system and lattice parameters

(phases I, II, III) exist at $m = 0.25$, 0.667 and 0.75. Charges of these compositions transported homogeneously, i.e., crystals of only one species formed; x-ray diffraction patterns and residual charge were identical. Charges of intermediate compositions disproportionated into crystals of two phases and mixed residues. At the Nb-rich end of the system, phases (IV, V) of considerable width exist.

2.2 Quaternary Chalcogenides

The quaternary chalcogenides that have been prepared[13] are listed in Table 3. They were obtained by reacting stoichiometric amounts of the elements at 1100°C in the presence of 5 mg I_2/cm^3 and transporting

Table 3—Quaternary Chalcogenides Prepared by Vapor-Phase Growth

Compound	Color	Shape	Crystal size (mm)	Lattice type	Unit cell (Å)			
					Type	a	b	c
Cu_2ZnSnS_4	black	needles	20 × 0.2 × 0.2	S	tetr.	5.43		10.83
Cu_2CdSnS_4	black	blades	8 × 1 × 0.1	S	tetr.	5.43		10.82
Cu_2FeSnS_4	black	plates	5 × 5 × 0.1	S	tetr.	5.44		10.74
Cu_2ZnGeS_4	red	blades	10 × 1 × 0.3	W	o.rh.	7.47	6.45	6.12
$Cu_2ZnGeSe_4$	dark red	blades	2 × 0.1 × 0.3	S	tetr.	5.61		11.02
Cu_2CdGeS_4	dark red	plates	5 × 5 × 0.1	W	o.rh.	7.72	6.57	6.29
Cu_2FeGeS_4	black	needles	10 × 1 × 0.1	S	tetr.	5.32		10.51
Cu_2MnGeS_4	black	blades	8 × 1 × 0.1	W	o.rh.	7.61	6.50	6.18
Cu_2NiGeS_4	black	plates	3 × 3 × 0.1	S	o.rh.	5.34	5.27	10.47
Cu_2ZnSiS_4	greenish	prisms	5 × 3 × 3	W	o.rh.	7.40	6.40	6.08
$Cu_2ZnSiSe_4$	orange	blades	10 × 3 × 0.1	W	o.rh.	7.80	6.70	6.46
Cu_2CdSiS_4	yellow	blades	10 × 3 × 0.1	W	o.rh.	7.58	6.44	6.17
Cu_2FeSiS_4	black	blades	10 × 2 × 0.1	W	o.rh.	7.43	6.43	6.16

the compound in a temperature gradient of 800-750°C. X-ray powder photographs showed that the basic diffraction patterns are ordered superstructures of either the sphalerite (S) or wurzite (W) type. For sphalerite-type lattices, tetragonal cells with $a_{tetr} \simeq a_s$, $c_{tetr} \simeq 2a_s$ were found. The wurzite-type pattern can be indexed on the basis of an orthorhombic unit cell with $a_{or} \simeq 2a_w$, $b_{or} \simeq a_w\sqrt{3}$, $c_{or} \simeq c_w$.

2.3 Ternary Oxides

The ternary oxides that have been grown[14,15] are listed in Table 4 with their growth conditions and structure type. The mechanism of transport of metal oxides is not as simple as in the case of chalcogenides. In the case of niobates and tantalates the Nb_2O_5 transport equilibrium can be described by the following overall reaction:

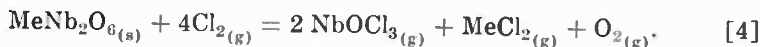

$$MeNb_2O_{6(s)} + 4Cl_{2(g)} = 2\,NbOCl_{3(g)} + MeCl_{2(g)} + O_{2(g)}. \qquad [4]$$

This can be divided into two transport equilibria:

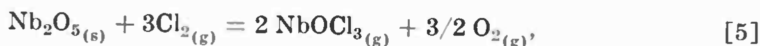

$$Nb_2O_{5(s)} + 3Cl_{2(g)} = 2\,NbOCl_{3(g)} + 3/2\,O_{2(g)}, \qquad [5]$$

$$MeO_{(s)} + Cl_{2(g)} = MeCl_{2(g)} + 1/2\,O_{2(g)}. \qquad [6]$$

This mechanism is readily understood for all niobates and tantalates except $CaNb_2O_6$. The transport of CaO cannot occur by Reaction [6] because the equilibrium lies too far over to the right and the vapor pressure of $CaCl_2$ at 1000°C is only 3.7×10^{-2} Torr. Possibly a more volatile gaseous complex, e.g., of the form $[(NbOCl_3)_x\,(CaCl_2)_y]$, is responsible for the increased volatility of $CaCl_2$.

Based on simple thermodynamic considerations it can be shown[15] that simultaneous transport and ternary compound formation from a mixture of two binary oxides will *not* occur if (a) the free energy of formation of the ternary compound is positive and (b) the free energies of formation of the binary oxides differ widely (eg. $\Delta G_1 < 0$, $\Delta G_2 > 0$). This results in the transport of only one oxide, since although the oxides might transport under similar conditions in separate experiments, the transport of one interferes with that of the other when simultaneous transfer is attempted.

The low-frequency dielectric constant ϵ of a number of niobates and tungstates $MeNb_2O_6$, $MeWO_4$ (Me = Mg, Ca, Mn, Fe, Co, Ni, Zn) has been measured at room temperature in the frequency range 5 to 500 kHz.[16] The effect of chemical substitution is small; $\epsilon'_{(100)} \simeq \epsilon'_{(010)} \simeq 18$ for both the niobates and tungstates. In the niobates, the dielectric anisotropy is very pronounced with $\epsilon'_{(001)} \simeq 32$.

Table 4—Ternary Oxides Prepared by Vapor-Phase Growth

Compound	Transport Agent	T_1 (°C)	T_2 (°C)	Crystals	Structure
$CrNbO_4$	$Cl_2 + NbCl_5$	980	860	prisms and pyramids 0.2 mm	rutile
$FeNbO_4$	$Cl_2 + NbCl_5$	920	750	prisms $2 \times 5 \times 0.5$ mm	wolframite
$FeNb_2O_6$	$Cl_2 + NbCl_5$	1005	935	prisms $2 \times 2 \times 2$ mm	columbite
$MnNb_2O_6$	$Cl_2 + NbCl_5$	1010	1010-970*	plates $4 \times 2 \times 0.5$ mm	
				prisms $3 \times 3 \times 2$ mm	columbite
$CoNb_2O_6$	Cl_2	1010	1010-970*	plates and prisms $4 \times 3 \times 1.5$ mm	columbite
$NiNb_2O_6$	Cl_2	1010	1010-970*	plates and prisms $5 \times 2 \times 1$ mm	columbite
$ZnNb_2O_6$	HCl	1020	975	prisms 1 mm	columbite
$MgNb_2O_6$	HCl	1005	935	prisms $5 \times 2 \times 1$ mm	columbite
$CaNb_2O_6$	Cl_2	1010	980	plates $1 \times 0.5 \times 0.2$ mm	columbite
$9Nb_2O_5 \cdot V_2O_5$	$NbCl_5 + Cl_2$	980	880	$5 \times 0.6 \times 0.6$ mm	tetragonal
$9Nb_2O_5 \cdot As_2O_5$	Cl_2	1020	975	$0.5 \times 0.2 \times 0.2$ mm	tetragonal
$9Nb_2O_5 \cdot GeO_2$	Cl_2	1000	900	$5 \times 0.6 \times 0.6$ mm	tetragonal
$MgTa_2O_6$	Cl_2	1060	980	microscopic	trirutile
$MnTa_2O_6$	Cl_2	1010	950	microscopic	trirutile
$CoTa_2O_6$	Cl_2	880	850	$1 \times 1 \times 1$ mm	trirutile
$NiTa_2O_6$	$TaCl_5 + Cl_2$	1000	900	$2 \times 2 \times 1$ mm (polycrystalline aggregates)	trirutile
$FeTaO_4$	$TaCl_5 + Cl_2$	1000	900	$1.5 \times 1 \times 1$ mm	rutile
$CrTaO_4$	Cl_2	1010	950	microscopic	rutile

Table 4 (continued)

Compound	Transport Agent	T_1 (°C)	T_2 (°C)	Crystals	Structure
$MgWO_4$	Cl_2	1060	980	3 × 0.5 × 0.5 mm	wolframite
$MnWO_4$	Cl_2	1000	900	6 × 1 × 1 mm	wolframite
$FeWO_4$	Cl_2	1010	980	2 × 2 × 1 mm	wolframite
$CoWO_4$	Cl_2	1000	905	2 × 2 × 2 mm	wolframite
$NiWO_4$	Cl_2	1040	1010	6 × 1 × 1 mm	wolframite
$ZnWO_4$	Cl_2	1075	1040	1.5 × 1.5 × 1 mm	wolframite
$MgMoO_4$	Cl_2	1060	980	5 × 0.3 × 0.3 mm	monoclinic
$MnMoO_4$	Cl_2	905	870	0.8 × 0.5 × 0.2 mm	monoclinic
$CoMoO_4$	Cl_2	1020	975	microscopic	monoclinic
$NiMoO_4$	Cl_2	905	870	0.2 × 0.2 × 0.1 mm	monoclinic
$MgTiO_3$	Cl_2	1060	980	0.5 × 0.5 × 0.1 mm	ilmenite
$NiTiO_3$	Cl_2	1030	960	microscopic	ilmenite
$MnCr_2O_4$	Cl_2	980	860	octahedra 1.2 mm side length	spinel
$CoCr_2O_4$	Cl_2	900	800	octahedra 2 mm side length	spinel
$NiCr_2O_4$	Cl_2	950	800	octahedra 1 mm side length	spinel
$Mn(Fe,Cr)_2O_4$	Cl_2	1000	900	octahedra 0.5 mm side length	spinel
$Ni(Fe,Cr)_2O_4$	Cl_2	1000	900	octahedra 1 mm side length	spinel
Co_2SnO_4	Cl_2	1030	1010	octahedra 1 mm side length	spinel

* By pulling the ampoule in a furnace with low temperature gradient, the growth zone (tip) was cooled at a rate of around 4°C/day while the charge remained at constant temperature.

2.4 Metal-Phosphorus-Sulfur Compounds

By reacting together stoichiometric amounts of the constituent elements, the metal–phosphorus–sulfur compounds shown in Table 5 have been prepared.[17] Except for Cu_3PS_4, which appeared to melt around 960°C, these compounds decompose between 500-700°C into the metal sulfides and volatile $P_2S_5(P_2S_4)$. The original composition can be inferred from the weight loss after completed decomposition.

3. Preparation of Ternary Phosphides in an Open-Flow System

Open-flow systems are potentially of more use for the preparation of materials by vapor-phase reactions when thin, epitaxial layers are desired and when the controlled introduction of dopants is required. The addition of dopants is much more easily controlled and the growth of p-n junctions is easily achieved by changing the gas composition. For this reason the preparation of a number of ternary compounds was attempted, but in many cases the material could not be prepared, probably because the required pressure of the volatile components for compound formation was greater than one atmosphere.

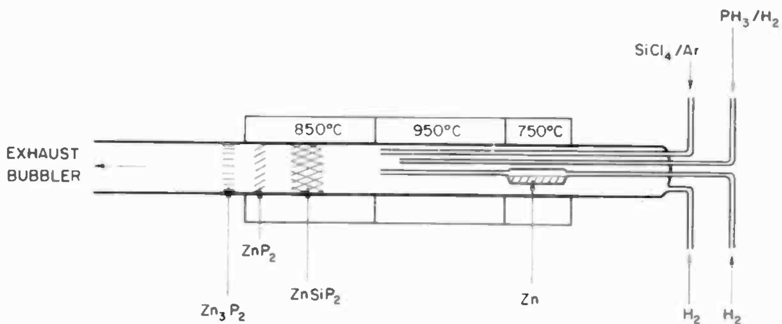

Fig. 5—Apparatus for the preparation of $ZnSiP_2$

3.1 Preparation of $ZnSiP_2$

$ZnSiP_2$ is prepared[18] in the apparatus shown in Fig. 5. $SiCl_4$ vapor in Ar is mixed with PH_3 (5% by volume in H_2) and Zn Vapor in H_2 at a reaction temperature of 850°C, using the gas-flow conditions shown in Table 6. The $SiCl_4$ is contained in a gas saturator held at 0°C, and argon is used as the carrier gas to ensure that premature reduction does not occur before the $SiCl_4$ reaches the reaction zone. Attempts to grow epitaxial layers produced only polycrystalline films with 3-4 μm

Table 5—Metal–Phosphorus–Sulfur Compounds Prepared by Vapor-Phase Growth

Crystal	Form	Color	Size (mm)	T_1 (°C)	T_2 (°C)	Type	Unit Cell			
							a	b	c	°
Cu_3PS_4	prisms	yellow-brown	4 × 4 × 8	850	800	o.rh.	6.43	7.55	6.12	
$InPS_4$	needles	colorless	0.5 × 0.5 × 15	640	580	tetr.	5.59		9.00	
$GaPS_4$	thin plates	colorless	5 × 5	450	430					
$BiPS_4$	prisms	dark red	3 × 3 × 6	660	610	o.rh.	5.24	5.50	9.75	
$Sn_2P_2S_6$	polyhedra	orange	5 × 5 × 5	660	630	monocl.	6.43	7.47	11.03	122.2
$Fe_2P_2S_6$	plates	black	0.1 × 10 × 10	670	620	pseudo rhombohedral				
$Mn_2P_2S_6$	plates	green	0.1 × 10 × 10	670	620	pseudo rhombohedral				
$Cd_2P_2S_6$	plates	colorless	0.1 × 4 × 4	630	600	pseudo rhombohedral				

Table 6—Flow Conditions for the Preparation of $ZnSiP_2$

Reactant	Gas Flow (cc/min)	Reactant Flow (Moles/hr)
$SiCl_4$ (0°C)	7.5 (Ar carrier)	2.1×10^{-4}
Zn (750°C)	200 (H_2 carrier)	4×10^{-2}
PH_3 (5 per cent mixture in H_2)	65	9×10^{-3}
Additional H_2	200	—

crystallites; the substrates used were GaP, Si, $ZnSiP_2$ and $CdSiP_2$. The preparation of $ZnSiP_2$ is critically dependent on the reactor geometry and conditions. A considerable excess of Zn and P relative to Si is required before compound formation occurs, presumably due to the relatively high equilibrium dissociation pressure of the compound. The failure to achieve epitaxial growth may also be linked to the thermodynamic instability of the compound under the conditions of reaction.

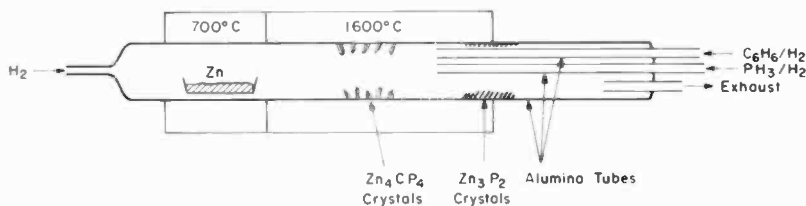

Fig. 6—Apparatus for the preparation of Zn_4CP_4

3.2 Preparation of Zn_4CP_4

Hydrogen streams (Fig. 6) containing Zn, C_6H_6 and PH_3 fed through alumina inlet tubes into an alumina reaction tube are mixed at 1600°C using a countercurrent system as shown. After about 1 hour, a small yield (~50 mg) of shiny black platelets about 1×1 mm and 20 μm thick are formed. These have a composition corresponding to Zn_4CP_4 (by electron-probe microanalysis). The compound has a hexagonal layer structure (easy basal plane cleavage) with $a = 7.33$ Å and $c = 10.00$ Å.

4. Conclusion

Vapor-phase transport reactions carried out in closed ampoules are a very convenient exploratory technique for certain types of compounds. The size of the crystals obtained is in most cases sufficient to enable

good physical characterisation of the material to be made with the reservation that incorporation of the transport agent may affect some properties. Open-flow systems may not be so generally useful for the preparation of complex ternary and quaternary compounds since all the reactions must be carried out at 1 atmosphere total pressure, which may not be sufficient for complete stability of the material.

Acknowledgments

The authors gratefully acknowledge the skilful assistance of M. Aschwanden, T. Petermann, E. Sturzenegger, P. Wettstein, and P. Wild.

References

[1] H. Schäfer, **Chemical Transport Reactions,** Academic Press, New York, 1964.

[2] J. A. Beun, R. Nitsche, H. U. Bölsterli, "Aftertreatment of CdS Single Crystals Grown by Vapour Transport with Iodine," **Physica,** Vol. 28, p. 184, 1962.

[3] R. Nitsche, "The Growth of Single Crystals of Binary and Ternary Chalcogenides by Chemical Transport Reactions," **J. Phys. Chem. Sol.,** Vol. 17, No. 1/2, p. 163, 1960.

[4] R. Nitsche, H. U. Bölsterli, and M. Lichtensteiger, "Crystal Growth by Chemical Transport Reactions—I Binary, Ternary, and Mixed-Crystal Chalcogenides," **J. Phys. Chem. Sol.,** Vol. 21, Nos. 3/4, p. 199, 1961.

[5] R. Nitsche, **Fortschr. der Min.,** Vol. 44, p. 231, 1967.

[6] R. Nitsche and W. J. Merz, "Zinc-Indium-Sulfide, a New Photoconductor," **Helv. Phys. Acta,** Vol. 35, Nos. IV/V, p. 274, 1962.

[7] L. Krausbauer, R. Nitsche, and P. Wild, **Proc. Int. Conf. Liem, Budapest,** p. 1107, 1966.

[8] E. Kaldis, L. Krausbauer, and R. Widmer, "Cd_4SiS_6 and Cd_4SiSe_6, New Ternary Compounds—Synthesis, Photoconductive and Fluorescent Properties," **J. Electrochem. Soc.,** Vol. 114, p. 1074, Oct. 1967.

[9] L. Krausbauer, R. Nitsche, and P. Wild, "Mercury Gallium Sulfide, $HgGa_2S_4$, A New Phosphor," **Physica,** Vol. 31, p. 113, 1965.

[10] J. A. Beun, R. Nitsche, and M. Lichtensteiger, "Photoconductivity in Ternary Sulfides," **Physica,** Vol. 26, p. 647, 1960.

[11] R. Nitsche and P. Wild, "Crystal Growth and Electro-Optic Effect of Copper-Tantalum-Selenide, Cu_3TaSe_4," **J. Appl. Phys.,** Vol. 38, p. 5413, Dec. 1967.

[12] R. Nitsche and P. Wild, "Vapour Growth of New Single-Crystalline Phases in the System Cu-Nb-S," **Proc. 2nd Int. Conf. Cryst. Growth,** Birmingham, U.K., **Jour. Cryst. Growth,** Vol. 3-4, p. 153, 1968.

[13] R. Nitsche, D. F. Sargent, and P. Wild, "Crystal Growth of Quaternary $1_2 2 4 6_4$ Chalcogenides by Iodine Vapor Transport," **J. Cryst. Growth,** Vol. 1, p. 52, 1967.

[14] F. P. Emmenegger and A. Petermann, "Transport Reactions and Crystal Growth of Transition Metal Niobates," **J. Cryst. Growth,** Vol. 2, p. 33, 1968.

[15] F. P. Emmenegger, "Crystal Growth of Ternary Metal Oxides by Chemical Transport," **Proc. 2nd Int. Conf. Cryst. Growth,** Birmingham, U.K., July 15-19, **Jour. Cryst. Growth,** Vols. 3, 4, p. 135, 1968.

[16] F. P. Emmenegger and H. Rötschi, to be published, **J. Phys. Chem. Solids.**

[17] R. Nitsche and P. Wild, "Crystal Growth of Metal-Phosphorus-Sulfur Components by Vapor Transport," **Mat. Res. Bull.,** Vol. 5, p. 419, June 1970.

[18] B. J. Curtis and P. Wild, "The Preparation and Growth of Polycrystalline Layers of $ZnSiP_2$ in an Open Flow System," **Mat. Res. Bull.,** Vol. 5, p. 69, Feb. 1970.

[19] B. J. Curtis and P. Wild, **Mat. Res. Bull.,** Vol. 4, p. 591, 1969.

Vapor Growth of (II-VI)–(III-V) Quaternary Alloys and Their Properties

W. M. Yim, J. P. Dismukes, and H. Kressel
RCA Laboratories, Princeton, N.J.

Abstract—Vapor growth of single-crystal (II-VI)–(III-V) quaternary alloys has been investigated using an open-tube vapor-phase epitaxial technique, with particular emphasis on the three completely miscible systems (ZnSe–GaAs, ZnSe–GaP, and ZnS–GaP) and one partly miscible system (CdS–InP) that were chosen from among the 16 quaternary alloy systems previously studied. Properties investigated include solid solubility, optical energy gap, electrical and doping behavior, and photo- and cathodoluminescence. In all alloy systems investigated, the compositional dependence of the bandgap was anomalously sublinear, and this behavior was explained in terms of impurity banding effects. The luminescence measurements revealed deep recombination centers of unknown nature. All of the II–VI rich alloys investigated that showed high, direct bandgaps ($>$2 eV) could not be doped low resistivity, either n- or p-type, with the exception of CdS-InP alloys, which were readily doped high n-type but not p-type. This difficulty in doping appears to be due to self-compensation by native lattice defects.

1. Introduction

Relatively little has been reported of quaternary alloys between the II-VI compounds and the III-V compounds. Part of the reason for this is that synthesis of these four-component alloys in the desired homogeneity and crystallinity is very difficult, because of their high melting points and large dissociation pressures. Recent exploratory investigations,[1-4] using mostly polycrystalline specimens, have shown that several II-VI compounds and II-V compounds form solid solutions over a wide range of compositions, and the dependence of the energy gap upon composition has been determined for three completely miscible systems (ZnSe–GaAs,[2,3] ZnSe–GaP,[2] and ZnS–GaP[2,4]) and for one partly miscible system (CdS–InP[2]).

In order to further characterize these materials, we have prepared single-crystal specimens of the above alloys, using an open-tube vapor-phase epitaxial growth technique.[5,6] This paper presents a review and an extension of previous results,[2-4,9,11] with the major emphasis on the

results obtained with epitaxially grown (II-VI)–(III-V) alloys. The results include growth morphology and crystalline perfection of the epitaxial layers, and some of the properties of the quaternary alloys, i.e., solid solubility, optical energy gap, electrical and doping behavior, and photo- and cathodoluminescent properties.

Our interest in the quaternary alloys had been motivated by the intriguing possibility that such alloys might combine certain desirable properties of the II-VI compounds and the III-V compounds. In particular, it was felt that a (II-VI)–(III-V) alloy might combine the high, direct bandgap (>2 eV) of II-VI luminescent materials with the ease of doping both n- and p-type of III-V semiconducting materials. However, this aim has not been achieved by the present approach. The inability to dope these quaternary alloys n- and p-type may be attributed to self-compensation by native lattice defects, much like that encountered in many high-bandgap II-VI compounds. This is briefly discussed in the following section, and more fully in a separate paper.[7]

2. Vapor-Phase Epitaxial Growth

In our early studies,[2] we used a closed-tube chemical transport technique to grow single crystals of the quaternary alloys. However, this technique gave single-crystal alloys only over a very narrow composition range (<5 mole %) near the II-VI or the III-VI end component compound, because of a considerably different rate of chemical transport for each component compound in a closed system. We therefore investigated an open-tube, vapor-phase epitaxial growth technique, which affords a greater flexibility. This technique has been particularly successful in preparing high-quality single-crystal layers of many ternary III-V compound alloys over the entire alloy composition. It is logical therefore that this technique be extended to preparation of the quaternary alloys.

2.1 Experimental Procedure

The open-tube quartz system used for vapor-phase growth is shown in Fig. 1. It is similar to that used by Tietjen and Amick[5] for epitaxial growth of GaAs and Ga(As, P) alloys, with the exception of a two-barrel source zone arrangement first designed by Richman[8] to accomodate two different source metals.

With this apparatus, the group II element (Zn or Cd) was transported most frequently as the vapor by passing H_2 over the molten metal located in the source zone at a temperature T_1. The group III element (Ga or In) was transported as a chloride by passing an H_2-HCl

mixture over the molten metal located in the second source zone at a temperature T_2. The group VI (Se or S) and group V (As or P) elements were introduced as gaseous hydrides (H_2Se, H_2S, AsH_3, or PH_3) diluted in H_2. These reactant gases were brought together in the reaction zone at a temperature T_3, and growth of a (II-VI)–(III-V) alloy occurred on a substrate in the deposition zone at a temperature T_5. Provisions have also been made for introducing desired doping impurities, in gaseous form, through the side arm at T_4 directly into the reaction zone.

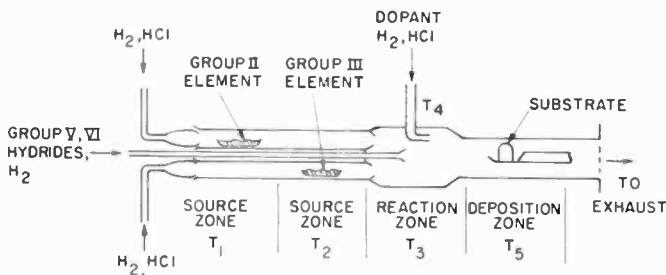

Fig. 1—Apparatus for vapor-phase epitaxial growth of (II-VI)–(III-V) alloys.

The substrate material most extensively used was GaAs of <100> orientation for the ZnSe–GaAs and ZnSe–GaP alloys, and of <111A> orientation for the ZnS–GaP and CdS–InP alloys. Strain-free substrates were prepared by using a procedure of mechanical and chemical polishing developed for GaAs.[5] Typical substrates had an area of 2 cm^2 and a thickness of 0.05 cm. In order to provide a close lattice and thermal expansion match between the substrate and the epitaxial layer, the GaAs substrates were first deposited with single-crystal layers of the following II-VI compounds prior to epitaxial growth of alloys: ZnSe for both ZnSe–GaAs and ZnSe–GaP, ZnS for ZnS–GaP, and CdS for CdS–InP. A detailed account of epitaxial growth of the above II-VI compounds is presented elsewhere.[6]

For successful growth of quaternary alloy single crystals by vapor-phase epitaxy, there are several factors that deserve careful consideration. These include, in addition to the choice of reactant gases and substrate materials, the occurrence of polymorphism and the possibility of forming various compounds other than those actually intended. Indeed, we have observed in preliminary experiments a mixture of zincblende–wurtzite polymorphs, and the formation of undesirable byproducts such as Ga_2Se_3, Zn_3As_2, Zn_3P_2, and As_2Se_3. These structural

and chemical inhomogeneities are often related to the composition and temperature of various reactant gases, and most importantly to the deposition temperature. Accordingly, we have conducted a comprehensive series of experiments with various reactant gas compositions, flow rates, and zone temperatures, in order to establish optimum conditions for epitaxial growth of (II-VI)–(III-V) alloys. Table 1 lists the optimum growth conditions for several II-VI rich ZnSe-based, ZnS-based, and CdS-based alloys, and it also includes the conditions for ZnSe, ZnS, and CdS epitaxial growth.[6]

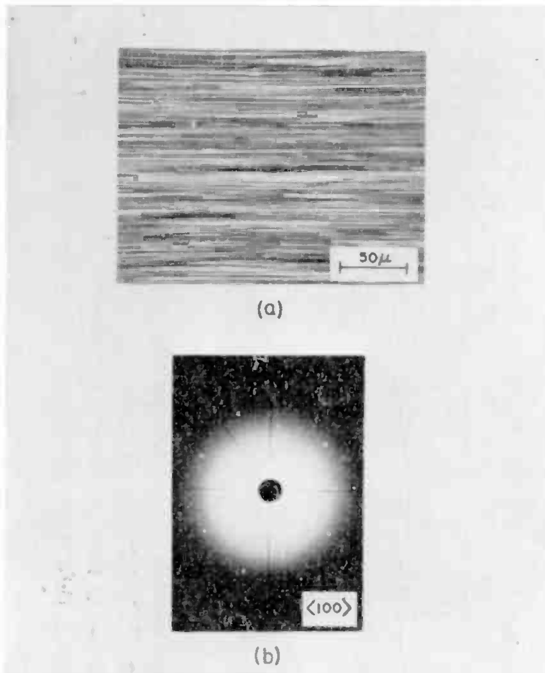

Fig. 2—(a) Photomicrograph and (b) Laue back-reflection pattern of $(ZnSe)_{0.94}(GaAs)_{0.06}$ alloy grown epitaxially on (100) GaAs.

2.2 Growth Morphology and Crystallinity of Epitaxial Layers

Figs. 2-5 show the microstructure and the corresponding Laue back-reflection pattern for as-grown single-crystal layers of $(ZnSe)_{0.94}(GaAs)_{0.06}$, $(ZnSe)_{0.82}(GaP)_{0.18}$, $(ZnS)_{0.65}(GaP)_{0.35}$, and $(CdS)_{0.84}(InP)_{0.16}$ alloys; these are typical of all other II-VI rich materials in each alloy system.

It is interesting to note that each alloy has its own particular

Table 1—Optimum Conditions for Vapor-Phase Epitaxial Growth of Several II-VI Compounds and (II-VI–(III-V) Alloys

Epitaxial Material	Cryst. Struct.	E_g (eV)	Substrate Material	Substrate (hkl)	Flow (cc/min) over Zn (530°C) H_2	Cd (580°C) H_2	Ga (825°C) H_2	Ga (825°C) HCl	In (900°C) H_2	In (900°C) HCl	Flow (cc/min) to Reaction Zone (925-1000°C) H_2Se	H_2S	AsH_3	PH_3	H_2	Substrate Temp. (°C)	Growth Rate (μm/hr)
ZnSe	Zb	2.7	GaAs	100	200	—	—	—	—	—	2.5	—	—	—	700	890	36
ZnS	W	3.7	GaAs*	111A	200	—	—	—	—	—	—	2.5	—	—	700	825	15
CdS	W	2.5	GaAs	111A	—	200	—	—	—	—	—	5	—	—	700	690	50
ZnSe-6% GaAs	Zb	2.2	GaAs+	100	200	—	300	1	—	—	2.5	—	10	—	350	890	18
ZnSe-20% GaP	Zb	2.2	GaAs+	100	200	—	350	1	—	—	2.5	—	—	2	350	890	24
ZnS-35% GaP	W	2.3	GaAs**	111A	200	—	350	1	—	—	—	2.5	—	3	300	810	20
Cds-16% InP	W	1.8	GaAs***	111A	—	200	—	—	350	1	—	10	—	2	200	690	65

Zb: Zinc blende structure

W: Wurtzite structure

GaAs*: Substrate graded in composition from GaAs to GaP prior to alloy deposition

GaAs+: Substrate deposited with a thin layer of ZnSe

GaAs**: Deposited with a thin layer of ZnS on GaAs* substrate

GaAs***: Substrate deposited with a thin layer of CdS

growth morphology, showing a sharp and somewhat diffused layer structure for ZnSe-GaAs and ZnSe-GaP, and a hexagonal and a circular growth feature for ZnS-GaP and CdS-InP, respectively. These growth patterns were no doubt influenced by the orientation of the substrates (<100> for the ZnSe-based alloys, and <111A> for the ZnS-based and the CdS-based alloy) as well as by the crystal structure of the epitaxial layers (both ZnSe-GaAs and ZnSe-GaP are of the zincblende form, while both ZnS-GaP and CdS-InP are in the wurzite form). More significantly, however, these growth features, although different for different alloys, are probably indicative of a particular common growth mechanism, possibly surface nucleation, which is responsible for all the epitaxial growth shown.

There is a close lattice and thermal expansion match between ZnSe and GaAs, and consequently ZnSe-GaAs alloys deposited on ZnSe on GaAs substrates had an excellent epitaxial quality, as shown in Figs. 2(a) and (b). On the other hand, ZnSe-GaP epitaxial layers grown on ZnSe on GaAs substrates were occasionally found to crack; the orthogonal crack lines in Fig. 3(a) are one such example. For epitaxial growth of ZnS-GaP, (111A) GaAs substrates were first deposited

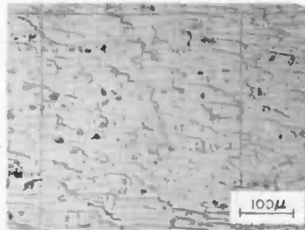

(a)

(b)

Fig. 3—(a) Photomicrograph and (b) Laue back-reflection pattern of $(ZnSe)_{0.82}(GaP)_{0.18}$ alloy grown epitaxially on (100) GaAs.

with thin single-crystal layers of ZnS after slowly varying the composion from pure GaAs to pure GaP, since high-quality ZnS or GaP single-crystal substrates were not readily available.* Because of this multilayered structure, ZnS-GaP epitaxial layers had a considerable strain, as evidenced by the diffused Laue diffraction spots in Fig. 4(b). Such strain can probably be minimized by proper grading of the alloy composition, and also by growing a thick epitaxial layer. The lattice mismatch between CdS and GaAs is considerably larger than that between ZnS and GaP; nevertheless a 100-μm-thick CdS-InP epitaxial layer grown on CdS on a GaAs substrate showed sharp Laue diffraction

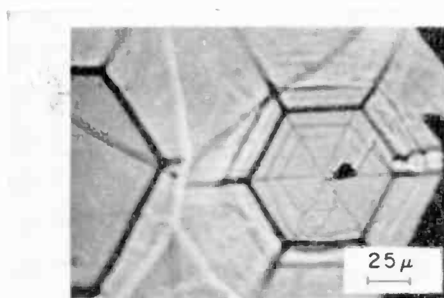

(a)

(b)

Fig. 4—(a) Photomicrograph and (b) Laue back-reflection pattern of $(ZnS)_{0.65}(GaP)_{0.35}$ alloy grown on (111A) GaAs. Sharp diffraction spots with a threefold symmetry are from the GaAs substrate.

* Although there is good lattice match between Si(5.43 Å) and ZnS (5.41 Å) or GaP (5.45 Å), silicon is not a suitable substrate material for ZnS or for GaP, since either compound deposited epitaxially on Si was found to crack badly due to a large thermal expansion mismatch between them.

spots, as in Fig. 5(b), indicating that the strain arising from the lattice mismatch between the epitaxial layer and the substrate had decreased considerably with increasing distance away from the CdS-GaAs interface.

With a given composition of reactant gases, materials grown at high deposition temperatures (≥800°C) were generally II-VI rich, and the deposits progressively became III-V rich toward lower growth temperatures down to about 700°C, the lowest temperature investigated for ZnSe- and ZnS-based alloys, where the deposits were substantially rich in the III-V component compound. Associated with the growth temperature dependence of alloy compositions was an occurrence of zincblende–wurtzite polymorph mixtures and an increasing tendency toward polycrystallinity. Using the conditions listed in Table 1, but with minor modifications in the reactant gas compositions and in the growth temperatures, single-crystal layers were obtained for all the four alloy systems in the II-VI rich regions ≥ 75 mole % II-VI).

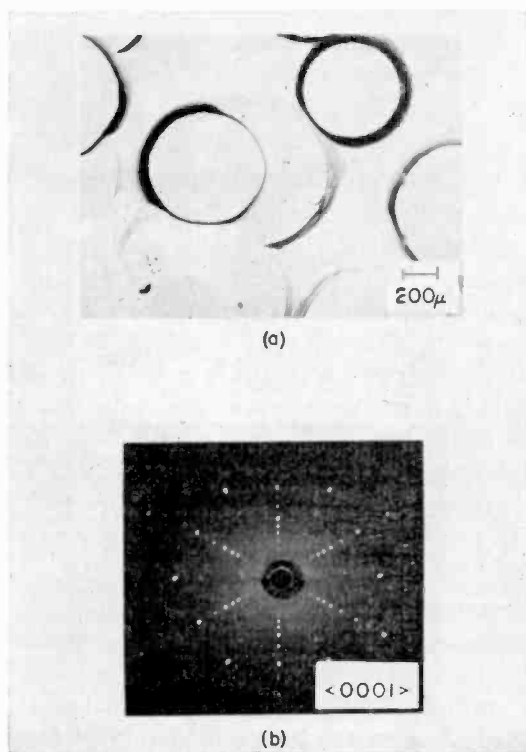

Fig. 5—(a) Photomicrograph and (b) Laue back-reflection pattern of $(CdS)_{0.84}(InP)_{0.16}$ alloy epitaxially grown on (111A) GaAs.

It should also be possible, with the present epitaxial technique, to prepare single crystals of III-V rich alloys; however, this was not investigated in detail since we were mainly interested in the II-VI rich alloys having a direct energy gap in excess of 2 eV.

3. Properties

The results presented below were obtained with specimens prepared by various techniques that include, in addition to the vapor-growth methods, such techniques[2] as direct fusion of component compounds under high pressure, flash evaporation, and solution growth. Values of the optical energy gap and, especially of the x-ray lattice parameter obtained with various specimens having the same composition, were generally the same irrespective of the synthesis technique used. However, the electrical and luminescent properties were shown to be significantly dependent upon the materials homogeneity and crystallinity, and hence only those that were obtained with well-characterized samples, namely the vapor-grown specimens, are to be considered the properties truly characteristic of the alloy.

3.1 Solid Solubility

Table 2 lists the sixteen (II-VI)–(III-V) quaternary systems investigated. The range of miscibility was determined from x-ray lattice parameters assuming Vegard's law, except in one partly miscible system (CdS-InP) and in three completely miscible systems (ZnSe-GaAs, ZnSe-GaP, and ZnS-GaP) for which wet-chemical or atomic absorption analysis was also made for all component elements. It is to be noted that the III-V and II-VI component compounds were chosen with the aim that their alloys, if they form, would have a bandgap energy >2 eV. Goryunova[1] lists, in addition to GaAs-ZnSe and InP-CdS, seven previously explored (III-V)–(II-VI) systems: AlSb-CdTe, InP-CdSe, InP-CdTe, InAs-CdTe, InAs-HgTe, and InSb-CdTe, all of which have a bandgap below 1.6 eV; and AlP-ZnS for which virtually no miscibility exists.

As seen in Table 2, only two systems (those containing ZnO) were completely immiscible, which would be expected since the lattice constants of the end component compounds differ by more than 20%. Partial miscibility was observed in eleven systems, but the mutual solubility is very limited when the lattice constants of the end components differ by more than 6%. The lack of extensive miscibility in the AlSb-ZnTe system is anomalous, since the lattice constant difference

Table 2—(II-VI)-(III-V) Quaternary Alloy Systems Investigated*

System				Range of Alloy Formation		Energy Gap (eV) (D = direct) (I = indirect)		Lattice Parameter (Å) (z.b.)		Difference in Lattice Parameter (%)
III-V		II-VI		III-V Region	II-VI Region	III-V	II-V	III-V	II-VI	
GaAs	z+	ZnO	w++	NONE		1.43 D	3.3 D	5.6533	4.56**	21.3
InP	z	ZnO	w	NONE		1.3 D	3.3 D	5.8694	4.56**	25.1
				Partial (approx. mole %)						
GaAs	z	ZnS	z, w	0-15 ZnS	0- 7 GaAs	1.43 D	3.7 D	5.6533	5.4093	4.4
GaAs	z	CdS	w, z	N. I.	0- 10 GaAs	1.43 D	2.5 D	5.6533	5.8378**	3.2
GaAs	z	ZnTe	z	0-25 ZnTe	N. I.	1.43 D	2.3 D	5.6533	6.1037	7.7
GaAs	z	CdSe	z	0- 3 CdSe	0- 18 GaAs	1.43 D	1.7 D	5.6533	6.05**	6.9
GaP	z	CdS	w, z	0- 4 CdS	0- 6 GaP	2.26 I	2.5 D	5.4506	5.8378**	6.8
GaP	z	ZnTe	z	0- 2 ZnTe	0- 5 GaP	2.26 I	2.3 D	5.4506	6.1037	11.3
GaP	z	CdSe	z	0- 1 CdSe	0- 4 GaP	2.26 I	1.7 D	5.4506	6.05**	10.4
InP	z	ZnS	z, w	0-10 ZnS	0- 2 InP	1.3 D	3.7 D	5.8694	5.4093	8.2
InP	z	ZnSe	z, w	0- 6 ZnSe	0-0.6 InP	1.3 D	2.7 D	5.8694	5.6687	3.5
InP	z	CdS	w, z	0-22 CdS	0- 26 InP	1.3 D	2.5 D	5.8694	5.8378**	0.5
AlSb	z	ZnTe	z	0-18 ZnTe	NONE	1.6 I	2.3 D	6.1356	6.1037	0.5
GaAs	z	ZnSe	z, w	Complete		1.43 D	2.7 D	5.6533	5.6687	0.3
GaP	z	ZnSe	z, w	Complete		2.26 I	2.7 D	5.4506	5.6687	3.9
GaP	z	ZnS	z, w	Complete		2.26 I	3.7 D	5.4506	5.4093	0.7

* All data at 300°K
+z Normally in zinc blende form
++w Normally in wurtzite form

** zinc blende a_o estimated as: $(\sqrt{3}\, a^2_{hex} \times c_{hex})^{1/3}$

N. I.: Not investigated

is very small (<0.5%). It should be noted that two CdS-based systems (CdS-GaAs and CdS-InP) were initially thought to be immisible.[2] However, more recent data showed that they are partly miscible, especially for the CdS-InP system for which up to 22 mole % CdS were found to be soluble in InP with alloys having the zincblende structure, and up to 26 mole % InP was soluble in CdS with alloys having the wurtzite structure. Vegard's law holds in both the InP-rich and the CdS-rich regions.

Complete miscibility was found in three systems: ZnSe-GaAs, ZnSe-GaP, and ZnS-GaP. The variation of the lattice constant with composition for each of these three systems is approximately linear. Since ZnSe and GaAs have the same zincblende structure with a very small (<0.3% at room temperature) lattice constant difference, and since both compounds are in an isoelectronic series, the formation of complete solid solutions between them is understandable. However, the complete alloy formation between ZnSe and GaP is somewhat surprising in view of a relatively large lattice constant difference of 3.9%. In the case of ZnS (which normally exists in either the zincblende or the wurtzite form, and frequently in a mixture of both) and GaP (which is nearly always in the zincblende form), they form complete solid solutions only when the alloys are in the zincblende form, as observed with chemically transported specimens.[2] The vapor-phase grown II-VI rich layers of ZnS-GaP alloys were, as mentioned previously, always of the wurtzite type, as contrasted to the layers of III-V rich GaP-ZnS alloys, which were always of the zincblende type. It thus appears that the occurrence of polymorphism in ZnS and particularly in the ZnS-GaP alloys is a sensitive function of such variables as the preparative technique and growth temperature used, as well as impurities present.

3.2 Optical Energy Gap

The bandgaps of various alloys were determined by optical absorption measurements at 300°K. The dependence of the optical energy gap upon composition for four alloy systems (ZnSe-GaAs, ZnSe-GaP, ZnS-GaP, and CdS-InP) is shown in Fig. 6. In all cases, the bandgap variation is sublinear, and one particular characteristic is immediately apparent in Fig. 6, namely, a very sharp drop in the bandgap as a small amount of the III-V compound is added to the II-VI host. No similar drop occurs, however, at the III-V end. Such "anomalous" bandgap variation was also observed in other quaternary systems, e.g., ZnS-GaAs, CdS-GaAs, CdS-GaP and ZnTe-GaP, and thus this seems a common behavior in these quarternary alloy systems.

An explanation of this anomalous behavior was proposed by Bloom[9] in terms of impurity banding effects. Starting at the II-VI end, the Group III (donor) and V (acceptor) atoms first enter the II-VI crystal host atomically, giving a *deep* donor level centered at approximately 0.3-0.4 eV from the II-VI conduction band edge, and a *deep* acceptor level centered at about 0.6-1.0 eV from the II-VI valence band edge. As the III-V "dopant" concentration is increased, the donor and acceptor levels are replaced by increasingly wide impurity bands that eventually merge with their adjacent II-VI intrinsic bands, resulting in an apparent bandgap shrinkage. Such bandgap shrinkage has been observed in many elemental and binary semiconductors such as germanium[10] at typical impurity concentrations of 10^{18}-$10^{20}/cm^3$.

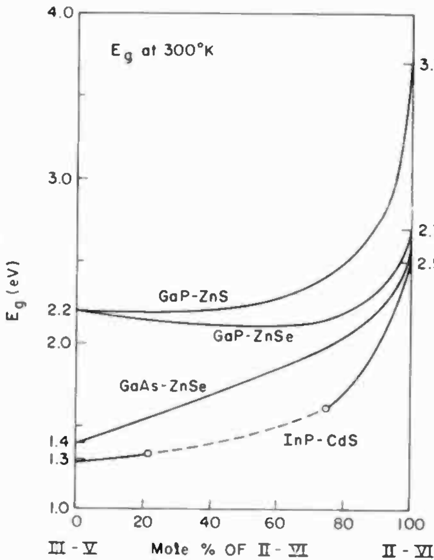

Fig. 6—The dependence of the optical energy gap upon composition for ZnSe-GaAs, ZnSe-GaP, ZnS-GaP, and CdS-InP alloys at 300°K. For CdS-InP, the portion of the curve drawn in broken line represents the two-phase region.

As the III-V "dopant" concentration is further increased, the donor and acceptor ions associate into close pairs. This tends to weaken the banding effects and results in a gradual change in slope of the bandgap variation, noticeable especially near 25 mole % III-V.

Finally, at the other end of the alloy system, the Group II (acceptor) and VI (donor) atoms also enter the III-V host atomatically. However, now the centers of the acceptor and donor bands are very shallow,

being only 0.005-0.02 eV from their intrinsic bands. Thus, as the II-VI "dopant" concentration is increased, the incipient bandgap shrinkage is quickly mitigated by the increasing degree of ion pairing, and therefore no large decrease in the bandgap is seen near the III-V end.

In addition to the behavior of bandgap variation, it is of particular interest to investigate whether the quaternary alloys have a direct or an indirect energy gap. In a system where both of the end components have a direct bandgap, it is reasonable that alloys between them should also have a direct energy gap. This was the case for the ZnSe-GaAs and the CdS-InP alloys throughout the alloy compositions, as determined from the relationship $\alpha \propto (h\nu - h\nu_t)^n$, where α is the absorption coefficient, $h\nu_t$ is the threshold energy, and the experimentally determined values of n were in the range 0.6-1.0. These n values are close to the theoretical value of 0.5 predicted for an allowed direct transition. For the systems involving a direct gap material (ZnSe or ZnS) and an indirect gap material (GaP), one would expect that the alloys undergo a transition at a certain composition from the direct to the indirect energy gap. Such a crossover composition for the ZnSe-GaP system appears to be near 75 mole % GaP, and for the ZnS-GaP system it is approximately 65 mole % GaP; since alloys having equal to or less than these GaP concentrations gave values of n ranging from 0.7 to 1.2.

3.3 Electrical Properties and Doping Behavior

All of those alloys that were not intentionally doped were high resistivity with the exception of vapor-grown CdS-InP alloys, which were highly n-type with resistivities of $\sim 10^{-3}$ ohm-cm, carrier concentrations of $10^{20}/cm^3$, and mobilities of $\sim 10^2$ cm^2/V sec. Early results[2] indicated that undoped ZnSe-GaAs alloys having larger than 40 mole % GaAs were p-type, and that phosphorus doping rendered $(ZnSe)_{0.8}(GaAs)_{0.2}$ p-type. However, these results have not been reproduced with epitaxially grown specimens, and the previous indication of p-type doping is now thought to be due to inhomogeneities in the specimens used.

The alloys with very small II-VI concentrations, typically less than 5 mole %, were, however, made relatively low resistivity by suitable impurity additions. The electronic transport properties of one such alloy, n-type Cu-doped $(GaP)_{0.95}(ZnSe)_{0.05}$, have been studied by Glicksman et al.[11] The electron mobility of this alloy at room temperature with carrier concentrations in the range of $0.2\text{-}1.2 \times 10^{18}/cm^3$ was about 6 cm^2/V-sec, as compared with 140-180 cm^2/V-sec for relatively pure GaP with carrier concentrations of $\sim 10^{17}/cm^3$. The mobility

of the alloy showed a $T^{3/2}$ temperature dependence in the range 175-300°K, as compared to the usual $T^{-3/2}$ dependence for pure GaP. At about 125°K the mobility value was only 1 cm^2/V-sec, and it fell steeply with decreasing temperature down to 77°K.

The explanation of the above electronic transport properties awaits further detailed experimental and theoretical analyses. However, a tentative interpretation is that the $T^{3/2}$ dependence of the mobility in the 175-300°K range is the result of ionized impurity scattering, and that the stronger temperature dependence and much reduced values of the mobility below 125°K are the results of trapping of carriers in partially localized states, where the mobility is now limited by a hopping and tunneling mechanism.

Attempts to dope II-VI rich alloys low resistivity (both n- and p-type) were not successful. In selecting doping impurities for the quaternary alloys, even assuming the simplest doping behavior, one must consider not only those elements that dope III-V compounds but also those that dope II-VI compounds. However, since we were primarily concerned with the II-VI rich alloys, we concentrated on those impurity elements that are either known to dope II-VI compounds or, based on valence considerations, would be expected to dope them. Upon careful survey of a wide variety of possible doping elements, we selected the following as being the most promising: for acceptors, Li, P, As, Sb, and Bi; for donors, Al, Ga, In, and Sc. We investigated two methods to incorporate these dopants—the addition of the impurities during the epitaxial growth, and the use of post-growth annealing treatments that have been frequently found necessary for obtaining low-resistivity material in many high-bandgap II-VI compounds, such as ZnSe and ZnS.

The impurity elements selected above were incorporated into the alloys during epitaxial growth, to a concentration as large as $10^{20}/cm^3$, as shown by emission spectroscopic analysis. However, in spite of this, the as-grown doped layers of those ZnSe-GaAs, ZnSe-GaP, and ZnS-GaP alloys investigated all remained high resistivity (10^7-10^8 ohm-cm). As for CdS-InP alloys, no p-type conversion occurred despite the incorporation of $\geq 10^{20}/cm^3$ acceptor impurities. For example, Li doping gave a four orders of magnitude reduction in the carrier concentration for a $(CdS)_{0.84}(InP)_{0.16}$ specimen, from 10^{19} down to $10^{15}/cm^3$; nevertheless the specimen remained n-type. Similarly, post-growth annealing treatments in either the vapor or the liquid of one of the major components of the alloys failed to induce the desired conductivity in these doped alloys.

The problem encountered above is reminiscent of the well-known difficulty in doping high-bandgap II-VI compounds. Although the (II-VI)–(III-V) alloys were selected with hope of overcoming this difficulty, it now appears unlikely that most of these materials can be doped low resistivity under equilibrium conditions. This is because the problem involved may be fundamental, i.e., self-compensation by native lattice defects,[12] as discussed further in a companion paper.[7]

3.4 Photo- and Cathodoluminescent Properties

Under cathode-ray excitation, a bright, visible light emission was observed at room temperature from many II-VI rich alloy specimens, e.g., red, orange, and green, respectively, for samples of $(ZnSe)_{0.95}(GaAs)_{0.05}$, $(ZnSe)_{0.93}(GaP)_{0.07}$, and $(ZnS)_{0.87}(GaP)_{0.13}$. In all cases, these colors correspond to peak photon energies below the respective bandgap energies. More quantitative information was obtained by photoluminescence and cathodoluminescence measurements at 77° and 300°K. The photoluminescence measurements were made using argon laser excitation (4880-Å line),[13] and the cathodoluminescence data were obtained using a 15-kV electron beam in the manner described by Nicoll.[14] Some of the photoluminescence and cathodoluminescence data obtained for ZnSe-GaP are listed in Table 3.

The photoluminescence observed at 300°K from all specimens was characterized by a broad-band emission, about 1000 Å wide, with the peak centered substantially below the bandgap energy. These data indicate that the emission involved deep recombination centers in all cases. At 77°K the width of the emission band decreased, which is to be expected, but it still remained relatively broad, and also the difference between the peak emission energy and the bandgap energy was still large, approximately 0.3 eV.

Since the excitation level for the photoluminescence measurements was small,* cathodoluminescence at much higher excitation levels should allow the observation of bandgap or near-bandgap emission by saturating those recombination processes that involve relatively deep centers and slow radiative transitions. This was the case for ZnSe and $(ZnSe)_{0.82}(GaP)_{0.18}$, as shown in Table 3. However, the nature of the recombination centers and radiative transitions cannot be determined without the knowledge of various energy levels involved, which are not known at present.

---

* For the photo-excitation, maximum density of non-equilibrium carriers generated is estimated to be in the $10^{13}/cm^3$ range, while it is in the 10^{17}-$10^{18}/cm^3$ range for the cathodo-excitation.

Table 3—Photo- and Cathodo-Luminescence Date for ZnSe-GaP

Sample	Dopant	Method of Measurement	T (°K)	λ peak (Å)	$\Delta\lambda\rho$ (Å)	$h\nu_\lambda$ (eV)	E_g (eV)	E_g-$h\nu_\lambda$ (eV)
GaP	Zn + 0	PL	300	6950	850	1.79	2.26	0.47
$(GaP)_{0.96}(ZnSe)_{0.04}$	Cu	PL	300	6720	1000	1.85	2.2	0.35
$(ZnSe)_{0.82}(GaP)_{0.18}$	—	PL	300	6500	1400	1.91	2.22	0.31
$(ZnSe)_{0.82}(GaP)_{0.18}$	—	PL	77	6100	900	2.02	2.35	0.33
$(ZnSe)_{0.82}(GaP)_{0.18}$	—	CL	77	5330	500	2.3	2.35	0.05
ZnSe	—	PL	300	6350	900	1.96	2.67	0.71
ZnSe	—	PL	77	5150	300	2.41	2.76	0.35
ZnSe	—	CL	77	4500	50	2.76	2.76	0

PL: Photoluminescence

CL: Cathodoluminescence

4. Conclusions

Because of the present inability to suitably dope them, the (II-VI)–(III-V) alloys are unlikely to find useful application in electronic devices. Nevertheless, these alloys remain of high scientific interest. Studies of the lattice-vibration spectra of (II-VI)–(III-V) alloys could provide[15] important information regarding the character of the ionic bonding in II-VI and III-V compounds. Further detailed analysis of the unusual and interesting bandgap variations could provide basic data in interpreting changes in the band structure especially on going from a direct-gap II-VI compound to an indirect-gap III-V compound. The atomic arrangement of the alloying elements in the host compound lattice is also of fundamental interest.

Acknowledgments

The authors are grateful to E. J. Stofko and R. J. Ulmer for most of the experimental work. The authors have been benefited by many valuable discussions with L. R. Weisberg, F. D. Rosi, D. Richman, J. J. Tietjen, F. H. Nicoll, and S. Bloom of RCA Laboratories; with M. Glicksman of Brown University; and with J. A. van Vechten of the U.S. Naval Research Laboratory.

The research herein reported was made possible in large measure by the support of the Advanced Research Projects Agency under Order No. 1034, through the U.S. Army Electronics Command, Fort Monmouth, New Jersey, under Contract Nos. DAAB07-68-C-0129 and DAAB07-69-C-0145.

References:

[1] N. A. Goryunova, **The Chemistry of Diamond-like Semiconductors,** p. 148, Chapman and Hall, Ltd., London, 1965.

[2] W. M. Yim, "Silid Solutions in the Pseudobinary (III-V)-(II-VI) Systems and Their Optical Energy Gaps," **Jour. Appl. Phys.,** Vol. 40, p. 2617, 1969; and W. M. Yim, J. P. Dismukes and E. J. Stofko, unpublished results.

[3] S. M. Ku and L. J. Bodi, "Synthesis and Some Properties of ZnSe: GaAs Solid Solutions," **Jour. Phys. Chem. Solids,** Vol. 29, p. 2077, 1968.

[4] I. Bertoti, M. Farkas-Jahnke, M. Harsy, T. Nemeth and K. Richter, "Preparation, Composition and Structure of Mixed Crystals in ZnS-GaP System," **Proc. International Conf. on Luminescence,** Budapest, 1966, p. 1261; and I. Bertoti, E. Barta, J. Schanda and P. Sviszt, "Luminescent Properties of ZnS-GaP Mixed Crystals," ibid., p. 1102.

[5] J. J. Tietjen and J. A. Amick, "The Preparation and Properties of Vapor-Deposited Epitaxial $GaAs_{1-x}P_x$ Using Arsine and Phosphine," **Jour. Electrochem. Soc.,** Vol. 113, p. 724, 1966.

[6] W. M. Yim and E. J. Stofko, "Vapor-Phase Epitaxial Growth of Several II-VI Compounds," to be published.

[7] J. P. Dismukes, W. M. Yim, J. J. Tietjen and R. E. Novak, "Vapor Deposition of Semiconducting Mononitrides of Sc, Y, and the Rare Earth Elements," **RCA Review**, Vol. 31, p. 680, Dec. 1970 (this issue).

[8] D. Richman, unpublished results; also see, e.g., D. Richman, C. J. Nuese and R. B. Clough, "Preparation and Properties of $In_xGa_{1-x}P$ Alloys," to be published in **Met. Trans.**

[9] S. Bloom, "Bandgap Variation in Quaternary Alloys," **Jour App. Phys.**, Vol. 41, p. 1864, 1970.

[10] J. I. Pankove, "Properties of Heavily Doped Germanium," p. 49, in **Progress in Semiconductors,** Vol. 9, ed. by A. F. Gibson and R. E. Burgess, Temple Press Books Ltd., London, 1965.

[11] M. Glicksman, D. Gutman and W. M. Yim, "Electronic Transport Properties in the Semiconductor Alloy $(GaP)_{0.95}(ZnSe)_{0.05}$," **Appl. Phys. Letters,** Vol. 16, p. 366, 1970.

[12] G. Mandel, "Self-Compensation Limited Conductivity in Binary Semiconductors. I. Theory," **Phys. Rev.**, Vol. 134, p. A1073, 1964.

[13] H. Kressel, F. Z. Hawrylo and P. LeFur, "Luminescence due to Ge Acceptors in GaAs," **Jour. App. Psys.,** Vol. 39, p. 4059, 1968.

[14] F. H. Nicoll, "Apparatus for Studying Electron Beam Pumped Semiconductor Lasers and Other High Excitation Density Phenomena," **Rev. Scientific Instr.,** Vol. 41, p. 1175, 1970.

[15] J. C. Phillips and J. A. van Vechten, "Charge Redistribution and Piezoelectric Constants," **Phys. Rev. Letters,** Vol. 23, p. 1115, 1969.

Vapor Deposition of Semiconducting Mononitrides of Scandium, Yttrium, and the Rare-Earth Elements

J. P. Dismukes,† W. M. Yim, J. J. Tietjen, and R. E. Novak*

RCA Laboratories, Princeton, N.J.

Abstract—The mononitrides LnN having the NaCl structure, where Ln=Sc, Y, or a rare-earth element, were grown epitaxially on α-Al_2O_3 by reaction of NH_3 gas with a volatile Ln chloride or with Ln vapor at about 925°C. The as-grown layers were all n-type. The optical energy gap of ScN is about 2.2 eV, whereas those of the other nitrides are in the range 0.9-1.6 eV. All the rare-earth nitrides except ScN are unstable in moist air. In contrast, ScN is inert to water and dilute acids and stable in air up to 550°C. Chemical analysis indicates that ScN is a stoichiometric 1:1 compound, in contrast to previously reported gross nitrogen deficiency. Mass spectrographic analysis shows chlorine to be the principal donor impurity.

The lowest carrier concentration thus far obtained in n-type ScN is $8.6\times10^{19}/cm^3$. However, the mobility values of 158 cm^2/volt-sec and 1940 cm^2/volt-sec at 300°K and 77°K, respectively, are relatively large. Calculations based on a simple thermodynamic model for self-compensation in semiconductors by lattice defects indicate that ScN should be particularly resistant to this effect, and hence should be readily doped n- and p-type in the absence of chlorine.

1. Introduction

Among the most important general materials requirements for a semiconductor useful in electronic devices are ease of high-conductivity n- and p-type doping to allow formation of good p-n junctions, high carrier mobility, simplicity of materials preparation and device fabrication, and chemical stability of the material under conditions of device use. Germanium, silicon, and the III-V compounds covering the bandgap range 0.2-2.26 eV have been extensively studied, and technologies have been developed for their application in p-n junction devices. However, there

† Present Address: Laboratories RCA, Ltd., Zurich, Switzerland.

* Present Address: Department of Ceramic Engineering, The University of Illinois, Urbana, Illinois.

is still a need for semiconductors with direct bandgaps in the 2-3 eV range, especially for use in efficient p-n junction electroluminescent diodes covering the spectral region from the orange to the blue.

For large-bandgap semiconductors, it is the requirement of n- and p-type doping that is the most difficult to satisfy. All previously available data on II-VI compounds and recent results at RCA Laboratories[1,2] on (III-V)-(II-VI) alloys indicate that inability to dope these materials n- and p-type is due to compensation by native lattice defects,

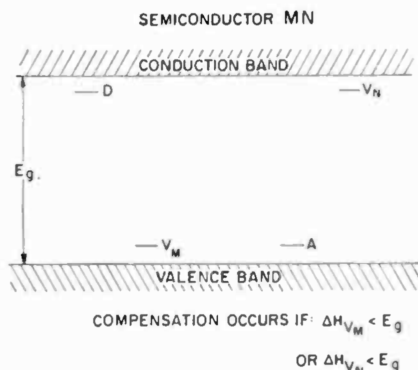

Fig. 1—Schematic diagram of self-compensation in a semiconductor of general formula MN.

namely vacancies and/or interstitials. Kroger[3] and Mandel[4] have discussed this type of compensation in terms of a model illustrated in Fig. 1. For a semiconductor of general formula MN, compensation of a substitutional donor impurity (D) by an acceptor vacancy (V_M) or of a substitutional acceptor impurity (A) by a donor vacancy (V_N) can occur if the enthalpy of vacancy formation (ΔH_{V_M} or ΔV_N) is less than the bandgap energy E_g.* This simple model predicts that the most promising compounds for amphoteric doping will be those with $E_g/\Delta H_v < 1$. Indeed, the plot of E_g versus $E_g/\Delta H_v$ in Fig. 2 shows that compounds that are readily doped p- and n-type (CdTe, GaP, InP, GaAs and SiC) have values of $E_g/\Delta H_v$ considerably less than unity, whereas those that cannot be doped both p- and n-type (CdSe, CdS, ZnTe, ZnSe, MgTe and

* Following Mandel, ΔH_v was taken as one-half the sublimation energy, and the energies of cation and anion vacancy formation were assumed equal. An exact treatment would take the free energy rather than the enthalpy of vacancy formation. This neglects the $T\Delta S$ terms involving the entropy of mixing, which is relatively small and can be neglected, and the vibrational entropy, accurate estimates of which are beyond the present state of theory and experiment.

ZnS) hve values of $E_g/\Delta H_v$ approaching or exceeding unity. It is important to note that prior to the investigation of the (II-VI)-(III-V) alloys[1,2] the value of $E_g/\Delta H_v$ that separates those materials that can be doped from those that cannot was relatively poorly defined, since the range of 0.6 to 1.0 had not been adequately characterized. Now, however, with the results for alloys such as $(GaAs)_{.2}(ZnSe)_{.8}$, not doped, and $(GaP)_{.1}(ZnSe)_{.9}$, readily doped, and with the recent successful n- and p-type doping[6] of GaN, it is evident that the most promising materials should have $E_g/\Delta H_v$ values of 0.75 or less.

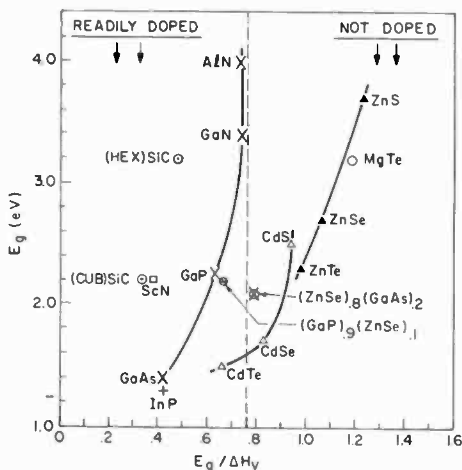

Fig. 2—The dependence of E_g upon $E_g/\Delta H_v$ for a number of semiconductors. E_g is the bandgap and ΔH_v is the enthalpy of vacancy formation in the compound.

Before conducting experimental work we made an extensive survey of a wide variety of semiconductors to determine those with large enthalpy of formation, and hence large enthalpy of vacancy formation, and small $E_g/\Delta H_v$. Thermodynamic data for these calculations were obtained from standard sources.[6,7] This survey indicated that of those materials expected[8,9] to have values of energy gap in excess of 2 eV, the nitrides LnN with the NaCl structure, where Ln = Sc, Y, or a rare-earth element, would have the smallest values of $E_g/\Delta H_v$. Initial experiments showed ScN to be a chemically stable compound, and to have $E_g \sim 2.2$ eV and $E_g/\Delta H_v \sim 0.4$. Accordingly, we selected these materials for thorough study in the present work.

2. Experimental

2.1 Vapor-Phase Growth

Although the mononitrides of Sc, Y and the rare-earth elements have been known for many years, relatively little has been learned of their electrical and optical properties,[10] due largely to the lack of synthetic techniques for preparing them in single-crystal form with controlled purity and stoichiometry. Bulk samples prepared by arc melting[11] the metal under nitrogen atmosphere are nonstoichiometric due to nitrogen deficiency as are also crystals grown by chemical transport reaction with I_2 in molybdenum crucibles[12] at $> 1500°C$. Reaction of nitrogen or ammonia with the metals or metal hydrides,[14] or of nitrogen with metal amalgams,[13] gives monitride powders that are also nitrogen deficient.

In this work we have developed a vapor-phase technique for growing single-crystal layers of the mononitrides of Sc, Y, or rare-earth elements on α-Al_2O_3 in the relatively low temperature range 850°-1000°C. Fig. 3 shows a schematic diagram of the apparatus used to grow these nitrides.

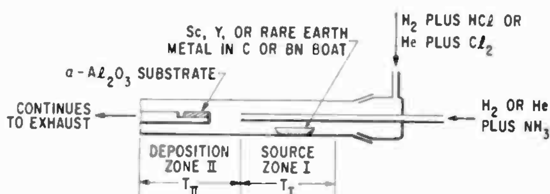

Fig. 3—Apparatus for vapor-phase epitaxial growth of mononitrides of Sc, Y, or rare-earth metals.

In most cases the metal contained in a carbon or boron nitride boat in zone I was reacted with HCl in H_2 carrier gas or with Cl_2 in He carrier gas to form a volatile metal chloride, which reacts further in zone II with NH_3 diluted with H_2 or He, to form the mononitride. However, in the case of a volatile metal such as Yb, the metal could be transported directly as its vapor. The experimental arrangement is similar to that employed for the epitaxial growth of GaN,[5] but with two important differences. First, the nitrides form by direct reaction of NH_3 gas with a volatile metal chloride at the junction of the two carrier gas streams in Fig. 3. Second, a temperature gradient need not be imposed between the source zone I and the deposition zone II. And, in fact, in most

experiments T_I equals T_{II}. A thin carbon liner in the reaction tube and a carbon coated sample holder are employed to prevent reaction of the metal chlorides with quartz.

Representative conditions for growth were: 25 cc/min NH_3 plus $\sim$ 1000 cc/min H_2 or He through the central tube (¼-inch O.D.), and 3 cc/min HCl plus $\sim$ 1000 cc/min H_2 or 3 cc/min Cl_2 plus $\sim$ 1000 cc/min He through the main tube (1.5-inch O.D.). Typical growth rates were about 2-3 μm per hour, and specimens 1-20 μm in thickness were conveniently grown.

Mononitrides of Sc, Y, and the rare-earth elements from the last half of the rare-earth series were readily grown by this vapor-growth technique. In marked contrast, no LaN nor GdN formed in the reaction tube under the same conditions, even though metal chlorides were transported. This behavior could be due to differences either in nucleation characteristics or in the thermodynamics of the reaction between NH_3 and the respective metal halide.

2.2 Physical Measurements

The lattice parameter of the mononitrides was determined from x-ray powder photographs taken using a 114.6-mm diameter camera. Laue photographs were taken by the back reflection technique using Cr-radiation. Optical absorption measurements were made on as-grown epitaxial layers on α-Al_2O_3, using a Cary Model No. 14 spectrophotometer. In the case of the mononitrides of Y and the rare-earth elements the apparatus was purged with dry nitrogen gas to prevent reaction with moisture from the atmosphere. The absorption coefficient α was calculated as $\alpha = (1/t)\ln(I_0/I_T)$, where t is the thickness in cm, and I_0 and I_T are the initial and transmitted intensities, respectively. The thickness of the samples was measured by an interferometric technique. Hall-effect measurements were made by an ac null method that eliminates thermoelectric effects. Bridge-shaped samples for Hall masurements were fabricated by sandblasting a pattern in the epitaxial layers. Pressed indium wire contacts were satisfactory since they gave ohmic I-V characteristics.

3. Results and Discussion

3.1 Chemical properties

Chemical Reactivity

The mononitrides of Y, Dy, Er, Yb, and Lu were stable indefinitely in dry air, but were unstable in moist air, with which they reacted to form

oxide-hydroxides, for example YOOH. Impurities and/or lattice defects are well known to affect the chemical reactivity of semiconductors. An interesting example is AlAs, whose reactivity with moisture is dependent on growth conditions.[15] In this regard we observed that LuN is stable in air for periods of up to one day, and that it is the most stable of the rare-earth nitrides listed above. However, Didchenko and Gortsema[14] observed that LuN prepared by reaction of lutetium hydride with ammonia was the most reactive of the nitrides they investigated.

In contrast, ScN is remarkably inert. It does not react with moist air after exposure for as long as one year, and does not react with water or dilute acids. Aqua regia or $HF\text{-}HNO_3$ must be used to dissolve ScN in a reasonable time. In addition, ScN is stable in air up to 550°C. Above 600°C it oxidizes to Sc_2O_3.

Table 1—Chemical Analysis of ScN

Sample #	Weight Percent Scandium	
	Actual	Calculated for ScN
1	76.0	
2	76.1	
3	75.9	
4	76.0	
	76.0	76.2

Chemical Composition

Since the nitrides of Y and the rare-earth elements were relatively unstable, they were not analyzed. Determinations of scandium in vapor-grown ScN using the method of Cheng[16] are shown in Table 1. The average weight percent scandium for four samples is 76.0%, compared with a calculated value of 76.2% for pure ScN. As shown in Table 2, which will be discussed further in connection with the electrical properties, metallic impurities and oxygen and carbon are present in relatively small concentrations, and the major impurity is chlorine. The close to theoretical analysis indicates that appreciable nitrogen vacancies are not present in the vapor-grown ScN. Thus ScN appears to be a stoichiometric 1:1 compound, in contrast to grossly nitrogen-deficient material prepared by previous methods.

3.2 Physical Properties

X-Ray Measurements

Measurements of Debye–Scherrer powder photographs showed that the mononitrides of Sc, Y, and the rare-earth metals have the NaCl structure, as previously reported. The lattice parameter of ScN was found to be 4.502 Å, which is about 1% higher than the literature value[17] of 4.44 Å. The other nitrides also exhibited slightly higher values of lattice parameter. For example, vapor-grown YN had a lattice parameter of 4.888 Å compared to the literature value[18] of 4.877 Å. This difference probably reflects the improved purity and stoichiometry of the vapor-grown nitrides.

Table 2—Correlation between Impurity Analyses and Electron Concentration in ScN[a]

Sample #	Metallic[b] Impurities	[C]	[O]	[F]	[Cl]	n ($10^{20}/cm^3$)	$\frac{[F]+[Cl]}{n}$
Sc Metal	1.8	0.64	2.3	0.58	—	—	—
A[c]	0.4	0.17	0.44	0.04	1.8	1.73	1.06

[a] Mass spectrographic determination. All analyses in units of 10^{20} atoms/cm^3.

[b] The major metallic impurities are miscellaneous rare-earth metals, Si, Fe, Al, Mg, and Ca.

[c] Sample removed from silicon substrate.

Laue photographs of ScN on $\langle 1\bar{1}02\rangle \alpha$-$Al_2O_3$ exhibited well-defined diffraction spots. But the determination of the orientation of ScN relative to the substrate proved generally difficult because interfering spots from the substrate were also observed even for ScN layers as thick as 20 μm. A $\langle 321\rangle$ orientation has been definitely identified, and another as yet unidentified orientation has been quite often observed. For LuN, which has a higher x-ray absorption coefficient than ScN, Laue spots exhibiting four-fold symmetry were obtained, indicating an epitaxial relation of $\langle 100\rangle$ LuN//$\langle 1\bar{1}02\rangle \alpha$-$Al_2O_3$. A Laue photograph of an LuN layer is shown in Fig. 4. Here a large number of weaker spots is due to the $\langle 1\bar{1}02\rangle \alpha$-$Al_2O_3$ substrate.

Optical Energy Gap

Values of optical energy gap for mononitrides of Sc, Y, and the rare-earth elements are shown in Table 3, which also compares the results of previous work on these compounds[9, 12]. The values of optical energy gap

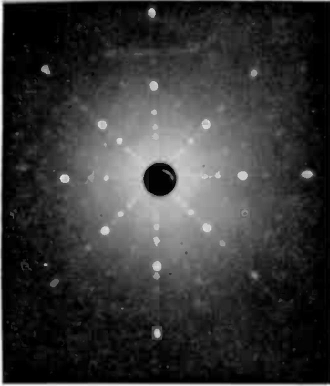

Fig. 4—Laue photograph of epitaxial layer of LuN grown on <1$\bar{1}$02> α-Al_2O_3. The spots showing four-fold symmetry are due to LuN. The weaker spots are due to the substrate.

in this work were derived from absorption edges such as that shown for ScN in Fig. 5. Due to the large electron concentrations in samples thus far prepared ($\sim 10^{20}/cm^3$), effects due to free carrier absorption and the Burstein shift may be present. Thus the uncertainty in the present bandgap values listed in Table 3 may be as much as 0.1 eV.

The results of Busch et al[12] for DyN, ErN, LuN, and YN determined by diffuse reflection are in good agreement with the present results for these compounds determined by absorption. However, the values meas-

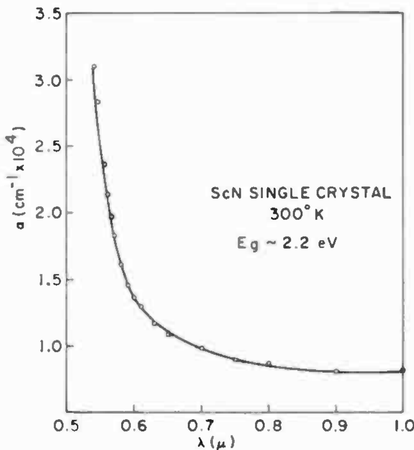

Fig. 5—The dependence of optical absorption coefficient (α) upon wavelength (λ) for single-crystal ScN.

used by us for YbN and ScN, which we believe to be more accurate, are about 0.4-0.5 eV higher than those measured by Busch et al. In any event, the large values in excess of 2 eV reported by Sclar[9] for DyN and ErN are not substantiated either by this work or the work of Busch et al. Thus ScN appears to be the only nitride in this materials class with an energy gap in excess of 2 eV, and consequently the only material of further interest for p-n junction electroluminescence.

Table 3—Optical Energy Gap of Mononitrides of Sc, Y, and the Rare-Earth Elements

COMPOUND	Optical Energy Gap (eV) This Work	Previous Work a	Previous Work b
ScN	2.15	1.75	—
YN	1.5	1.45	—
LaN	—	0.82	—
CeN	—	—	—
PrN	—	1.03	—
NdN	—	0.80	—
SmN	—	0.70	—
EuN	—	0.76	—
GdN	—	0.98	—
TbN	—	—	—
DyN	0.95	0.91	2.60
HoN	—	1.06	1.88
ErN	1.3	1.20	2.40
TmN	—	1.10	—
YbN	1.5	1.03	—
LuN	1.6	1.55	—

[a] Reference (12).
[b] Reference (9).

Electrical Properties

The epitaxial layers of the mononitrides of Sc, Y, and the rare-earth elements were all high-conductivity n-type as determined by thermal probe testing. Hall measurements were readily made on ScN, but could not be conveniently made on the other nitrides because of their sensitivity to moisture.

Electrical data both at 300°K and 77°K for representative samples of vapor-grown, single-crystal, n-type ScN covering the range of carrier

concentration from $8.6 \times 10^{19}/cm^3$ to about $2.3 \times 10^{21}/cm^3$ are given in Table 4. Values of carrier concentration lower than $8.6 \times 10^{19}/cm^3$ at 300°K were not obtained, even though extensive variations in growth temperature and other deposition parameters were made. The major metallic impurities (Table 2) in ScN were Si, Fe, Al, Mg, and Ca, which are either acceptors or electrically neutral. Moreover, the bulk concentration of the donor impurity oxygen is probably considerably lower than the observed value of $4.4 \times 10^{19}/cm^3$, since the analyses were performed on powders with large surface area. Thus chlorine, which is the major impurity, appears to be the principal donor impurity. And in fact Table 2 indicates a 1:1 relation between donor concentration and halogen concentration.

Table 4—Electrical Properties of Vapor-Grown, Single-Crystal, n-Type ScN[a]

	Sample					
	A ($t = 4.8\ \mu m$)		B ($t = 13.5\ \mu m$)		C ($t = 7.9\ \mu m$)	
	300°K	77°K	300°K	77°K	300°K	77°K
ρ (10^{-4} ohm-cm)	4.61	0.47	2.11	0.23	1.73	—
n ($10^{20}/cm^3$)[b]	0.86	0.69	4.25	3.51	23.4	—
μ (cm^2/V-sec)[c]	158	1940	70	775	11	—

[a] All samples grown on <1$\bar{1}$02> α-Al_2O_3
[b] Carrier concentration = $1/Re$
[c] Hall mobility = R/ρ.

Although controlled doping of ScN has thus far been prevented by the incorporation, during vapor-phase growth, of chlorine as a donor, this compound could become a useful semiconductor material if n- and p-type doping can be achieved. As discussed earlier in this paper, based on thermodynamic arguments, there are no fundamental limitations on p- and n-type doping of ScN. Indeed it has a very small $E_g/\Delta H_v$ ratio (Fig. 2) of 0.4, and thus it should be resistant to self-compensation by lattice defects.

Furthermore, the electron mobilities of 158 cm^2/volt-sec and 1940 cm^2/ volt-sec, at 300°K and 77°K, respectively, shown in Table 4 are relatively large for such heavily doped material. The favorable electron mobility of ScN is more clearly shown in Fig. 6, which compares the dependence of mobility upon electron concentration for ScN with that for the III-V compound semiconductors AlAs[18], GaP[19,20], GaN[5], and

GaAs[14]. Clearly ScN (2.2 eV) could have considerably higher electron mobility than GaN (3.50 eV) GaP (2.26 eV), or AlAs (2.16 eV) in the $10^{17} - 10^{18}/\ cm^3$ range of carrier concentration. And in fact an optimistic extrapolation suggests that the mobility of ScN at lower carrier concentration might approach that of GaAs (1.43 eV). Thus further study of ScN is warranted to determine if its properties can be tailored for semiconductor device application.

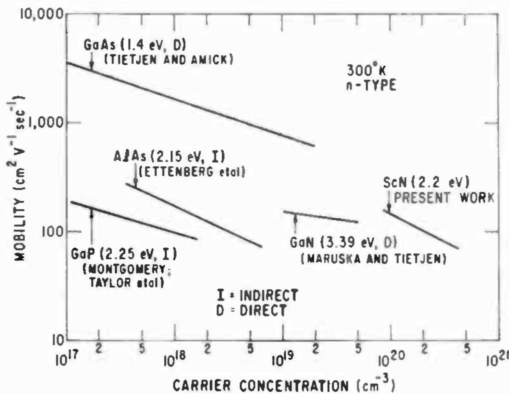

Fig. 6—The dependence of Hall mobility upon electron concentration for ScN and for several III-V compound semiconductors.

Acknowledgments

The authors are indebted to H. P. Maruska for initial experiments, to R. J. Ulmer and E. J. Stofko for most of the experimental work, to R. J. Paff for x-ray powder photographs, to R. T. Smith for Laue photographs, to W. C. Roth for electron diffraction, to B. L. Goydish and Mrs. A. W. Murray for wet chemical analysis, and to W. L. Harrington for mass spectrographic analysis. The authors also thank Dr. E. Kaldis for making available a copy of reference (12) prior to its appearance in the open literature.

The research reported herein was made possible by the support of the Advanced Research Projects Agency under Order No. 1034, through the United States Army Electronics Command, Forth Monmouth, New Jersey, USA 07703, under Contracts Nos. DAAB07-69-C-0145 and DAAB07-70-C-0155.

References:

[1] W. M. Yim, "Solid Solutions in the Pseudobinary (III-V)-(II-VI) Systems and Their Optical Energy Gaps," **Jour. Appl. Phys.**, Vol. 40, p. 2617 (1969).

[2] W. M. Yim, J. P. Dismukes, and H. Kressel, "Vapor Growth of (II-VI)-(III-V) Quaternary Alloys and Their Properties," **RCA Review**, Vol. 31, p. 662, Dec. 1970 (this issue).

[3] F. A. Kroger and H. J. Vink, "Relations between the Concentrations of Imperfections in Crystalline Solids," in **Solid State Physics** edited by F. Seitz and D. Turnbull (Academic Press Inc., N. Y., 1956), Vol. III, p. 310.

[4] G. Mandel, "Self-Compensation Limited Conductivity in Binary Semiconductors. I. Theory," **Phys. Rev.**, Vol. 134, p. A1073 (1964).

[5] H. P. Maruska and J. J. Tietjen, "The Preparation and Properties of Vapor-Deposited Single-Crystalline GaN," **Appl. Phys. Letters**, Vol. 15, p. 327 (1969).

[6] C. E. Wicks and F. E. Block, "Thermodynamic Properties of 65 Elements—Their Oxides, Halides, Carbides, and Nitrides," Bureau of Mines Bulletin 605, U. S. Government Printing Office, Washington, 1963.

[7] O. Kubaschewski, E. Ll. Evans, and C. B. Alcock, **Metallurgical Thermochemistry**, Fourth Edition, Pergamon Press Ltd., 1967.

[8] N. Sclar, "Energy Gaps of the III-V and the (Rare Earth)-V Semiconductors," **Jour. Appl. Phys.**, Vol. 33, p. 2999 (1962).

[9] N. Sclar, "Properties of Rare-Earth Nitrides," **Jour. Appl. Phys.**, Vol. 35, p. 1534 (1964).

[10] F. Hulliger, "On the Conductivity Character of Rare-Earth Compounds," **Helv. Phys. Acta**, Vol. 41, p. 945 (1968).

[11] R. J. Gambino and J. J. Cuomo, "Preparation of Rare Earth Nitrides by Reactive Arc Melting," **Jour Electrochem. Soc.**, Vol. 113, p. 401 (1966).

[12] G. Busch, E. Kaldis, E. Schaufelberger-Teker and P. Wachter, "Synthesis, Crystal Growth and Physical Properties of Rare-Earth Nitride Phases," conference proceedings of the Colloque International du C.N.R.S. sur les Elements des Terres-Rares, Paris-Grenoble, May 5-10, 1969.

[13] R. Didchenko and F. P. Gortsema, "Some Electronic and Magnetic Properties of Rare Earth Monosulfides and Nitrides," **Jour. Phys. Chem. Solids**, Vol. 24, p. 863 (1963).

[14] J. J. Tietjen and J. A. Amick, "The Preparation and Properties of Vapor-Deposited Epitaxial $GaAs_{1-x}P_x$ Using Arsine and Phosphine," **Jour. Electrochem. Soc.**, Vol. 113, p. 724 (1966).

[15] W. M. Yim, "Direct and Indirect Optical Energy Gaps of AlAs," submitted to **Jour. Appl. Phys.**

[16] K. L. Cheng, "Analysis of Lead Telluride with an Accuracy to Better than 0.1%," **Anal. Chem.**, Vol. 33, p. 761 (1961).

[17] R. W. G. Wyckoff, **Crystal Structures**, Second Edition, Vol. 1, pp. 85-94, John Wiley and Sons, New York, 1963.

[18] M. Ettenberg, A. G. Sigai, S. Gilbert and A. Dreeben, "Properties and Vapor Growth of AlAs", to be published.

[19] R. C. Taylor, J. F. Woods, and M. R. Lorenz, "Electrical and Optical Properties of Vapor-Grown GaP," **Jour. Appl. Phys.**, Vol. 39, p. 5404 (1968).

[20] H. C. Montgomery, "Hall Measurements of Te-Doped Gallium Phosphide of Improved Homogeneity," **Jour. Appl. Phys.**, Vol. 39, p. 2002 (1968).

Vapor-Phase Growth of Magnetic Semiconducting Spinels

H. L. Pinch and L. Ekstrom
RCA Laboratories, Princeton, N.J.

Abstract—The chromium chalcogenide spinels (ACr_2X_4) have been found to be both magnetic and semiconducting. The electronic transport properties and the optical band edge are strongly influenced by the degree of magnetic order. Single crystals and single-crystal films of these compounds have been prepared by chemical vapor transport methods, and the crystal growth processes and mechanisms are discussed. Prospective novel devices using these new materials are also examined.

Introduction

A new class of magnetic compounds has recently been the focus of much scientific and technological investigation. These compounds have the spinel structure as do the oxide ferrites and have the general formula $A[Cr_2]X_4$. Here A can be either diamagnetic or magnetic cations (such as Cd^{2+}, Zn^{2+}, $Ag^{+}_{0.5}In^{3+}_{0.5}$, Co^{2+}, Cu^{+}, or Fe^{2+}) and X can be either a single anion or a combination of anions (such as S, Se or combinations of these with Cl, Br, or I). The type and strength of the magnetic interactions varies greatly among the many compounds.[1] Several of the materials such as $CdCr_2S_4$ and $CdCr_2Se_4$ are ferromagnets.[2,3] These compounds have extremely low magnetocrystalline anisotropies and very narrow microwave line widths.[4,5] The optical absorption edge of many of the chromium chalcogenide spinels is strongly influenced by the magnetic behavior.[6-9] Most important, many of the compounds are respectable semiconductors.[10,11] It is the combination of these various effects occurring simultaneously in a given material and the possibility of devices that could utilize these properties concurrently that has been the stimulus of the recent activity. Devices may be envisioned in which electronic properties are magnetically controlled or vice versa. Alternatively, there is the prospect of using the different properties independently on the same chip of material to construct arrays of magnetic and semiconducting elements.

To test these materials for device applications and to make more

meaningful physical measurements, a program of crystal growth was undertaken. This review describes the application of vapor-transport techniques in the preparation of crystals and films of these magnetic semiconductors.

Crystal Growth

All of these materials are high-temperature peritectics, and decompose in varying degrees above 700°C. Crystal-growth methods that can be carried out at temperatures near or below the stability range are needed. Some success was achieved in growing crystals of $CdCr_2Se_4$ from molten $CdCl_2$[6] or $CdCl_2$-$CrCl_2$ mixtures,[12] but these flux methods proved to be specific for $CdCr_2Se_4$ alone. The growth of complex sulfides and selenides by vapor transport is well known,[13,14] and these techniques were found to be useful for the crystal growth of the chromium chalcogenide spinels.

Open-Tube Vapor Transport

The open-tube vapor-phase growth of $CdCr_2S_4$ and $ZnCr_2S_4$ films has been accomplished by reacting the vapors of Cd or Zn, $CrCl_3$ and S_2 in a He atmosphere. The equation for the formation of $CdCr_2S_4$ in this manner is

$$4Cd(g) + 2S_2(g) + 2CrCl_3(g) = CdCr_2S_4(s) + 3CdCl_2(g). \quad [1]$$

However, other reactions yielding solid products can occur between these reactants, and must be avoided in order to obtain a single-phase deposit. The most important of these are

$$Cd(g) + \tfrac{1}{2}S_2(g) = CdS(s) \quad [2]$$

and

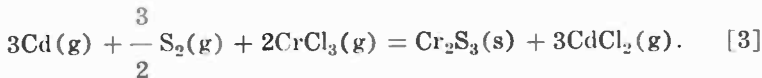

$$3Cd(g) + \frac{3}{2}S_2(g) + 2CrCl_3(g) = Cr_2S_3(s) + 3CdCl_2(g). \quad [3]$$

From considerations of the law of mass action, the conditions for driving Eq. [1] to the right are the same as those for driving Eqs. [2] and [3] to the right simultaneously. In order for it to form, the ternary compound must be thermodynamically more stable than a mixture of the binary solids at the deposition temperature. Thus, in devising conditions that make reaction [1] occur, it is convenient to think of making Eqs. [2] and [3] occur simultaneously. The main

criteria for conditions under which the spinel forms and the formation of CdS or Cr_2S_3 is minimized are first, the partial pressure of Cd, p_{Cd} must be made larger than p_{S_2} or p_{CrCl_3} and second, values of both p_{Cd} and p_{S_2} greater than equilibrium must be used. Because of the reaction

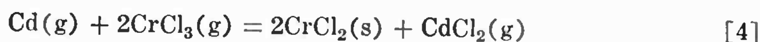

$$Cd(g) + 2CrCl_3(g) = 2CrCl_2(s) + CdCl_2(g) \quad [4]$$

the $CrCl_3$ can be premixed only with the S_2.

The effect of varying the reactant concentrations at constant temperature on the deposit composition obtained from the Cd-$CrCl_3$-S_2 system is illustrated in Fig. 1. In these experiments, the p_{Cd} was constant at 0.13 Torr while p_{S_2} and p_{CrCl_3} varied in the range from 4×10^{-3} to 8×10^{-3} Torr. It is seen that a clear division exists at a S_2 to $CrCl_3$ concentration ratio of 0.9. Below this value the deposits were $CdCr_2S_4$ and/or Cr_2S_3, while above this value $CdCr_2S_4$ and/or CdS formed. In no cases were CdS and Cr_2S_3 present simultaneously. The main reason that the same S_2 to $CrCl_3$ ratios give single-phase $CdCr_2S_4$ in some experiments and mixtures of phases in others is variations in the geometry of the deposition chamber, including the shape and position of the substrate. Fig. 2 shows the effect of temperature on the S_2 to $CrCl_3$ ratio at which single-phase $CdCr_2S_4$ is obtained.

The fused-quartz reactor used in this work is shown in Fig. 3. The reactants are evaporated in the tubes shown. These tubes extend into the reaction chamber to serve as nozzles that direct the gas streams to meet in the center of the chamber. A sleeve with a reduced opening downstream increases mixing and then directs the gas stream onto the substrate. The geometry of the nozzles, sleeve, and substrate is critical, as is the use of a high carrier-gas flow rate. The third tube entering the reaction chamber is used to introduce Cl_2 to prevent any deposition until thermal equilibrium is established. The phases present in the deposit on the substrate were determined from Debye–Scherrer x-ray powder pattern photographs. The crystal structure and orientation of the film were obtained by low-angle electron diffraction.

When Zn is substituted for Cd in otherwise similar experiments, the results are not only of the same form, but single-phase $ZnCr_2S_4$ is obtained at almost the same partial pressures of the reactants. However, when Se is substituted for S, only mixtures of Cr_2Se_3 and CdSe are obtained, with no $CdCr_2Se_4$ detectable. Similarly, on substituting Hg for Cd, only mixtures of the corresponding binary compounds are obtained.

The substances on which single-crystal films of $CdCr_2S_4$ have been

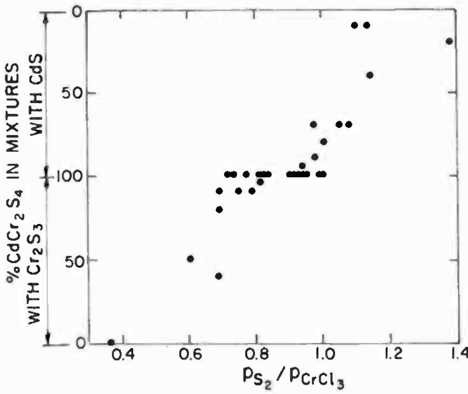

Fig. 1—Effect of vapor composition, p_{S_2}/p_{CrCl_3}, on deposit composition with excess Cd vapor at 740°.

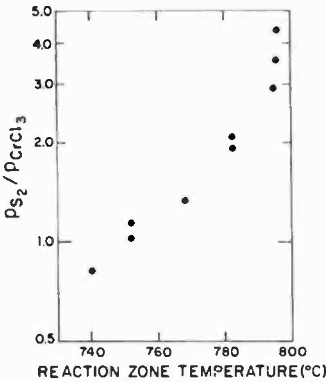

Fig. 2—Temperature dependence of the vapor composition needed to obtain single-phase $CdCr_2S_4$ deposit with excess Cd vapor.

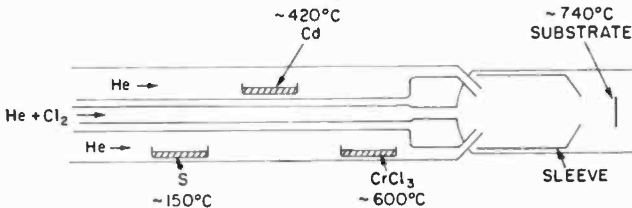

Fig. 3—Apparatus for the preparation of epitaxial films of $CdCr_2S_4$.

deposited include sapphire and spinel. The crystallographic relationships between these substrates and the films are shown in Table 1. Only polycrystalline films of $ZnCr_2S_4$ have been observed.

A two-hour deposition time typically results in a $CdCr_2S_4$ film about 1 micron thick. The single-crystal films are a deep red color in transmitted light and have an extremely high electrical resistivity.

Table 1—Orientation of $CdCr_2S_4$ Films on Various Substrates

Substrate Material and Orientation	Deposit Orientation
sapphire $(\bar{1}012)$	(100)
spinel (111)	(111)
spinel (110)	(110)
spinel (100)	(100)

Closed-Tube Vapor Transport

For many complex sulfides and selenides, crystal growth in sealed quartz ampoules with a halide transport agent is a straightforward process. The reversible equilibria involved can generally be determined readily, and crystals of near centimeter dimensions can be grown with little experimental difficulty. The distressing thing about the chromium chalcogenide spinels is their nonstraightforward behavior with respect to transport growth. As in the open-tube method just described, the closed-tube transport suffers from the same tendency to form unwanted phases at the expense of the desired spinel.

All of the spinels that were transported moved from higher (900°-775°C) to lower (800°-725°C) temperatures. The transport agent found to be most effective was chlorine, added either as the gas itself or that obtained from the high-temperature disproportionation of $CrCl_3$. The halide pressures were estimated to be about 2-3 atmospheres under the conditions of transport. To increase the rate of crystal growth, transport was carried out inclined from the horizontal or vertically to make maximum use of convection, and large-diameter quartz tubes (up to 5 cm) and short transport lengths (2.5 cm) were also used.

The compounds can be divided into two groups with respect to their transport equilibrium reactions. The first group contains those spinels with high-vapor-pressure metals (e.g., Zn, Cd, and Hg) as the A-site cations. These spinels decompose thermally most readily, and the probable decomposition reaction is

$$ACr_2X_4(s) = A(g) + \tfrac{1}{2}X_2(g) + Cr_2X_3(s). \qquad [5]$$

Thus a good part of the transport of the A-site ions is as the free metal, as proposed by Wehmeier.[15]. The residual solid Cr_2X_3 is transported by reactions [6] and [7].

$$Cr_2X_3(s) + 3Cl_2(g) = 2CrCl_3(g) + 3/2\,X_2(g) \qquad [6]$$

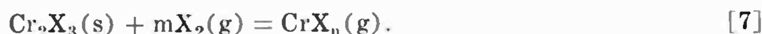

$$Cr_2X_3(s) + mX_2(g) = CrX_n(g). \qquad [7]$$

The transport of $CrCl_3$ in Eq. [6] is a complex process in itself.[16] The transport of transition metal chalcogenides (Eq. [7]) by excess chalcogen was recently described by Shafer.[17] A final probable transport mechanism is that involving ACl_2 in the vapor phase.

$$ACr_2X_4(s) + 4Cl_2(g) = ACl_2(g) + 2CrCl_3(g) + 2X_2(g). \qquad [8]$$

Under typical conditions used for the growth of $CdCr_2Se_4$ ($T_h = 825°C$, $T_c = 780°C$) a yield of ~25% transport was obtained at a transport rate of $\sim 1 \times 10^{-2}$ mmol/day. The crystals were flattened octahedra, $3 \times 3 \times 1$ mm,[3] and were intermixed with platelets of CdSe. As a comparison, under similar conditions $CdIn_2S_4$, whose transport equilibrium can be represented best as an equation similar to Eq. [8], was transported in almost 100% yield at an approximate rate of 1 mmol/day. Crystals of the other 5 spinels of this group, especially those with Hg on the A-site, are more difficult to grow, but these too have also been obtained by chemical vapor transport.[8,18]

The second group of spinels are those where the A-site cations are occupied by divalent transition metal ions (Mn, Fe, or Co) or a mixture of mono- and trivalent cations ($Cu_{1/2}Ga_{1/2}$, $Ag_{1/2}In_{1/2}$ or $Cu_{1/2}Fe_{1/2}$). The transport is probably governed by equations similar to Eq. [8].

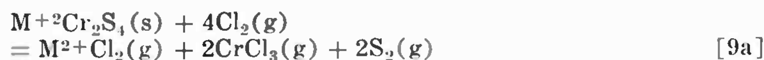

$$M^{+2}Cr_2S_4(s) + 4Cl_2(g) = M^{2+}Cl_2(g) + 2CrCl_3(g) + 2S_2(g) \qquad [9a]$$

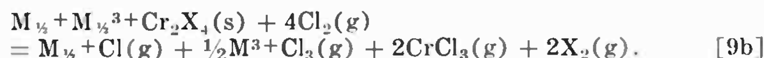

$$M_{1/2}^{+}M_{1/2}^{3+}Cr_2X_4(s) + 4Cl_2(g) = M_{1/2}^{+}Cl(g) + \tfrac{1}{2}M^{3+}Cl_3(g) + 2CrCl_3(g) + 2X_2(g). \qquad [9b]$$

The extent and ease of crystal growth for these materials range from very poor (for $FeCr_2S_4$,[19] where growth rates of less than 10^{-3} mmol/day have been reported) to about the same as that reported for $CdCr_2Se_4$. Again, other phases are transported along with the spinels (e.g., $CuGaS_2$, $AgCrSe_2$, Cr_2X_3). Even more deliterious efforts often occur. The transport is entirely limited by side reactions and processes,

and chemical species less complex than the spinel are formed at the source end of the closed tube. The rates of transport for the selenide spinels are from one to two orders of magnitude greater than those of the corresponding sulfides for this group.

Crystals of the mixed anion compounds (e.g., $CuCr_2Se_3Br$, $CuCr_2Te_3I$) can be grown by transport either using the intrinsic halide present in the material or with extra copper halide added as the source of additional halide.[20] The crystals of these materials are best prepared by pulling the sealed ampoules slowly through the temperature gradient. Crystals up to 3 mm along an edge have been obtained in this manner.[21]

Physical Properties of the Chromium Chalcogenide Spinels

The macroscopic magnetic behavior of the single crystals of the spinels is similar to that of the corresponding polycrystalline samples that were prepared and studied initially. The magnetic ordering temperatures are the same. Sample-to-sample variation in magnetic moment due to anion nonstoichiometry is found in both single-crystal and polycrystalline specimens.[22]

Electrical transport studies have been carried out, and most of the detailed work was done on $CdCr_2Se_4$.[11,23] As grown, crystals of undoped $CdCr_2Se_4$ are slightly p-type and of high resistivity. They can be made strongly p-type by the substitution of Ag for Cd on the A-site and n-type conductivity is achieved by substitution of In for Cd. The resistivity of p-type crystals increases monotonically with decreasing temperature. There is only a slight change in slope when the resistivity is measured through the Curie temperature. The calculated Hall mobility is 20 cm^2/V sec at room temperature and increases to 700 $cm^2/$ V sec near T_c (129°K). The electrical transport characteristics of n-type $CdCr_2Se_4$ are vastly different.[11] The resistivity initially increases with decreasing temperatures, and as magnetic order is approached there is an abrupt turn-around near 150°K and the resistivity decreases by a factor of 10^4 between 150° and 50°K. In n-type $CdCr_2Se_4$[11,23] the transverse magnetoresistance is negative and large, and peaks sharply at T_c, where $\Delta\rho/\rho_0 \approx -0.9$ at 10 kOe. Other unusual features also occur in the Seebeck effect and Hall-effect measurements[24] and are associated with the paramagnetic-to-ferromagnetic transition. A phenomenological model that postulates a hole band moving relative to the donor levels has been presented[25] to account for the anomalous temperature dependencies of the electrical parameters.

In all of the magnetic semiconducting spinels that have been meas-

ured, the optical bandgap shifts to lower energies as the temperature is decreased and magnetic order increases.[6-9] The deviation of the bandgap, E_g, from that expected from a high-temperature extrapolation begins 60° above the Curie temperature for $CdCr_2Se_4$.[6,7] In the case of $HgCr_2S_4$[8,9] the total energy shift is the largest seen. E_g has a maximum of 1.42 eV at 260°K and drops to 1.04 eV at 20°K. In the region of magnetic order, especially at T_c, a shift in E_g is also seen upon application of a magnetic field. For $HgCr_2Se_4$[26] at $T_c = 108$°K the effect is the largest seen, 0.042 eV for a 7 kOe field. Optical absorption measurements on the $CdCr_2S_4$ films[27] have been carried out to much shorter wavelengths than was possible with thinned bulk crystals. As a result, the shift of the absorption edge near T_c was found to be towards lower energies as is the case for the other spinels. Previous data[6,7] on bulk crystals had suggested that E_g was shifted to higher energies for $CdCr_2S_4$.

Applications

The areas of application of the chromium chalcogenide spinels can be expected to be those that will make use of their unique combination of properties and interaction of effects. Admittedly, as a semiconductor these spinels compare very unfavorably with present elemental and III-V materials. However, one can reasonably expect that as single crystals and films of greater perfection and purity are obtained, substantial increases in the mobilities, for example, will result. A further drawback to the application of this class of materials is the low Curie temperatures, which require operation of a possible device at below room temperature. This objection might be overcome, since several of the compounds, e.g., $CuCr_2Se_3Br$ and $Cu_{1/2}Fe_{1/2}Cr_2S_4$, have Curie temperatures near or above room temperature.

To date, p-n junctions made from single crystals of $CdCr_2Se_4$ have operated from room temperature to well below the Curie temperature.[27] The existence of this first active device raises the possibility of magnetically controlled diodes, laser diodes, and the like.

The use of these spinels in monolithic microwave integrated circuits has been discussed.[28,29] In this application the semiconducting properties and magnetic properties are used separately. On certain areas of the single crystal or thin single-crystal film, the gyromagnetic properties would be used to make nonreciprocal microwave devices. On other portions of the sample, using techniques of selective doping, arrays of diodes would be fabricated.

A survey of the potential devices and applications of these materials

as well as a compilation of the physical properties are presented in a recent paper by Wojtowicz.[30]

Acknowledgment

The authors gratefully acknowledge the many discussions and correspondence during the course of this work with their colleagues including P. J. Wojtowicz and Stuart B. Berger at RCA Laboratories in Princeton, K. Kato, F. Okamoto, T. Takahashi, and Y. Wada at RCA Research Laboratories, Inc., Tokyo, and F. P. Emmenegger and H. von Philipsborn at Laboratories RCA, Ltd., Zurich.

References:

[1] P. K. Baltzer, P. J. Wojtowicz, M. Robbins and E. Lopatin, "Exchange Interactions in Ferromagnetic Chromium Chalcogenide Spinels," **Phys. Rev.**, Vol. 151, p. 367 (1966).

[2] P. K. Baltzer, H. W. Lehmann and M. Robbins, "Insulating Ferromagnetic Spinels," **Phys. Rev. Letters**, Vol. 15, p. 493 (1965).

[3] N. Menyuk, K. Dwight and R. J. Arnott, "Ferromagnetism in $CdCr_2S_4$ and $CdCr_2Se_4$," **Jour. Appl. Phys.**, Vol. 37, p. 1387 (1966).

[4] S. B.Berger and H. L. Pinch, "Ferromagnetic Resonance of Single Crystals of $CdCr_2S_4$ and $CdCr_2Se_4$," **Jour. Appl. Phys.**, Vol. 38, p. 949 (1967).

[5] R. C. LeCraw, H. von Philipsborn and M. D. Sturge, "Ferromagnetic Resonance and Other Properties of $CdCr_2Se_4$," **Jour. Appl. Phys.**, Vol. 38, p. 965 (1967).

[6] G. Harbeke and H. Pinch, "Magnetoabsorption in Single-Crystal Semiconducting Ferromagnetic Spinels," **Phys. Rev. Letters**, Vol. 17, p. 1090 (1966).

[7] G. Busch, B. Magyar and P. Wachter, "Optical Absorption of Some Ferro- and Antiferromagnetic Spinels Containing Cr^{3+} Ions," **Phys. Letters**, Vol. 23, p. 438 (1966).

[8] G. Harbeke, S. B. Berger and F. P. Emmenegger, "Anomalous Absorption Edge Shift in Magnetic $HgCr_2S_4$," **Solid State Comm.**, Vol. 6, p. 533 (1968).

[9] H. W. Lehmann and G. Harbeke, "Anomalous Absorption Edge Shift in the Metamagnetic Temperature Range of $HgCr_2S_4$," **Phys. Rev.**, Vol. B1, p. 319 (1970).

[10] H. W. Lehmann and M. Robbins, "Electrical Transport Properties of the Insulating Ferromagnetic Spinels $CdCr_2S_4$ and $CdCr_2Se_4$," **Jour. Appl. Phys.**, Vol. 37, p. 1389 (1966).

[11] H. W. Lehmann, "Semiconducting Properties of Ferromagnetic $CdCr_2Se_4$," **Phys. Rev.**, Vol. 163, p. 488 (1967).

[12] H. von Philipsborn, "Growth of Single Crystals of $CdCr_2Se_4$ by Liquid Transport with Platinum Catalyst," **Jour. Appl. Phys.**, Vol. 38, p. 955 (1967) and "Crystal Growth by Topochemical Reactions: $CdCr_2Se_4$ in the System $CdSe$-$CrCl_3$-Pt," **Jour. Cryst. Growth**, Vol. 5, p. 135 (1969).

[13] R. Nitsche, H. Bolsterli and M. Lichtensteiger, "Crystal Growth by Chemical Transport Reactions—I. Binary Ternary, and Mixed Crystal Chalcogenides," **Jour. Phys. Chem. Solids**, Vol. 21, p. 199 (1961).

[14] H. Schafer, **Chemical Transport Reactions**, Academic Press, Inc., New York, 1964.

[15] F. H. Wehmeier, "The Growth of $CdCr_2Se_4$ by Chemical Transport," **Jour. Crystal Growth**, Vol. 5, p. 26. (1969).

[16] H. Opperman, "Das Reaktionsgleichgewicht $2CrCl_3(s,g) + Cl_2(g) = 2CrCl_4(g)$," **Z. Anorg. Allg. Chem.**, Vol. 359, p. 51 (1968).

[17] H. Schafer, F. Wehmeier, and M. Trenkel, "Chemisher Transport mit Schwefel als Transportmittel," **Jour. Less-Common Met.**, Vol. 16, p. 290 (1968).

[18] T. Takahashi, "Growth of $HgCr_2Se_4$ Single Crystals by Chemical Transport," **Jour. Crystal Growth**, Vol. 6, p. 319 (1970).

[19] P. Gibart and A. Begouen-Demeau, "Preparation de Monocristeaux de $FeCr_2S_4$," **C. R. Acad. Sc. Paris**, Vol. 268C, p. 816 (1969).

[20] K. Miyatani, Y. Wada and F. Okamoto, "Magnetic Properties of Single Crystal Chalcogenide Spinels; $CuCr_2X_3Y$ (X=S, Se and Te, Y=Cl, Br and I) System," **Jour. Phys. Soc. (Japan),** Vol. 25, p. 369 (1968).

[21] K. Kato, private communication.

[22] H. L. Pinch and S. B. Berger, "The Effects of Non-Stoichiometry on the Magnetic Properties of Cadmium Chromium Chalcogenide Spinels," **Jour. Phys. Chem. Solids,** Vol. 29, p. 2091 (1968).

[23] C. Haas, A. M. J. G. van Run, P. F. Bongers and W. Albers, "The Magnetoresistance of n-Type $CdCr_2Se_4$," **Solid State Comm.,** Vol. 5, p. 657 (1967).

[24] A. Amith and G. Gunsalus, "Unique Behavior of Seebeck Coefficient in n-Type $CdCr_2Se_4$," **Jour. Appl. Phys.,** Vol. 40, p. 1020 (1969).

[25] A. Amith and L. R. Friedman, "Mixed Conduction Model for Charge Transport in n-Type $CdCr_2Se_4$," **Phys. Rev.,** Vol. B2, p. 4311 (1970).

[26] H. W. Lehmann and F. P. Emmenegger, "Crystal Growth, Optical and Semiconducting Properties of Ferromagnetic $HgCr_2Se_4$," **Solid State Comm.,** Vol. 7, p. 965 (1969).

[27] S. B. Berger and L. Ekstrom, "Optical Properties of Single-Crystal Films of $CdCr_2S_4$," **Phys. Rev. Letter,** Vol. 23, p. 1499 (1969).

[28] C. P. Wen, B. Hershenov, H. von Philipsborn and H. L. Pinch, "Device Application Feasibility of Single-Crystal $CdCr_2Se_4$, a Ferromagnetic Semiconducting Spinel," **IEEE Trans. Magnetics,** Vol. MAG-4, p. 702 (1968).

[29] B. Hershenov, "Microstrip Junction Circulator for Microwave Integrated Circuits," **IEEE Trans. Microwave Theory and Techniques,** Vol. MTT-15, p. 748 (1967).

[30] P. J. Wojtowicz, "Semiconducting Ferromagnetic Spinels," **IEEE Trans. Mag.,** Vol. MAG-5, p. 840 (1969).

Compounds and Alloys for Superconducting Applications

R. E. Enstrom, J. J. Hanak, and G. W. Cullen
RCA Laboratories, Princeton, N.J.

Abstract—A review is given of several variations of a chemical vapor deposition process for Nb_3Sn based on the hydrogen reduction of niobium and tin chlorides. These methods are used for preparing Nb_3Sn in forms including single crystals and polycrystalline films on ceramic or metal substrates, particularly long lengths of ribbon. Growth techniques have been described that make this material available (1) as a highly perfect nearly dislocation-free material suitable for basic studies of properties needed for theoretical work and (2) as a heavily doped material with maximum concentration of defects necessary for flux pinning and high current-carrying capability in high-field-solenoid applications. This technology has culminated not only in the construction of the highest field superconducting magnets to date, but also in a successful commercial product.

1. Introduction

Nb_3Sn is of interest as a superconducting material because of its high transition temperature, 18.3°K, and its high upper critical field, 225 kG. The high upper critical field, H_{c_2}, implies that superconducting magnets fabricated from Nb_3Sn can be used to generate very high magnetic fields. To be able to realize high-field superconducting magnets, the Nb_3Sn conductor must be able to achieve a high critical current, I_c, so that a sufficient resistanceless current can be carried to generate the magnetic field without an inordinate length of wire. A major thrust of the research on Nb_3Sn has been to increase the current-carrying ability of ribbon intended for superconducting magnet applications. The successful achievement of this goal has led to the fabrication of superconductive Nb_3Sn ribbon on a commercial basis and to the generation of fields as high as 140 kG in a core as large as 6 inches in diameter. This represents the highest field achieved in such a large volume.[1]

Nb_3Sn is a weak, nonductile compound, and therefore wire drawing procedures used for copper and for the ductile metallic alloy superconductors, such as Nb-Zr and Nb-Ti, cannot be employed. Therefore, it was necessary to develop other procedures to prepare a practical Nb_3Sn

superconducting magnet wire. The approach taken by others was to use a composite wire consisting of an Nb jacket with an Nb + Sn powder core[2] or an Nb wire coated with a layer of Sn.[3] Both of these types of wire, however, must be wound onto the magnet form and subsequently heated to about 1000°C to form the Nb_3Sn by reaction of the elements. The approach developed by Hanak[4,5] has been to vapor deposit a thin layer of Nb_3Sn on a high-strength, flexible metal substrate ribbon by means of hydrogen reduction of the metal chlorides. Thus, the superconducting composite is pre-reacted, so that a subsequent Nb_3Sn formation step is not required. This type of superconducting ribbon is strong and flexible. It can be bent to a radius as small as ½ inch and can be rewound without degradation of I_c.

The materials investigated for use as the Nb_3Sn superconductive deposit substrate have included refractory (Mo, Ta, and W) and precious (Pt) metals. The coefficient of thermal expansion (CTE) for Mo and W is less than that for Nb_3Sn, so that the Nb_3Sn is under tension and therefore can crack easily on cooling to room temperature after deposition. Pt, Ni, and Ni alloys (such as Hastelloy) have a CTE greater than Nb_3Sn, so that the Nb_3Sn on Hastelloy is under a longitudinal compressive stress.[6] These stresses do not lead to cracking since brittle materials are relatively stable in compression. Based on cost and strength considerations, Hastelloy has been adopted as the preferred substrate material for commercial applications.[5,7] This alloy contains 62% Ni, 5% Fe, and 28% Mo and has an ultimate tensile strength of about 150,000 psi at 4.2°K. For most magnet applications, Hastelloy ribbon 0.090 inch wide by 0.002 inch thick has been utilized. As described later, interdiffusion between the metal substrate and the vapor-grown Nb_3Sn can occur, but this can be avoided with ceramic substrates. Ceramic materials with the proper CTE and chemical inertness were examined, and the magnesium silicates ($3MgO.4SiO_2$ to $4MgO.3SiO_2$) were found to be the most satisfactory. They are not corroded by halides at 900°C, no reaction between the substrate and deposit is observed by optical microscopy or x-ray diffraction, and the deposits are nonporous, adherent, and crack-free.[8] Other ceramics are either attacked by the halides or have a low CTE.

The prepartion of Nb_3Sn and its alloys by several chemical vapor deposition methods on various substrates, methods of increasing I_c and H_{c_2}, the properties of these materials, and the device applications are discussed in the following sections.

2. Experimental Apparatus and Procedures

Nb_3Sn crystals and layers can be grown by the hydrogen reduction of niobium and tin chlorides.[4,5] Several different vapor-growth procedures

have been developed including: (1) HCl transport[9] from a pre-reacted Nb_3Sn source at temperature T_1 to a substrate or a spontaneous nucleation site at a higher temperature, T_2; (2) reaction of chlorine with a pre-reacted Nb_3Sn source followed by H_2 reduction of the resulting metal chloride gases and redeposition of Nb_3Sn onto a heated ceramic or metal substrate[4]; (3) reaction of chlorine with separate Nb and Sn metal sources and the subsequent H_2 reduction of the resulting metal chlorides onto a heated metal substrate[5]; (4) the H_2 reduction of $SnCl_2$ and $NbCl_5$ vapors fed into the growth tube and the subsequent formation of Nb_3Sn on a heated metallic ribbon[4] or on a ceramic substrate.[8] Each of these growth methods has its special area of application. HCl transport, method 1, is useful for the growth of single crystals and polycrystalline deposits of Nb_3Sn and a wide variety of other superconducting materials.[9] These single crystals have been used in the determination of the low-temperature structural transformation[10] and elastic constants,[11] which have been of paramount importance in furnishing data for the recently introduced simple band-model theory.[12] Method 2 was used initially for the growth of Nb_3Sn films, but because the composition of the vapors changed with time as the more reactive Sn was depleted from the Nb_3Sn source, method 3 is preferred for the preparation of long lengths of ribbon coated with Nb_3Sn. Method 4 has been used extensively for the growth of Nb_3Sn on ceramic substrates for a variety of scientific investigations.

The apparatus used by Cullen[8] for the growth of Nb_3Sn on flat and cylindrical ceramic substrates using $NbCl_5$ and $SnCl_2$ powders (method 4) is shown in Fig. 1. Pure (99.9%) $NbCl_5$ and $SnCl_2$ powders are fed into a vaporizer, and the rate of feed is controlled by a vibrator. Although the Nb_3Sn resultant layer has an Nb to Sn ratio of 3 to 1, the halide powders have to be introduced in the ratio of 1 Nb to 1 Sn in the vapor to achieve the correct stoichiometry in the deposit. Other ratios of the metal chloride gases produce deposits containing either excess Nb (7 Nb:3 Sn yields a deposit containing 79% Nb) or free Sn (3 Nb:7 Sn). In this process, the furnace and the substrate temperature are the same, 900°C, since the insulating substrates cannot be conveniently heated to temperatures greater than their surroundings as can a metallic ribbon. Ultrapure H_2 from a palladium diffuser is passed counterstream to the halides and results in Nb_3Sn deposited in a zone about 3 inches long according to the following reaction:

$$3NbCl_5 + SnCl_2 + 8.5H_2 \rightarrow Nb_3Sn + 17HCl$$

Polycrystalline Nb_3Sn deposits ranging from 0.5 to 5 mils thick can be

prepared on either flat or cylindrical substrates. Single-crystal whiskers sometimes also grow at spontaneous nucleation sites.

Initially, the vapor growth of Nb_3Sn on a continuous length of metal ribbon[4] utilized the reaction between chlorine and presintered Nb_3Sn as the source of metal chlorides. During deposition, the moving ribbon was resistance heated to about 1000°C while the furnace temperature

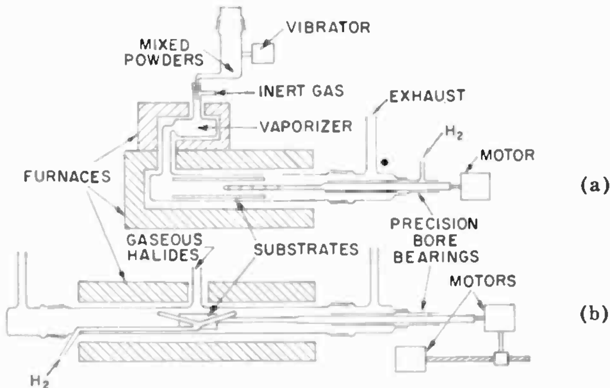

Fig. 1—(a.) Apparatus for vapor deposition of Nb_3Sn on flat surfaces and (b.) apparatus for vapor deposition of Sb_3Sn on cylinders.

was maintained at about 700°C. In this case some additional HCl was introduced along with the metal chlorides to prevent the formation of $NbCl_3$ and Nb_3Sn on the walls of the apparatus. This permitted continuous operation for times as long as 90 hours, so that ribbons coated with Nb_3Sn as long as 1000 meters could be produced.

The clorination of elemental Sn and Nb metal sources has subsequently been adopted for the production of long lengths of Nb_3Sn-coated ribbon. The apparatus used in this method is shown in Fig. 2. High-purity Nb metal bars and molten Sn are reacted with Cl_2 at 900°C and 800°C, respectively, to form the metal chlorides, and these are introduced directly into the deposition chamber, thereby avoiding problems related to the handling of hygroscopic chloride powders. H_2 and HCl are also introduced into the deposition chamber where reduction to Nb_3Sn takes place according to the reaction shown in Fig. 2. The reaction products, HCl, and excess reactant gases are vented at the opposite end of the chamber. The ribbon moves in a direction opposite to the gas flow, and the speed determines the deposit thickness, e.g., ¼ μm/side at 15 m/hr and ½ μm/side at 7 m/hr. The equilibrium constant for the

reaction increases with temperature.[5] Therefore, the ribbon is heated to a higher temperature than the reaction tube in order to produce a deposit of sufficient thickness on the ribbon while the furnace is maintained at 700°C to keep the incoming metal chlorides volatile and to suppress Nb_3Sn deposition on the tube walls. The ribbon temperature

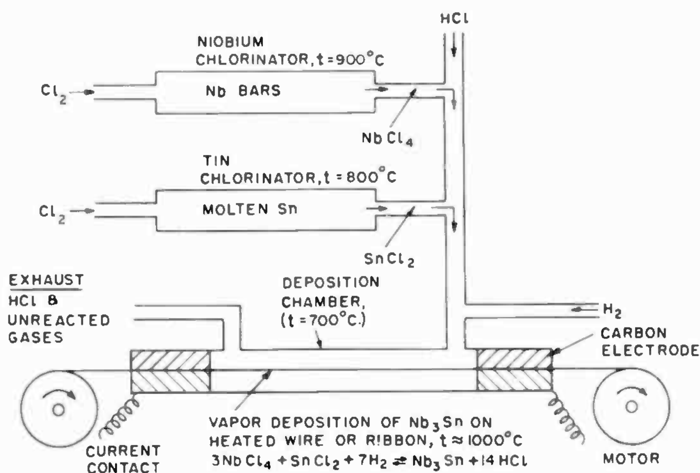

Fig. 2—Apparatus for continuous vapor deposition of Nb_3Sn on metallic ribbon and wire.

somewhat affects the composition of the Nb_3Sn layer. Higher ribbon temperatures result in Nb-rich deposits (76.1% Nb) while lower temperatures achieve nearly stoichiometric composition (75.1% Nb) when an Nb:Sn chloride ratio of 1:3 to 1:4 is used.[5] For the preparation of Nb_3Sn alloys containing Bi, Mo, Si, Ta, Ti, and V, a separate chlorination chamber parallel to the Nb chlorinator at 900°C was used.[13] To dope the Nb_3Sn to achieve a high I_c, various gasese were introduced along with the metal chlorides and H_2. For these studies, gases such as CO_2, CO, C_2H_6, C_3H_8, N_2O_2, SO_2, N_2O, and BCl_3 were used.[13,14]

3. Properties of Vapor deposited Nb_3Sn and Nb_3Sn Alloys

3.1 Physical Properties

Single-phase Nb_3Sn can be vapor deposited over a range of compositions by both the static (Fig. 1) and the continuous (Fig. 2) processes. This range includes from the stoichiometric ratio (75% Nb) to Nb-rich (82.3% Nb) with a corresponding range in the lattice parameter from

5.290 to 5.282 Å. As discussed in a later section, the highest T_c is observed for stoichiometric material. The stoichiometric material is from 98.8 to 100% of the theoretical density,[5] and the Nb_3Sn layer grows with a columnar structure that is perpendicular to the substrate surface. The average coefficient of thermal expansion[5] over the temperature range from 25° to 700°C is 9.8×10^{-6}/°C.

3.2 Superconducting Properties

T_c

The superconducting transition temperature is given as a function of composition in Fig. 3.[5] Here it may be seen that the highest T_c occurs

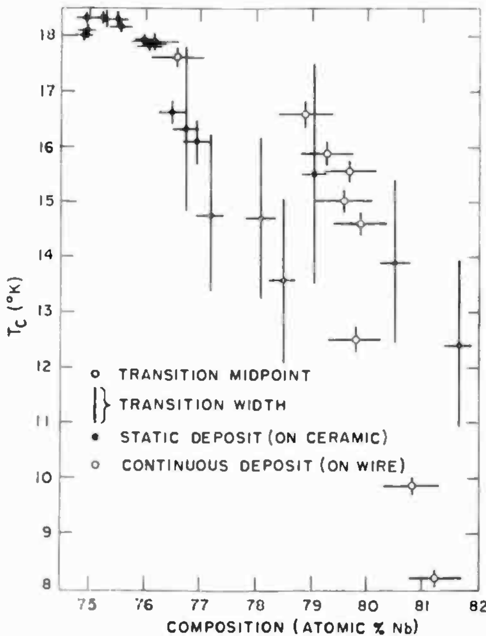

Fig. 3—Transition temperature as a function of composition for vapor-deposited Nb_3Sn.

for near stoichiometric Nb_3Sn and that excess Nb decreases T_c to values as low as 8°K. Therefore, the vapor-grown layers should be prepared as close as possible to 75 atomic percent Nb, and this requires careful adjustment of the Nb:Sn chloride vapor ratio.

Stress in the Nb_3Sn can also affect T_c. For example, it was found that an 80,000 psi compressive longitudinal stress, as is produced in the

Nb_3Sn on Hastelloy on cooling to room temperature from the deposition temperature, can reduce the T_c by 0.9°K.[6] On the other hand, Nb_3Sn on ceramic is not stressed on cooling to room temperature because of the close match of the CTE of the layer and the substrate; accordingly, the T_c is 18.31°K, about the maximum observed for stoichiometric Nb_3Sn.[16]

The T_c can be influenced also by the dopant that is used to enhance the current-carrying ability of the Nb_3Sn-coated ribbon, by alloying elements added to the Nb_3Sn, and by diffusion of elements from the substrate into the vapor-grown Nb_3Sn layer. The addition of CO_2 to Nb_3Sn on Hastelloy reduces the T_c to 14.65°K from 16.4°K observed for a comparable, undoped Nb_3Sn ribbon.[13] For ribbon containing small amounts of alloying elements in addition to the CO_2 dopant, T_c values range from 13.85°K (Si) to 16.25°K. (Ta).[13] The high-magnetic-field properties of these alloys are discussed in a later section.

I_c

As mentioned previously, the I_c is an important parameter in the construction of superconducting magnets. Accordingly, the effects on I_c in vapor-grown Nb_3Sn of various dopant additions,[13, 14] orientation within the magnetic field,[17-19] and defects[20-22] such as induced by a fast neutron flux, have been examined. The addition of CO_2, CO, and N_2 gases to the gas stream during vapor growth of Nb_3Sn ribbon has been shown to be effective in increasing the critical current by a factor of up to 5, as shown in Fig. 4, compared to undoped ribbon.[13,14] In addition, doping gases such as C_2H_6 and C_3H_8 have been found that are equally effective[14] in enhancing the I_c, while others have been found to degrade the critical currents. The current-carrying capacity of Nb_3Sn vapor deposited on a ceramic substrate can be increased very substantially by the introduction of structural defects resulting from neutron irradiation[20-22] without seriously degrading T_c.[16] It was found that the change in I_c per unit of neutron flux is a function of the initial perfection of the material. Thus, the more perfect samples with initially lower values of I_c were improved by factors of up to 15 (to $JH = 18 \times 10^6$ kGA/cm^2) while for the less perfect high initial I_c samples, the increase in I_c is a factor of only about 2 (to 9.7×10^6 kGA/cm^2) for neutron fluxes on the order of 1×10^{18} neutrons/cm^2. Higher dosages subsequently decrease I_c as does annealing at elevated temperatures. During neutron irradiation the metallic alloy substrates become quite radioactive compared to the magnesium silicate substrates. Consequently, neutron irradiation is impractical for Nb_3Sn deposited on a Hastelloy ribbon substrate, and therefore doping with impurity gases is the preferred method of in-

troducing defects to increase I_c. To avoid erratic behavior and thereby increase the stability of the current in applied magnetic fields, the Nb_3Sn on Hastelloy ribbon must be plated with a normal metal conductor such as Cu or Ag for both short sample tests and magnet applications.[23,24]

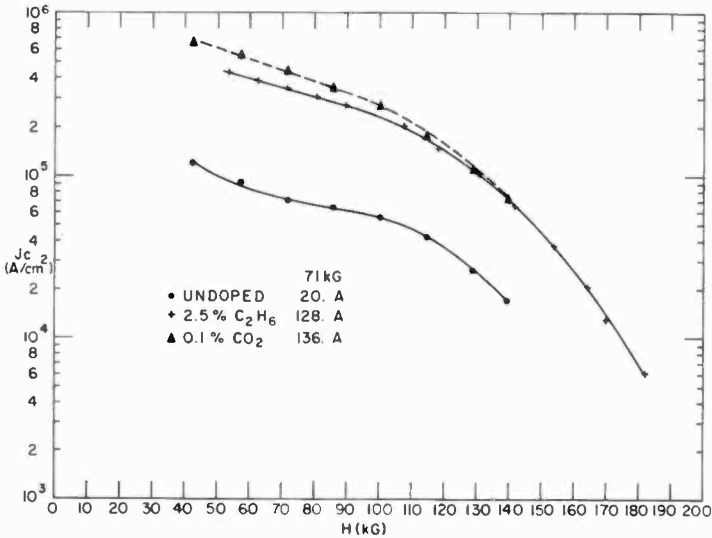

Fig. 4—Critical current density as a function of applied magnetic field for undoped, CO_2-doped, and C_2H_6-doped Nb_3Sn ribbon.

The dependence of I_c on the applied magnetic field in fields above 100 kG is of importance when considering Nb_3Sn ribbons for use in magnets capable of attaining fields as high as 150 kG in the center of the air core since the local field at the windings can reach fields as high as 170 kG. As can be seen from Fig. 4, I_c decreases rapidly in the region 100 to 170 kG. Therefore, special attention had to be directed towards increasing I_c in this range, and a number of approaches were taken[13] to solve this problem. The most satisfactory, simplest, and direct method found was to increase the thickness of the Nb_3Sn layer by a factor of about two.[13] In this way, the last-grown Nb_3Sn is far enough away from the Hastelloy interface so that the H_{c_2} of the material is high enough to allow a substantial resistanceless current to flow at the highest fields; Nb_3Sn near the interface has a lower H_{c_2} and a lower I_c at a given value of H because of diffusion of metallic alloying elements from the Hastelloy ribbon during growth.

The angular dependence of I_c on the magnetic field has been studied in some detail,[17-19] and it has been found that transport behavior in Nb_3Sn on ceramic substrates is in good agreement with the Lorentz-force flux-creep model.

H_{c_2}

The upper critical field at 4.2°K for Nb_3Sn has been found to be as high as 225 kG for Nb_3Sn produced both by the static process and the continuous process. In the former, the Nb_3Sn is grown on a ceramic substrate[8] while for the latter, this high value is only achieved when the Nb_3Sn is deposited on an Nb substrate.[13] Deposition of the same amount of Nb_3Sn on Hastelloy reduces H_{c_2} to about 195 kG, but this can be increased to 211 kG by increasing the thickness of the Nb_3Sn layer.[13] As noted previously, the thicker deposit results in a significantly increased I_c at the higher magnetic fields. Addition of alloying elements to the Nb_3Sn also affects H_{c_2}; Mo reduces H_{c_2} to about 140 kG, while Si increases H_{c_2} to 225 kG.[13]

Other superconducting parameters have also been examined for Nb_3Sn samples, including the penetration depth,[25] the energy gap,[26] the lower critical field,[27] and the specific heat.[15]

3.3 Microstructure

As noted previously, I_c is a strong function of the dopant gas additions. To try to understand the mechanism of this enhancement, several methods of materials characterization were employed including x-ray diffraction, electron microprobe analysis, optical microscopy, transmission electron microscopy (TEM), and radioactive tracer analysis. Examination of the subgrain size as a function I_c for Nb_3Sn ribbons doped with several different gases[14,28] showed that the subgrain size decreases from about 1500 Å for an undoped sample with low I_c to about 380 Å for samples with nearly optimum I_c values (i.e., about 5 times higher). Thus, it appears that the subgrain boundaries are the principal agents pinning the flux lines and thus serving to increase I_c. The role of the dopant gas was further examined by substituting radioactive CO_2 for the CO_2 source normally employed. Here it was determined that carbon does enter the Nb_3Sn during vapor growth and that a near optimum concentration of carbon in the Nb_3Sn layer is about 2000 ppm.[13] Further, since the solubility limit of carbon in Nb_3Sn is about 200 ppm, most of the carbon in excess of the solubility limit is present as a second phase, probably as NbC, that most likely resides on the subgrain boundaries.[13]

The oxygen associated with the CO_2 does not take part in the I_c enhancement since C_2H_6 has been found to be equally effective. TEM of Nb_3Sn thinned to less than 2000 Å shows the presence of grain boundaries and a second phase.[29]

Unlike the clean interface noted for Nb_3Sn on ceramic, the interface between the Nb_3Sn and the Hastelloy is a complex region consisting of Ni_3Sn, $NbNi_3$, and a molybdenum-rich phase.[13] That these phases should form is not surprising, since Nb, Sn, Ni, and Mo are present in large amounts in close proximity to one another. In addition to the formation of intermediate phases, Ni and Fe diffuse into the Nb_3Sn layer. Thus, it is probably a combination of the intermediate phases and alloy interdiffusion zones that decrease H_{c_2} for Nb_3Sn on Hastelloy compared to vapor-grown Nb_3Sn on Nb or ceramic.

4. Device Applications

Vapor-deposited Nb_3Sn has found use at RCA in commercial production of high-field superconducting solenoids. The fields of interest are primarily in the range of 100 kG and higher, because at lower fields less expensive alloys such as NbTi can be used. The use of vapor-deposited ribbon in magnets presented many technical problems to be overcome. Paramount among these problems was the so-called "degradation" of the current-carrying capacity of the superconductor when used in long lengths in the construction of sizable magnets. This puzzling problem was overcome by plating or cladding the superconductor with highly conductive normal metals such as silver or copper.

Among superconducting ribbons and magnets offered commercially by RCA[30] are the six-inch bore magnet built for NASA that achieved a test field of 140 kG (Fig. 5); a 150-kG 1.5-inch-bore magnet; 100-kG, split-coil, 2.5-inch-bore magnets with optical path access; concentric coils for multipurpose use; and others. RCA superconducting ribbon has also been used by other manufacturers of magnets and by private institutions to build special solenoids. Significant special designs include dipole and quadruple magnets built by several national laboratories[30] for use in particle accelerators and doughnut-shaped, 20- and 36-inch-bore magnets for plasma research purposes.[31]

Another interesting application developed at RCA is a superconducting cylinder consisting of a multitude of superconducting rings of Nb_3Sn vapor deposited on metallic substrates.[32] This is a 1-inch-diameter cylinder (Fig. 6) capable of either shielding or trapping a magnetic field of 60 kG in its 0.2-inch annulus; for its size it is the strongest magnet ever built. As the field strength per unit volume, field grad-

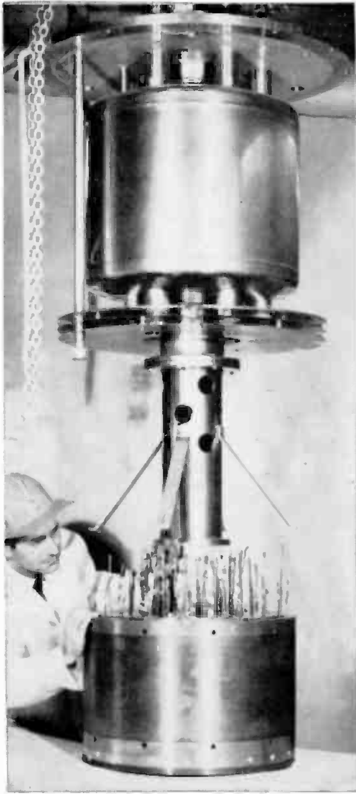

Fig. 5—140-kilogauss, 6-inch-bore magnet fabricated from about 55 miles of Nb_3Sn ribbon.

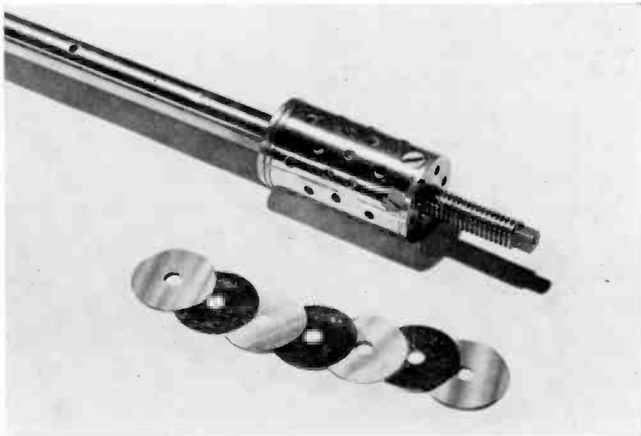

Fig. 6—60-kilogauss, 0.2-inch-bore magnet fabricated from numerous rings of Nb_3Sn vapor deposited on platinum strip.

ient, and stability of such a device exceed those of any other magnet device, similar cylinder devices made by RCA were successfully used in the construction of an experimental electron microscope magnetic lens having a resolution superior to that of normal magnet lenses.[33]

The foregoing magnet devices can be classified as laboratory test instruments that require relatively modest amounts of the vapor-deposited material. Large-scale use is envisioned in power-generating equipment that is under development and in electric power lines, which are believed to be technically and economically feasible.

5. Conclusions

A review is given of several variations of a chemical vapor-deposition process for Nb_3Sn based on the hydrogen reduction of niobium and tin chlorides. These methods are used for preparing Nb_3Sn in forms including single crystals, and polycrystalline films on ceramic or metal substrates, particularly long lengths of ribbon. Growth techniques have been described that make this material available in highly perfect, nearly dislocation-free material suitable for basic studies of properties needed for theoretical work and heavily doped material with maximum concentration of defects necessary for flux pinning and high-current-carrying capability in high-field solenoid applications. This technology has culminated not only in the construction of the highest field superconducting magnets to date, but also in a successful commercial product.

References:

[1] W. D. Coles, E. R. Schrader, and P. A. Thompson, "A 14-Tesla 15-cm Bore Superconductive Magnet," **Advances in Cryogenic Engineering**, Vol. 13, Plenum Press (1968) p. 142.

[2] E. Buehler, J. H. Wernick, K. M. Olsen, F. S. L. Hsu, and J. E. Kunzler, "Preparation and Properties of Cored Wire Containing Nb_3Sn and V_3Ga," p. 105 in **Metallurgy of Advanced Electronic Materials**, G. E. Brock, Ed., Interscience Publishers, New York (1963).

[3] C. L. Kolbe and C. H. Rosner, "Processing and Superconducting Properties of Nb_3Sn Wires," p. 17 in **Metallurgy of Advanced Electronic Materials**, G. E. Brock, Ed., Interscience Publishers, New York (1963).

[4] J. J. Hanak, "Vapor Deposition of Nb_3Sn," p. 161 in **Metallurgy of Advanced Electronic Materials**, G. E. Brock, Ed., Interscience Publishers, New York (1963).

[5] J. J. Hanak, K. Strater, and G. W. Cullen, "Preparation and Properties of Vapor-Deposited Niobium Stannide," **RCA Review**, Vol. 25, p. 342 (1964).

[6] R. E. Enstrom, "Residual Stresses in Nb_3Sn-Coated Stainless Steel Ribbon," **Phenomenon of Superconductivity**, Technical Report AFML-TR-65-169, prepared by RCA Laboratories, June 1965, p. 223.

[7] H. C. Schindler and F. R. Nyman, "Electromagnetic Performance of Niobium-Stannide Ribbon," **RCA Review**, Vol. 25, p. 570 (1964).

[8] G. W. Cullen, "Preparation and Properties of Niobium Stannide on Insulating Substrates," **Trans. Met. Soc. AIME**, Vol. 230, p. 1494 (1964).

[9] J. J. Hanak and H. S. Berman, "The Growth of Single Crystals of Nb_3Sn by Chemical Transport," p. 249 in **Crystal Growth**, H. S. Peiser, Ed., Pergamon Press, New York (1966).

[10] R. Mailfert, B. W. Batterman, and J. J. Hanak, "Low Temperature Structural Transformation in Nb_3Sn," **Physics Letters,** Vol. 24A, p. 315 (1967); and R. Mailfert, B. W. Batterman, and J. J. Hanak, "Observations Related to the Order of the Low Temperature Transformation in V_3Si and Nb_3Sn," **Physica Status Solidi,** Vol. 32, p. K67 (1969).

[11] W. Rehwald, "Lattice Softening and Stiffening of Single Crystal Niobium Stannide at Low Temperatures," **Physics Letters,** Vol. 27A, p. 287 (1968); and K. R. Keller and J. J. Hanak, "Ultrasonic Measurements in Single Crystal Nb_3Sn," **Phys. Rev.,** Vol. 154, p. 628 (1967).

[12] R. W. Cohen, G. D. Cody, and J. J. Halloran, "Effect of Fermi-Level Motion on Normal-State Properties of β-Tungsten Superconductors," **Phys. Rev. Letters,** Vol. 19, p. 840 (1967).

[13] R. E. Enstrom and J. Appert, "Superconductors," U.S. Patent No. 3,484,208, issued Dec. 16, 1969; also R. E. Enstrom and J. R. Appert, to be published.

[14] R. E. Enstrom, J. J. Hanak, F. R. Nyman, and K. Strater, "Method of Coating Superconducting Niobium Tin with Lattice Defects," U.S. Patent No. 3,400,016, issued Sept. 3, 1968; also R. E. Enstrom, J. J. Hanak and J. R. Appert, to be published.

[15] L. J. Vieland and A. W. Wicklund, "Specific Heat in Niobium Tin," **Phys. Rev.,** Vol. 166, p. 424 (1968).

[16] J. L. Cooper, "Transition Temperature of Niobium Stannide," **RCA Review,** Vol. 25, p. 405 (1964).

[17] G. W. Cullen, G. D. Cody, and J. P. McEvoy, "Field and Angular Dependence of Critical Currents in Nb_3Sn," **Phys. Rev.,** Vol. 132, p. 577 (1963).

[18] G. D. Cody, G. W. Cullen, and J. P. McEvoy, "Field and Angular Dependence of Critical Currents in Nb_3Sn II," **Rev. Mod. Phys.,** Vol. 36, p. 95 (1964).

[19] G. D. Cody and G. W. Cullen, "Critical Currents and Lorentz-Force Model in Niobium Stannide," **RCA Review,** Vol. 25, p. 466 (1964).

[20] G. W. Cullen and R. L. Novak, "Effect of Neutron-Induced Defects on the Current-Carrying Behavior of Nb_3Sn," **Appl. Phys. Letters,** Vol. 4, p. 147 (1964).

[21] G. W. Cullen, R. L. Novak, and J. P. McEvoy, "Effect of Neutron-Induced Defects on the Current-Carrying Behavior of Niobium Stannide," **RCA Review,** Vol. 25, p. 479 (1964).

[22] G. W. Cullen and R. L. Novak, "Effect of Neutron-Induced Defects on the Current-Carrying Behavior of Vapor-Deposited Niobium Stannide," **J. Appl. Phys.,** Vol. 37, p. 3348 (1966).

[23] H. C. Schindler and F. R. Nyman, "Electromagnetic Performance of Niobium Stannide Ribbon," **RCA Review,** Vol. 25, p. 570 (1964).

[24] E. R. Schrader and F. Kolondra, "Analysis of Degradation Effects in Superconductive Niobium Stannide Solenoids," **RCA Review,** Vol. 25, p. 582 (1964).

[25] G. D. Cody, "The Superconducting Penetration Depth of Niobium Stannide," **RCA Review,** Vol. 25, p. 414 (1964).

[26] G. D. Cody, Y. Goldstein, and R. Cohen, "The Superconducting Energy Gap of Niobium Stannide," **RCA Review,** Vol. 25, p. 433 (1964).

[27] R. L. Hecht, "Lower Critical Field of Niobium Stannide," **RCA Review,** Vol. 25, p. 453 (1964).

[28] J. J. Hanak and R. E. Enstrom, "Flux Pinning in Nb_3Sn by Grain Boundaries," **Proc. Tenth International Conf. on Low Temperature Physics,** Vol. IIB, Moscow, USSR (1967), p. 10.

[29] M. C. Inman, "Examination of As-Grown and Neutron-Irradiated Nb_3Sn Single Crystals by Transmission Electron Microscopy," **Phenomenon of Superconductivity** (Phase II), Oct. 1966, prepared by RCA Laboratories, Princeton, N. J., for Air Force Materials Laboratory, Wright-Patterson Air Force Base, Ohio, p. 56.

[30] R. B. Britton, "Brookhaven Superconducting dc Beam Magnets," **Proc. 1968 Summer Study on Superconducting Devices and Accelerators,** Brookhaven National Laboratories, July 1968, p. 893.

[31] J. File, G. D. Martin, R. G. Mills, and J. L. Upham, "Princeton Floating Multipole-Superconducting Ring Progress," **J. Appl. Phys.,** Vol. 40, p. 2106 (1969); and J. File, G. D. Martin, R. G. Mills, and K. E. Wakefield, "Operation of a Levitated Superconducting Ring in a Plasma Physics Experimental Device," in print, **J. Appl. Phys.**

[32] J. J. Hanak, "Magnetization of Nb_3Sn Films in Transverse Fields," **RCA Review,** Vol. 25, p. 551 (1964).

[33] N. Kitamura, M. P. Schulhof, and B. M. Siegel, "Superconducting Lens for Electron Microscopy," **Appl. Phys. Letters.** Vol. 9, p. 10, 377 (1966).

Deposition and Properties of Silicon Dioxide and Silicate Films Prepared by Low-Temperature Oxidation of Hydrides

Werner Kern and A. W. Fisher
RCA Laboratories, Princeton, N.J.

Abstract—The deposition of pure and doped silicon dioxide and binary glass films based on the controlled gas-phase oxidation of diluted silane, diborane, and phosphine is described. Simultaneous oxidation of the hydrides and aluminum or zinc alkyls yield binary and ternary alumino and zinc glasses. The effects of system variables in the temperature range of 250° to 500°C are discussed. Chemical, dielectric, thermal, and optical properties of the various films and their applications in semiconductor device technology are reviewed, with particular emphasis on doped oxide diffusion sources and borosilicate glasses for silicon device passivation and sealing.

1. Introduction

Pure silicon dioxide, doped silicon dioxide, and silicate glass films deposited by chemical vapor reactions are extensively used in the fabrication of semiconductor devices.[1,2] Principal applications of these dielectric films are (a) surface protection and masking, (b) solid-to-solid diffusion sources, (c) electrical insulation and isolation of micro-circuit components, (d) dielectric layers for multilayer metallization, and (e) surface and junction passivation.

Both organic and inorganic source materials have been employed to deposit these dielectrics by either pyrolytic decomposition or chemical synthesis techniques. These are based on either high-temperature (600°-1200°C) or low-temperature (250°-500°C) gas-phase reactions.

The deposition of silicon dioxide films by pyrolysis of tetraethyl siloxane at 740°C is a typical high-temperature process.[3] The addition of volatile organoboron or organophosphorus compounds to this silicon ester yields doped oxide layers suitable for diffusion sources.[4] Simultaneous pyrolytic oxidation at 730°C of tetraethyl siloxane and trialkyl borates or phosphates yields borosilicate and phosphosilicate films, as described in previous papers.[5] The synthesis of high-quality lead sili-

cate and lead borosilicate glasses is achieved by incorporating tetraethyl lead in the vapor mixture, followed by a thermal densification treatment of the films.[5] Hydrolysis of silicon tetrachloride at 1200°C,[6] or of silicon tetrabromide with carbon dioxide at 800°-850°C,[7] yields vitreous silicon dioxide films. Aluminosilicates can be formed similarly from silicon tetrachloride and aluminum trichloride in the temperature range of 900°-1200°C.[8] Oxidation of silane with oxygen at 750°-1050°C,[9] or with carbon dioxide at 700°-1000°C,[10] can also be used for depositing silicon dioxide layers. The major drawback these processes have in common is the relatively high temperature required for the deposition. This condition is undesirable, and in many cases unacceptable, for device processing for several reasons.

Chemical vapor deposition by controlled oxidation of gaseous metal hydrides (silane, diborane, phosphine, arsine, germane) is thermochemically and kinetically more advantageous as it allows deposition at much lower temperatures (250°-500°C), eliminating a number of restrictions. Furthermore, processing is simplified and can be readily adapted for the coating of several semiconductor substrate wafers simultaneously. The present paper summarizes and references the techniques, and briefly reviews important reaction parameters as well as properties and applications of the resulting silicon dioxide, doped oxide, and silicate glass films.

2. Deposition Techniques

2.1 Deposition Apparatus

Several deposition systems designed especially for coating semiconductor wafers by hydride oxidation reactions have been built at RCA.[5,11] These consist essentially of a heated gear assembly that rotates substrates, preferably in planetary fashion, in a controlled atmosphere chamber. A commercial high-temperature hotplate with thermostatic control is used to attain substrate temperatures up to 500°C. An opening between the glass chamber and the hotplate surface serves as exit for the spent gases. The apparatus (Fig. 1) is capable of reproducibly depositing uniform films simultaneously on three semiconductor substrate wafers of up to 1.5 inches in diameter. A complete description of the equipment has been published previously,[12] and a schematic of the gas distributing and metering systems has also been presented.[2,12-15]

2.2 Silicon Dioxide films

Silane reacts exothermically with oxygen by a stepwise free radical mechanism leading to SiO_2 and H_2O as end products.[16] Under the

proper conditions, silane gas can be oxidized to form continuous, uniform silicon dioxide films at low temperatures.[17,5] A detailed description of the conditions required for the safe, controlled oxidation of silane in the temperature range of 250°-550°C in various deposition systems has been presented in a previous paper.[11] Nitrogen is used as a diluent. The N_2/SiH_4 ratio is kept relatively large to suppress homogeneous gas phase nucleation that would lead to colloidal SiO_2 coatings.

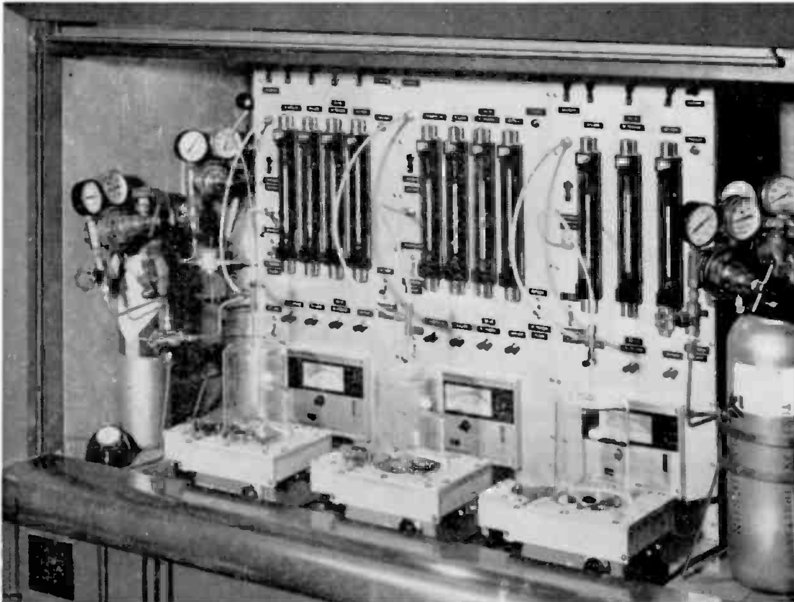

Fig. 1—System for depositing layers of pure silicon dioxide, doped oxides, and silicate glasses from the hydrides.

Film deposition rate increases linearly with increasing silane input so long as excess oxygen is present in the system. The deposition rate increases sharply with increasing temperature. However, this temperature dependence can be modulated by varying the O_2/SiH_4 ratio. For example, at an O_2/SiH_4 ratio of 3:1 the deposition rate remains nearly constant over the temperature range of 300°-350°C. This temperature independence is an important consideration in the practical application of the process. A temperature of 325°C is usually employed. The deposition rate above 350°C keeps increasing with rising temperature, but a larger excess of oxygen is required for optimum film growth. For example, at 475°C a constant maximum deposition rate of typically 3000 Å/min is attained with an O_2/SiH_4 ratio between 14:1

and 33:1. These results have been corroborated by workers at RCA and elsewhere, even for deposition systems of different geometry.[18] To simplify the flow controls, premixing of the SiH_4-N_2-O_2 can be employed if the SiH_4 concentration is kept below 0.8% to prevent reaction at room temperature.[19] Nozzle-type reactor designs[17,20] have also been described that can be readily optimized for continuous film deposition.[21]

2.3 Doped Silicon Dioxide Layers as Diffusion Sources

Doped silicon dioxide films have been prepared by simultaneously reacting silane and a suitable hydride such as diborane or phosphine to form a silicon dioxide deposit containing B_2O_3 or P_2O_5, respectively.[22-25]

The gaseous reactants used included silane diluted in argon, phosphine diluted in argon, diborane diluted in argon, or, alternatively, appropriate mixtures of silane and dopant (either phosphine or diborane) diluted in argon. The use of separate cylinders of silane and dopant allows one to prepare doped oxides having any desired doping level. If separate hydrides are used, each gas must be accurately metered individually into the reaction chamber.

When one doping level is used repeatedly, it is desirable to have the silane and dopant contained in one cylinder. With such premixed gases diffusion results are more controllable and the operation of the apparatus is simplified since careful control over flow rates is not as important as when separate cylinders are employed. Depositions are carried out at $325°C \pm 15°$ using 7000 cm^3 of nitrogen per minute to dilute 10 to 20 cm^3 of hydride. The ratio of oxygen to silane is kept at 3:1.

For phosphorus-doped oxide layers, the oxide composition is not affected appreciably by changes in the deposition temperature over a range of 270° to 380°C. The diffusion results obtained from oxides prepared at these different temperatures are equivalent, even though the deposition rate varies somewhat.

For boron-doped oxide layers, only oxides with high concentrations of boron oxide, i.e., capable of yielding surface concentrations of 2×10^{20} atoms/cm^3, yielded diffusion results that were independent of deposition temperature. Boron-doped layers capable of giving surface concentrations of 5×10^{18} atoms/cm^3 had to be deposited at 325°C $\pm 15°$ to maintain good control over the diffusion results.

A study of hydride oxidation reactions pertinent to doped oxide has been reported recently,[26] and a model for the diffusion of dopants from a deposited oxide source into a semiconductor substrate has been discussed.[27,28]

2.4 Silicate Glasses

The incorporation of substantial amounts of diborane or phosphine in the reactant gas stream leads to borosilicate or phosphosilicate films, respectively. Ternary glass compositions can be synthesized by simultaneous gas phase oxidation of silane, diborane, and metal alkyls.[13-15]

A complete description of these systems has been published recently.[15] The salient features can be summarized as follows. The reaction of hydrides, or mixtures of hydrides and metal alkyl vapors, with oxygen at 275°-475°C in the 3-gear planetary rotary reactor[12] has been used for the deposition of glass films. Reactants were silane, diborane, phosphine, trimethyl aluminum, diethyl zinc, and oxygen. Nitrogen and argon were the carrier gases. Glass compositions that can be deposited include borosilicates, phosphosilicates, aluminosilicates, zinc silicates, aluminoborosilicates, zinc borosilicates, and phosphoborosilicates.

A detailed study of the deposition parameters for binary borosilicates synthesized from silane, diborane, and oxygen has led to the following conclusions: (1) the molar boron/silicon ratio in the deposited films is lower than that in the reactant gas; (2) the oxygen/hydride ratio should be at least 20:1 to assure complete oxidation of the hydrides; (3) starting at 280°C, the deposition rate of borosilicate films increases steeply as the substrate temperature is increased to 375°, but the rate declines with a further temperature increase because of the formation of powdery deposits on the reactor walls (Fig. 2); (4) the distribution of glassy substrate deposit and reactor wall deposit can be affected by varying the deposition parameters (Fig. 3); (5) the deposition temperature also affects the composition of the glass films, the boron content in the glass decreasing with decreasing temperatures, especially below 400°C; (6) the film deposition rate up to 3000 Å/min increases linearly with the hydride concentration in the feed stream (Fig. 4); (7) the glass films grow linearly with time to a thickness of at least 40 μm (Fig. 5); (8) borosilicate glasses with a high silica content that are difficult to prepare homogeneously by conventional ceramic techniques (because of their high viscosity and liquidus temperature) can be readily prepared.

For phosphosilicate films containing up to 5 mol% P_2O_5, the deposition from silane, phosphine, and oxygen at 400°C proceeds stoichiometrically, but at higher concentrations the yield of phosphorus oxide diminishes.

The simultaneous gas phase oxidation at 450°-475°C of trimethyl aluminum or diethyl zinc vapor with the silane or silane–diborane yields aluminosilicate, zinc silicate, aluminoborosilicate, or zinc borosilicate compositions.

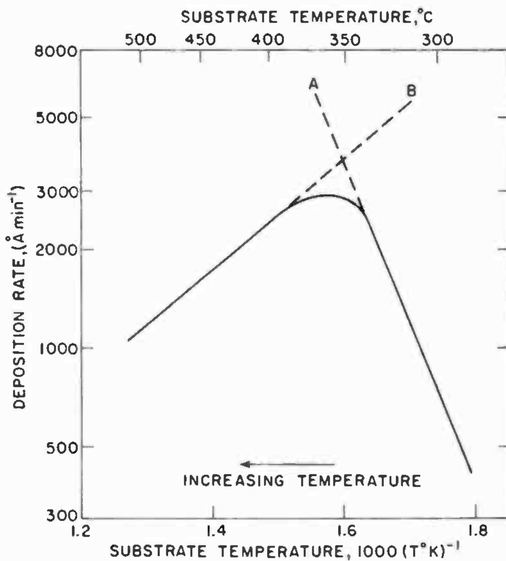

Fig. 2—Borosilicate glass deposition rate as a function of substrate temperature. Curve A increases with temperature; curve B decreases due to the formation of wall deposits.

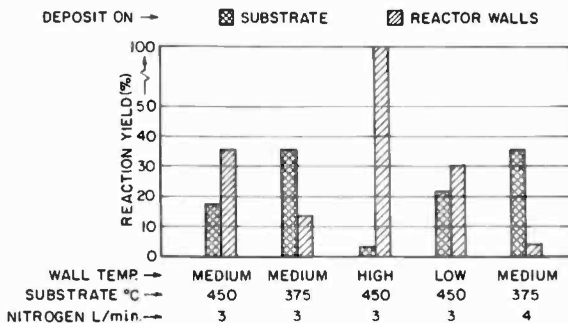

Fig. 3—Distribution of borosilicate reaction products on the substrate (always glassy deposits) and the reactor walls (usually powdery deposits) shown as a function of several critical deposition conditions.

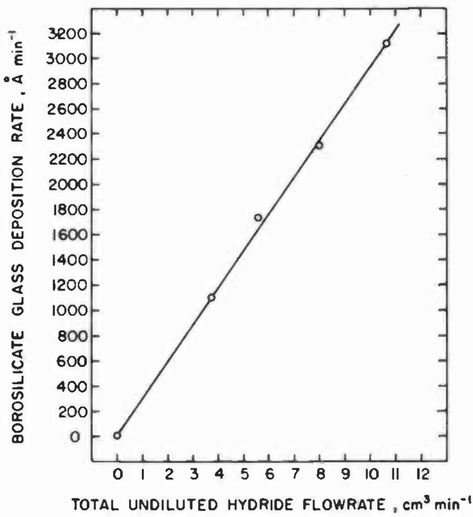

Fig. 4—Borosilicate glass deposition rate as a function of undiluted, combined silane and diborane flow rate of fixed ratio.

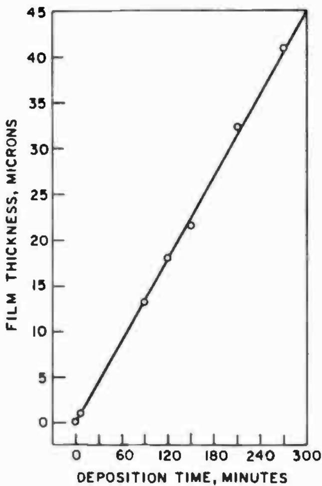

Fig. 5—Film thickness of borosilicate glass on silicon substrates as a function of deposition time.

3. Characteristics of the Films

3.1 Silicon Dioxide

Films deposited by silane oxidation are glassy and amorphous, like most deposited silica films. The deposition rate and the structural integrity of the films are strongly influenced by the nature of the substrate surface.[11,18] The deposition of a 1,500 to 3,000 Å layer serves as a very sensitive test for the cleanliness of a silicon wafer surface and can be used to monitor the relative effectiveness of various surface cleaning treatments.[29,30] Improper precleaning of the silicon results in film defects in the deposit such as non-uniform thickness, pinholes, and particulate contaminants. On properly cleaned wafers, the films are uniform across the entire surface of a 1.5-inch-diameter silicon wafer, 6,000 ± 200 Å being a typical example. The porosity of the films is considerably greater than that of thermally grown silicon dioxide films, as indicated by the high etch rate. Heat treatment for a few minutes at typically 800°C[11] or longer treatments (several hours) at 450°C in the presence of water vapor as catalyst[31,32] leads to a densification approaching that of the best thermally grown oxides.[33,34] Additional important properties of the films relevant to device fabrication have been presented in the original paper.[11] Other investigators have reported in detail on electrical and interface properties[18,33,34] mechanical stress behavior,[35] and pinholes,[36] etch rates,[9,33] and application to devices.[34] In general, the densified films obtained on silicon wafers are comparable in their properties to those normally found for oxides thermally grown on silicon.

3.2 Doped Silicon Dioxide Layers

Phosphorus-doped silicon dioxide films have been prepared from diluted gas mixtures having phosphine concentrations of 0.01 to 50 mole% of phosphine in silane. These diffusion sources yielded sheet resistivities of 1600 to 1.5 ohms/square when diffused into 1-2 ohm-cm p-type silicon at 1200°C in a dry nitrogen atmosphere for 1 hour. Assuming an error-function distribution for the dopant, the corresponding surface concentrations ranged from 1.7×10^{17} to 1.4×10^{21} atoms/cm^3 for the different oxide compositions. The reproducibility of sheet resistivity from day to day is about ±10%. Across any wafer the variation is about ±3%. The best diffusion results were obtained in the range of 2×10^{18} to 4×10^{20} atoms/cm^3.

For the preparation of boron-doped silicon dioxide films, gas mixtures with concentration of diborane ranging from 0.005 to 15 mole%

of diborane in silane were used. When these oxides were used as diffusion sources at 1200°C for 1 hour in a nitrogen ambient, sheet resistivities ranged from 10,000 to 1.6 ohms/square when diffused into 1-2 ohm-cm n-type silicon. Control over sheet resistivity was about ±6% on a day-to-day basis in the range of 2×10^{18} to 2×10^{19} atoms/cm^3. For doping levels near 1×10^{20} atoms/cm^3 or greater, variations of ±15% were observed.

A summary of typical surface concentrations resulting from both phosphorus- and boron-doped oxide sources prepared from various silane-to-dopant gas ratios is presented in Table 1.

The doped oxide sources provide a constant level reservoir of dopant for diffusion up to at least 2 hours at 1200°C in nitrogen when 3000 Å of doped oxide are present as the source.

Table 1—Doping Concentrations Resulting From Various Gas Concentrations

Mole Ratio of Silane to Dopant used to Prepare Oxide Sources	Surface Concentration (Atoms/cm^3) from Diffusion into 1-2 ohm-cm silicon at 1200°C in N_2 for 1 hour	
	Phosphorus-Doped Oxide Diffusion Source	Boron-Doped Oxide Diffusion Source
1000:1	4.3×10^{17}	1.9×10^{18}
500:1	1.3×10^{18}	3.4×10^{18}
300:1	1.8×10^{18}	4.6×10^{18}
200:1	3.0×10^{18}	6.5×10^{18}
100:1	5.5×10^{18}	1.1×10^{19}
50:1	1.8×10^{19}	1.8×10^{19}
33:1	3.8×10^{19}	2.6×10^{19}
25:1	4.6×10^{19}	5.0×10^{19}
10:1	3.8×10^{20}	1.4×10^{20}

3.3 Silicate Glasses

Properties relevant to device applications of chemically deposited borosilicate films have been presented in a recent paper.[38] Synthesized under proper conditions, these films have the expected silicate glass structure, as can be shown by infrared absorption and chemical etch rate measurements. The thermal expansion coefficient can be made to match that of

silicon for compositions of typically 17 mole% B_2O_3. The crack-free build-up of several-micron-thick layers glass can be achieved with this composition. A thermal densification treatment is essential to produce stable films of optimum properties; water vapor accelerates the rate of densification significantly, particularly at low temperatures.[32]

The dielectric properties of borosilicate films deposited under a variety of conditions were found to be relatively independent of deposition parameters. For densified films of glasses containing 17-19 mole% B_2O_3, the dielectric values are as follows: dielectric constant, 3.8-4.1; dissipation factor, 0.10-0.15; dc dielectric breakdown field strength sustained, $6\text{-}8 \times 10^6$ V/cm. The electrical stability on life testing of borosilicate glassed planar transistors indicates that the glass layer was effective in preventing moisture penetration. Densified borosilicate films are smooth, uniform, transparent, free of cracks or crazing, resist moisture penetration, and are well suited for silicon device glassing.

The ratios of absorbance of the B-O and the Si-O infrared absorption maxima are related to the glass composition and have been utilized for quantitative film composition analysis.[32,38] The etch rate of borosilicates in specific etchants is a characteristic function of the boron oxide content and can be utilized to check the approximate glass composition. In aqueous HF solutions, the etch rate increases exponentially with increasing boron oxide. In buffered HF, it decreases steeply to a minimum and then increases rapidly with increasing boron oxide concentration due to free B_2O_3. Densification of the films at temperatures from 450° to 800°C lowers the etch rates markedly, indicating an increase of the apparent film density. Densification of borosilicates at 800°C proceeds without weight loss and leads to densities comparable to bulk borosilicate glasses.

The dielectric constant of phosphosilicate films chemically vapor deposited from silane, phosphine, and oxygen did not change on densification, in contrast to all other vapor-synthesized silicate films. The sustained dielectric breakdown field of films as deposited was 8×10^6 V/cm, and remained stable over 3 years of storage in air at room temperature. Phosphosilicates require a protective cover layer because of their hygroscopic nature. Layers up to 25 microns thick were deposited on silicon single-crystal substrates without cracking.

The properties of silicate glasses containing the oxides of aluminum or zinc showed no distinct advantages over the simpler binary borosilicates for passivating silicon devices.

4. Applications

Application of these chemically vapor deposited dielectric films within semiconductor device technology are numerous. Densified silicon dioxide films have high-quality dielectric properties that make them suitable for both passive and active components, for insulation and isolation of microcircuit components, for use as dielectrics in multilevel metallized integrated circuits, and in MOS field-effect transistors. The films are also used for surface protection of sensitive surfaces; for masking during chemical etching of silicon nitride; for masking against diffusion of dopants into a semiconductor substrate; for capping of doped oxide layers to prevent out-diffusion in the ambient; for surface passivating multilayer structures developed for bipolar transistors, integrated circuits, and mesa power devices.

Doped silicon dioxide diffusion sources have been used successfully to prepare emitter and base regions in both n-p-n and p-n-p silicon devices. For less critical applications, such as n^+ and p^+ contact regions for bipolar and MOS transistors, the diffusion sources are also very useful. With doped oxide diffusion sources, the fabrication of complementary devices on one substrate is greatly simplified, since n-type and p-type doped oxide can be selectively deposited onto a given substrate. A single heat treatment can then be used to form both the n- and p-type silicon regions. P-channel enhancement-type MOS transistors have been fabricated successfully by application of these doped oxide sources.[39]

Densified binary borosilicates in conjunction with silicon dioxide top layers are particularly attractive for passivating silicon devices because of their excellent dielectric properties and relative ease of preparation. Lower concentration phosphosilicate compositions are potentially useful for stabilizing bipolar silicon devices and MOS field-effect devices,[37] since they can mask against the migration of sodium ions[40] and can getter impurities from the device surface. However, special precautions must be observed to minimize the well-known electrical polarization effects associated with phosphosilicate glasses.[37,40]

5. Conclusions

The oxidation of diluted silane with oxygen at temperatures of 250°-500°C yields vitreous silicon dioxide films at deposition rates of several thousand angstroms per minute. On clean substrates, the films are of excellent quality, especially after they have been densified by a suitable

heat treatment, and as such have found numerous applications in solid-state device technology.

Doped silicon dioxide layers deposited at 325°C from mixtures of hydrides, either premixed or in separate cylinders, provide uniform, highly reproducible and controllable diffusion sources for the fabrication of silicon devices. Principal advantages of these doped-oxide sources are improved control over dopant concentration, lower sensitivity of the devices to contamination during diffusion, and simplified processing procedures.

Binary and ternary silicate glasses have been synthesized by oxidation of hydride mixtures at typically 450°C, with and without the use of metal alkyls. Densified borosilicate compositions have expansion coefficients matching that of silicon and can be useful in passivating silicon devices.

References:

[1] T. L. Chu, "Dielectric Materials in Semiconductor Devices," **Jour. Vac. Sc. & Technol.**, Vol. 6, p. 25 (1969).

[2] J. A. Amick and W. Kern, "Chemical Vapor Deposition Techniques for the Fabrication of Semiconductor Devices," p. 551, in **Chemical Vapor Deposition,** Second Internatl. Conf.; T. M. Blocher, Jr. and J. C. Withers, Editors; The Electrochem. Soc., Inc., New York 1970.

[3] E. L. Jordan, "A Diffusion Mask for Germanium," **Jour. Electrochem. Soc.**, Vol. 108, p. 478 (1961).

[4] J. Scott and J. Olmstead, "A Solid-to-Solid Diffusion Technique," **RCA Review**, Vol. 26, p. 357 (1965).

[5] W. Kern, N. Goldsmith, and A. Mayer, "Surface Passivation Techniques for Compound Solid State Devices," AF33 (657)-11615, Interim Tech. Doc. Prog. Rep. No. 1-4, 6/1/63 to 5/31/64; Techn. Rep. AFAL-TR-75-213, 1965.

[6] W. Steinmaier and J. Bloem, "Successive Growth of Si and SiO_2 in Epitaxial Apparatus," **Jour. Electrochem. Soc.**, Vol. 111, p. 206 (1964).

[7] M. J. Rand and J. L. Ashworth, "Deposition of Silica Films on Germanium by the Carbon Dioxide Process," **Jour. Electrochem. Soc.**, Vol. 113, p. 48 (1966).

[8] S. K. Tung and R. E. Caffrey, "The Deposition and Physical Properties of Alumino-Silicate Films," **Jour. Electrochem. Soc.**, Vol. 117, p. 91 (1970).

[9] T. L. Chu, J. R. Szedon, and G. A. Gruber, "Silica Films by the Oxidation of Silane," **Trans. Met. Soc. AIME**, Vol. 242, p. 532 (1968).

[10] R. C. G. Swann and A. E. Pyne "The Preparation and Properties of Silica Films Deposited from Silane and Carbon Dioxide," **Jour. Electrochem. Soc.**, Vol. 116, p. 1014 (1969).

[11] N. Goldsmith and W. Kern, "The Deposition of Vitreous Silicon Dioxide Films from Silane," **RCA Review**, Vol. 28, p. 153 (1967).

[12] W. Kern, "Apparatus for Chemical Vapor Deposition of Oxide and Glass Films," **RCA Review,** Vol. 29, p. 525 (1968).

[13] W. Kern and R. C. Heim, "Chemical Vapor Deposition of Silicate Glasses for use with Silicon Devices," **Jour. Electrochem. Soc.**, Vol. 116, p. 70C (1968).

[14] W. Kern, "Silicate Glass Coating of Semiconductor Devices," U. S. Pat. 3,481,781 (Dec. 2, 1969).

[15] W. Kern and R. C. Heim, "Chemical Vapor Deposition of Silicate Glasses for use with Silicon Devices—1. Deposition Techniques," **Jour. Electrochem. Soc.**, Vol. 117, p. 562 (1970).

[16] H. J. Emeleus and K. Stewart "Oxidation of the Silicon Hydrides (I and II)," **Jour. Chem. Soc.**, p. 1182 (1935); p. 677 (1936).

[17] S. S. Flaschen, H. C. Evitts, and J. R. Black, "Large Area Semiconductor Surface Passivation Production Refinement Program," AD439885, AMC7-879(XI) Interim-Techn. Progr. Rep. No. 2, Jan. 1964.

[18] M. L. Hammond and G. M. Bowers, "Preparation and Properties of SiO_2 Films Deposited from SiH_4 and O_2," **Trans. Met. Soc. AIME**, Vol. 242, p. 546 (1968).

[19] K. Strater, "Controlled Oxidation of Silane," **RCA Review**, Vol. 29, p. 618 (1968).

[20] **Vapor Deposition**, L. F. Powell, T. H. Oxley, and T. M. Blocher, Jr., Editors, John Wiley & Sons, Inc., New York, 1966.

[21] M. L. Barry, "A Continuous Process for the Deposition of Silicon Oxide from the Oxidation of Silane," p. 595 in **Chemical Vapor Deposition**, Second Internatl. Conf., J. M. Blocher, Jr. and T. C. Withers, Editors, The Electrochem. Soc., Inc., New York 1970.

[22] A. W. Fisher, J. A. Amick, H. Hyman, J. H. Scott, Jr., "Diffusion Characteristics and Applications of Doped Silicon Dioxide Layers Deposited from Silane," **RCA Review**, Vol. 29, p. 533 (1968).

[23] A. W. Fisher, J. A. Amick, "Diffusion Characteristics of Doped Silicon Dioxide Layers Deposited from Premixed Hydrides," **RCA Review**, Vol. 29, p. 549 (1968).

[24] A. W. Fisher and J. A. Amick, "Doped Oxide Diffusion Sources for Silicon," presented at NEPCON WEST, Feb. 1970 and NEPCON EAST, June 1970.

[25] B. M. Mecs, "Oxidized SiH_4 as a Diffusion Source," **Jour. Electrochem. Soc.**, Vol. 115, p. 70C (1968).

[26] K. Strater and A. Mayer, "The Oxidation of Silane, Phosphine, and Diborane during Deposition of Doped-Oxide Diffusion Sources," p. 469 in **Semiconductor Silicon**, The Electrochem. Soc., Inc., New York, 1969.

[27] M. L. Barry and P. Olofsen, "Doped Oxides as Diffusion Sources," **Jour. Electrochem. Soc.**, Vol. 116, p. 859 (1969).

[28] M. L. Barry and J. Manolin, "Further Verification of a Model for Diffusion from Doped Oxides," **Jour. Electrochem. Soc.**, Vol. 117, p. 258, (1970).

[29] W. Kern, unpublished work.

[30] W. Kern and D. Puotinen, "Cleaning Solutions Based on Hydrogen Peroxide for use in Silicon Semiconductor Technology," **RCA Review**, Vol. 31, p. 187 (1970).

[31] B. Swaroop, "Low-Temperature Densification of Silica Films," **Jour. Electrochem. Soc.**, Vol. 115, p. 239C (1968).

[32] W. Kern, "Densification of Chemically Vapor Deposited Borosilicate Glasses," **Jour. Electrochem. Soc.**, Vol. 116, p. 251C (1969).

[33] B. E. Deal, R. J. Fleming, and P. L. Castro, "Electrical Properties of Vapor-Deposited Silicon Nitride and Silicon Oxide Films on Silicon," **Jour. Electrochem. Soc.**, Vol. 115, p. 300 (1968).

[34] J. P. Biet, C. Dam, and P. Pinchon, "Silicon-Pyrolytic Oxide Interface," **Jour. Electrochem. Soc.**, Vol. 117, p. 97C (1970).

[35] R. Lathlaen and D. A. Diehl, "Stress in Thin Films of Silane Vapor-Deposited Silicon Dioxide," **Jour. Electrochem. Soc.**, Vol. 116, p. 620 (1969).

[36] V. Y. Doo and V. M. L. Sun, "Pinholes in Pyrolytic Oxide Deposited on Silicon and Metals," **Metallurg. Transact.**, Vol. 1, p. 741 (1970).

[37] K. Sato, T. Abe, and Y. Nishi, "An Optimum P_2O_5-SiO_2/SiO_2 Structure for Stable MOS Field-Effect Devices," **Jour. Electrochem. Soc.**, Vol. 116, p. 209C (1969).

[38] W. Kern and R. C. Heim, "Chemical Vapor Deposition of Silicate Glasses for Use with Silicon Devices; Part II-Film Properties," **Jour. Electrochem. Soc.**, Vol. 117, p. 568 (1970).

[39] P. Delivorias, "Development of p-Channel Enhancement MOS Triodes," **RCA Review**, Vol. 29, p. 630 (1968).

[40] E. H. Snow and B. E. Deal, "Polarization Phenomena and other Properties of Phosphosilicate Glass Films on Silicon," **Jour. Electrochem. Soc.**, Vol. 113, p. 263 (1966).

Vapor Deposition and Characterization of Metal Oxide Thin Films for Electronic Applications

C. C. Wang, K. H. Zaininger, and M. T. Duffy

RCA Laboratories, Princeton, N.J.

Abstract—The rapid progress of solid-state electronics technology has stimulated the development of chemical vapor-deposition techniques for thin-film materials with functional properties for device applications. Research results are reviewed in this paper on the vapor deposition and characterization of transition-metal oxides (TiO_2, Ta_2O_5, and Nb_2O_5) dielectric films and lead oxide (PbO) photoconductive films. Potential device applications are presented.

1. Introduction

The development of chemical vapor-deposition technology has made possible the use of a variety of new thin-film components to improve the present capability of many electronic devices for better performance, greater versatility, higher reliability, and lower cost. In the micro-electronic field new thin-film dielectrics[1-4] have been in demand because of the manifold functional requirements in devices and integrated circuits including, among others, dielectric insulation, surface passivation, diffusion masking, radiation resistance, and hermetic encapsulation. Research results are reviewed in this paper on the synthesis of transition-metal oxides (TiO_2, Ta_2O_5, and Nb_2O_5) dielectric films by chemical vapor deposition techniques, and the characterization of the films by physical and electrical methods. Metal–oxide–semiconductor (MOS) units were fabricated and evaluated using these films deposited on silicon.

In another area of application, thin-film oxides exhibiting desirable photoconductive properties are useful as the target material for vidicon camera tubes. Lead monoxide (PbO, tetragonal red form) has been used in commercial Vistacon* and Plumbicon* camera tubes. The lead oxide targets are characterized by high sensitivity, very low dark current and lag, and linear light-transfer characteristics. Research results

* "Vistacon" and "Plumbicon" are, respectively, trademarks of RCA and Philips television camera tubes.

on the vapor deposition and characterization of PbO thin films are also presented in this paper.

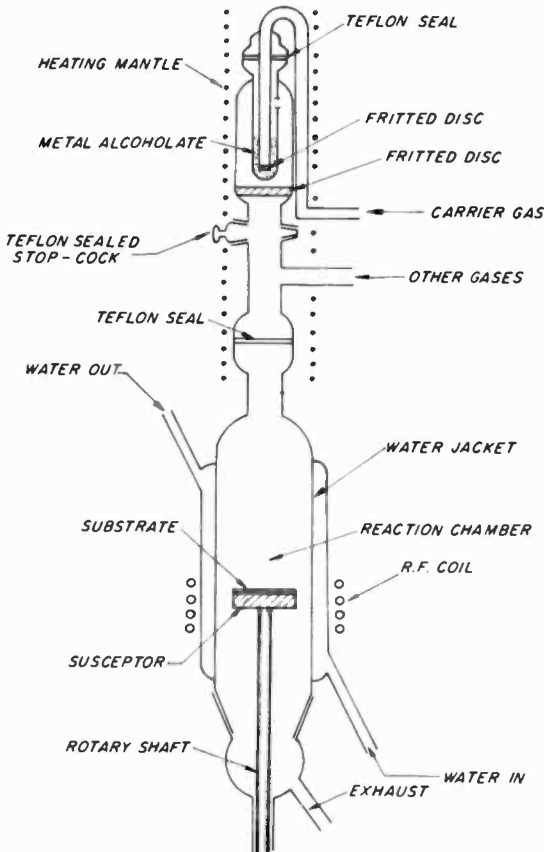

Fig. 1—Apparatus for thin film deposition.

2. Thin-Film Deposition

2.1 Ta_2O_5 Films

Thin dielectric films of tantalum oxide have been deposited on a variety of substrates including silicon, germanium, quartz, and platinum by the pyrolysis of tantalum pentaethylate, Ta $(OC_2H_5)_5$, in an oxidizing ambient. The deposition apparatus is illustrated in Fig. 1. The quartz reaction chamber is 20 cm long with an internal diameter of 35 mm. A graphite susceptor having a pyrolytic graphite coating was used for heating the substrates. It was cylindrical in shape; 1¼ inches in diameter and ¾ inch long. The apparatus was arranged in the vertical

position, and the vapor path between generator and deposition chamber was kept as short as possible. Air or water was circulated through the outer jacket of the deposition chamber to cool the inner tube. The susceptor was rotated at 10 rpm during film formation in order to facilitate uniform deposition.

The tantalum alcoholate vapors were transported to the rf heated substrates by helium carrier gas. Deposition conditions were optimized by varying the alcoholate vapor pressure, the deposition temperature, and total flow rate of gases. The following deposition parameters gave best results for the particular apparatus geometry used:

Substrate temperature:	450°C
Metal pentaethylate source temperature:	115°C
Helium carrier flow rate:	325 cc/min
Other gases: Helium flow rate:	2500 cc/min
Oxygen flow rate:	820 cc/min

Faster flow rates than indicated here favored heavy deposition at the center of the substrate, while slower flow rates favored deposition at the periphery of the substrate.

2.2 Nb_2O_5 Films

Nb_2O_5 thin films have also been successfully deposited on silicon, germanium, quartz, and platinum substrates by the pyrolysis[5] of niobium pentaethylate, $Nb(OC_2H_5)_5$ under the conditions cited above for deposition of Ta_2O_5 films. In addition to the pyrolysis of metal alcoholate, a halogen transport process[6] was used to deposit Nb_2O_5 films on platinum and silicon substrates by the reaction,

$$2NbOCl_3 + 3/2\ O_2 = Nb_2O_5 + 3Cl_2$$

The deposition appartus is shown in Fig. 2. It consists of a system of quartz tubing heated by split ovens. Gas is supplied through calibrated flowmeters. A gas mixture consisting of 3% chlorine and 97% argon was streamed at a flow rate of 100 cm^3/min over a boat containing high-purity Nb_2O_5 powder. After entering the deposition zone, the argon stream carrying the $NbOCl_3$ was mixed with pure oxygen flowing at a rate of 70 cm^3/min. Reaction of the oxygen with the $NbOCl_3$ takes place preferentially on the substrate and on the walls of the quartz tubing, generating Nb_2O_5 films.

2.3 TiO_2 Films

TiO_2 films[7] were deposited on various substrates including silicon, germanium, platinum, quartz, and aluminum by the pyrolysis in an oxidizing ambient of titanium tetraisopropylate, $Ti(C_2H_5O)_4$. The experimental setup and deposition conditions are similar to those used for deposition of Ta_2O_5 and Nb_2O_5 films by the pyrolysis of metal alcoholates as shown in Fig. 1.

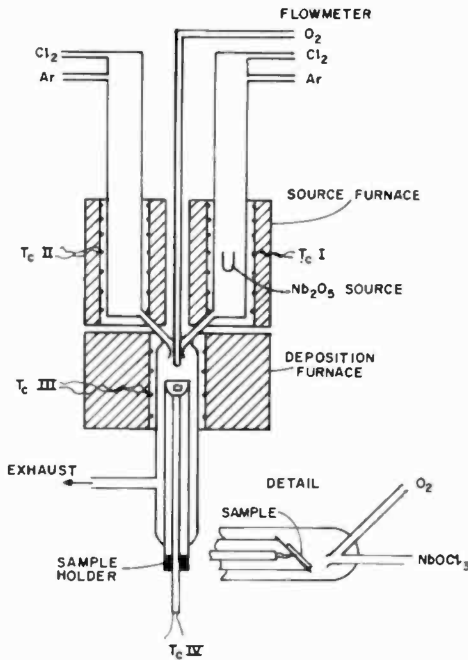

Fig. 2—Apparatus for growing Nb_2O_5 films.

TiO_2 films have also been prepared by the pyrohydrolysis of titanium tetrachloride, $TiCl_4$ according to the reaction:

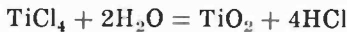

$$TiCl_4 + 2H_2O = TiO_2 + 4HCl$$

The $TiCl_4$ and H_2O source materials were kept in Pyrex vessels at, respectively, 10° and 80°C. The vapor streams were carried by O_2 at flow rates of 200 cc/min (for $TiCl_4$) and 1500 cc/min (for H_2O) through concentric Pyrex tubings. Reaction of the streams took place on the substrates which were heated in the temperature range 100° to 1000°C.

2.4 PbO Films

PbO films were prepared by heating tetragonal PbO (red form) at a temperature of about 900°C in a residual atmosphere (total pressure of about 10^{-2} Torr) of O_2 and H_2O. The apparatus consists of a vacuum system with residual pressure of 10^{-7} Torr. Substrates employed include Corning 7056 glass and thin-film tin oxide coating (transparent iridescent conductive coating, TIC) on the 7056 glass. The substrate temperature was generally kept at about 120°C.

The presence of O_2 serves the purposes of (1) preventing the formation of free lead caused by the decomposition of PbO, and (2) maintaining the stoichiometry and the conductiivty type of the layers. The H_2O vapor, which is probably the transporting agent, has the effect of controlling the crystalline size of the PbO layers. The crystallite size determines the resolution of the camera-tube target.

3. Properties of Oxide Films

3.1 Measurement Techniques

The surface crystallinity of the metal oxide thin films was examined by glancing-angle electron diffraction using a Model EMU electron microscope. The samples were examined at a glancing angle of less than 1° using 100-kV electrons, and the diffraction took place from over the whole surface (~1 cm²) of each sample. In addition to electron diffraction measurements, x-ray diffractometry was used to determine the preferred orientations and phases. A x-ray unit and the attached diffractometric tracer were used for this study. A Cambridge Stereoscan Mark II scanning electron microscope was used to examine the surface structures of the films.

Optical measurements have been made on the oxide films. Transmission spectra were obtained on films deposited on quartz or glass in the spectral region 0.2 to 2.6 μm using a Cary Model 14 spectrometer. Information on dispersion and fundamental absorption edge (energy gap) has been obtained. Ellipsometric measurements[8] were made on films deposited on silicon to determine thickness and refractive index. Dielectric properties of the oxide films were determined from capacitance measurements on MOS units using the automatic MOS measurement arrangement.[9]. Supplementary results were obtained from measurements on films deposited on platinum substrates using a General Radio Model 1615 capacitance bridge.

The MOS capacitance–voltage (C-V) technique[10] was used to determine the electrical properties of the MOS structures using transition-metal oxide/Si composites. This method was employed because of the simplicity of fabricating test structures, the ease of making

(automatic) measurements, and the large amount of information that can be obtained. The C-V characteristics of the MOS structures provide information on oxide changes, surface-state densities, hysteresis, and bias instability effects. Details on the measurement techniques have been published[9] elsewhere.

Radiation sensitivity of the transition-metal oxide films was determined from radiation damage tests carried out using a 1 MeV van de Graff generator. The units were subjected to electron fluxes ranging from 10^{11} to 10^{15} electrons/cm^2 at intensities from 5×10^{10} to 2×10^{13} electrons/cm^2-min. The observed changes in the C-V characteristics of MOS structures were used as a measure of the radiation damage.

Electrical properties of lead oxide layers were determined on films deposited on (SnO_2) TIC using RCA C-23097 vidicon electron gun. The light sensitivity, resolution, dark current, and speed of response (lag) have been measured. Details of the measurement techniques have been published[11,12] elsewhere.

3.2 Results and Discussion

3.2.1 *Crystallinity and Physical Properties of Ta_2O_5, Nb_2O_5, and TiO_2 Films*

Ta_2O_5 and Nb_2O_5 films with thicknesses ranging from 500 to 3000 Å have been deposited on substrates using the process of pyrolysis of metal alcoholates. The deposition rate was generally ~80 Å/min at a substrate temperature of about 450°C. Adhesion of the films to substrates is good. The films are inert to most acids but can be etched in HF. The films exhibit very smooth surfaces as shown in the scanning electron micrograph (Figs. 3a and 3b).

The Ta_2O_5 and Nb_2O_5 films are amorphous as revealed by x-ray and electron-diffraction studies. After annealing a tantalum oxide film in He for 30 minutes at 800°C, electron diffraction indicates that polycrystalline β-Ta_2O_5 was obtained. Films of niobium oxide, which were treated in a similar manner, remained amorphous after a heat treatment at 850°C. The amorphous films start to crystallize at temperatures higher than 1200°C. This contrasts with the case of anodic niobium oxide, which has been reported[13] to "recrystallize" at 500 to 600°C, and seems to support the argument that in the latter case recrystallization is due to the presence of impurities, and is not an intrinsic characteristic of amorphous Nb_2O_5.

Nb_2O_5 films prepared by the chloride transport process at about 1000°C were polycrystalline (H-modification of Nb_2O_5). Films up to 50 μm were prepared with a transport rate of ~160 Å/min.

TiO_2 films with thicknesses ranging from 500 Å to several μm have

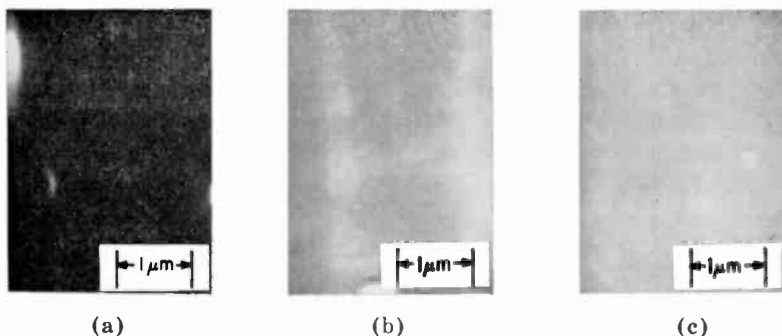

Fig. 3—Scanning electron micrographs of thin films, beam-sample angle 45°. (a) Ta_2O_5, (b) Nb_2O_5, (c) TiO_2.

been deposited using the processes described in Section II on a variety of substrates with good adhesion. The surfaces of the films are smooth, as shown in the scanning electron micrograph (Fig. 3c). In contrast to the Ta_2O_5 and Nb_2O_5 films, which are synthesized using similar processes and are amorphous, the TiO_2 films were polycrystalline. The structure is highly dependent on the deposition temperature. At substrate temperatures of 100° to 400°C, the films are polycrystalline TiO_2 (anatase) with (101) preferred orientation. A typical x-ray diffractometric trace (Cu/Ni radiation) of a TiO_2 film deposited on fused quartz substrate is presented in Fig. 4, showing the single-phase

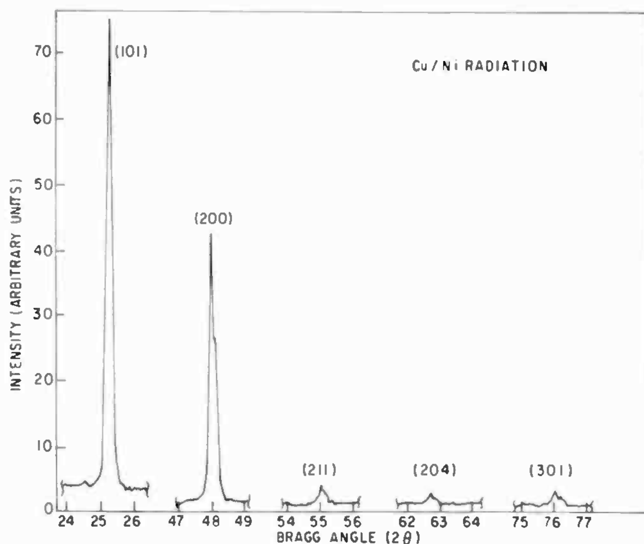

Fig. 4—X-ray diffractometric trace of TiO_2 (anatase) thin film.

Table 1—Properties of Thin-Film Metal Oxides

	TiO_2	Ta_2O_5	Nb_2O_5	Nb_2O_5
Film Structure	polycrystalline (anatase)	amorphous	amorphous	polycrystalline (H-modification)
Energy Gap (eV)	3.0	4.2	3.5	3.4
Refractive Index (at 5461 Å)	2.0	2.3	2.2	2.6
Dielectric Constant	20-50	22	11	100
Loss Tangent (at 1 kHz)	$\sim 10^{-2}$	$\sim 10^{-2}$	$\sim 10^{-2}$	$\sim 10^{-2}$
Breakdown Strength (V/cm)	5×10^5	5×10^6	5×10^6	$>5 \times 10^5$

anatase structure with preferred orientation. The anatase phase transfers to the rutile phase upon a post deposition annealing treatment at elevated temperatures (800°-1000°C).

The various properties of the oxide films are summarized in Table 1.

3.2.2 *MOS Characteristics of Ta_2O_5, Nb_2O_5, and TiO_2 Films*

MOS capacitors were fabricated using the transition-metal oxide thin films as the gate insulators on (111) silicon. The *C-V* characteristics of the MIS structures were determined.

Typical *C-V* curves for Ta_2O_5-Si and Nb_2O_5-Si contacts are shown in Figs. 5 and 6, respectively. It is seen that the curves are scattered around zero bias and are steep. This indicates that interface state

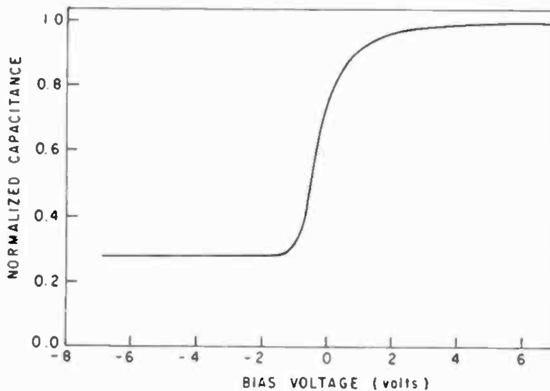

Fig. 5—Normalized *C-V* curve for an n-type MOS capacitor with 1100 Å of Ta_2O_5 as gate insulator.

density and oxide charge can be kept to values that readily allow modulation of the silicon surface potential.

Generally, the positive oxide charge for Nb_2O_5 and Ta_2O_5 can be kept below $5 \times 10^{11}/cm$ so that flat-band voltages for a 1000 Å oxide film on 10 ohm-cm p-type silicon are less than 1 V. This number includes oxide charge as well as work-function difference due to gate metallization.

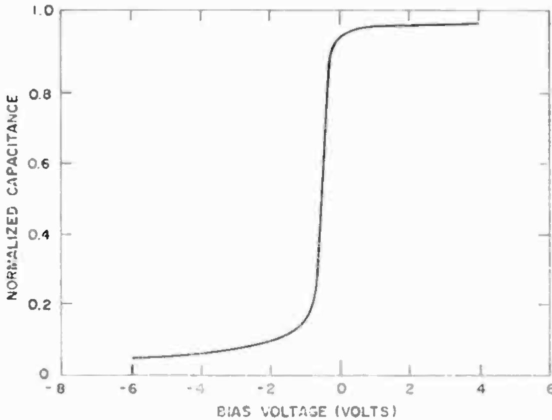

Fig. 6—Normalized *C-V* curve for an n-type MOS capacitor with 900 Å of Nb_2O_5 as gate insulator.

The Nb_2O_5-Si and Ta_2O_5-Si interfaces generally exhibit a room-temperature hysteresis of the slow trapping type. That is, for increasing negative gate voltage, the flat-band voltage shifts to more negative values. Generally, this type of hysteresis is strongly dependent on deposition conditions, but can be reduced by annealing at high temperatures.

Bias-temperature tests at 200°C in an inert ambient show that these films are not an effective barrier against ionic motion. Positive charge is observed to move toward the silicon interface under the influence of positive gate voltage.

In general, the TiO_2 films showed such high conductance that no MOS behavior could be observed. However, some films had no conduction and thus allowed the examination of the TiO_2-Si interface. Typical *C-V* characteristics of a nonconducting TiO_2 (anatase)-Si contact are shown in Fig. 7. In contrast to the Nb_2O_5-Si and Ta_2O_5-Si systems, the density of both oxide charge and interface states is quite high, making the modulation of the silicon surface very difficult. Flat-band voltage is typically between −5 and −10 V. This, combined with the high

dielectric constant for this oxide film is an indication of the large amount of oxide charges. In addition, the *C-V* curve is not sharp, and inversion sets in at about −35 V, indicating a very high density of interface states.

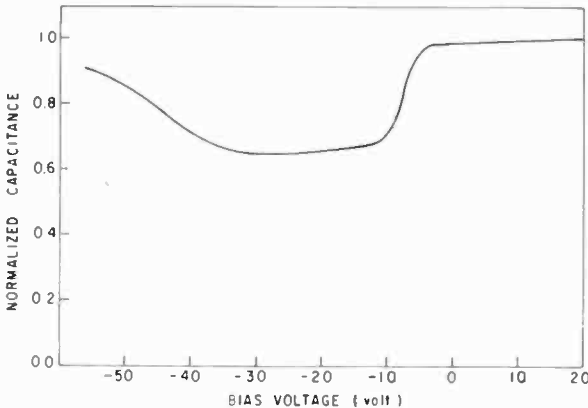

Fig. 7—Normalized *C-V* curve for an n-type MOS capacitor with 1000 Å of TiO_2 as gate insulator.

The radiation behavior of the Ta_2O_5-Si system has been examined by bombarding the wafer with 1 MeV electrons over a total flux range from 10^{13} to 10^{15} e/cm^2. Up to 10^{13} there was no radiation-induced shift, but for larger fluence values, the *C-V* curves shifted to the left, with the shifts saturating at about 10^{15} e/cm^2. The same samples were subsequently bombarded with 10^{13} e/cm^2 under the application of positive bias. Even under 10 V bias no further shift was observed.

3.2.3 *Physical and Electrical Characteristics of PbO Films*

PbO films with thicknesses up to about 25 μm have been prepared. The scanning electron micrographs of a typical film deposited on a tin oxide coated glass are presented in Fig. 8, showing the surface structures of both sides of the films. The film was stripped off mechanically from the substrate for examination. It is seen that the side (TIC side) adjacent to the substrate exhibits smoother texture than the opposite side (target side). The crystallites in the layer (Fig. 8a) are in the form of upright platelets. The texture[14] is very similar to that in the Plumbicon target. The dimensions of these crystals are approximately 1-2 × 0.5-1 × 0.05-0.1 μm. The porosity of the films is generally in the range 45-60%. Extensive studies have revealed that the PbO layers

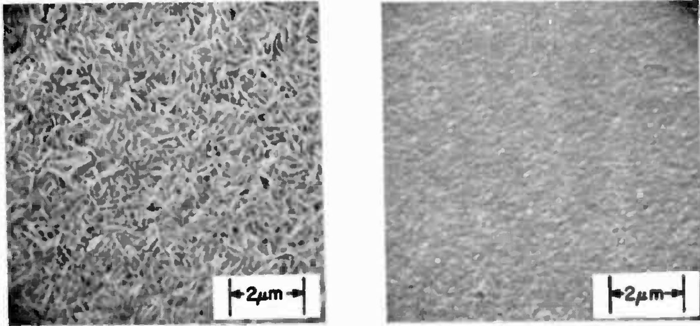

Fig. 8—Scanning electron micrograph of PbO films, beam-sample angle 45°. (a) Target-side texture, (b) TIC-side texture.

are composed of two phases. Within the first 10^2-10^3 Å the films exhibit the orthorhombic PbO structure with (001) preferred orientation. Upon further growth the films change to the tetragonal PbO with a strong degree of (110) preferred orientation. This orientation is caused by evolutionary selection[15, 16] during the layer deposition. X-ray diffractometric traces of the TIC and target sides of a typical PbO layer are shown in Fig. 9. The differences between the two sides are clearly

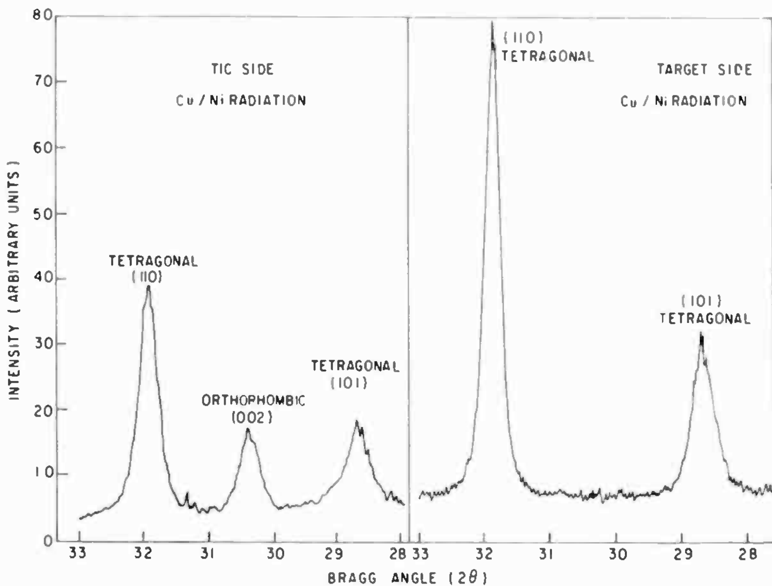

Fig. 9—X-ray diffractometric trace of PbO films. (a) Target side, (b) TIC side.

seen. The target side exhibits a higher degree of (110) preferred orientation, and the (002) reflection peaks of the orthorhombic PbO is only seen in the TIC side material. Some films examined by x-ray diffractometry (x-ray penetration of several μm) showed absence of orthorhombic PbO in the TIC sides. However, electron diffraction

Table 2—Properties* of Lead Oxide PbO) Films

Film Structure	
Target Side	Tetragonal red PbO with (110) preferred orientation.
TIC Side	Orthorhombic yellow PbO layer (10^2-10^3 Å) with (002) preferred orientation adjacent to TIC; tetragonal red PbO with (110) preferred orientation (less preferred oriented than on the target side)
Film Density	4.3-5.7 g/cc
Film Porosity	45-60%
Stability in Air	Films degrade to form $3PbCO_3 \cdot 2PbO_2 \cdot H_2O$ and $Pb_3(CO_3)_2(OH)_2$
Energy Gap	1.94 eV
Dielectric Constant	24
Refractive Index	2.66
Threshold Wavelength of Photosensitivity	6500 Å
Dark Current	< 1 nA
White Light Sensitivity (2870°K tungsten illumination)	~400 μA/lumen
Lag (% of initial value of 100 nA signal 1/20 sec after removal of illumination)	< 10
Amplitude Response (to a 400 line TV test pattern at center of picture)	> 20

* Electrical properties are determined at a target voltage of 50 V.

(electron penetration of about 50 Å) studies revealed that the target and TIC sides of a film are always composed of respectively single phase tetragonal and orthorhombic PbO. The presence of a small amount of orthorhombic phase in the tetragonal phase does not degrade the PbO tube performance. However, a large amount of orthorhombic PbO in the layer may cause deterioration effect.

The physical and electrical properties of the PbO films are summarized in Table 2.

4. Potential Device Applications

The vapor-phase-deposited thin oxide films have potential for various device applications depending on the functional requirements.

The Ta_2O_5 films exhibit good radiation-resistance properties. The interface state density and oxide charge of the Ta_2O_5/Si and Nb_2O_5/Si MOS structures can be kept to values that allow modulation of the silicon surface potential. These films may be useful, upon further improvements in fabrication techniques, as the gate insulators for MOS integrated electronic devices.

TiO_2 has a high dielectric constant. The dielectric constant values are relatively insensitive to temperature up to 300°C and to frequencies into the gigahertz range. Therefore, the TiO_2 films are attractive for use as passive components in thin-film circuits and in microwave devices. Ta_2O_5 and Nb_2O_5 may be also useful as resistive and capacitive elements in thin-film circuits.

In another area of application, Nb_2O_5 films may be useful as resistive discharge layers for improvements in beam-landing efficiency[17] and signal output uniformity of vidicon-type tubes. Nb_2O_5 films exhibit desirable resistivity, permittivity, and thermal stability, and are attractive for this use in high-resolution silicon vidicons.[18]

PbO films have been widely used as the target photosensitive layers of the commercial lead oxide vidicon. This vidicon is presently the leading contender among broadcast television pickup tubes, particularly for use in color cameras. It is smaller and simpler to operate than the image orthicon, and its electrical and optical performance have some advantages compared to the conventional vidicons employing antimony trisulfide or other targets. The superior characteristics include extremely low dark current, high resolution, high sensitivity, and low lag.

5. Conclusions

Metal oxide films prepared by chemical vapor deposition are of potential for various solid-state device applications. The applications are determined by the fundamental behavior and functional properties of the constituent materials. The transition-metal oxide dielectric films possess some outstanding properties and are attractive for micro-electronic applications as active and/or passive elements. The current trend of research in this class of material is to improve the preparation techniques and to understand the fundamental nature of materials, the parameters that influence their behavior, and the effects of associated processes. The PbO photoconductive films have been used in the vidicon camera tubes. The current interest in this material is the development

of a doped-PbO target layer with an extended red response characteristic.

Acknowledgment

The authors are grateful to R. Bates, R. Soltis, and B. Halon for thin film deposition work. They also wish to thank R. Lanskold, E. Luedicke, R. J. Paff, W. Roth, and B. Seabury for experimental measurements. Stimulating discussions with R. G. Neuhauser and M. D. Coutts are also appreciated.

References:

[1] K. H. Zaininger and C. C. Wang, "Thin Film Dielectric Materials for Microelectronics," **Proc. IEEE,** Vol. 57, p. 1564, (1969).

[2] L. V. Gregor, **Physics of Thin Films, Vol. III,** Ed. G. Hass and R. E. Thun, Academic Press, New York, 1966.

[3] Editorial Staff, **Dielectric Films in Microelectronics** (NBS Rpt. OTR-117), U. S. Dept. of Commerce, Washington, D. C., 1965.

[4] L. V. Gregor, "Dielectric Films/Semiconducting Films/Superconducting Films," **Electro-Technology,** Vol. 57, p. 95, Sept. 1963.

[5] M. T. Duffy, C. C. Wang, A. Waxman, and K. H. Zaininger, "Preparation, Optical and Dielectrical Properties of Vapor-Deposited Niobium Oxide Thin Films," **Jour. Electrochem. Soc.,** Vol. 116, p. 234, (1969).

[6] H. R. Brunner, F. P. Emmenegger, M. L. A. Robinson, and H. Rötschi, "Growth of Nb_2O_5 Thin Film Capacitors," **Jour. Electrochem. Soc.,** Vol. 115, p. 1287, Dec. 1968.

[7] C. C. Wang and K. H. Zaininger, "Transition Metal Oxide Thin-Film Microelectronic Components," **Proc. 1969 Electronic Comp. Conf.,** p. 345, 1969.

[8] K. H. Zaininger and A. G. Revesz, "Ellipsometry—A Valuable Tool in Surface Research," **RCA Review,** Vol. 25, p. 85 (1964).

[9] K. H. Zaininger, "Automatic Display of MIS Capacitance-Versus-Bias Characteristics," **RCA Review,** Vol. 27, p. 341 (1966).

[10] K. H. Zaininger and F. P. Heiman, "The C-V Technique as an Analytical Tool—Part 1," **Solid State Tech.,** Vol. 13, p. 49, May 1970.

[11] P. K. Weimer, S. V. Forgue, and R. R. Goodrich, "The Vidicon—Photoconductive Camera Tube," **RCA Review,** Vol. 12, p. 306 (1951).

[12] P. K. Weimer, "Television Camera Tubes: A Research Review," **Adv. Electronics and Electron Phys.,** Vol. 13, p. 387, Academic Press, New York, 1960.

[13] L. Young, **Anodic Oxide Films,** Academic Press, N. Y. (1961).

[14] E. H. Stupp and R. S. Levitts, **The Plumbicon,** Lecture on Photo-Electronic Imaging Devices, Univ. of Rhode Island, R. I., and reprinted by Amperex Electronic Corporation (1968).

[15] A. Van der Drift, "Evolutionary Selection, A Principle Governing Growth Orientation in Vapor-Deposited Layers," **Philips Res. Rpt.,** Vol. 22, p. 267 (1967).

[16] A. Van der Drift, "Texture of a Vapor-Deposited Lead-Monoxide Layer," **Philips Res. Rpt.,** Vol. 21, p. 289 (1966).

[17] R. G. Neuhauser and L. D. Miller, "Beam-Landing Errors and Signal-Output Uniformity of Vidicon Tubes," **Proc. National Electronics Conf.,** Vol. 13, p. 846, National Electronics Conf. Inc., Chicago, Ill., 1957.

[18] M. H. Crowell and E. F. Labuda, "The Silicon Diode Array Camera Tube," **Bell System Tech. Jour.,** Vol. 48, p. 1481, May 1969.

Preparation, Properties, and Applications of Chemically Vapor Deposited Silicon Nitride Films

M. T. Duffy and Werner Kern
RCA Laboratories, Princeton, N.J.

Abstract—The formation and use of amorphous films of silicon nitride by the silane–ammonia and the silicon-tetrachloride–ammonia reactions are reviewed and recent results are presented. Substrates employed included chemically cleaned silicon substrates, controlled surface oxide layers, and GaAs. The electrical film and interface properties were evaluated as functions of the type of carrier gas (H_2, N_2, NH_3), the NH_3:SiH_4 ratio (200:1 to 10,000:1), and the deposition temperature (650°-1100°C). Films deposited at relatively low temperature (700°C) and in a large excess of ammonia were superior for applications involving MNOS structures. The silicon nitride films were also useful for insulation, passivation, and sealing of devices and integrated circuits.

1. Introduction

The application of amorphous silicon nitride films in the passivation of bipolar semiconductor devices and as a dielectric component in field-effect devices has become well established in recent years. Silicon nitride films are formed quite readily by chemical vapor deposition using either (1) the silane–ammonia reaction or (2) the silicon-tetrachloride–ammonia reaction according to the following overall equations:

$$3SiH_{4(g)} + 4NH_{3(g)} \rightarrow Si_3N_{4(s)} + 12H_{2(g)} \quad [1]$$

$$3SiCl_{4(g)} + 4NH_{3(g)} \rightarrow Si_3N_{4(s)} + 12HCl_{(g)} \quad [2]$$

The silane reaction can be effected at low temperature in an rf glow discharge or, preferably, by heating to temperatures in the range of 700°-1100°C in hydrogen[3-7] or in excess anhydrous ammonia.[8] At temperatures of 900°C and above a large excess of hydrogen tends to lead to undesirable crystallites.[3,4] The reaction utilizing silicon tetrachloride and ammonia can be conducted in the temperature range of 550°-1250°C (typically 850°) using either hydrogen[7,8] or nitrogen[9] as the carrier gas. The advantage of this process lies in its ability to yield silicon nitride films that exhibit lower electrical conductivity and polarization

effects, but it has the disadvantage of requiring a higher deposition temperature than does the silane reaction.[7]

Properties of chemically vapor deposited silicon nitride films relevant to semiconductor device applications that have been characterized in considerable detail include mechanical properties and chemical composition,[4,7,8] film structure,[3,4,8-10] ion migration and masking,[7-13] interfacial characteristics on silicon substrates,[5,7,10,12,14] and dielectric properties such as conduction and breakdown strength.[5-7,10,12,15,16] Optical properties and infrared absorption characteristics have also been studied by several investigators.[3-5,8,10,12] Chemical etch rate determinations, important both for characterizing[3-5,7-9,14] and for patterning[17-20] of silicon nitride films, have been studied extensively. Applications of silicon nitride films for junction sealing,[21,22] passivation of mesa diodes,[23] and power rectifiers[24] have been recently reported.

This paper discusses recent results obtained on the deposition of silicon nitride films based on the silane–ammonia process, and some properties of the resulting films with emphasis on metal-nitride-oxide-silicon structures. Several novel applications of silicon nitride films in solid-state technology are briefly discussed.

2. Deposition Process and Film Properties

The physical, electrical, mechanical, and interface properties of pyrolytic silicon nitride films on silicon substrates depend strongly upon the deposition conditions. Of primary importance among these are deposition temperature, reactants employed and their purity, ratio of reactants, gas flow rate, geometry of deposition chamber, and silicon surface preparation. Consequently, it is necessary to employ deposition conditions that will yield film properties compatable with the intended application.

2.1 Deposition on Chemically Cleaned Silicon Substrates

Initially, the feasibility of the deposition process was tested in a conventional resistively heated system. The furnace tube was 30 inches long with an internal diameter of 2.5 inches. The furnace flat zone was about 12 inches long. The NH_3:SiH_4 ratio was 200:1, and the deposition temperature was 700°C. Both N_2 and H_2 were used as carrier gases, and the total flow rate was about 2 l/min. The SiH_4 component was 0.2% of the total flow.

Deposition was performed on p-type silicon substrates of (100) and (111) orientation (resistivity 10 ohm-cm). Various substrate cleaning procedures were performed prior to deposition but, since no clear cor-

relation was found between these procedures and interface properties in the early stages of the investigation, no further discussion of surface preparation will be presented at this stage.

Film Properties

Thickness and refractive index measurements were made by ellipsometry at the mercury wavelength 5461 Å. Uniform films in the thickness range up to about 3000 Å were obtained by suitably positioning the substrates in the furnace tube. The refractive index showed a dependence on the carrier gas used. For nitrogen the range was 1.80

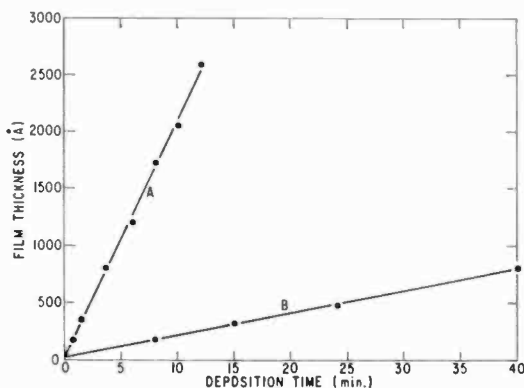

Fig. 1—Dependence of film thickness on deposition time: for curve A, the NH_3/SiH_4 ratio is 10^2; for curve B, the ratio is 10^4.

to 1.90, and for hydrogen the range was 1.90 to 2.04. (This may be due to the relatively impure N_2 used, which probably contained some oxygen, whereas the hydrogen was palladium diffused.) The above values were affected by the residual oxide thickness on the silicon substrates, which varied from about 15 to 35 Å depending upon surface preparation. This caused a detectable change in the second decimal place of the refractive-index value. For both carrier gases the relative dielectric constant ranged from 6.0 to 6.3.

In general, films deposited in the presence of nitrogen carrier gas showed inferior properties to those resulting from the use of hydrogen carrier gas. For example, in the latter case films had higher dielectric strength and showed fewer instances of excessive localized conduction. Consequently, these films were studied in greater detail.

The deposition rate was determined in order to test the reproducibility of the deposition process. The results are presented in Fig. 1

(curve A) showing film thickness as a function of deposition time. As expected, the thickness can be predicted with reasonable accuracy provided the substrate is located at the same position in the furnace tube, and the temperature and gas flow rates are maintained constant for each deposition.

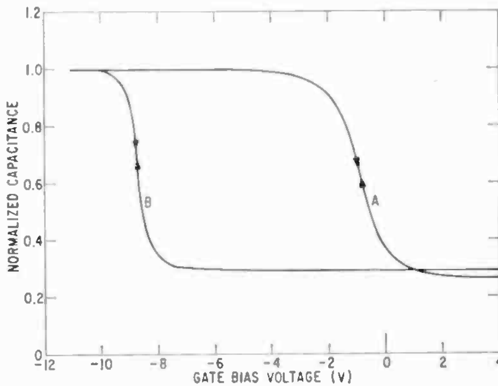

Fig. 2—MOS capacitance curves for Si_3N_4-Si structures prepared in nitrogen (curve A) and hydrogen (curve B) carrier gas.

Interface Properties

The most striking differences between samples prepared in N_2 and H_2 were observed in MOS capacitance (*C-V*) and conductance (*G-V*) measurements[25,26] on the interface properties of MNS (metal–silicon-nitride–silicon) capacitors. Although the residual silicon surface oxide, which strongly influences interface properties,[27] was ill-defined in these experiments, certain differences were immediately apparent. Fig. 2 shows examples of typical normalized *C-V* curves obtained on two such samples. Curve "A" corresponds to a sample prepared in N_2 carrier gas and curve "B" to a sample prepared in H_2 carrier. There is approximately a 7 *V* difference in flat-band voltage value between the two cases; those films deposited in the presence of H_2 having the larger flat-band voltage value. A computer evaluation of the MOS capacitance data[28] yielded interface state density distributions similar to those shown in Figs. 3 and 4, which are representative of the trends observed for both carrier gases. In both figures the interface state density (states/$cm^2 \cdot eV$) is plotted as a function of energy above the valence band of silicon (in eV units). Fig. 3 shows results obtained on three samples prepared in N_2 carrier gas, and Fig. 4 shows results obtained

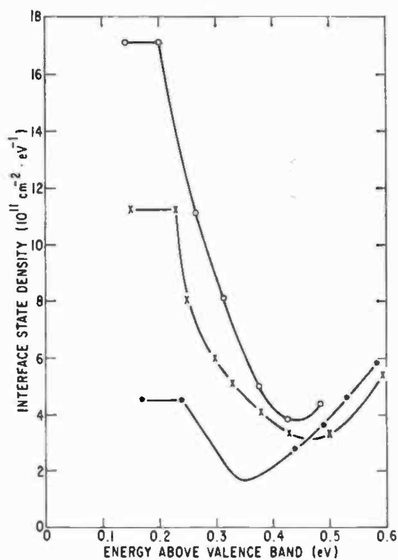

Fig. 3—Interface-state density distributions of three Si_3N_4-Si samples prepared in nitrogen carrier gas.

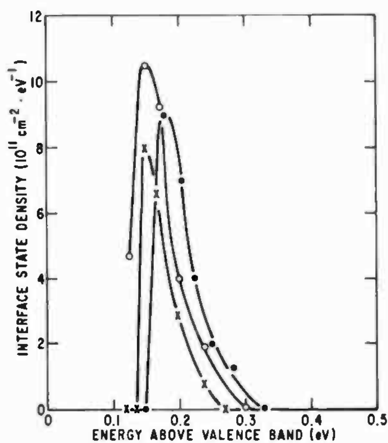

Fig. 4—Interface-state density distributions of three Si_3N_4-Si samples prepared in hydrogen carrier gas.

on three samples that were prepared in H_2 carrier. As can be seen, samples prepared in N_2 carrier gas have a distribution of interface states over a wide range of energy with a minimum density near mid bandgap. Samples prepared in H_2 carrier gas have a distribution of interface states more localized in energy than those prepared in N_2 carrier, and the density of states is significantly reduced over most of the energy range studied. The peak value occurs between 0.15 and 0.2 eV above the silicon valence band. The results of G-V measurements also confirm these trends. Low-voltage hysteresis effects ($E = \pm 10^6$ V/cm) were negligible in both cases. High-voltage hysteresis or "memory" effects were present at higher fields. This latter effect was subsequently investigated in the MNOS (metal-nitride-oxide-silicon) memory element.

2.2 Silicon Nitride Deposition Over Controlled Surface Oxide

These studies were initiated in order to investigate charge storage phenomena associated with the MNOS memory element.[29] Deposition was performed over a controlled thin tunnelable oxide, the thickness of which was varied from 15 to 50 Å. The preparation of this oxide has been described previously.[30]

In this study, certain basic criteria are essential for successful device operation. Among these are the requirements that silicon nitride films must be pinhole free, uniform, exhibit low "conductivity", be reproducible with respect to film thickness and composition, and have high dielectric strength.

It had been observed in the initial experiments discussed in section 2.1 that if the NH_3:SiH_4 ratio was decreased an increasing accumulation of white powder formed on the colder parts of the furnace tube walls. As the ratio was increased, this wall deposit decreased significantly. Consequently, in order to minimize the occurrence of powder formation and the risk of incorporating powder particles in the film during deposition, a high NH_3:SiH_4 ratio of 10,000:1 was used. A high ratio is also thermodynamically favorable and has been reported by others.[31,15] In the present case no gases other than NH_3 and SiH_4 (~3% in H_2) were admitted to the gas stream, and the total flow rate was approximately 6.5 l/min in a resistively heated system similar to the one described previously. Flow rates up to 13 l/min have also been used. Depositions were performed at temperatures from 650° to 1100°C.

Film Properties

The deposition rates in these experiments were intentionally low. This allowed greater control over the desired film thickness. Curve "B" in

Fig. 1 gives film thickness dependence on deposition time at 800°C for a series of samples when the flow rate was 6.5 l/min. As can be seen, film thickness can be predicted with good accuracy. Film uniformity was controlled to better than 3% variation in thickness over a 1¼-inch-diameter silicon wafer. These films had a significantly lower pinhole density than films deposited at a ratio of 200:1. The criterion used for estimating this density was the frequency of dielectric failure under applied gate bias during measurement of charge storage phenomena and current–voltage characteristics of MNOS

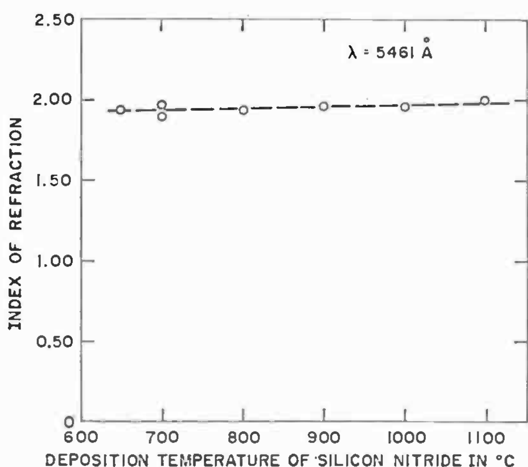

Fig. 5—Index of refraction of silicon nitride as a function of deposition temperature.

structures.[29] Failure was sufficiently rare for films in the thickness range 400 to 800 Å that this problem was regarded as negligible at this stage of the investigation. This can be attributed in part to the high ratio of reactants used, which minimizes the incorporation of powder particles in the films and also to careful surface preparation.[30,*]

The refractive index dependence on deposition temperature is shown in Fig. 5. Only slight variation in refractive index was observed from sample to sample. Again, this is probably due to the high NH_3/SiH_4 ratio, which helps to maintain constant film composition despite possible fluctuations in flow rates.

---

* The presence of silicon surface defects has been observed to lower the breakdown strength of Al_2O_3 films by as much as 50%.[32]

Electrical Measurements

For these measurements, silicon nitride films ranging in thickness from 500 to 750 Å were deposited over a controlled 20 Å silicon dioxide film.[30] Aluminum contacts of 25 mils diameter were vacuum evaporated through a metal mask to form MNOS capacitors. The exact capacitor areas were determined by taking photomicrographs of known magnification and subsequently measuring the micrograph areas with a planimeter. An evaporated aluminum back contact to the silicon was provided.

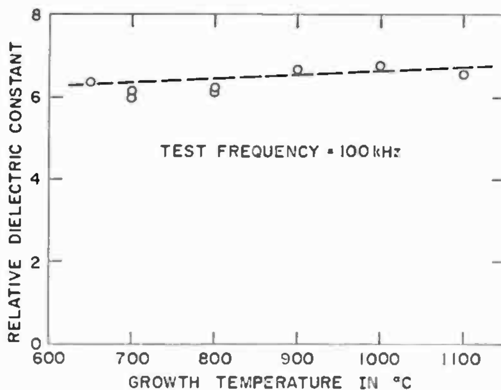

Fig. 6—Relative dielectric constant of silicon nitride as a function of deposition temperature.

Measurements of the capacitance of the MNOS structure were made at 100 kHz with the silicon surface biased heavily into the accumulation region. The relative dielectric constant of the silicon nitride was calculated from the capacitance and dimensions of the structures and is shown in Fig. 6 as a function of deposition temperature. The dielectric breakdown strength of these samples was approximately 10^7 V/cm.

The results of other electrical measurements have been reported previously, including capacitance–voltage characteristics, current–voltage characteristics, charge storage and retention, and the dependence of these properties on the deposition temperature.[29]

3. Device Application

The application of amorphous silicon nitride films in planar silicon technology is well known. The superior resistance of silicon nitride to

ionic contaminants and dopants, amongst other properties, has led to various important applications of this material, including gate insulator in IGFETS (over silicon dioxide), surface passivation of both MOS and bipolar IC's and transistors, diffusion masking, and dielectric isolation. More recently, the high-voltage hysteresis effects associated with MNOS structures have stimulated interest in its use as a memory element material.

At RCA, silicon nitride films deposited by the silane–ammonia reaction have also been applied in several other areas of solid-state technology, as exemplified by the following work.

Gallium arsenide insulated-gate field-effect transistors have been devised using silicon nitride as the gate dielectric.[33,34] Compared with metal–silicon-dioxide–gallium-arsenide structures, the metal–silicon-nitride–gallium-arsenide devices proved superior due to a lower interface state density ($\leqslant 10^{12}$ cm^{-2} $(eV)^{-1}$), the higher dielectric constant of the nitride films, and the greatly improved diffusion masking against zinc and tin dopants.

Silicon planar transistors and integrated circuits having chemically vapor deposited tungsten as metallization and interconnection material have been passivated with silicon nitride films.[35,36] The silicon–tungsten system readily withstands the relatively high temperatures required for silicon nitride deposition, and yields seals of excellent quality. In these devices the silicon nitride layer covers the metallization pattern as well as the active areas of the structure. Openings are prepared in the contact-pad regions along the periphery of the chip, using a layer of silicon dioxide deposited by the silane–oxygen reaction[37,38] as a mask for the phosphoric acid etchant[17] to free the bonding pads and grid lines from silicon nitride. Alternatively, chemically vapor deposited borosilicate glass layers of substantially greater thickness can be used by the process described in previous papers.[38-40] An example of an integrated circuit prepared by this method, combined with an rf sputter-etching technique,[41] is presented in Fig. 7.

Silicon nitride films have also been utilized in the dielectric air isolation scheme named "Decal", developed at RCA for fabricating integrated circuits.[42] Here, the tungsten metallized device wafer is coated with a silicon nitride layer to provide an impurity barrier. The wafer is then bonded face-down to a glass substrate by pressure fusion. The excess silicon is removed in a series of operations from the back side of the device wafer, leaving only islands of silicon and exposed tungsten bonding pads on the glass, all of which are bonded to the glass via silicon nitride.

A novel technique for forming glass-to-metal seals employing silicon

nitride as an interface layer has been described recently.[43] This method offers a number of significant advantages over standard glass-to-metal seal formation. For example, inert atmospheres are not required in the glassing step, so that more readily oxidizable metals can be sealed in ordinary room ambient. Furthermore, there is no adverse reaction of the glass with the metal or its oxide, and the composition of an alloy to be sealed to glass can be selected without regard to the nature or adherence of the oxide that it forms.

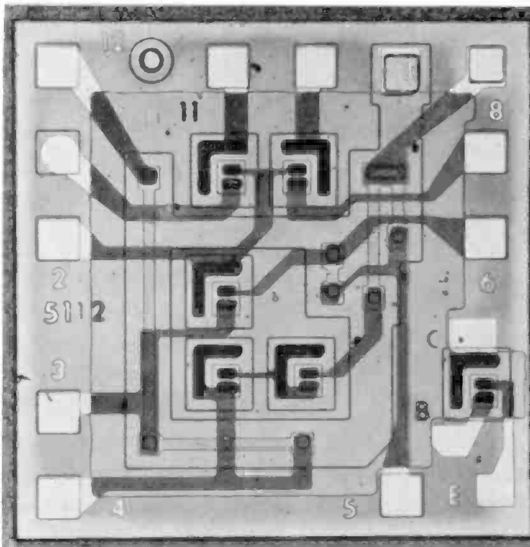

Fig. 7—Silicon nitride/glass passivated and sputter etched experimental integrated circuit. Chemically vapor deposited tungsten is used as the metallization and interconnection material.

4. Conclusions

The properties of silicon nitride films formed by the reaction between silane and ammonia have been studied in MNS and MNOS structures. The influence of carrier gas and deposition temperature on interface and electrical properties has been investigated.

The electrical and interface properties of Si_3N_4-Si structures formed in hydrogen carrier gas were found to be superior to those formed in nitrogen carrier, except for the flat-band voltage value.

Films formed in a large excess of ammonia (NH_3:SiH_4 ratio 10,000:1) had a relatively low pinhole density and exhibited more reproducible properties than films formed at the lower ratios (e.g., 200:1). Previously published results[29] on the electrical properties of MNOS

structures incorporating these films showed that films become more conducting with increasing deposition temperature (probably due to increasing silicon content in the films). Simultaneously the ability of the MNOS structure to retain stored charge decreased very significantly. Consequently, low deposition temperatures (~700°C) are more favorable for memory retention and for attaining less conducting films. This is also an important consideration in Si_3N_4/SiO_2 structures, since differences in conduction behavior in both dielectrics may lead to device failure.

Although the purpose of this work was primarily directed toward investigating the properties of MNOS memory element, these films can be and have been successfully utilized in other applications.

Acknowledgments

The authors gratefully acknowledge the contributions made by R. A. Soltis, J. M. Breece, and D. J. Maurizi for assisting in the experimental work, and G. W. Cullen for reviewing the manuscript.

References:

[1] H. F. Sterling and R. C. G. Swann, "Chemical Vapour Deposition Promoted by r.f. Discharge," **Solid State Electronics,** Vol. 8, p. 653 (1965).

[2] R. C. G. Swann, R. R. Mehta, and T. P. Cauge, "The Preparation and Properties of Thin Film Silicon-Nitrogen Compounds Produced by a Radio Frequency Glow Discharge Reaction," **J. Electrochem. Soc.,** Vol. 114, p. 713 (1967).

[3] V. Y. Doo, D. R. Nichols, and G. A. Silvey, "Preparation and Properties of Pyrolytic Silicon Nitride," **J. Electrochem. Soc.,** Vol. 113, p. 1279 (1966).

[4] K. E. Bean, P. S. Gleim, and R. L. Yeakley, "Some Properties of Vapor Deposited Silicon Nitride Films using the SiH_4-NH_3-H_2 System," **J. Electrochem. Soc.,** Vol. 114, p. 733 (1967).

[5] V. Y. Doo, D. R. Kerr, and D. R. Nichols, "Property Changes in Pyrolytic Silicon Nitride with Reactant Composition Changes," **J. Electrochem. Soc.,** Vol. 115, p. 61 (1968).

[6] J. R. Yeargan and H. L. Taylor, "Conduction Properties of Pyrolytic Silicon Nitride Films," **J. Electrochem. Soc.,** Vol. 115, p. 273 (1968).

[7] W. A. Kohler, "Structural Properties of Vapor Deposited Silicon Nitride," **Tran. AIME,** Vol. 1, p. 735 (1970).

[8] T. L. Chin, C. H. Lee, and G. A. Gruber, "The Preparation and Properties of Amorphous Silicon Nitride Films," **J. Electrochem. Soc.,** Vol. 114, p. 717 (1967).

[9] J. V. Dalton and J. Drobek, "Structure and Sodium Migration in Silicon Nitride Films," **J. Electrochem. Soc.,** Vol. 115, p. 865 (1968).

[10] S. M. Hu, "Properties of Amorphous Silicon Nitride Films," **J. Electrochem. Soc.,** Vol. 113, p. 693 (1966).

[11] F. K. Heumann and D. M. Brown, "Diffusion Masking of Silicon Nitride and Silicon Oxynitride Films on Si," **J. Electrochm. Soc.,** Vol. 115, p. 99 (1968).

[12] M. J. Grieco, F. L. Worthing, and B. Schwartz, "Silicon Nitride Thin Films from $SiCl_4$ plus NH_3: Preparation and Properties," **J. Electrochem. Soc.,** Vol. 115, p. 525 (1968).

[13] T. E. Burgess, J. C. Baum, F. M. Fowkes, R. Holmstrom, and G. A. Shirn, "Thermal Diffusion of Sodium in Silicon Nitride Shielded Silicon Oxide Films," **J. Electrochem. Soc.,** Vol. 116, p. 1005 (1969).

[14] B. E. Deal, E. L. MacKenna, and P. L. Castro, "Characteristics of Fast Surface States Associated with SiO_2-Si and Si_3N_4-SiO_2-Si Structures," **J. Electrochem. Soc.,** Vol. 116, p. 997 (1969).

[15] G. A. Brown, W. C. Robinette, Jr., and H. G. Carlson, "Electrical Characteristics of Silicon Nitride Film Prepared by Silane-Ammonia Reaction," **J. Electrochem. Soc.**, Vol. 115, p. 948 (1968).

[16] P. S. Schaffer and B. Swaroop, "Vapor Phase Growth and DC Breakdown of Silicon Nitride Films," **American Ceramic Soc. Bull.**, Vol. 49, p. 536 (1970).

[17] W. Van Gelder and V. E. Hauser, "The Etching of Silicon Nitride in Phosphoric Acid with Silicon Dioxide as a Mask," **J. Electrochem. Soc.**, Vol. 114, p. 809 (1967).

[18] N. C. Tombs and F. A. Sewell, Jr., "Silicon Oxide as an Etch Mask for Silicon Nitride," **J. Electrochem. Soc.**, Vol. 115, p. 101 (1968).

[19] P. F. Schmidt and D. R. Wonsidler, "Conversion of Silicon Nitride Films to Anodic SiO_2," **J. Electrochem. Soc.**, Vol. 114, p. 603 (1967).

[20] T. B. Tripp, "The Anodic Oxidation of Silicon Nitride Films on Silicon," **J. Electrochem. Soc.**, Vol. 117, p. 157 (1970).

[21] M. P. Lepselter, "Beam Lead Sealed Junction Technology," **Bell Lab. Rec.**, Vol. 44, p. 299 (1966).

[22] S. S. House and R. A. Whitner, "Manufacturing Beam-Lead Sealed-Junction Monolithic Integrated Circuits," **Western Electric Engineer**, Vol. 11, p. 3 (1967).

[23] G. A. Gruber and R. R. Verderben, "The Effects of Film Thickness and Deposition Temperature on SiO_2/Si_3N_4 Passivated High Voltage Mesa Diodes," **J. Electrochem. Soc.**, Vol. 117, p. 98C (1970).

[24] K. S. Tarneja and D. M. Gillott, "Silicon Nitride Passivated Power Rectifiers for High Reliability," **J. Electrochem. Soc.**, Vol. 117, p. 101C (1970).

[25] For a review, see A. G. Revesz and K. H. Zaininger, "The Si-SiO_2 Solid—Solid Interface System," **RCA Review**, Vol. 29, p. 22 (1968).

[26] E. H. Nicollian and A. Goetzberger, **Bell System Tech. J.**, Vol. 46, p. 1055 (1967).

[27] J. Scott and J. T. Wallmark, "Switching and Storage Characteristics of MIS Memory Transistors," **RCA Review**, Vol. 30, p. 335 (1969).

[28] K. H. Zaininger, private communication.

[29] A. M. Goodman, E. C. Ross, and M. T. Duffy, "Optimization of Charge Storage in the MNOS Memory Device," **RCA Review**, Vol. 31, p. 342 (1970).

[30] A. M. Goodman and J. M. Breece, "Thin Tunnelable Layers of Silicon Dioxide Formed by Oxidation of Silicon," **J. Electrochem. Soc.**, Vol. 117, p. 982 (1970).

[31] D. M. Brown, P. V. Gray, F. K. Heumann, H. R. Philipp, and E. A. Taft, "Properties of $Si_xO_yN_z$ Films on Silicon," **J. Electrochem. Soc.**, Vol. 115, p. 311 (1968).

[32] M. T. Duffy, J. E. Carnes, and D. Richman, "Dielectric and Interface Properties of Pyrolytic Aluminum Oxide Films on Silicon Substrates," to be published.

[33] H. W. Becke and J. P. White, "Gallium Arsenide Insulated Gate Field Effect Transistors," p. 219 in **International Symposium on Gallium Arsenide**, Reading, England, Sept. 1966

[34] H. W. Becke and J. P. White, "GaAs FET's outperform conventional silicon MOS devices," **Electronics**, Vol. 40, p. 82 (1967).

[35] J. A. Amick and J. M. Shaw, "Vapor-Deposited Tungsten as a Metallization and Interconnection Material for Silicon Devices," **J. Electrochem. Soc.**, Vol. 116, p. 376C (1969).

[36] J. M. Shaw and J. A. Amick, "Vapor-Deposited Tungsten as a Metallization and Interconnection Material for Silicon Devices," **RCA Review**, Vol. 31, p. 306 (1970).

[37] N. Goldsmith and W. Kern, "The Deposition of Vitreous Silicon Dioxide Films from Silane," **RCA Review**, Vol. 28, p. 153 (1967).

[38] W. Kern and A. W. Fisher, "Deposition and Properties of Silicon Oxide and Silicate Film Prepared by Low-Temperature Oxidation of Hydrides," **RCA Review**, Vol. 31, No. 4, p. 715 (1970).

[39] W. Kern and R. C. Heim, "Chemical Vapor Deposition of Silicate Glasses for use with Silicon Devices—I. Deposition Techniques," **J. Electrochem. Soc.**, Vol. 117, p. 562 (1970).

[40] W. Kern and R. C. Heim, "Chemical Vapor Deposition of Silicate Glasses for Use with Silicon Devices—II. Film Properties," **J. Electrochem. Soc.**, Vol. 117, p. 568 (1970).

[41] J. L. Vossen and J. J. O'Neill, Jr., "R-F Sputtering Processes," **RCA Review**, Vol. 29, p. 149 (1968).

[42] A. I. Stoller and W. H. Schilp, Jr., "Isolation Techniques for Fabricating Integrated Circuits—II. Dielectric Refill Techniques and Decal Air Isolation," **RCA Review**, Vol. 29, p. 485 (1968).

[43] A. I. Stoller, W. C. Schilp, Jr., and J. Benbenek, "A Novel Technique for Forming Glass-to-Metal Seals Using a Silicon Nitride Interface Layer," **RCA Review**, Vol. 31, p. 443 (1970).

Chemical Vapor Deposition of Aluminum Oxide Films from Organo-Aluminum Compounds

M. T. Duffy and Werner Kern
RCA Laboratories, Princeton, N.J.

Abstract—Aluminum oxide films have been deposited on silicon substrates by thermal decomposition of aluminum isopropoxide and by oxidation of trimethyl aluminum vapor at temperatures in the range of 400°-500°C. MOS capacitance measurements have been made on Al_2O_3-Si and Al_2O_3-SiO_2-Si structures and the influence of deposition parameters on interface properties examined. Several other film properties, such as chemical etch rate, dielectric breakdown, refractive index, and IR absorption have also been studied as functions of deposition conditions and heat treatments. Post deposition heat treatment in O_2 eliminates hysteresis effects and reduces the scatter in flat-band voltage values. The density of interface states varies from 10^{10} to 10^{11} cm^{-2} $(eV)^{-1}$ and the flat-band voltage (for ~ 1000 Å oxide) can vary between zero and several volts positive depending upon the deposition parameters and silicon surface preparation. Bias-temperature stress can increase the flat-band voltage value under negative gate bias. Excessive localized conduction and dielectric breakdown can be correlated with the occurrence of silicon surface defects. The interface properties of Al_2O_3-SiO_2-Si structures depend upon the silicon orientation. For the (100) orientation, the interface state density for Al_2O_3 synthesized from aluminum-isopropoxide is about 10^{10} cm^{-2} $(eV)^{-1}$ and the flat-band voltage is zero.

1. Introduction

The use of aluminum oxide (alumina) films for semiconductor device applications has recently received much attention. Advantages of alumina over silica include its greater density, which makes it a more effective barrier to migrating impurities, its better radiation resistance, and its high dielectric constant. The fact that alumina can be deposited, by the methods to be described, so as to yield films with associated positive flat-band voltage values stimulates additional interest.

Chemical vapor deposition is particularly attractive for forming Al_2O_3 films because uniform films of excellent quality for device applications can be obtained at relatively low temperatures. Deposition from a CO_2-H_2-Al_2Cl_6 reaction mixture at 850°-1200°C has been utilized by several investigators,[1-5] but the use of organic starting materials per-

mits lowering the substrate temperature considerably. The pyrolysis of aluminum acetylacetonate at 480°C has been reported to yield good films of Al_2O_3.[6] The pyrolysis of aluminum triethoxide at 300°-500°C[7-9] and the oxidation of tri-isobutyl aluminum with oxygen at 250°-500°C[10] tend to yield porous films with poor electrical properties. Al_2O_3 films obtained from trimethyl aluminum and nitrous oxide at 650°C have recently been reported to have better quality.[11]

We have focused our attention on two chemical vapor reactions for forming Al_2O_3 films: (1) oxidation of trimethyl aluminum, and (2) pyrolysis of aluminum tri-isopropoxide, which is similar to the process reported by Aboaf.[12] The second process has been studied more extensively and consequently is discussed in greater detail.

2. Aluminum Oxide Films Prepared from Trimethyl Aluminum

2.1 Deposition Process

This process is a chemical vapor synthesis based on the controlled oxidation of trimethyl aluminum vapor with oxygen in the temperature range of 275°-475°C.[13] Trimethyl aluminum, $Al_2(CH_3)_6$, was selected from the group of aluminum alkyl compounds because of (1) its favorable aluminum-to-organic ratio, which facilitates attaining pure films; (2) its high reactivity, which allows film deposition below 500°; and (3) its relatively high vapor pressure (8.4 Torr at 20°C), which permits handling in apparatus without heated lines. Nitrogen is used as a diluent and carrier gas. A stoichiometric excess of oxygen minimizes the formation of aluminum hydroxide and promotes oxidation of the organic breakdown products to volatile compounds. A relatively large nitrogen flow rate is beneficial as it tends to suppress the formation of the hydroxide by eliminating water vapor by-product at a rapid rate. A schematic of the alkyl-dispensing and gas-metering system is shown in Fig. 1. Nitrogen passes through a small (10-20 ml) quantity of the liquid alkyl contained in a specially constructed glass bubbler built inside a shock-proof Transite box. The nitrogen carrying the alkyl vapor is further diluted with nitrogen and is then combined with oxygen at the inlet to the reaction chamber. The deposition apparatus consists essentially of a bell jar resting on a hotplate on which the substrates rotate in a planetary motion. Details of the apparatus,[14] the reagents and general techniques,[15] and the physical–chemical principles involved[16] have been presented in previous papers.

Polished (111) and (100) oriented p- and n-type silicon wafers of various resistivities were used as substrates. They were chemically

cleaned[17] and, just before coating, dipped in 5% HF followed by rinsing in pure water. The substrate deposition temperature was normally 450°C. Films were deposited under oxygen-poor* or oxygen-rich** conditions at growth rates ranging from 150 Å/min to 750 Å/min (usually 500 Å/min). The cold substrate wafers are heated in the chamber while flushing with nitrogen prior to deposition to prevent thermal oxidation of the silicon surface. The aluminum alkyl vapor is

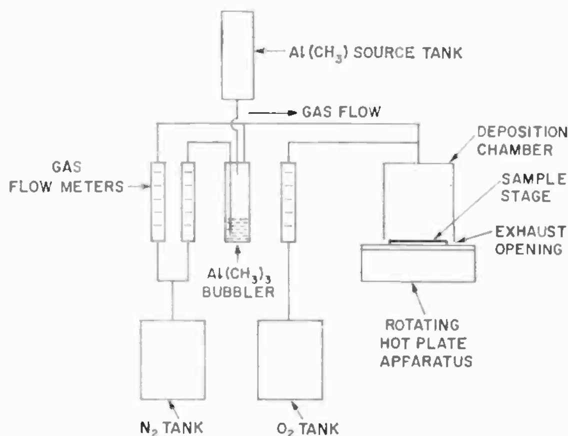

Fig. 1—Schematic of vapor-deposition system for preparing Al_2O_3 films for aluminum trimethyl and oxygen.

then introduced into the chamber, followed 20 seconds later by the oxygen (no deposits form under these conditions). The time required to deposit a film of only a few hundred angstroms thickness is estimated from a graph of film thickness versus deposition time, extrapolated to time zero; a delay time occurs before film deposition commences, which must be taken into account.

2.2 Film Properties

Films Deposited at 275-300°C at Low Oxygen Ratios

Clear films of uniform appearance in the thickness range 200 to 6000 Å were deposited on silicon wafers of 1.25 inch diameter. Films deposited under the above conditions had an average dielectric constant of 6 to 9

* Low oxygen-ratios are O_2:(N_2 through Alkyl) = 1:10 and 1:32.
** High oxygen-ratios are O_2:(N_2 through Alkyl) = 1:1 and 1:2.5.

at 10 kHz. For these measurements, circular top electrodes of 0.014-inch-diameter aluminum were vacuum-evaporated on the films to form parallel plate MOS capacitors. Capacitance measurements were made with a capacitance bridge using at least six capacitors per sample to obtain reliable average values. Several thousand angstroms thick films maintained d-c dielectric breakdown fields up to 8×10^6 V/cm. Transmission electron microscopy revealed an extremely smooth, pinhole-free surface structure, and the diffuse electron diffraction rings indicated a vitreous state of Al_2O_3. The as-deposited films were readily soluble in HF solutions and in 30% KOH, but became insoluble in KOH after a 10-minute densification treatment at 1200°C in argon.

Films Deposited at 450° and 475°C at Low Oxygen Ratios

Thickness and refractive index values of all films were determined by ellipsometry at the mercury wavelength 5461 Å. Films deposited under these conditions had a refractive index (n) of typically 1.64. Heat treatments densify the films and increase the refractive index to a value (1.75) identical with that reported for Al_2O_3 prepared by the H_2-CO_2-$AlCl_3$ process[1-4] at 900°-1200°C, and is close to that reported for pure α-Al_2O_3 (1.765),[18] or for γ-Al_2O_3 (1.76).[19] Low-angle electron diffraction analysis employed for structural investigation showed that 300-600 Å thick films (deposited at 450°C at an oxygen ratio of 1:10) were predominantly polycrystalline (α- and β-Al_2O_3). Scanning electron microscopy at ×10,000 magnification generally showed very smooth, clean, and structureless surface morphology. Thick layers up to 6000 Å were free from cracking or spalling. Layers thicker than this cracked on most substrate materials including vitreous alumina disks. The maximum dielectric breakdown fields estimated from point-contact breakdown tests of film several thousand angstroms thick on single-crystal silicon were in the 10^6 V/cm range.

Etch rates of those films deposited at low oxygen ratios were obtained for 4.9% HF at 25.0°C and for 85% H_3PO_4 at 55°C before and after densification at 700°C in argon or at 800°C in wet oxygen. The film thickness after various periods of etching was determined by interferometric techniques. The last 500 Å of the films was not included in the determination since the Al_2O_3/Si interface of the heat-treated samples exhibited irregular behavior due to residual impurities. Typical results are shown in Table 1. Pattern etching of Al_2O_3 films deposited on metallized silicon, sapphire, and glazed ceramic substrates could be best carried out before densification using photomasking techniques and 30% KOH at 50°C. An IC test pattern etched in a 2750-Å-thick

Table 1—Etch Rates of Al_2O_3 Films from Trimethyl Aluminum as Functions of Synthesis and Densification Conditions

	Synthesis Conditions		Film	Etch Rates (Å/min)					
				4.9% HF* at 25°C			85% H_3PO_4 at 55°C		
Sample	Temp. (°C)	O_2/Alkyl	Thickness (Å)	as dep.	700°	800°	as dep.	700°	800°
1	475	1:32	5000	5640	2100	1330	328	109	53
10	475	1:32	1200	5600	1290	1115	250	72	48
I-8	450	1:1	6000	7780	2280	1930	418	116	100
II-4	450	1:1	3200	7510	2250	1940	358	125	102

* "4.9% HF" = 1 vol 49% (w/w) HF + 9 vol H_2O

Densification Conditions were as follows:

700°C in dry argon for 30 min; or

800°C in wet oxygen for 30 min. followed by a 3 hours anneal to 500°C.

Al_2O_3 film on a silicon substrate is shown in Fig. 2 as an example of the definition obtainable. (This pattern was obtained with the aid of a metallization mask; the dark pattern corresponds to Al_2O_3 in the light colored silicon background. Capacitors prepared on sapphire substrates by this technique were usable with good results up to the 500-MHz range.[20]

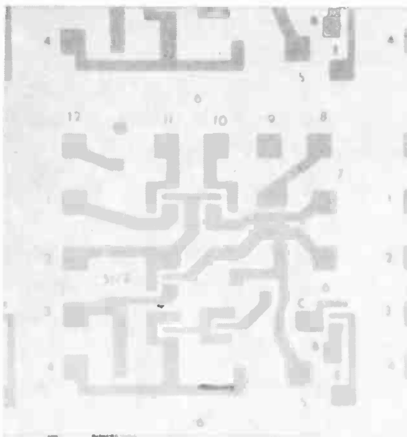

Fig. 2—IC pattern (0.043 × 0.043 inch) prepared from a 2750 Å thick Al_2O_3 film on silicon by photomasking and etching in 30% KOH at 50°C. Dark areas are Al_2O_3; light areas are Si.

Films Deposited at 450° at High Oxygen Ratios

Al_2O_3 films deposited in this manner showed several significant differences in their physical properties from those prepared at low oxygen ratios. Electron diffraction analysis indicated an amorphous film structure in most samples, both before and after heat treatments at 700° or 800°C. The refractive indices were typically 1.60 for as-deposited films, rising to 1.73 on densification at 800°C. However, heat treatment of these films generally lead to defects, such as pinholes and line cracks, more readily than for the films formed under oxygen-poor conditions. Slow cooling (3 hrs from 800° down to 500°C) did not eliminate this tendency. An example of a severe case of this type of

Fig. 3—Optical micrograph of a heat-treated thick Al_2O_3 film showing pinholes and line cracks (approx. 200× before reduction).

defect is shown in Fig. 3. Some dielectric breakdown strength measurements were made by the "self-healing" technique,[23] but most samples exhibited variable behavior. Exceptionally good results were obtained from a 545-Å-thick Al_2O_3 film deposited on p-type silicon and densified for 15 minutes in wet oxygen at 800°C. The breakdown fields were 7.0×10^6 V/cm for positive silicon polarity, and 3.0×10^7 V/cm for negative silicon polarity. This indicates that films of excellent breakdown strength can be deposited under certain substrate preparation and deposition conditions.

Chemical etch rates of these films deposited at high oxygen ratios were determined as described above. Typical values are shown in Table 1 for comparison. The considerable difference for the two etch-

ants between films deposited under various oxygen conditions indicates differences in the film stoichiometry both before and after densification treatments. The relatively small differences in the etch rates of films heated at 700°C in dry argon and those heated at 800°C in wet oxygen indicate that the temperature rather than the ambient is the primary factor in the densification mechanism.

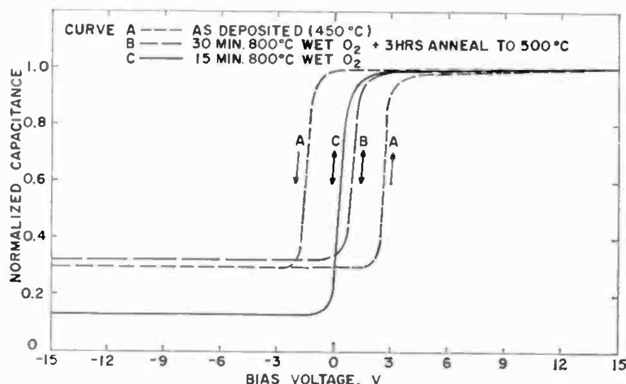

Fig. 4—Typical MOS *C-V* curves for an Al_2O_3 film deposited on silicon from aluminum trimethyl and oxygen before and after heat treatments at 800°C (500 Å Al_2O_3 on 30 ohm-cm n-type silicon wafer using Hg probe).

2.3 Interface Properties

Electrical interface properties were tested with Al_2O_3 films of typically 500 Å thickness, deposited at 450°C both at low and at high oxygen ratios. The *C-V* characteristics, measured at 100 kHz with the aid of a mercury probe, are shown in Fig. 4A for a typical as-deposited film at high oxygen ratio on a (111)-oriented 30 ohm-cm n-type silicon substrate. The large hysteresis effect can be readily reduced or eliminated by a suitable post-deposition heat treatment. Fig. 4B shows the *C-V* characteristics of a sample taken from the same wafer after a 30-minute anneal in moist oxygen at 800°C followed by a 3-hour anneal in argon to 500°C; no hysteresis can be detected any longer. In addition to the disappearance of the hysteresis, the flat-band voltage of the heated sample has decreased to +1 V. Curve 4C shows the result obtained on a portion of the same wafer after heat treatment for only 15 minutes in wet oxygen without annealing in argon, which decreased

the flat-band voltage to only +0.5 V while also eliminating hysteresis effects. The density of interface states determined from *C*-*V* measurements[30] (at 100 kHz) for samples that received a heat treatment in oxygen at 800°C was in the range of 5×10^{11} states/cm^2-eV. Heat treatments at 700°C in argon were much less effective in reducing the flat-band voltage, although the hysteresis could be reduced in most cases. Samples prepared under oxygen-poor synthesis conditions behaved similarly. Essentially the same results were obtained using evaporated gold dots as electrodes on the Al_2O_3 surface and evaporated gold films as back contact to the silicon, except for changes due to work function difference.

Using a semitransparent gold film as a counter electrode, measurements were also made to compare the current flowing through the Al_2O_3 layers due to photoexcitation in the p-type silicon substrate. Thin films of Al_2O_3 deposited at low and at high oxygen ratios were used for this purpose. Both the offset voltage and the apparent Si-Al_2O_3 barrier height for electrons increased with successive voltage pulses for films made under oxygen-rich oxidation conditions, whereas they were relatively constant for oxygen-poor samples. In addition, it was determined that the oxygen-rich films tended to break-down at lower current levels than did oxygen-poor samples. A more detailed discussion of these phenomena will be presented in a forthcoming paper.[21]

3. Aluminum Oxide Films Prepared from Aluminum Isopropoxide

3.1 Deposition Process

Vapor of aluminum isopropoxide was transported to the rf-heated substrates by bubbling helium as carrier gas through the molten metal alcoholate maintained at 125°-130°C. This gas stream was subsequently mixed with nitrogen diluent gas as shown in Fig. 5. This apparatus has been previously described in detail.[21a] Depositions were performed both in the presence and absence of added oxygen. The susceptor deposition temperature* was usually 425° to 500°C, but depositions have also been performed at temperatures as low as 250°C and as high as 900°C.

Both p- and n-type silicon substrates of (111) and (100) orientation were used. The resistivity was usually ~10 ohm-cm; some degenerate substrates were used for dielectric investigations. The wafers were

* The actual substrate temperature was lower.

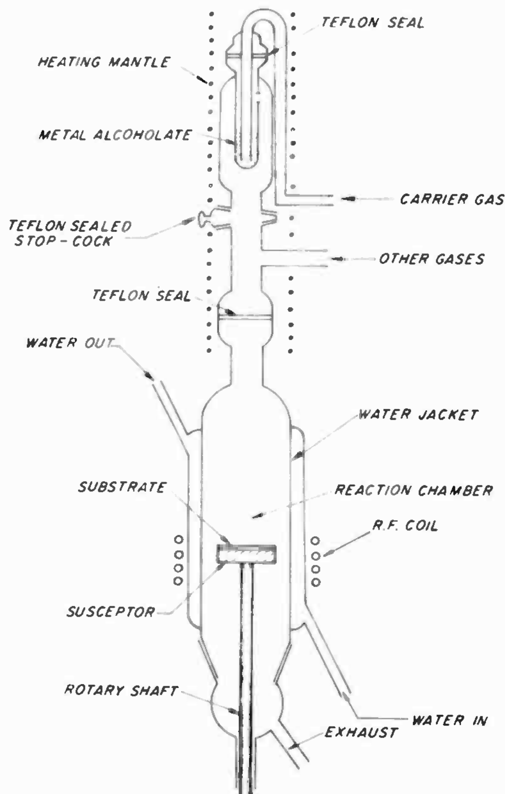

Fig. 5—Apparatus for depositing Al_2O_3 films from aluminum isopropoxide.

cleaned by standard chemical means prior to deposition and had a residual SiO_2 film of 10 to 15 Å. Al_2O_3 films were also deposited on samples prepared by thermally oxidizing silicon wafers in dry O_2 at 1100°C to form an SiO_2 film of 200 Å thickness, followed by annealing in helium for 15 minutes at 1100°C; these processes were performed *in situ* in the Al_2O_3 reactor prior to film deposition.

3.2 Film Properties

Uniform Al_2O_3 films ranging in thickness up to 1.2 μm have been prepared at deposition rates of about 100 Å/min. The etch rates for films prepared at 425°C were typically 200 Å/ min in 85% H_3PO_4 at 55°C, and 80 Å/min at 40°C. Films deposited at 500°C without oxygen had

etch rates of 118 Å/min in 85% H_3PO_4 at 55°C, and 1940 Å/min in 4.9% HF† at 25.0°C. Heat treatment in wet oxygen at 800°C for 15 min decreased these values to 51% and 62%, respectively.

The refractive index varied from 1.60 to 1.68 depending upon deposition temperature in the range of 425° to 500°C. Films deposited at temperatures up to 700°C were amorphous, and remained amorphous even after heat treatment for 30 min at 700°C in oxygen. By contrast, films deposited at temperatures above 800°C and also those heated in O_2 at 800°C showed some crystallinity when examined by electron diffraction.

Electron-probe measurements were made on films that had been deposited at 500°C both in the presence and in the absence of oxygen. The O/Al ratio in both cases was higher than for sapphire, indicating that the films were oxygen rich.[23] The results also showed that no elements with atomic number greater than 11 were present in detectable quantities. Carbon was the only element sought with atomic number less than 11, and was found present in both films at levels of the order of 0.3%.

Infrared studies were initiated in conjunction with post-deposition heat treatments in both moist and dry O_2 at 800°C. These treatments modify the interface properties.[23] The spectra reveal that crystallization of the Al_2O_3 and formation of SiO_2, probably at the Al_2O_3 interface, results from these heat treatments. The infrared data also show that the rate of formation of this oxide is several times greater in the case of the moist-O_2 treatment than when dry O_2 is used. The rates of crystallization are not significantly different for both treatments. Consequently, the moist-O_2 treatment is preferable for reducing the flat-band voltage (as shown later), because of the shorter annealing time required, resulting in a lesser degree of crystallization. Crystallized films cannot be etched controllably in either hydrofluoric acid or phosphoric acid.

The dielectric constant and loss tangent are frequency dependent; typical curves (for films deposited at 425°C) are presented in Figs. 6 and 7. The curves labeled "1" in both figures represent data obtained on an untreated film that was deposited on degenerate silicon, while the curves labeled "2" represent the data from measurements on a sample that received an *in situ* post deposition O_2 treatment at 700°C. The substrate in this latter case was ~10 ohm-cm silicon; the series resistance of this substrate accounts for the upward trend in curve "2", Fig. 7. The dashed curve approximates the expected effect. These results indicate that the O_2 treatment increases the dielectric constant and decreases the apparent value of the loss tangent.

† Vol. 49% (w/w) HF + 9 vol. H_2O.

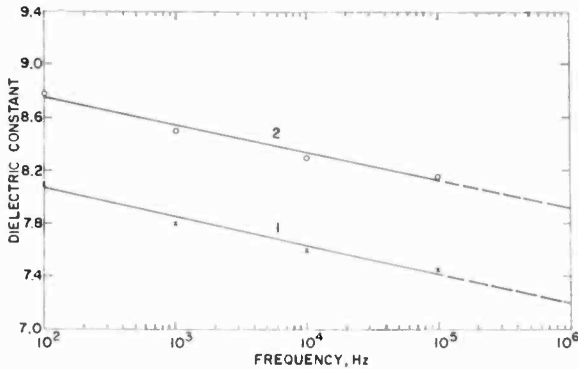

Fig. 6—Frequency dependence of dielectric constant of Al_2O_3: curve 1, as-deposited; curve 2, oxygen-treated.

It has been demonstrated in self-healing breakdown measurements and by dark-field microscopy that excessive localized conduction and low breakdown strength can be associated with silicon surface defects prior to deposition.[23] The final breakdown strength (after weak spots are eliminated) is common to all samples prepared in similar fashion. For Au-Al_2O_3-Si structures, this value was approximately 7.5×10^6 to 1×10^7 V/cm (Al_2O_3 film thickness 1000 Å). These values were obtained for films deposited at 500°C. Values for films deposited at 400°C were approximately half of those quoted above. By suitable surface

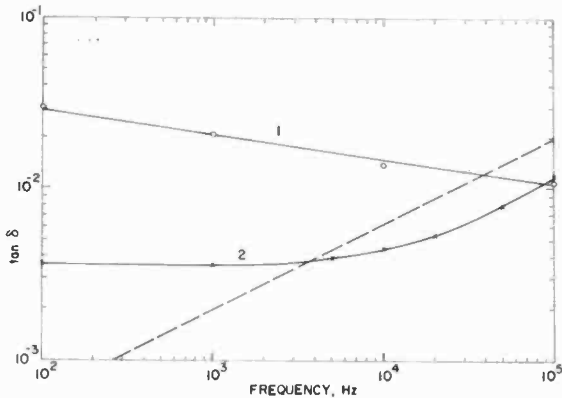

Fig. 7—Loss tangent versus frequency: curve 1, as deposited Al_2O_3 on degenerate silicon; curve 2, deposited on ~10 ohm-cm Si and heat treated in O_2. The upward trend of curve 2 results from the resistance of the substrate; the broken curve approximates the expected effect.

preparation and deposition procedure, it is now possible to prepare Al_2O_3 films whose initial breakdown voltage is as high as the final "intrinsic" value.[24]

3.3 Interface Properties

The *C-V* characteristics of as-prepared Al_2O_3-Si structures depend upon the deposition temperature and silicon surface preparation.[22,23] In general, higher deposition temperatures favor reduced hysteresis and more positive flat-band voltage values.

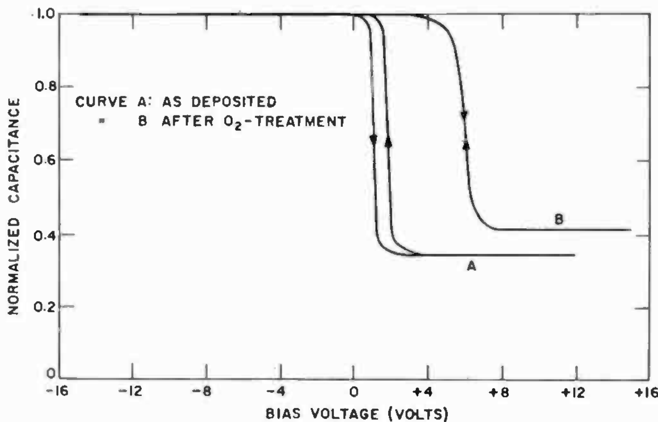

Fig. 8—Effect of O_2 treatment at 700°C for 15 min on interface behavior of Al_2O_3-Si structure.

Hysteresis effects can be removed by post-deposition annealing in O_2 at 700°C. An example is shown in Fig. 8. After this treatment, the flat-band voltage is usually +2 to +4 V (using aluminum contacts on 1000-Å Al_2O_3) and the density of interface states varies from 10^{10} to 10^{11} states/cm^2 eV.[22]

It is possible to decrease the value of the flat-band voltage by post-deposition annealing in moist or dry O_2 at 800°C.[23] Such a decrease in flat-band voltage could be expected with the growth of a thin SiO_2 interface layer, as has been indicated by infrared measurements.

Interface properties can be modified considerably by the silicon surface preparation. Fig. 9 shows the *C-V* characteristics corresponding to different surface preparations (deposition temperature 500°C). A pre-deposition heat treatment in H_2 at 1200°C results in a flat-band

voltage of +8 V, while the growth of approximately 50 Å SiO_2 on a chemically cleaned substrate prior to deposition results in zero flat-band voltage.* Various intermediate values result from different substrate cleaning procedures, which, in turn, influence the properties of the residual surface oxide and the nature of surface adsorbates.[25,26]

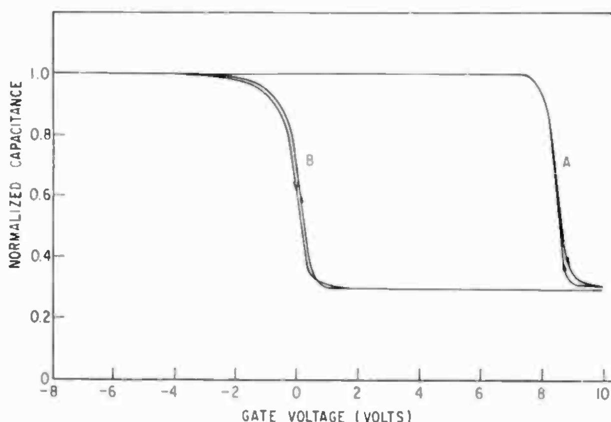

Fig. 9—*C-V* characteristics of two samples showing flat-band voltage dependence on Si surface oxide (film thickness ~1000 Å): curve A is for Si substrate heated in H_2 at 1200°C prior to deposition; curve B is for ~50 Å SiO_2 grown on chemically cleaned substrate prior to deposition.

The corresponding high-voltage hysteresis or "memory" effect associated with the films characterized in Fig. 9 is illustrated in Fig. 10, where the same designations apply. It can be seen that the presence of a thin interface SiO_2 film (~50 Å) is sufficient to eliminate high-voltage hysteresis effects associated with charge transfer at the Al_2O_3-Si interface.[23]

The interface properties of double insulator structures (200 Å SiO_2 and 1000 Å Al_2O_3), in contrast to Al_2O_3-Si structures, depend upon the silicon crystallographic orientation.[22] Typically, for (111) orientation, the flat-band voltage is about −2.5 V, and the interface state density varies from 4×10^{10} to 2×10^{11} states/cm^2 eV. For (100) orientation, the flat-band voltage is approximately zero, and the interface state density varies from 1×10^{10} to 4×10^{10} states/cm^2 eV.

The results of bias-temperature stability measurements on Al_2O_3-Si

* Capacitance–voltage measurements were made with the aid of an Hg probe.

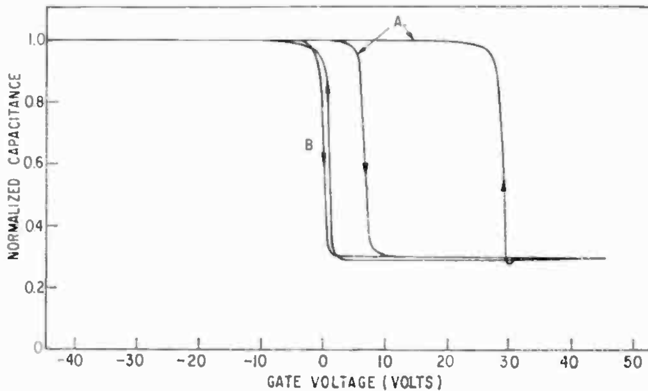

Fig. 10—*C-V* characteristics of samples shown in Fig. 9 showing high-voltage hysteresis effects in relation to Si surface oxide.

samples[23] show that a change of approximately +4 V in flat-band voltage occurs after application of −10 V gate bias for 5 min at 250°C (1000 Å Al_2O_3). Little change is observed for positive gate biasing. A possible explanation for these results has been given previously.[22]

The results of irradiation measurements are presented in Fig. 12. These measurements were made by irradiating MOS units, while under applied gate bias, with 1 MeV electrons. The fluence level corresponding to each bombardment was 10^{14} e/cm^2, and a bombardment was made at each of a series of applied gate voltages. MOS capacitance measure-

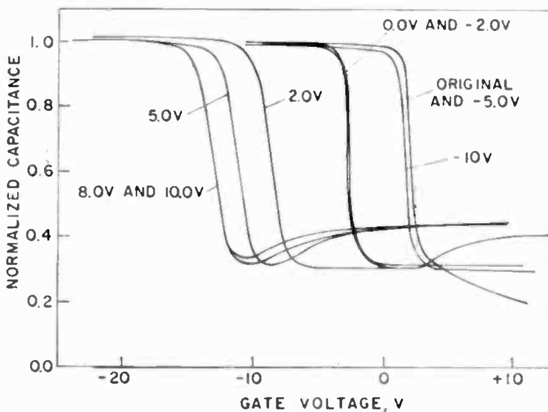

Fig. 11—Effect of electron irradiation on MOS capacitance of 1400 Å Al_2O_3 film. The parameter in the figure refers to the gate bias during irradiation.

ments were performed and the density of induced charge determined after each bombardment. The principal radiation effect occurs under positive gate bias. The increased radiation resistance of Al_2O_3 over that of SiO_2 can be explained in terms of electron trapping in Al_2O_3.[22, 27, 28]

4. Device Applications

Aluminum oxide has emerged as a radiation-hard thin-film dielectric that forms good interface properties with silicon. It has been demonstrated that Al_2O_3-Si structures can be prepared without hysteresis and with an interface state density of $\sim 10^{10}$ states/cm^2 eV without the application of ultraclean technology.[24] This value is comparable with that obtained for ultraclean SiO_2-Si structures and 10 to 100 times better than for the Si_3N_4-Si system. Like silicon nitride, Al_2O_3 is a good diffusion mask and has a dielectric constant about double that of SiO_2. Considerable interest and research has been devoted to the possible substitution of this material for SiO_2 for specialized applications, particularly radiation-hard MOS devices. It can also be used in conjunction with SiO_2 in composite insulator structures and allows an alternative choice to Si_3N_4 with corresponding difference in interface properties.

To test the device potential of the films prepared by the aluminum isopropoxide pyrolysis, discrete "ring-dot" MOS transistors were fabricated.[29] The dimensions of this test structure were relatively large in order to ease the processing requirements. These tests were oriented toward meeting the requirements of complementary-symmetry application. Because the flat-band voltage of alumina MOS capacitors is too large for this purpose, it was necessary to perform a post-deposition heat treatment in moist O_2 in order to obtain the desired device threshold voltage. Encouraging results were obtained in this manner.[23, 29]

5. Conclusions

Techniques have been described for depositing aluminum oxide films from the vapor phase by oxidation of trimethyl aluminum and by pyrolysis of aluminum isopropoxide. The properties relevant to solid-state device technology of the films obtained by these two processes have been explored with emphasis on the films obtained by the pyrolysis process, which exhibited particularly good interface properties on silicon without using special clean technology. Consequently, chemically

vapor deposited Al_2O_3 can be used either alone or in conjunction with a thin film of SiO_2 for device purposes. However, more precise control of the flat-band voltage value is required before these advantages and other benefits (such as radiation resistance) of the films can be fully exploited. One method of accomplishing this—namely post-deposition heat treatment in moist oxygen—has been demonstrated to be an effective technique that simultaneously eliminates *C-V* hysteresis effects. Good MOS transistor characteristics have been obtained by this means.

Although Al_2O_3-Si structures formed by the oxidation of trimethyl aluminum have not been as extensively studied as those prepared by the pyrolysis of aluminum isopropoxide, the available results show that both structures exhibit parallel behavior in many respects. Optimization of the deposition parameters could lead to similar properties.

Trimethyl aluminum as source material allows control of one additional and interesting parameter, namely control of the oxygen content of the resulting Al_2O_3 films.

Acknowledgments

The authors gratefully acknowledge the contributions made by R. Soltis, G. Mark, F. Kolondra, and G. O. Fowler for assisting in the experimental work, J. Carnes for dielectric measurements, D. G. Fisher for photoexcitation studies, E. P. Bertin and D. A. Kramer for electron microprobe analysis, J. T. McGinn and W. C. Roth for electron diffraction, J. M. Shaw for ellipsometric measurements, P. J. Zanzucchi for infrared analysis, F. B. Micheletti and C. W. Benyon for transistor fabrication and measurements, and G. W. Cullen for reviewing the manuscript.

Portions of this work have been performed under Contract N-00019-69-C-0042 sponsored by the Naval Air Systems Command, Department of the Navy.

References:

[1] S. K. Tung and R. E. Caffrey "The Deposition of Oxide on Silicon by the Reaction of a Metal Halide with a Hydrogen-Carbon Dioxide Mixture," **Trans. Met. Soc. AIME**, Vol. 233, p. 572 (1965).

[2] S. K. Tung and R. E. Caffrey, "Pyrolytic Deposition and Properties of Aluminum Oxide Film," **J. Electrochem. Soc.**, Vol. 114, p. 275C (1967).

[3] V. Y. Doo and P. J. Tsang, "Morphology, Structure and Properties of Pyrolytic Aluminum Oxide," **J. Electrochem. Soc.**, Vol. 116, p. 116C (1969).

[4] S. K. Tung and R. E. Caffrey, "The Deposition and Physical Properties of Aluminosilicate Films," **J. Electrochem. Soc.**, Vol. 117, p. 91 (1970).

[5] T. Tsujide, S. Nakanuma, and Y. Ikushima, "Properties of Aluminum Oxide Obtained by Hydrolysis of $AlCl_3$," **J. Electrochem. Soc.**, Vol. 117, p. 703 (1970).

[6] V. F. Korzo, N. S. Ibraimov, and B. D. Halkin, "The Structure of Pyrolytically Grown Al_2O_3 Films," **J. Appl. Chem.**, Vol. 42, p. 989 (1969).

[7] L. A. Ryabova and Ya. S. Savitskaya, "The Preparation of Thin Films of Some Oxides by the Pyrolysis Method," **Thin Solid Films,** Vol. 2, p. 141 (1968).

[8] M. Matsushita and Y. Koga, "Thin Alumina Films Prepared by Thermal Decomposition of Aluminum Triethoxide," **J. Electrochem. Soc.,** Vol. 115, p. 69C (1968).

[9] L. A. Ryabova and Ya. S. Savitskaya, "Preparation of Oxide Films by Pyrolysis and Investigation of their Structure Sensitive Properties," **J. Vacuum Science and Technol.,** Vol. 6, p. 934 (1970).

[10] F. C. Evenstijn, "Low-Temperature Deposition of Alumina-Silica Films," **Philips Res. Repts.,** Vol. 21, p. 379 (1966).

[11] L. Hall and B. Robinette, "Properties of Aluminum Oxide Films obtained from Nitrous Oxide and Aluminum Trimethyl," p. 637 in **Chemical Vapor Deposition,** Sec. Intern. Conf., ed. by J. M. Blocher, Jr., and J. C. Withers, The Electrochem. Soc., Inc., New York, 1970.

[12] J. A. Aboaf, "Deposition and Properties of Aluminum Oxide Obtained by Pyrolytic Decomposition of an Aluminum Alkoxide," **J. Electrochem. Soc.,** Vol. 114, p. 948 (1967).

[13] W. Kern and R. C. Heim, "Chemical Vapor Deposition of Silicate Glasses for Use with Silicon Devices," **J. Electrochem. Soc.,** Vol. 116, p. 70C (1969).

[14] W. Kern, "Apparatus for Chemical Vapor Deposition of Oxide and Glass Films," **RCA Review,** Vol. 29, p. 525 (1968).

[15] W. Kern and R. C. Heim, "Chemical Vapor Deposition of Silicate Glasses for Use with Silicon Devices—I. Deposition Techniques," **J. Electrochem. Soc.,** Vol. 117, p. 562 (1970).

[16] J. A. Amick and W. Kern, "Chemical Vapor Deposition Techniques for the Fabrication of Semiconductor Devices," p. 551, in **Chemical Vapor Deposition,** Second Internatl. Conf., ed. by J. M. Blocher, Jr., and J. C. Withers, The Electrochem. Soc., Inc., New York (1970).

[17] W. Kern and D. Puotinen, "Cleaning Solutions Based on Hydrogen Peroxide for use in Silicon Semiconductor Technology," **RCA Review,** Vol. 31, p. 187 (1970).

[18] R. C. Weast, Ed., p. B-86 in **Handbook of Chemistry and Physics,** 50th Ed., The Chem. Rubber Co., Cleveland, Ohio (1969).

[19] P. W. Lee, p. 15 in **Ceramics,** Reinhold Publ. Co., New York (1961).

[20] L. Norton. RCA Laboratories, Private Communications.

[21] D. G. Fisher and W. Kern, to be published.

[21a] M. T. Duffy, C. C. Wang, A. Waxman, and K. H. Zaininger, **J. Electrochem. Soc.,** Vol. 116, p. 234 (1969).

[22] M. T. Duffy and A. G. Revesz, "Interface Properties of Si-(SiO_2)-Al_2O_3 Structures," **J. Electrochem. Soc.,** Vol. 117, p. 372 (1970).

[23] M. T. Duffy, J. E. Carnes, and D. Richman, "Dielectric and Interface Properties of Pyrolytic Aluminum Oxide Films on Silicon Substrates," paper given at The Metallurgical Society Technical Conf. on Preparation and Properties of Electronic and Magnetic Materials for Computers, New York, Aug. 30-Sept. 2, 1970 (to be published).

[24] J. E. Carnes, M. T. Duffy, C. W. Mueller, D. Richman, and P. J. Zanzucchi, "Improved Dielectric films for Semiconductor Application," Final Report, Oct. 1970, Contract N00019-70-C-0129.

[25] W. Kern, "Radiochemical Study of Semiconductor Surface Contamination—I. Adsorption of Reagent Components," **RCA Review,** Vol. 31, p. 207 (1970).

[26] W. Kern, "Radiochemical Study of Semiconductor Surface Contamination—II. Deposition of Trace Impurities on Silicon and Silica," **RCA Review,** Vol. 31, p. 234 (1970).

[27] J. P. Mitchell, **IEEE Trans. on Nucl. Science,** Vol. NS-15, p. 154 (1968).

[28] K. H. Zaininger and A. G. Holmes-Siedle, "A Survey of Radiation Effects in Metal-Insulator-Semiconductor Devices," **RCA Review,** Vol. 28, p. 208 (1967).

[29] F. B. Micheletti, K. H. Zaininger and W. J. Dennehy, "Fabrication of Radiation-Resistant Al_2O_3 MOS Circuits," Techn. Rep. AFAL-TR-70-53, May 1970.

[30] E. H. Nicollian and A. Goetzberger, **Bell System Tech. J.,** Vol. 46, p. 1055 (1967).

Interface Properties of Chemically Vapor Deposited Silica Films on Gallium Arsenide

Werner Kern, RCA Laboratories, Princeton, N.J.
J. P. White, RCA Solid State Division, Somerville, N.J.

Abstract—The average numerical distribution and frequency response of states at the GaAs/SiO_2 interface has been determined from the C-V characteristics of MOS surface varactors as a function of several variables. These include technique of oxide deposition, post-deposition heat treatment, dopant type of substrate, crystallographic orientation of the substrate, and chemical treatment of the GaAs crystal surface. The SiO_2 layers were deposited primarily by pyrolysis of tetraethyl siloxane under various temperature and pressure conditions. The influence of various deposition variables on some film properties was also investigated. Silane-derived SiO_2 deposited at low temperature was examined in an exploratory manner. The interface state density can be reduced significantly by using $(\bar{1}\bar{1}\bar{1})$ crystal face plus a combination of specific chemical treatments followed by rapid deposition of SiO_2 at low temperature. The lowest values achieved by this method is 1×10^{11} interface states/cm^2 eV, which made the construction of a GaAs MOS transistor feasible.

1. Introduction

A considerable amount of work has been done in the industry on developing the technology for the production of gallium arsenide devices. Although there have been some studies on the state density at the gallium arsenide surface,[1] little information is available on the density of states at gallium arsenide/silicon dioxide interface. The work described in this paper was undertaken as part of a study of surface passivation techniques[2] and was directed toward attaining optimum conditions for a gallium arsenide/silicon dioxide interface with a low state density.

The MOS surface varactor[3,4] was chosen as the test vehicle because of its sensitivity and its simplicity of construction. The capacitance–voltage characteristic of this device was used to estimate the average density of interface states. The effects of the crystallographic orientation of the substrate and the type of chemical surface treatment of the gallium arsenide surface were investigated. Furthermore, the effects

on the state density of variations in the oxide deposition techniques were studied, and some properties of the resulting films determined.

Two methods for depositing silicon dioxide films on gallium arsenide were examined: (1) pyrolysis of tetraethyl siloxane vapor,[5] and (2) gas-phase oxidation of silane.[6] However, at the time these studies were conducted the structural quality of the silane-derived silica layers had not been developed to the present stage of perfection; the major portion of the investigation was therefore based on the more conventional siloxane-derived silica deposition.

2. The MOS Surface Varactor for Determining Interface States

The capacitance of the surface varactor is usually measured with a low-voltage ac signal (typically 1 mV at 1 MHz) and is equivalent to the oxide capacitance, C_{ox}, in series with the parallel combination of the surface-state capacitance, C_{ss}, and the semiconductor space-charge capacitance, C_s.

In general, both slow and fast states exist at the semiconductor–oxide interface within the energy range of the forbidden gap. The slow states may be associated with the charge trapped in the oxide and have virtually no charge exchange with the bulk semiconductor during the measurements. These charges have response times ranging in periods from minutes to months. Their effect on the *C-V* characteristic of the surface varactor is merely a displacement of the voltage axis.

In contrast, the fast states have a marked effect on the *C-V* characteristics because their response varies from seconds to microseconds, or less, and there is charge transfer from these states to the bulk material. It will be shown that the density of fast states is dependent on the surface treatment, direction of crystal orientation, and the method of oxide deposition.

The effect of interface states on the *C-V* characteristic is shown in Fig. 1. The fraction f of fast states that respond at the test frequency have a capacitance associated with them that shunts the space-charge capacitance of the semiconductor, and so reduces the total capacitance change, i.e., $C_1'' - C_2'' < C_1 - C_2$. The surface states also reduce the field terminating at the charges at the surface of the semiconductor, requiring more voltage to swing the surface potential from level bands to the point of inversion, i.e., $V_1'' - V_2'' > V_1 - V_2$. The exact distribution of the state density as a function of energy over the forbidden gap is unknown. However, by assuming a uniform distribution, estimates of the average state density can be made from the *C-V* characteristics.[4]

3. Preparation and Measurements of Test Devices

Surface varactors were fabricated from gallium arsenide wafers that had been coated with silicon dioxide by the techniques described in the next section. A 9-mil-diameter silver gate electrode was formed by evaporation. The scribed pellets were mounted with lead on T0-5 headers at 400°C in 10% hydrogen–90% nitrogen. The device was completed by bonding a 0.5-mil-diameter gold wire from the header post to the gate of each unit.

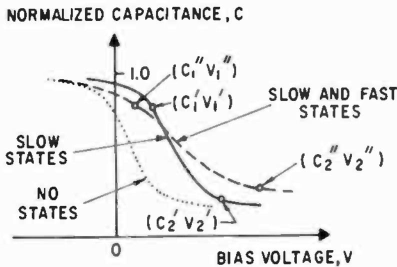

C_{so} = space-charge capacitance at flat-band condition

C_{sm} = space-charge capacitance minimum

$$C_1'' = \frac{C_{so} + C_{ss}(V_1'')}{C_{ox} + C_{so} + C_{ss}(V_1'')}, \quad C_2'' = \frac{C_{sm} + C_{ss}(V_2'')}{C_{ox} + C_{sm} + C_{ss}(V_2')}$$

$$V_2'' - V_1'' > V_2' - V_1'$$

Fig. 1—Effect of interface states on the capacitance–voltage characteristic of MOS surface varactor.

The capacitance was measured on a capacitance bridge using a 1-mV signal at 1 MHz. The capacitance was determined to an accuracy of better than 1 percent. A copper shield was used to minimize the effect of light and stray capacitance. A dc voltage was applied and varied to produce a complete variation in capacitance. In some cases the readings drifted, but appeared to stabilize within a few seconds. All measured points were normalized with respect to the oxide capacitance. An experimental curve was then plotted from the data and analyzed using the method described in Ref (4) to determine the state density, K, and the fraction of states responding at 1 MHz, f.

The maximum dielectric breakdown field sustained by the devices was determined under dc bias conditions. The dielectric constant of the films was calculated from the film thickness and the maximum capacitance at 1 MHz.

The thickness of the silicon dioxide films was determined by optical interference microscopy using monochromatic thallium light and metallized sample surfaces.[7] The accuracy of a typical film thickness of 2,000 Å is estimated at ±7 per cent. The chemical etch rate was determined at 25.0°C using dilute HF. The etching end point was determined by the hydrophobicity technique described in an earlier paper.[8]

4. Techniques of Oxide Deposition

Pyrolysis of tetraethyl siloxane* vapor was carried out in an argon atmosphere using horizontal and vertical quartz reaction tubes with suitable joints and provision for inserting a thermocouple. Three techniques of film deposition were investigated: (1) high temperature, normal pressure, fast deposition rate; (2) high temperature, reduced pressure, slow deposition rate; (3) low temperature, reduced pressure, slow deposition rate.

In the high-temperature, normal-pressure technique the substrate wafers were introduced in a horizontal tube furnace heated to 600°C and flushed with argon. The siloxane vapor was introduced with argon carrier gas from a source bubbler kept at 23°C. It is important to start the deposition at the lowest possible (600°C) temperature so that some silica is deposited immediately to prevent the gallium arsenide surface from dissociating subsequently at the higher temperatures. The temperature of the furnace was then rapidly increased to 730°C and maintained at that value until the desired film thickness resulted. Typical gas flow rated through the siloxane bubbler, oxide deposition rates, and other data are summarized in Table 1. An automated version of the apparatus employing programmed solenoid valves was also used.

The high-temperature, low-pressure deposition was conducted the same way except that the pressure in the reactor was reduced to 50 Torr. In this method the mean deposition rate was much lower, and decreased with deposition time as the furnace tubes became coated (Table 1). Typical runs of 15 minutes yielded 1600-Å-thick films. The uniformity of film thickness over the wafers with this technique was generally better than that obtained with the normal-pressure deposition, and the build-up of decomposition products in the pyrolysis tube was substantially reduced.

The low-temperature, low-pressure depositions were done in a vertical quartz tube reactor. The argon carrying the siloxane vapor

---

* $Si(OC_2H_4)_4$, also known as "tetraethyl orthosilicate" or "tetraethoxysilane".

Table 1—Evaluation of Pyrolytic SiO_2 Films Chemically Vapor Deposited by Various Techniques

Deposition Conditions					Film Analysis			
Temp (°C)	Pressure (Torr)	Time (min)	Flow Rate** (cm^3/min)	Mean Deposition Rate (Å/min)	Film Thickness (Å)	Dielectric Constant	Dielectric Breakdown Field E_{max}, (V/cm)	Etch Rate in 4.9% HF (Å/sec)
High Temperature, Normal Pressure								
730	760	1	850	2,290	2,290	4.7	3.5×10^6	45
High Temperature, Normal Pressure, Automatic								
730	760	2	850	1,200	2,400	4.9	4.0×10^6	45
730	760	2	850	1,250	2,500	4.5	3.5×10^6	45
High Temperature, Low Pressure								
733	50	7.5	123	170	1,270	4.8	7.0×10^6	53
733	50	15	123	108	1,620	4.2	5.0×10^6	41
733	50	30	123	81	2,400	4.3	3.0×10^6	40
733	50	10	425	270	2,700	6.2	2.5×10^6	
Low Temperature, Low Pressure								
275*	50	20	450	108	2,160	5.4	4.0×10^5	86
275*	50	30	450	90	2,700	5.2	5.5×10^6	71
~350*	50	30	460	235	2,700	5.2	5.5×10^6	71
450*	50	10	460	270	2,700	6.0	$>3.5 \times 10^6$	117
450*	50	20	460	232	4,640	6.9	$>3.5 \times 10^6$	101
~500*	50	10	460	540	5,400	>5	2.0×10^6	60

Substrate: Standard Polish-etched GaAs, $(\bar{1}\bar{1}\bar{1})$ plane, n-type, 3×10^{16} carriers/cm^3.

* Pedestal temperature.

** Argon carrier gas through tetraethyl siloxane bubbler.

passed downward through a short 740°C hot zone and then impinged onto the substrate wafer positioned on a water-cooled horizontal pedestal just below the hot zone. Substrate temperatures as low as 150°C and as high as 500°C were used. The pressure was maintained at 50 Torr. Uniform, hard, clear, and glassy silica films were obtained, but close control of the deposition parameters was required to attain reproducible results.

Some properties of the as-deposited films on gallium arsenide wafers are presented in Table 1. There is no marked difference between the dielectric constants, the dielectric breakdown values, and the etch rates of film deposited at normal or reduced pressure at high temperature. Films deposited by the low-temperature, low-pressure technique have a significantly higher dielectric constant and etch rate due to lower film density, but the dielectric breakdown fields, with a few exceptions, are only slightly lower. The adherence of all films to the gallium arsenide substrate was excellent, judged by the fact that no peeling or cracking of the layers occured. The low-temperature, low-pressure films deposited at 450°C were uniform in thickness and exhibited infrared adsorption spectra on silicon that were very similar to those obtained from 730°C samples or from other siloxane-derived films reported in the literature.[9]

Silicon dioxide films from nitrogen-diluted silane, SiH_4, and oxygen were deposited at 300°C by the technique described earlier,[6] employing the planetary rotation hot-plate reactor.[10] Additional details concerning both deposition reactions and the various deposition systems have been discussed recently.[11,12]

5. Density of Interface States as a Function of Various Parameters

The average density of states at the gallium arsenide/silica interface was determined separately each as a function of the method and specific technique of deposition of the silicon dioxide films, post-deposition heat treatment, semiconductor dopant type, crystallographic orientation of the substrate crystals, and chemical treatment of the gallium arsenide surfaces.

Effects of Oxide Deposition Parameters

The influence of the deposition parameters for depositing silicon dioxide films on the interface state density were assessed by coating $(\overline{1}\overline{1}\overline{1})$ oriented and chemically polished gallium arsenide wafers that were then fabricated into surface varactors. The results obtained are summarized in Table 2. The trend in the data indicates that the lower temperatures

Table 2—GaAs/SiO_2 Interface State Density as a Function of Oxide Deposition Conditions

Deposition Conditions				Interface State Density	
Temp. (°C)	Pressure (Torr)	Time (min)	Mean Deposition Rate, (Å/min)	K	f
High Temperature, Normal Pressure					
730	760	1	2,290	4×10^{12}	0.07
High Temperature, Normal Pressure Automatic					
730	760	2	1,200	9×10^{11}	0.99
730	760	2	1,250	3×10^{12}	0.80
High Temperature, Low Pressure					
733	50	7.5	170	8×10^{12}	0.03
733	50	15	108	$>10^{13}$	
733	50	30	81	$>10^{13}$	
733	50	10	270	5×10^{12}	0.01
Low Temperature, Low Pressure					
~350*	50	30	235	3×10^{12}	0.01
~500*	50	10	540	3×10^{12}	0.07

Substrate: Standard polish-etched GaAs, $(\bar{1}\bar{1}\bar{1})$ plane, n-type, 3×10^{16} carriers/cm^3.
f value: denotes the fraction of the total state densities which respond at 1 MHz.
K value: interface state density, $(cm^2\,eV)^{-1}$.
* Pedestal temperature.

and shorter periods of heat exposure favor the reduction of interface states.

MOS capacitors fabricated from substrates coated at 300°C by the silane oxidation process resulted in a wide variation of oxide capacitance between units due to nonuniformities in thickness and dielectric constant of the films. The interface state density ranged between 6×10^{11} and 2×10^{12}/cm^2-eV. The f factor was in general less than 0.01, indicating a predominance of slower states, with frequency response less than 1 MHz. Lower deposition temperatures tended to increase the interface state density above 2×10^{12}/cm^2-eV, in contrast to films deposited by the pyrolysis of tetraethyl siloxane.

Effects of Dopant Type and Post-Deposition Heat Treatment

These effects were studied with oxide coated n- and p-type gallium arsenide wafers that were $(\overline{1}\overline{1}\overline{1})$ oriented and chemically polished by standard techniques; no additional surface treatment was used. After depositing 2000 Å of silicon dioxide by the fast deposition technique (730°C, 760 Torr), the wafers were divided; one half of each was heated in vacuum for 15 hours at 800°C. MOS varactors were then fabricated from each half of the wafer. The C-V characteristics with the corresponding numerical average interface state density values of these devices are shown in Figs. 2 and 3. Although the heat treatment causes a considerable shift in the C-V curves, the interface state density is hardly affected both for p-type and n-type substrates. The frequency response factor (f), however, does change significantly.

Effects of Crystallographic Orientation

A single-crystal n-type gallium arsenide ingot was grown using silicon as the dopant to yield a concentration of 4 to 6×10^{17} carriers/cm^3. The crystal was sectioned into four groups of wafers oriented on the (111), $(\overline{1}\overline{1}\overline{1})$, (110), and (211) planes. They were lapped and chemically polished with a mixture of 5 vol H_2SO_4 98%, 1 vol H_2O, and 1 vol H_2O_2 30% for one hour at room temperature in a rotary beaker followed by rinsing in deionized and quartz-distilled water at 20°C. This process removes approximately 200 microns of the gallium arsenide surface and results in polished, hydrophylic surfaces of high quality except in the case of the gallium (111) plane, which exhibits etch pits. The wafers were dried and coated immediately with pyrolytic silica films prepared at high temperature by the reduced-pressure technique (slow deposition rate) and also by the normal-pressure technique (fast

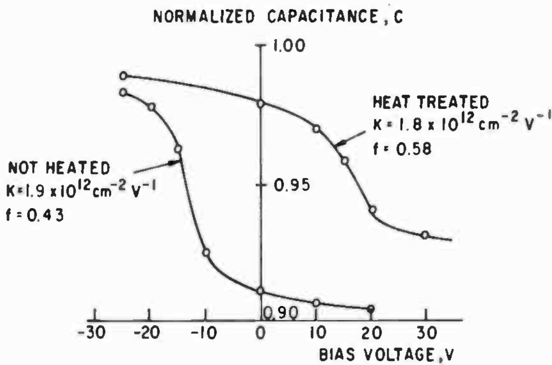

Fig. 2—Effect of heat treatment on the capacitance–voltage characteristic of MOS surface varactor for p-type GaAs (dopant concentration $= 1 \times 10^{17}/\text{cm}^3$).

deposition rate). The results presented in Table 3 show that under the high-temperature conditions discussed here, the lowest average state density was attained with the $(\overline{1}\overline{1}\overline{1})$ plane under fast deposition conditions ($K = 9 \times 10^{11}$ states/cm^2 eV, $f = 0.99$).

It is also of interest to note that the mean rate of silicon dioxide film growth under standard deposition conditions depends upon the crystallographic orientation. The data shown in Table 4 indicate that rate on the (110) plane is considerably higher than on the other planes. Furthermore, the deposition rate on gallium arsenide is higher than that on silicon single-crystal slices. This and the fact that the rate

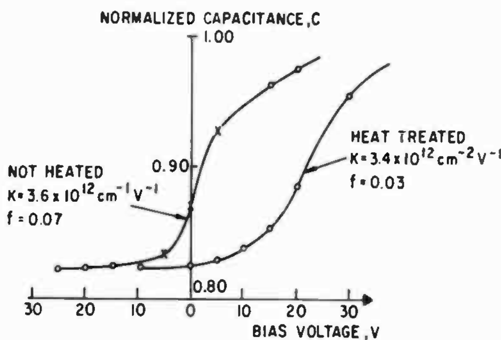

o Experimentally measured points
× Average measurements where drift occurred

Fig. 3—Effect of heat treatment on the capacitance–voltage characteristic of MOS surface varactor for n-type GaAs (dopant concentration $= 3 \times 10^{16}/\text{cm}^3$).

Table 3—Effect of Crystal Orientation on Interface State Density of High Temperature SiO_2 Films on GaAs

Crystal Plane	Interface State Density			
	Slow SiO_2 Deposition*		Fast SiO_2 Deposition**	
	K	f	K	f
$(\bar{1}\bar{1}\bar{1})$	$>10^{13}$		9×10^{11}	0.99
(211)	2×10^{12}	0.59	3×10^{12}	0.05
(110)	$>10^{13}$		8×10^{12}	0.25
(111)	Not determinable, surface pitted from etching			

Substrate: Uniformly doped GaAs crystal, n-type, 5 to 6×10^{17} carriers/cm^3, polish-etched by standard techniques.
f Value: Denotes the fraction of the total state densities which respond at 1 MHz.
K Value: Interface state density, $(cm^2\, eV)^{-1}$.
* 30 min 733°C, 50 Torr, 2000 to 3000 Å SiO_2.
** 2 min 730°C, 760 Torr, 2500 Å SiO_2.

Table 4—Rate of SiO_2 Deposition as a Function of Crystallographic Orientation of the GaAs Substrate

Crystallographic Plane	Film Thickness (Å)	Mean Deposition Rate (Å/min)
(211)	2,070	69
(111)	2,438	81
$(\bar{1}\bar{1}\bar{1})$	2,438	81
(110)	3,046	102

Deposition conditions: Tetraethyl siloxane in argon, 123 cm^3/min carrier flow rate of argon, 50 Torr, 30 min at 733°C.

decreases with increasing thickness suggests that the initial deposition may involve a surface-catalized reaction.

Effects of Chemical Surface Treatments

Standard gallium arsenide wafers (3×10^{16} n-type carriers/cm^3), oriented to the ($\bar{1}\bar{1}\bar{1}$) face and polished by the standard etching technique, were additionally treated with various other types of solutions or polishing etches, as indicated Table 5. The rinsed and dried wafers were then oxide coated for 15 minutes by the fast deposition technique (730°C, 50 Torr) to obtain a silica thickness of 1600 Å. The wafers were then processed to MOS surface varactors and analyzed for the average density of interface states. Samples that showed low densities were reprocessed by the fast deposition (733°C, 760 Torr). Again, substrates coated by the fast deposition rate generally yielded lower interface state densities than the slow rate. The best surface properties in both cases were achieved by a treatment with a hydrogen peroxide/hydrofluoric acid mixture, resulting in state densities as low as 2.5×10^{12}/cm^2-eV with a response factor of 95%. The quantities of trace impurities that can deposit on the gallium arsenide surface under such conditions has been discussed in a previous paper.[13]

By combining this surface treatment with the low-temperature (450°C), reduced-pressure oxide deposition technique and retaining the ($\bar{1}\bar{1}\bar{1}$) crystal orientation that has been shown to be most desirable, the interface state density was further decreased by more than one order of magnitude ($K = 1 \times 10^{11}$/cm^2 eV; $f = 0.55$). Thicker oxide layers, probably because of the longer heat treatment time required, led to an increased state density. These data are exhibited in Table 6; also included are some additional data on surface treatments of (211) oriented crystals.

6. Conclusions

The MOS surface varactor was used as a test device for the semiquantitative analysis of the GaAs/SiO_2 interface state density. The *C-V* measurements of the varactor, the basis for this analysis, were reasonably repeatable although some drifting was generally observed. The oxide thickness was usually not less than 2000 Å to reduce the error in measuring the film thickness and to minimize any field caused by built-in potentials.

The silicon dioxide films were deposited primarily by pyrolysis of tetraethyl siloxane in argon at typically 730°C/760 Torr, 730°C/50 Torr, or 450°C/50 Torr. Generally, minimum heat exposure (low tem-

Table 5—Interface State Density of Etched GaAs Surfaces Given Additional Chemical Treatments and Coated with High-Temperature SiO_2

Additional Surface Treatment				Interface State Density			
				Slow SiO_2 Deposition*		Fast SiO_2 Deposition**	
Composition	Concentrations†	Time (min)	Temp. (°C)	K	f	K	f
Control	—	—	—	$>10^{13}$		3×10^{12}	0.80
H_2O_2:HF	22:4	1.0	23	2×10^{12}	0.17	3×10^{12}	0.95
HNO_3:HF:H_2O	2:1:4	1.0	23	2×10^{12}	0.13	6×10^{12}	0.25
HCOOH:H_2O_2	100:1	0.5	23	3×10^{12}	0.07	$>10^{13}$	
Trace Fe $(NO_3)_3$ in H_2SO_4:Tartaric Acid: $NaNO_3$:H_2O	50ml + 25g + 15g + 100ml	1.5	150	3×10^{12}	0.02		
H_2SO_4:Tartaric Acid: $NaNO_3$:H_2O	50ml + 25g + 15g + 100ml	1.5	150	$>10^{13}$			
NH_4OH:H_2O_2:H_2O	1:2:7	1.0	75	$>10^{13}$			
$KMnO_4$:H_2O	3:97	5.0	23	$>10^{13}$			
CrO_3:H_2O	3:97	20.0	85	$>10^{13}$			

Substrate: GaAs, $(\overline{111})$ plane standard polish-etched before additional surface treatments.
Doping: 3×10^{16} carriers/cm^3, n-type.
f Value: Denotes the fraction of the total state densities which respond at 1 MHz.
K Value: Interface state density, $(cm^2\text{-}eV)^{-1}$.
* 15 min 730°C, 50 Torr, 1600 Å SiO_2.
** 2 min 733°C, 760 Torr, 2500 Å SiO_2, Automatic.
† Concentrated reagents were used.

Table 6—Interface State Density of GaAs/SiO_2 as a Function of Crystallographic Plane, Surface Treatment, and Silica Deposition Conditions.

Crystallographic Plane	Additional Etching Treatment			Silica Coating Conditions				Interface State Density	
	Composition†	Time (sec)	Temp. (°C)	Time (min)	Pressure (Torr)	Temp. (°C)	Thickness (Å)	K	f
$(\bar{1}\bar{1}\bar{1})$	$HF:H_2O_2$ (4:22)	10	23	10	50	450	2700	1×10^{11}	0.55
$(\bar{1}\bar{1}\bar{1})$	$HF:H_2O_2$ (4:22)	10	23	20	50	450	4640	6×10^{11}	0.01
(211)	$HCOOH:H_2O$ (100:1)	30	23	2	760	730	2200	6×10^{11}	0.99
(211)	$HNO_3:HF:H_2O$ (2:1:4)	60	23	2	760	730	2200	3×10^{12}	0.01
(211)	$HNO_3HF:H_2O$ (2:1:4)	60	23	7.5	50	730	1350	1×10^{13}	0.01

Substrate: GaAs, standard polish-etched before additional etching treatment (both were n type).
Doping: $(\bar{1}\bar{1}\bar{1})$ plane 3×10^{16} carriers/cm^3; (211) plane 5 to 6×10^{17} carriers/cm^3.
f value: denotes the fraction of the total state densities which respond at 1 MHz.
K value: interface state density, (cm^2-eV)$^{-1}$.
† Concentrated reagents were used.

perature, short heating periods) tended to decrease the interface state density, although the structural quality of the films deposited at the high temperature was superior.

Silicon dioxide layers deposited at 300°C by oxidation of silane indicated potential benefits of this low-temperature process for lowering the interface state density. However, structural defects in these films prevented their full exploitation at that time.

Heat treatment of oxide-coated gallium arsenide substrate crystals had no marked effect upon the state density. However, a noticeable displacement of the *C-V* characteristic in the positive voltage direction occured which may be associated with an increase of negative charge in the oxide. The *C-V* characteristics further indicate that, for both p- and n-type substrates, a depletion region exists at the gallium arsenide surface.

The crystallographic orientation of the substrate influenced both the interface state density and the oxide deposition rate. The lowest state density (for oxide deposited rapidly at 730°C, 760 Torr) was attained with $(\overline{1}\overline{1}\overline{1})$ oriented crystals.

It has been demonstrated that additional brief chemical treatments of standard etch-polished substrate crystals with special etchants or ionic solutions can further significantly decrease the interface state density.

By combining the optimum conditions for each of the variables studied a decrease of the interface state density has been achieved from values of greater than 10^{13} to $1 \times 10^{11}/\text{cm}^2$ eV, which has made the fabrication of MOS transisters possible.[14] This optimum combination of processing techniques can be summarized as follows:

1)	Crystal Orientation:	$(\overline{1}\overline{1}\overline{1})$
2)	Polish Etch:	95% H_2SO_4:30% H_2O_2:H_2O, (5:1:1); etch while rotating until polished surface is attained.
3)	Sulfate Desorption:*	29% NH_4OH:H_2O:30%H_2O_2, (1:18:4); immerse for 60 seconds.
4)	Final Etch:	49% HF: 30% H_2O_2, (4:22), immerse for 10 seconds.
5)	Final Rinse	Dilute final etch with cold deionized and distilled water; rinse repeatedly with cold deionized and distilled water. Spin dry.

* Trace amounts of sulfate are adsorbed on gallium arsenide surface during polish etching, but can be removed if treated as described.

6) Oxide deposition: Deposit silicon dioxide films by pyrolysis of tetraethyl siloxane vapor at low temperature under reduced pressure.

Acknowledgments

The authors are indebted to R. Hall for electrical measurements and data analysis, and to D. Bergman, J. Di Piazza, D. Jacukowicz, and W. C. Stever for their technical assistance in various phases of this project, and to J. E. Carnes for critically reading the manuscript.

This work was supported by the United States Air Force under Contracts AF33(657)-11615 and AF33(657)-2057.

References:

[1] M. H. Pilkuhn, "Study of GaAs Surfaces," **J. Phys. and Chem.**, Vol. 25, p. 141 (1964).

[2] W. Kern et al., "Surface Passivation Techniques for Compound Solid State Devices," Interim Techn. Doc. Progr. Rept. Nos. 1-4, 6/1/1963 to 5/31/1964, AF33(657)-11615; H. Becke and J. P. White, "Development of a Gallium Arsenide Metal-Oxide-Semiconductor Transistor," Summary Progress Rept. BPSN No. 4(6399-44600-1), Oct. 10, 1965, AF33(657)-2057.

[3] S. R. Hofstein, K. H. Zaininger, and G. Warfield, "Frequency Response of the Surface Inversion Layer in Silicon," **Proc. IEEE**, Vol. 52, No. 8 (1964).

[4] R. Hall and J. P. White, "Surface Capacity of Oxide-Coated Semiconductors," **Solid-State Electronics**, Vol. 8, p. 211 (1965).

[5] E. L. Jordan, "A Diffusion Mask for Germanium," **J. Electrochem. Soc.**, Vol. 108, p. 478 (1961).

[6] N. Goldsmith and W. Kern, "The Deposition of Vitreous Silicon Dioxide Films from Silane," **RCA Review**, Vol. 28, p. 153 (1967).

[7] G. R. Booker and E. E. Benjamin, "Measurement of Thickness and Refractive Index of Oxide Films on Silicon," **J. Electrochem. Soc.**, Vol. 109, p. 1206 (1962).

[8] W. Kern, "A Technique for Measuring Etch Rates of Dielectric Film," **RCA Review**, Vol. 29, p. 557 (1968).

[9] W. A. Pliskin and H. S. Lehman, "Structural Evaluation of Silicon Oxide Films," **J. Electrochem. Soc.**, Vol. 112, p. 1013 (1965).

[10] W. Kern, "Apparatus for Chemical Vapor Deposition of Oxide and Glass Films," **RCA Review**, Vol. 29, p. 525 (1968).

[11] J. A. Amick and W. Kern, "Chemical Vapor Deposition Techniques for the Fabrication of Semiconductor Devices," p. 551 in **Chemical Vapor Deposition**, Second International Conf., ed. by T. M. Blocher, Jr., and J. C. Withers, The Electrochem. Soc., Inc., N.Y., 1970.

[12] W. Kern and A. W. Fisher, "Deposition and Properties of Silicon Oxide and Silicate Films Prepared by Low-Temperature Oxidation of Hydrides," **RCA Review**, Vol. 31, No. 4, p. 715 (1970).

[13] W. Kern, "Radiochemical Study of Semiconductor Surface Contamination, III—Deposition of Trace Impurities on Germanium and Gallium Arsenide," to be published in **RCA Review.**

[14] H. Becke, R. Hall, and J. P. White, "GaAs MOS Transistors," **Solid-State Electronics**, Vol. 8, p. 813 (1965).

RCA Technical Papers Third Quarter, 1970

July

"An Adaptive Ferroelectric Transformer—A Solid-State Analog Memory Device," J. H. McCusker and S. S. Perlman, **IEEE Trans. GED** (July)

"Apollo Black-and-White Television Scan Converter," M. V. Sullivan, **Jour. SMPTE** (July)

"A Compatible High-Resolution TV System for Cablecasting," E. W. Herold, **Proc. IEEE** (July)

"Elastic Surface Waves: Thin-Film Transducers and Layered-System Dispersion," P. Schnitzler and Coauthors, **IEEE Trans. GSU** (July)

"IC's for Microwaves," R. B. Schilling, **Electronics World** (July)

"Generating Cold Gas for Photomultiplier Cooling," J. Gerber, **Rev. Sci. Instr.** (July)

"Monolithic LIC's for Consumer Products," R. A. Santilli, **Electronics World** (July)

"Performance of Broad-Band Microwave-Biased Extrinsic Photoconductive Detectors at 10.6 μ," C. Sun and T. E. Walsh, **IEEE Jour. Quantum Electronics** (July)

"Principles Involved in the LM Rendezvous Radar Redundant Gyro System," J. Dubbury, **IEEE Trans. GAES** (July)

"A Review of the Graphic Arts Industry," J. J. Walsh, **IEEE Trans. GAES** (July)

"S-Band CW Power Module for Phased Arrays," E. Belohoubek, A. Presser, D. M. Stevenson, A. Rosen, and D. Zieger, **Microwave Jour.** (July)

"Self-Pulsed High-Efficiency Avalanche-Diode Oscillators," S. G. Liu and J. J. Risko, **Proc. IEEE** (Letters) (July)

"Stable One-IC Reference Supply," H. A. Wittlinger, **Electronics World** (July)

"Now That the Heat is Off, Liquid Crystals Can Show Their Colors Everywhere," J. A. Castellano, **Electronics** (July 6)

"Mixed-Conduction Model for Charge Transport in n-Type $CdCr_2Se_4$," A. Amith and L. Friedman, **Phys. Rev. B** (15 July)

August

"Apparatus for Studying Electron Beam Pumped Semiconductor Lasers and Other High Excitation Density Phenomena," F. H. Nicoll, **Rev. Sci. Instr.** (August)

"Criterion for Nonreciprocal Injection Locking of Bilateral Microwave Oscillators," B. S. Perlman and T. E. Walsh, **IEEE Trans. GMTT** (Correspondence) (August)

"Defect Centers in $GaAs_{1-x}P_x$ Electroluminescent Diodes Due to High-Energy Electron Irradiation," H. Schade, C. J. Nuese, and D. Herrick, **Jour. Appl. Phys.** (August)

"Effects of Deep Centers on n-Type GaP Schottky Barriers," C. R. Wronski, **Jour. Appl. Phys.** (August)

"Electronic Color Separation with Laser Light Sources," D. Meyerhofer, A. W. Stephens, and J. J. Walsh, **IEEE Trans. GCOM** (August)

"Feasibility of Electrooptic Devices Utilizing Ferroelectric Bismuth Titanate," G. W. Taylor and A. Miller, **Proc. IEEE** (August)

"High-Resolution Return-Beam Vidicon Cameras: A Comparison with High-Resolution Photography," O.H. Schade, Sr., **Jour. SMPTE** (August)

"MOSFET Utility Preamp for Test Equipment," J. F. Sterner, **Electronics World** (August)

"Properties of a Blue-Emitting IR Pumped YF_3:Yb, Tm Diode," J. P. Wittke, I. Ladany, and P. N. Yocom, **Proc. IEEE** (Letters) (August)

"A Universal Threshold Extending Frequency-Modulated Feedback Demodulator," M. M. Gerber, **IEEE Trans. GCOM** (August)

"All-Weather Eye Opens Up With Millimeter Wave Imaging," B. J. Levin and B. R. Feingold, **Electronics** (August 17)

September

"To Clear the Image," B. J. Levin, **Electronics** (Readers Comment), (August 17)

"Characteristics of Coupled Microstrip Lines," L. S. Napoli and J. J. Hughes, **RCA Review** (September)

"Chromatic-Aberration-Limited Image-Transfer Characteristics of Image-Tube Lenses of Simple Geomerty," I. P. Csorba, **RCA Review** (September)

"Computer-Aided Design of a Fast-Wave Coupler," M. J. Schindler, **RCA Review** (September)

"A Design Criterion and Means of Quantitative Measurements of Magnetic Videotape Recorder Servo Performance," K. Sadashige, **Jour. SMPTE** (September)

"Effective of Electric Charge on the Evaporation of Napthalene Single Crystals," R. Williams and Coauthor, **Jour. Appl. Phys.** (September)

"Electronically Generated Halftone Pictures," R. J. Klensch, D. Meyerhofer, and J. J. Walsh, **RCA Review** (September)

"Epitaxial π-ν n-p-n High-Voltage Power Transistors," R. Denning and D. A. Moe, **IEEE Trans. GED** (September)

"On the Fabrication of High-Efficiency Silicon Avalanche Diodes," J. M. Assour, J. Murr, Jr., and D. Tarangioli, **RCA Review** (September)

"IC Capacitance Meter," H. A. Wittlinger, **Electronics World** (September)

"Operational Dependence of the Direct-Tunneling Mode MNOS Memory Transistor on the SiO_2 Layer Thickness," E. C. Ross, A. M. Goodman, and M. T. Duffy, **RCA Review** (September)

"Quantum Efficiency and Photoconductivity in Dye-Sensitized ZnO-Resin Binder Layers," R. B. Comizzoli, **Jour. Appl. Phys.** (September)

"Synthesis of Optimum Reflection Type Microwave Equalizers," C. M. Kudsia, **RCA Review** (September)

"Tehnology and Design of GaAs Laser and Non-Coherent IR-Emitting Diodes, Part 1," R. Glicksman, **Solid State Tech.** (September)

"Thermal Expansion of AlAs," M. Ettenberg and R. J. Paff, **Jour. Appl. Phys.** (September)

"Thermal Fatigue in Silicon Power Transistors," G. A. Lang, B. J. Fehder, and W. D. Williams, **IEEE Trans. GED** (September)

"TV Antenna Performance Evaluation with RF Pulse Techniques," M. S. Siukola, **IEEE Trans. GBC** (September)

"Use of Diode Lasers to Recover Holographically Stored Information," A. H. Firester and M. E. Heller, **IEEE Jour. Quartum Electronics** (Correspondence) (September)

"Vibration Control of Printed-Circuit Boards in a Dynamic Environment," E. D. Veilleux, **IEEE Trans. GPMP** (September)

"Measurement of Electron Energy-Loss Function in Bulk Strontium Titanate," J. M. Hammer, **Phys. Rev. B** (1 September)

"Energy Levels of the F_A Center," R. C. Alig, **Phys. Rev. B** (15 September)

"Luminescent Properties of Energy-Band-Tail States in GaAs:Si," D. Redfield, J. P. Wittke, and J. I. Pankove, **Phys. Rev. B** (15 September)

"Torques in Sheared Nematic Liquid Crystals: A Simple Model in Terms of the Theory of Dense Fluids," W. Helfrich, **Jour. Chem. Phys.** (15 September)

Patents Issued to RCA Inventors Third Quarter 1970

July

S. A. Ahmed, T. J. Faith, Jr., and G. W. Hoffman, RF Excitation Pumping of Gas Lasers by Means of a Wave Guide and Coupling Coils (3,521,119)

J. Avins, Angle Modulation Discriminator-Detector Circuit (3,519,944)

H. N. Crooks, Holograms for Reconstruction of Objects of Equal Intensity (3,519,324)

D. P. Dorsey, Apparatus for Preventing Receiver Recording of Partial Multiplexed Message Transmissions (3,519,736)

G. H. Heilmeier, Turnoff Method and Circuit for Liquid Crystal Display Element (3,519,330)

G. V. Jacoby and J. C. Kmiec, Synchronizing Servosystem with Memory Means (3,-520,993)

S. Katz, Complementary Transistor Write and NDRO for Memory Cell (3,521,242)

M. B. Knight, Regulated High Voltage Power Supply (3,519,741)

J. R. Leaman, Photoconductive Pickup Tube Having Opaque Gold Pattern Encapsulated in Tin Oxide Layer (3,519,866)

H. J. Mackway, Pushbutton Mechanism (3,519,766)

J. C. Marsh, Jr., Resonant Bandpass Filter Having Two Undesired Frequency Cancellation Traps (3,519,737)

J. L. McLaughlin, Photomasks for Fabrication of Semiconductor Devices (3,519,348)

J. C. Miller and C. M. Wine, Data Conversion and Display Apparatus (3,521,268)

L. E. Norton, Method of Making Gunn-Effective Devices (3,518,749)

W. L. Oates, Microminiature Electrical Component Having Integral Indexing Means (3,521,128)

J. H. Scott, Jr., Fabrication of Semiconductive Devices with Silicon Nitride Coatings (3,520,722)

R. A. Shahbender, Electronically Controlled Delay Line (3,521,198)

M. L. Topfer and R. E. Quinn, Stabilization of Thin Film Transistors (3,520,051)

D. H. R. Vilkomerson and R. S. Mezrich, Radiation-Sensing Matrix Circuit (3,519,996)

P. K. Weimer, Electrical Circuit for Processing Periodic Signal Pulses (3,521,244)

R. O. Winder, Threshold Gate Counters (3,519,941)

August

A. E. Bishop, Electron Tube Multicolor Dual Persistence Screen Comprising Phosphor-Coated Particles (3,522,463)

D. F. Bowman, Antenna Arrays with Elements Aperiodically Arranged to Reduce Grating Lobes (3,524,188)

F. Caprari, Apparatus for Regulating the Light Output of a Flash Lamp (3,525,016)

H. B. Currie, Character Reader (3,524,166)

J. R. Fendley, Jr., Laser Tube Construction (3,522,551)

R. C. Heuner and F. I. Ostroff, Temperature Tracking of Emitter Coupled Differential Amplifier Stage (3,522,548)

P. K. Hsieh and J. L. Freeman, Jr., Two-Element-Per-Bit Random Access Memory with Quiet Digit-Sense System (3,522,593)

D. J. Kanter, Limiting Network (3,522,443)

M. M. Kaufman, Translating Information with Multi-Phase Clock Signals (3,524,077)

M. H. Lewin, Character Selector and Generating Device (3,523,161)

A. Lichowsky, Storage System Employing Magnetic Tape Cartridges (3,525,086)

D. H. Montgomery and J. R. Oberman, Transistor Amplifier Having Emitter Bypass Through an Auxiliary Transistor (3,524,141)

P. K. Mrozek, Temperature Compensated Crystal Oscillator (3,525,055)

F. H. Nicoll, Thermoplastic Deformation Imaging Process (3,525,613)

R. C. Peyton, Printer Paper Feed Control System (3,524,528)

W. E. Salzer, Current Pulse Driver Apparatus Employing Nonsaturating Transistor Switching Techniques and Having Low Power Drain During Non-Pulse Periods (3,-523,197)

A. Sheng, Current Mode Circuit (3,523,194)

W. W. Siekanowicz, D. J. Blattner, and T. E. Walsh, Duplexer Having Two Non-Reciprocal Phase Shifting Means (3,525,952)

M. E. Steiner and G. J. Waas, Read-Only Magnetic Memory (3,522,592)

L. J. Striednig, Cascade Connected Regenerative Amplifiers (3,525,051)

M. C. Wang. Binary Coded Decimal to Binary Conversion (3,524,976)

M. C. Wang, Binary Multiplier Employing Multiple Input Threshold Gate Adders (3,524,977)

D. H. Willis, Service Aid for Color Television Receiver (3,525,801)

September

J. Avins, Integrated Circuit Amplifier Biasing Arrangement (3,531,657)

L. J. Baun, Composite Television Video Switching Circuit (3,527,886)

C. R. Corson, Bilevel Video Signal Reconstruction Circuit (3,528,018)

E. Deger and J. B. Schultz, Statistical Method, Under Computer Control, for the Manufacture and Test of Mass Produced Articles (3,526,836)

W. J. Hannan, Triangulation Radar System (3,530,468)

H. E. Haynes, Photocomposing Apparatus (3,530,780)

M. M. Hopkins and A. Miller, Method for Poling Bismuth Titanate (3,531,779)

P. K. Hsieh and D. Benima, Random Access Memory with Quiet Digit-Sense System (3,530,445)

J. I. Pankove, Filamentary Structure Injection Laser Having a Very Narrow Active Junction (3,526,851)

D. H. Pritchard, Color Image Projection System (3,527,879)

F. D. Rando, Voltage Regulated Signal Translating Circuit (3,528,020)

R. D. Smith, Computer Memory Address Generator (3,530,439)

S. A. Steckler, Signal Translating Stage (3,531,730)

B. Zuk, Information Switching and Storage Circuitry (3,529,294)

AUTHORS

Yuen-Sheng Chiang was born in 1936 in Tsingtao, China. He received his B.S. degree in chemical engineering from National Taiwan University (Taipei, Taiwan, China) in 1956 and M.Ch.E degree from the University of Louisville (Louisville, Kentucky) in 1960. In 1964 he was conferred the Ph.D. degree in Physical Chemistry by Princeton University. His thesis research dealt wth crystal growth.

He served as a consultant to the Research Divisions of Burroughs Laboratories, Burroughs Corporation from 1962 thru 1963, and was appointed as a research associate in the Chemistry Department of Princeton University in November 1963, upon completion of his Ph.D. studies. At Princeton, he engaged in research in the area of electron paramagnetic resonance studies of fast reactions. In 1964, he joined the Fundamental Research Laboratory of Xerox Corporation as a Scientist and was made a Senior Scientist in 1968. He has worked in the field of surface physics and chemistry of solids, ultra-high vacuum technology and electron microscopy and diffraction studies. Since joining the staff at RCA Laboratories in 1969, he has been involved with low temperature epitaxial growth of silicon.

He is a member of American Physical Society, American Chemical Society, American Crystallographic Association, Electron Microscopy Society of America, sigma Xi and the Electrochemical Society.

Glenn W. Cullen received the B.S. degree in chemistry from the University of Cincinnati in 1953, and the Ph.D. degree in inorganic chemistry from the University of Illinois in 1956. During the following two years he served on the teaching staff and as a Group Supervisor in the Electronics Department of the U. S. Army Air Defense School (Surface to Air Missiles) at Ft. Bliss, Texas. On release from the Army in 1958 he joined the staff of RCA Laboratories, Princeton, N. J., and initially worked on the chemical stabilization of semiconductor surfaces. Subsequent to this work he was involved in the chemical vapor deposition of Nb_3Sn, Nb, Ta and Nb-Ta superconducting thin films. This activity included the characterization of the electrical properties of the deposits at low temperatures in high magnetic fields. For the past three years Dr. Cullen has been involved in the preparation and characterization of silicon thin films epitaxially deposited on insulating substrate materials. Dr. Cullen is the Head of the Materials Applied Synthesis Group within the Process and Materials Applied Research Laboratory.

Dr. Cullen is a member of the American Chemical Society, the Electrochemical Society, the Society of Sigma Xi, and Alpha Chi Sigma.

Bernard J. Curtis received the B.Sc. and Ph.D. degrees in chemistry from Imperial College, London, England in 1955 and 1958, respectively. From 1958 to 1960 he worked as a Patent Examiner in the Board of Trade, London. The period 1960 to 1967 was spent at Mullard Research Laboratories, Redhill, England where he worked on the vapor growth of oxides and semiconductors and on the preparation of thin film transducers. During this time, a year was spent as a visiting scientist at the Philips Research Laboratories, Aachen, Germany, where a method for the melt growth of LaB_6 was developed. Dr. Curtis joined RCA Laboratories, Zurich, in 1967 where he has worked on the vapor phase and flux growth of semiconducting compounds in connection with electroluminescence and photoluminescence studies. He is a member of the Electrochemical Society and the British and Swiss Crystal Growth Societies.

John P. Dismukes received the B.S. degree from Auburn University in 1955 and the Ph.D. degree in inorganic chemistry from the University of Illinois in 1959. In 1959 he joined RCA Laboratories, but shortly thereafter he spent a year's leave of absence as a NSF Postdoctoral Fellow at the University of Munster, Germany, where he studied the preparation of CrTe by the chemical transport technique. Since returning to RCA in 1960, he has carried out materials research on a wide variety of thermoelectric materials, including $AgSbTe_2$-GeTe system, Ce_2S_3 and other rare-earth chalcogenides, and Ge-Si alloys. The Ge-Si alloys were used in the SNAP-10A system which generated 500 watts of electric power in space. He has also carried out hydrothermal synthesis of ferromagnetic CrO_2 and vapor-phase etching of silicon. More recently, he has been concerned with vapor-phase growth of compound and alloy semiconductors. Currently, Dr. Dismukes is on temporary assignment with RCA Laboratories, RCA, Ltd., Zurich for one year starting July 1, 1970.

Dr. Dismukes is a member of the American Chemical Society, the Metallurgical Society of AIME, and the Electrochemical Society.

Michael T. Dufty received the B.Sc. degree from University College, Dublin, in 1958 and completed his Ph.D. studies in Solid State Chemistry in 1963. He was a teaching assistant at this University from 1961 to 1963. In 1964, he joined the University of Toronto as a Research Associate, engaged in molecular beam studies. In July 1966, he joined the staff of RCA Laboratories, Princeton, N. J. Since then, he has been engaged in materials research in the field of integrated electronics and particularly in the area of thin film dielectrics and MIS structures.

David J. Dumin received the B.E.S. degree from Johns Hopkins University in 1957, the M.S.E.E. degree from Purdue University in 1961 and the Ph.D. degree from Stanford University in 1965. His doctoral dissertation concerned the properties of gallium arsenide diodes from room temperature to liquid helium temperatures and the effects of tunnelling currents on diode characteristics. From 1957 to 1960 he worked at the IBM Research Laboratories studying the electrical properties of thin superconducting films and their use in high speed logic circuits. He became a Member of the Technical Staff of the RCA Laboratories in 1964 where he has been studying the electrical and mechanical properties of thin silicon films grown epitaxially on sapphire. He is a member of Eta Kappa Nu and the American Physical Society.

F. P. Emmenegger was educated in Switzerland, receiving his Ph.D. in inorganic Chemistry from the Federal Institute of Technology, E.T.H., Zurich, Switzerland, in 1963. During 1964, he was employed by the University of Maryland as a research assistant. He joined Laboratories RCA Ltd., Zurich, Switzerland, in March 1965, working mainly on single-crystal growth of oxides by vapor-phase transport. In September 1969, he became an assistant professor in the Inorganic Chemistry Laboratory of the University of Fribourg, Switzerland.

Lincoln Ekstrom received his Sc.B. in Chemistry from Brown University in 1953 and his Ph.D. in physical chemistry from M.I.T. in 1957. His thesis was a spectrophotometric study of the nature of ferric ions in water solution. He joined RCA Laboratories in 1957 where he has done materials research on III-V compounds, thermoelectric materials, and magnetic materials. He is currently interested in plated-metal magnetic memory disks, as well as the vapor-phase deposition of thin film of ferromagnetic semiconductors.

Dr. Ekstrom is a Fellow of the American Institute of Chemists and a member of Sigma Xi, the American Chemical Society, the American Physical Society, and AAAS.

Ronald E. Enstrom received the S.B., S.M., and Sc.D. degrees in metallurgy from the Massachusetts Institute of Technology in 1957, 1962 and 1963, respectively, and has had extensive experience working on various materials. From 1957 to 1960 he worked at Union Carbide and Nuclear Metals, Inc., on materials for high temperature oxidation resistance and nuclear fuel elements, respectively. At M.I.T., his doctoral thesis forcussed on the metallurgy and superconductivity of the three compounds in the Nb-Sn system, and at RCA Laboratories he was instrumental in making Nb_3Sn ribbon a highly successful high-field magnet material. More recently, Dr. Enstrom has worked on the vapor phase synthesis and characterization of GaAs and GaAs-GaP alloys for high power rectifiers and solid-state microwave oscillators, and on the vapor-growth of GaAs-InAs alloys for infra-red sensitive negative electron affinity photocathode applications.

Dr. Enstrom is a member of Sigma Xi, AIME, the American Physical Society, and the Electrochemical Society.

A. Wayne Fisher attended Newark College of Engineering prior to joining RCA Laboratories in 1959, as a research technician. In 1966, he was promoted to technical staff associate. In his initial assignment, he was concerned with the fabrication and testing of germanium and gallium arsenide devices, especially varactors, tunnel diodes, and injection lasers. In 1964 he joined the Process Research and Development Laboratory where he has worked on techniques for providing dielectric isolation for silicon integrated circuits, methods of characterizing defects due to work damage in silicon, and, more recently, new diffusion sources for silicon devices.

G. Eugene Gottlieb received the B.S. degree in chemistry from Rutgers University in 1956, the M.S. degree in physical chemistry from Temple University in 1958, the M.B.A. degree from Rutgers University in 1964, and is currently completing his thesis for a Ph.D. in ceramics from Rutgers University. From 1958 to 1960, he was associated with the Philco Corporation, working on the selection, preparation, and evaluation of thermoelectric materials. In 1960 he joined RCA Laboratories, where he has been engaged in vapor phase transport of III-V semiconductors, single crystal growth of electro-optic materials from the vapor phase, and the synthesis and crystal growth of organic semiconductors. For the past four years Mr. Gottlieb has concentrated on the epitaxial growth of silicon films on insulating substrates.

Mr. Gottlieb is a member of the American Chemical Society, American Ceramic Society, Keramos, The Electrochemical Society, and is listed in American Men of Science.

Joseph J. Hanak received his B.S. in Chemistry at Manhattan College in 1953, his M.S. in Physical Chemistry at the University of Detroit in 1956 and his Ph.D. in Physical Chemistry at the Iowa State University in 1959. He was a Teaching Fellow in Chemistry at the University of Detroit in 1953 and 1954, worked for the Ethyl Corporation as a Chemist in 1955, and was a research assistant at the AEC Institute for Atomic Research (Ames, Iowa) from 1955 to 1959. He has been a Member of The Technical Staff at RCA Laboratories since 1959. Dr. Hanak has been active in the field of chemistry, metallurgy, and crystallography of the rare-earth elements. He had done research on superconducting materials and ferrites as well as on the processes of chemical vapor deposition and sputtering. He is the inventor of the RCA vapor-deposition process of Nb_3Sn, and of stable, permanent, high-field superconducting magnets. For the past three years he has worked in the field of rf sputtering of superconductors and dielectrics. He introduced novel co-sputtering compositional analysis and testing methods applicable to a large variety of materials, thereby greatly increasing productivity in materials research. In 1969-70, he spent a year at RCA Laboratories, Ltd., Zurich, Switzerland on a European Research Fellowship.

Dr. Hanak is a member of the American Chemical Society, Phi Lambda Upsilon, and Sigma Xi.

Werner Kern received a certificate in chemistry in 1944 from the University of Basle, Switzerland, and a diploma in chemical technology in 1946. He published a thesis on the chromatographic isolation and characterization of fluorescing polynuclear hydrocarbons which he discovered in soil. He was analytical research chemist with Hoffmann-LaRoche in Switzerland, and in 1948 transferred to their research division in New Jersey specializing in developing radiochemical and microanalytical methods. In 1955 he received an AB degree in chemistry from Rutgers University. In 1958 he joined Nuclear Corporation of America where he became chief chemist directing research in nuclear and radiation chemistry. He joined RCA Electronic Components and Devices Division in 1959 to conduct radiochemical investigations devoted mainly to the study of semiconductor surface contamination. Since 1964 he has been at RCA Laboratories as Member of the Technical Staff, where his activity has centered in semiconductor process research in the areas of solid-state device passivation, new methods of chemical vapor deposition of oxide and glass films, and the development of analytical methods for controlling these processes.

Mr. Kern is a member of the American Chemical Society, the Electrochemical Society, the Society of Sigma Xi, the Geological Society of New Jersey, and is listed in American Men in Science.

Henry Kressel received the B.A. degree from Yeshiva College in 1955. He received the S.M. degree in Applied Physics from Harvard University in 1956, and the M.B.A. and Ph.D. degree from the University of Pennsylvania in 1959 and 1965, respectively. Dr. Kressel joined RCA Electronic Components and Devices, Somerville, N. J., in 1959. He has been instrumental in the research and development of high-frequency mesa, planar, and planar epitaxial silicon transistors. In 1961 Dr. Kressel became head of the microwave diode group, where he was responsible for research, development, and pilot-line engineering of gallium arsenide and silicon varactor diodes. From 1963 to 1965, he was on leave of absence doing doctoral work in metallurgy. Upon his return to RCA in 1965, he became head of the Device Physics Group in the Technical Programs Laboratory (Somerville, N. J.). He joined RCA Laboratories, Princeton, in 1966. He is currently head of the semiconductor Optical Devices Research Group. Dr. Kressel is a member of the IEEE, The American Physical Society, and Sigma Xi.

R. Nitsche graduated from the University of Heidelberg, Germany, receiving his Ph.D. in Physical Chemistry in 1951. From 1951 to 1954, he was employed by I. E. DuPont De Nemours Co., Photo Products Research Laboratory, in Parlin, N.J., performing work on the synthesis of phosphors for television and electroluminescent and x-ray devices. In 1954, he returned to Germany to take up an appointment with Siemens-Reiniger Werke, A.G., in Erlangen, working on the synthesis of phosphors and photoconductors for light-amplifying devices. He joined Laboratories RCA Ltd., Zurich, Switzerland, in 1957. His main interest at RCA was the study of the mechanisms in chemical transport reactions for single-crystal growth. In September 1968, he became a professor at the Institute of Crystallography, University of Freiburg, Germany.

Richard E. Novak received his B.S. and M.S. degrees in Ceramic Engineering from the University of Illinois, Urbana, Illinois, in 1967 and 1969, respectively. He is presently working toward his doctorate, preparing a thesis on the determination of the structure and thermal stability of B_6O. During the summers of 1968 and 1969, he worked at RCA Laboratories, Princeton, N.J., doing research on PbTe thermoelectric materials and ScN vapor synthesis. Mr. Novak is a member of the American Ceramic Society.

Harry L. Pinch received the B.S. degree in Chemistry in 1951 from the City College of New York, N.Y. and the Ph.D. in Physical Chemistry in 1955 from the Pennsylvania State University. He held the Allied Chemical and Dye Fellowship for the academic year 1952-1953. Since 1957 he has been employed by RCA Laboratories and has worked in the fields of thin phosphor films, thin magnetic films, growth of halide crystals for laser materials, and the preparation and crystal growth of magnetic chalcogenides. Presently he is interested in the crystal growth of ferrites, garnets, and other magnetic oxides.

Dr. Pinch is a member of the American Chemical Society, the American Physical Society and Sigma Xi.

D. Richman received his B.S., cum laude, from Yale University in 1954 and Ph.D. from Cornell University in 1959, majoring in physical chemistry. Since joining the staff of RCA Laboratories in 1959, Dr. Richman has worked on the preparation and physical chemical properties of III-V compound semiconductors and, more recently, silicon. In April 1970, he was appointed Head, Semiconductor Research, Materials Research Laboratory. He is currently a member of Sigma Xi, the American Chemical Society, and the Electrochemical Society.

Paul H. Robinson graduated with a Bachelor of Arts in Chemistry, June 1951 from New York University College of Pure Arts and Science and received a Master Degree in Physical Chemistry for Polytechnic Institute of Brooklyn and the Massachusetts Institute of Technology in 1955. He was employed by M.I.T. as a staff member at Lincoln Laboratory from 1952-1959. While at Lincoln Laboratory he was part of a group which was first to determine the oxidation kinetics, thickness, and isosteric heat of adsorption of oxygen on atomically clean germanium surfaces after oxidation. This work was published and presented at the First Conference on Semiconductor Surfaces held in Philadelphia in 1956. He also worked on the electrochemical preparation of manogermane. From 1959 to 1962 he worked at Raytheon's Semiconductor Division Advanced Development Laboratories and was mainly involved with surface studies on silicon and silicon devices. He joined the research staff at RCA Laboratories in February 1962 and developed the closed-spaced technique for the vapor transport of germanium and III-V semiconductors. For the past 7 years he has worked on the epitaxial growth of silicon, silicon device structures, and the characterization of silicon on insulators. He was first to use the silane system for this purpose. He reported along with C. W. Mueller in 1964 the first MOS devices using these films. He also reported the first useful bipolar transistors on insulators using an all epitaxial approach and helped develop a technology for improving minority carrier lifetime in silicon on insulator films. He is a member of the American Chemical Society and the Electrochemical Society.

J. J. Tietjen received a B.S. degree, cum laude, from Iona College in 1956 and the M.S. and Ph.D. degrees from the Pennsylvania State University in 1958 and 1963, respectively. He was awarded the Speer Carbon Company research fellowship in 1959, 1960, and 1961. Since joining RCA Laboratories, in 1963, Dr. Tietjen has primarily worked on the preparation of a broad range of III-V compound semiconductors by chemical vapor transport reactions. This work has significantly affected both research and development at RCA, since it has led to the preparation of a series of new and improved devices. In 1966, Dr. Tietjen was appointed a Research Leader in the Semiconductor Materials Research Group and in 1969 became Head of the Semiconductor and Luminescence Research Group. In 1970, he was appointed Director of the Materials Research Laboratory.

Dr. Tietjen has been elected to the honorary societies of Pi Mu Epsilon and Phil Lambda Epsilon and has held the office of President in Mu chapter of the latter organization. He is a member of Sigma Xi, the American Chemical Society, the Electrochemical Society, and the Electronic Materials Committee of the AIME.

Chih-Chun Wang received his B.S. degree in Chemical Engineering in 1955 from the National Taiwan University, Taiwan, China, his M.S. degree at Kansas State University in 1959, and his Ph.D. degree in Physical Chemistry in 1962 from Colorado State University. From 1962 to 1963 he received the postdoctoral training in high temperature physical chemistry research group of the University of Kansas. In 1963 Dr. Wang joined the research staff of RCA Laboratories where he has been engaged in research on synthesis and characterization of electronic materials, including wide-bandgap III-V semiconductors, ferromagnetic transition metal oxides, refractory dielectrics, and thin films. Dr. Wang has specialized in crystal growth and vapor-phase deposition of electronic materials, thermodynamics and kinetics of high temperature systems, x-ray crystallography, and mass spectrometry.

Dr. Wang is a member of the American Chemical Society, Electrochemical Society, Sigmi Xi, Sigma Pi Sigma, and Phi Lambda Upsilon. He is listed in American Men of Science, Leading Men in the United States of America, and International Biography of Contemporary Achievement.

Leonard R. Weisberg received his B.A. degree from Clark University in 1950, Magna Cum Laude with honors in Physics. In 1952, he received his M.A. degree in physics from Columbia University. His Ph.D. thesis at Columbia was concerned with the physics of metals and was published in 1957. From 1953 to 1955 he was employed by the IBM Watson Laboratories in New York City, working on the preparation and properties of germanium. In 1955 he joined RCA Laboratories where he carried out materials research on III-V compound semiconductors, especially GaAs. In 1966, he became Head of the Semiconductor and Luminescence Research Group, and in 1969 he was appointed Director of the Semiconductor Device Research Laboratory.

He is a Past Chairman of the Electronic Materials Committee of the AIME and is an Associate Editor of the Materials Research Bulletin. He has been a member of the American Committee for Crystal Growth, the American Committee for Thin Film Growth, the IEEE Committee for Materials, a Study Panel of the Materials Advisory Board, and a Lecture Series Committee of the American Chemical Society. He is also a member of Sigma Xi, the American Physical Society, the Electrochemical Society, the Metallurgical Society of the AIME, and is a senior member of IEEE. He is listed in the American Men of Science, Who's Who in the East, and the Dictionary of International Biography.

Joseph P. White received his B.S. degree (1959) and M.S. degree (1964) in Physics, from the Polytechnic Institute of Brooklyn. Prior to joining RCA in November, 1962, he worked for three years at Tung-Sol Electric, Inc., in product development of germanium high-frequency and power transistors. In the Advanced Technology Center at RCA, Somerville, he has worked on GaAs bipolar and field-effect transistors and on complementary integrated circuits. He is currently in the Advanced Power Development section, where he is engaged in the development of high-power silicon devices and laminated power integrated circuits.

W. Michael Yim received the B.S. degree from the Montana College of Mineral Science and Technology in 1951, the M.S. degree from the University of Washington in 1953, and the Sc.D. degree in metallurgy with minor in physics from the Massachusetts Institute of Technology in 1961. From 1961 to 1962 he was with the Union Carbide Corporation. Dr. Yim joined RCA Laboratories in 1962, and has since been engaged in the preparation and properties of a wide variety of solid-state materials. These included thermoelectric materials based on Bi_2Te_3 and related V-VI compounds, Group V semimetals including Bi-Sb alloys, eutectic materials, and high-bandgap II-VI compounds and their solid-solution alloys with III-V semiconducting compounds. More recently, he has been concerned with studies of nitrides, phosphides, arsenides, and various chalcogenides of Groups II and III elements including rare-earth metals.

Dr. Yim is a Fellow of the American Institute of Chemists, and a member of the Metallurgical Society of AIME, the American Physical Society, and the Society of Sigma Xi.

Karl H. Zaininger received the BEE degree (magna cum laude) from City College of New York in 1959; the MSE in 1961, the MA in 1962, and the Ph.D. in Engineering Physics in 1964 from Princeton University. In 1959, Dr. Zaininger joined the staff of RCA Laboratories. At RCA, he worked in research on various semiconductor devices, and has been involved in research on silicon-based MOS devices since their original inception. His research activities with the MOS devices have included basic studies in the area of semiconductor surface physics. He is presently concerned with MIS device physics and technology, with measurement techniques, and with the physics of radiation damage in MIS systems. In August 1968, Dr. Zaininger was appointed Head of the Solid-State Device Technology group at RCA Laboratories.

Dr. Zaininger is a Senior Member of the Institute of Electrical and Electronics Engineers, and a member of Tau Beta Pi, Eta Kappa Nu, Sigma Xi, and the Shevchenko Scientific Society.

RCA Review

A technical journal published quarterly
by RCA Research and Engineering
in cooperation with the subsidiaries
and divisions of RCA.

Index 1970 Volume 31

March 1970 Volume 31 Number 1

3 Fabrication and Performance of Kilowatt L-Band Avalanche Diodes
S. G. Liu and J. J. Risko

20 High-Power L- and S-Band Transferred Electron Oscillators
B. E. Berson, R. E. Enstrom, and J.F. Reynolds

39 Sonic Film Memory
R. Shahbender, P. Herkart, K. Karstad,
K. Kurlansik, and L. Onyshkevych

60 Electron Optics and Signal Read-Out of High-Definition
Return-Beam Vidicon Cameras
O. H. Schade, Sr.

120 Stable Solid-State Vertical Deflection for High-Definition
Television Systems
O. H. Schade, Jr.

148 Linear Solid-State Horizontal Deflection Circuit for
High-Definition Television Systems
O. H. Schade, Jr.

171 RCA Technical Papers

173 Patents

175 Authors

June 1970 Volume 31 Number 2

New Process Technologies for Microelectronics

Guest Editor, J. A. Amick

185 **Foreword**
P. Rappaport and J. A. Amick

Aqueous Etching and Cleaning Techniques for Silicon

187 Cleaning Solutions Based on Hydrogen Peroxide
for Use in Silicon Semiconductor Technology
W. Kern and D. Puotinen

207 Radiochemical Study of Surface Contamination
I. Adsorption of Reagent Components
Werner Kern

234 Radiochemical Study of Surface Contamination
II. Deposition of Trace Impurities on Silicon and Silica
Werner Kern

265 A New Technique for Etch Thinning Silicon Wafers
A. I. Stoller, R. F. Speers, and S. Opresko

271 The Etching of Deep Vertical-Walled Patterns in Silicon
A. I. Stoller

Techniques for Metallizing Devices

276 Evaporation of Aluminum with RF-Induced Substrate Bias
J. L. Vossen and J. J. O'Neill, Jr.

293 Back Scattering of Material Emitted from RF-Sputtering Targets
J. L. Vossen, J. J. O'Neill, Jr., K. M. Finlayson and L. J. Royer

306 Vapor Deposited Tungsten as a Metallization and Interconnection Material for Silicon Devices
J. M. Shaw and J. A. Amick

317 Two Room-Temperature Electroless Nickel Plating Baths
N. Feldstein

MOS Device Processing

330 Fabrication of Al_2O_3 COS/MOS Integrated Circuits
F. B. Micheletti, P. E. Norris, and K. H. Zaininger

342 Optimization of Charge Storage in the MNOS Memory Device
A. M. Goodman, E. C. Ross, and M. T. Duffy

355 The Epitaxial Growth of Silicon on Sapphire and Spinel Substrates: Suppression of Changes in the Film Properties During Device Processing
G. W. Cullen, G. E. Gottlieb, and C. C. Wang

372 The Performance of Complementary MOS Transistors on Insulating Substrates
E. J. Boleky

Process Control and Defect Characterization

396 Monitoring Silicon Tetrachloride Concentration in Hydrogen Carrier Gas
G. A. Riley and J. A. Amick

407 An Inexpensive Integrating Photoresist Exposure Control System
G. A. Riley

414 Detection of Damage on Silicon Surfaces: Origin and Propagation of Defects
A. Mayer

431 A Study of Dielectric Defect Detection by Decoration with Copper
W. J. Shannon

Special Technologies

439 Selective Electroless Plating by Selective Deactivation
N. Feldstein and T. S. Lancsek

443 A Novel Technique for Forming Glass-to-Metal Seals Using a Silicon Nitride Interface Layer
A. I. Stoller, W. C. Schilp, Jr. and J. Benbenek

450 **RCA Technical Papers**

452 **Patents**

455 **Authors**

September 1970 Volume 31 No. 3

467 Operational Dependence of the Direct-Tunneling Mode MNOS Memory Transistor on the SiO_2 Layer Thickness
E. C. Ross, A. M. Goodman, and M. T. Duffy

479 Characteristics of Coupled Microstrip Lines
L. S. Napoli and J. J. Hughes

499 On the Fabrication of High-Efficiency Silicon Avalance Diodes
J. M. Assour

517 Electronically Generated Halftone Pictures
R. J. Klensch, D. Meyerhofer, and J. J. Walsh

534 Chromatic-Aberration-Limited Image-Transfer Characteristics of Image-Tube Lenses of Simple Geometry
I. P. Csorba

553 Computer-Aided Design of a Fast-Wave Coupler
M. J. Schindler

571 Synthesis of Optimum Reflection Type Microwave Equalizers
C. M. Kudsia

596 RCA Technical Papers

598 Patents

601 Authors

December 1970 Volume 31 No. 4

Chemical Vapor Phase Deposition of Electronic Materials

607 **Foreword**
L. R. Weisberg and G. W. Cullen

Semiconductors

613 Low-Temperature Vapor Growth of Homoepitaxial Silicon
D. Richman, Y. S. Chiang, and P. H. Robinson

620 Heteroepitaxial Growth of Germanium and Silicon on Insulating Substrates
D. J. Dumin, P. H. Robinson, G. W. Cullen, and G. E. Gottlieb

635 Vapor-Phase Growth of Several III-V Compound Semiconductors
J. J. Tietjen, R. E. Enstrom, and D. Richman

647 The Preparation of Ternary and Quaternary Compounds by Vapor-Phase Growth
B. J. Curtis, F. P. Emmenegger, and R. Nitsche

662 Vapor Growth of (II-VI)-(III-V) Quaternary Alloys and Their Properties
W. M. Yim, J. P. Dismukes, and H. Kressel

680 Vapor Deposition of Semiconducting Mononitrides of Scandium, Yttrium, and the Rare-Earth Elements
J. P. Dismukes, W. M. Yim, J. J. Tietjen, and R. E. Novak

692 Vapor-Phase Growth of Magnetic Semiconducting Spinels
H. L. Pinch and L. Ekstrom

Superconductors

702 Compounds and Alloys for Superconducting Applications
R. E. Enstrom, J. J. Hanak, and G. W. Cullen

Insulators

715 Deposition and Properties of Silicon Dioxide and Silicate Films Prepared by Low-Temperature Oxidation of Hydrides
W. Kern and A. W. Fisher

728 Vapor Deposition and Characterization of Metal Oxide Thin Films for Electronic Applications
C. C. Wang, K. H. Zaininger, and M. T. Duffy

742 Preparation, Properties, and Applications of Chemically Vapor Deposited Silicon Nitride Films
M. T. Duffy and W. Kern

754 Chemical Vapor Deposition of Aluminum Oxide Films from Organo-Aluminum Compounds
M. T. Duffy and W. Kern

771 Interface Properties of Chemically Vapor Deposited Silica Films on Gallium Arsenide
W. Kern and J. P. White

786 Technical Paper

788 Patents

790 Authors

798 Index to Volume 31, 1970

Index to Authors, Volume 31, 1970

J. A. Amick (coauthor) Foreword to Issue on New Process Technologies In Microelectronics, March, p. 183
— Vapor Deposited Tungsten as a Metallization and Interconnection Material for Silicon Devices, March, p. 306
— Monitoring Silicon Tetrachloride Concentration in Hydrogen Carrier Gas, March, p. 396

J. M. Assour, On the Fabrication of High-Efficiency Silicon Avalanche Diodes, Sept., p. 499

J. Benbenek (coauthor) A Novel Technique for Forming Glass-to-Metal Seals Using a Silicon Nitride Interface Layer, June, p. 443

B. E. Berson (coauthor) High-Power L- and S-Band Transferred Electron Oscillators, March, p. 20

E. J. Boleky, The Performance of Complimentary MOS Transistors on Insulating Substrates, June, p. 372

Y. S. Chiang (coauthor) Low-Temperature Vapor Growth of Homoepitaxial Silicon, Dec., p. 613

I. P. Csorba, Chromatic-Aberration-Limited Image-Transfer Characteristics of Image-Tube Lenses of Simple Geometry, Sept., p. 534

G. W. Cullen (coauthor) The Epitaxial Growth of Silicon on Sapphire and Spinel Substrates: Suppression of Changes in the Film Properties During Device Processing, June, p. 355
— (coauthor) Foreword to Special Issue on Chemical Vapor Phase Deposition, Dec., p. 607
— (coauthor) Heteroepitaxial Growth of Germanium and Silicon on Insulating Substrates, Dec., p. 620
— (coauthor) Compounds and Alloys for Superconducting Applications, Dec., p. 702

B. J. Curtis (coauthor) The Preparation of Ternary and Quaternary Compounds by Vapor-Phase Growth, Dec., p. 647

J. P. Dismukes (coauthor) Vapor Growth of (II-VI)-(III-V) Quaternary Alloys and Their Properties, Dec., p. 662
— (coauthor) Vapor Deposition of Semiconducting Mononitrides of Scandium, Yttrium, and the Rare-Earth Elements, Dec., p. 680

M. T. Duffy (coauthor) Optimization of Charge Storage in the MNOS Memory Device, June, p. 342
— (coauthor) Operational Dependence of the Direct Tunneling Mode MNOS Memory Transistor on the SiO_2 Layer Thickness, Sept., p. 467
— (coauthor) Vapor Deposition and Characterization of Metal Oxide Thin Films for Electronic Applications, Dec., p. 728
— (coauthor) Preparation, Properties, and Applications of Chemically Vapor Deposited Silicon Nitride Films, Dec., p. 742
— (coauthor) Chemical Vapor Deposition of Aluminum Oxide Films for Organo-Aluminum Compounds, Dec., p. 754

D. J. Dumin (coauthor) Heteroepitaxial Growth of Germanium and Silicon on Insulating Substrates, Dec., p. 620

L. Ekstrom (coauthor) Vapor Phase Growth of Magnetic Semiconducting Spinels, Dec., p. 692

F. P. Emmenegger (coauthor) The Preparation of Ternary and Quaternary Compounds by Vapor-Phase Growth, Dec., p. 647

R. E. Enstrom (coauthor) High-Power L- and S-Band Transferred Electron Oscillators, March, p. 20
— (coauthor) Vapor-Phase Growth of Several III-V Compound Semiconductors, Dec., p. 635
— (coauthor) Compounds and Alloys for Superconducting Applications, Dec., p. 702

N. Feldstein Two Room-Temperature Electroless Nickel Plating Baths, June, p. 317
— (coauthor) Selective Electroless Plating by Selective Deactivation, June, p. 439

K. M. Finlayson (coauthor) Back Scattering of Material Emitted from RF-Sputtering Targets, June, p. 293

A. W. Fisher (coauthor) Deposition and Properties of Silicon Dioxide and Silicate Films Prepared by Low-Temperature Oxidation of Hydrides, Dec., p. 715

A. M. Goodman (coauthor) Optimization of Charge Storage in the MNOS Memory Device, June, p. 342
— (coauthor) Operational Dependence of the Direct-Tunneling Mode MNOS Memory Transistor on the SiO_2 Layer Thickness, Sept., p. 467

G. E. Gottlieb (coauthor) The Epitaxial Growth of Silicon on Sapphire and Spinel Substrates: Suppression of Changes in the Film Properties During Device Processing, June, p. 355

— (coauthor) Heteroepitaxial Growth of Germanium and Silicon of Insulating Substrates, Dec., p. 620

J. J. Hanek (coauthor) Compounds and Alloys for Superconducting Applications, Dec., p. 702

P. Herkart (coauthor) Sonic Film Memory, March, p. 39

J. J. Hughes (coauthor) Characteristics of Coupled Microstrip Lines, Sept., p. 479

K. Karstad (coauthor) Sonic Film Memory, March, p. 39

W. Kern (coauthor) Cleaning Solutions Based on Hydrogen Peroxide for Use in Silicon Semiconductor Technology, June, p. 187

— Radiochemical Study of Surface Contamination: I. Adsorption of Reagent Components, June, p. 207; II. Deposition of Trace Impurities on Silicon and Silica, June, p. 234

— (coauthor) Deposition and Properties of Silicon Dioxide and Silicate Films Prepared by Low-Temperature Oxidation of Hydrides, Dec., p. 715

— (coauthor) Preparation, Properties, and Applications of Chemically Vapor Deposited Silicon Nitride Films, Dec., p. 742

— (coauthor) Chemical Vapor Deposition of Aluminum Oxide Films from Organo-Aluminum Compounds, Dec., p. 754

— (coauthor) Interface Properties of Chemically Vapor Deposited Silica Films on Gallium Arsenide, Dec., p. 771

R. J. Klensch (coauthor) Electronically Generated Halftone Pictures, Sept., p. 517

H. Kressel (coauthor) Vapor Gowth of (II-VI)-(III-V) Quaternary Alloys and Their Properties, Dec., p. 662

C. M. Kudsia Synthesis of Optimum Reflection Type Microwave Equalizers, Sept., p. 571

K. Kurlansik (coauthor) Sonic Film Memory, March, p. 39

T. S. Lancsek (coauthor) Selective Electroless Plating by Selective Deactivation, June, p. 439

S. G. Liu (coauthor) Fabrication and Performance of Kilowatt L-Band Avalanche Diode, March, p. 20

A. Mayer Detection of Damage on Silicon Surfaces: Origin and Propagation of Defects, June, p. 414

D. Meyerhofer (coauthor) Electronically Generated Halftone Pictures, Sept., p. 517

F. Micheletti (coauthor) Fabrication of Al_2O_3 COS/MOS Integrated Circuits, June, p. 330

L. S. Napoli (coauthor) Characteristics of Coupled Microstrip Transmission Lines, Sept., p. 479

R. Nitsche (coauthor) The Preparation of Ternary and Quaternary Compounds by Vapor-Phase Growth, Dec., p. 647

P. E. Norris (coauthor) Fabrication of Al_2O_3 COS/MOS Integrated Circuits, June, p. 330

R. E. Novak (coauthor) Vapor Deposition of Semiconducting Mononitrides of Scandium, Yttrium, and the Rare-Earth Elements, Dec., p. 680

J. J. O'Neill, Jr. (coauthor) Evaporation of Aluminum with RF-Induced Substrate Bias, June, p. 676

— (coauthor) Backscattering of Material Emitted from RF-Sputtering Targets, June, p. 293

S. Opresko (coauthor) A New Technique for Etch Thinning Silicon Wafers, June, p. 265

L. Onyskevych (coauthor) Sonic Film Memory, March, p. 39

H. L. Pinch (coauthor) Vapor-Phase Growth of Magnetic Semiconducting Spinels, Dec., p. 692

D. Puotinen (coauthor) Cleaning Solutions Based on Hydrogen Peroxide for Use in Silicon Semiconductor Technology, June, p. 187

P. Rappaport (coauthor) Foreword to Special Issue on New Process Technologies for Microelectronics, June, p. 185

J. F. Reynolds (coauthor) High-Power L- and S-Band Transferred Electron Oscillators, March, p. 20

D. Richman (coauthor) Low-Temperature Vapor Growth of Homoepitaxial Silicon, Dec., p. 613
— (coauthor) Vapor-Phase Growth of Several III-V Compound Semiconductors, Dec., p. 635

G. A. Riley (coauthor) Monitoring Silicon Tetrachloride Concentration in Hydrogen Carrier Gas, June, p. 396
— An Inexpensive Integrating Photoresist Exposure Control System, June, p. 407

J. J. Risko (coauthor) Fabrication and Performance of Kilowatt L-Band Avalanche Diodes, March, p. 3

P. H. Robinson (coauthor) Low-Temperature Vapor Growth of Homoepitaxial Silicon, Dec., p. 613
— (coauthor) Heteroepitaxial Growth of Germanium and Silicon on Insulating Substrates, Dec., p. 620

E. C. Ross (coauthor) Optimization of Charge Storage in the MNOS Memory Device, June, p. 342
— (coauthor) Operational Dependence of the Direct-Tunneling Mode MNOS Memory Transistor on the SiO_2 Layer Thickness, Sept., p. 467

L. J. Royer (coauthor) Back Scattering of Material Emitted from RF-Sputtering Targets, June, p. 293

O. H. Schade, Sr. Electron Optics and Signal Read-Out of High-Definition Return-Beam Vidicon Cameras, March, p. 60

O. H. Schade, Jr. Stable Solid-State Vertical Deflection for High Definition Television Systems, March, p. 120
— Linear Solid-State Horizontal Deflection Circuit for High-Definition Television Systems, March, p. 148

W. C. Schilp, Jr. (coauthor) A Novel Technique for Forming Glass-to-Metal Seals Using a Silicon Nitride Interface Layer, June, p. 443

M. J. Schindler Computer-Aided Design of a Fast-Wave Coupler, Sept., p. 553

R. Shahbender (coauthor) Sonic Film Memory, March, p. 39

W. J. Shannon A Study of Dielectric Defect Detection by Decoration with Copper, June, p. 431

J. M. Shaw (coauthor) Vapor-Deposited Tungsten as a Metallization and Interconnection Material for Silicon Devices, June, p. 306

R. F. Speers (coauthor) A New Technique for Etch Thinning Silicon Wafers, June, p. 265

A. I. Stoller (coauthor) A New Technique for Etch Thinning Silicon Wafers, June, p. 265
— The Etching of Deep Vertical-Walled Patterns in Silicon, June, p. 271
— (coauthor) A Novel Technique for Forming Glass-to-Metal Seals Using a Silicon Nitride Interface Layer, June, p.443

J. J. Tietjen (coauthor) Vapor-Phase Growth of Several III-V Compound Semiconductors, Dec., p. 635
— (coauthor) Vapor Deposition of Semiconductor Mononitrides of Scandium, Yttrium, and the Rare-Earth Elements, Dec., p. 680

J. L. Vossen (coauthor) Evaporation of Aluminum with RF-Induced Substrate Bias, June, p. 276
— (coauthor) Back Scattering of Material Emitted from RF-Sputering Targets, June, p. 293

J. J. Walsh (coauthor) Electronically Generated Halftone Pictures, Sept., p. 517

C. C. Wang (coauthor) The Epitaxial Growth of Silicon on Sapphire and Spinel Substrates: Suppression of Changes in the Film Properties During Device Processing, June, p. 355
— (coauthor) Vapor Deposition and Characterization of Metal Oxide Thin Films for Electronic Applications, Dec., p. 728

L. R. Weisberg (coauthor) Foreword to Special Issue on Chemical Vapor Deposition of Electronic Materials, Dec., p. 607

J. P. White (coauthor) Interface Properties of Chemically Vapor Deposited Silica Films on Gallium Arsenide, Dec., p. 771

W. M. Yim (coauthor) Vapor Growth of (II-VI)-(III-V) Quaternary Alloys and Their Properties, Dec., p. 662
— (coauthor) Vapor Deposition of Semiconducting Mononitrides of Scandium, Yttrium, and the Rare-Earth Elements, Dec., p. 680

K. H. Zaininger (coauthor) Fabrication of Al_2O_3 COS/MOS Integrated Circuits, June, p. 330
— (coauthor) Vapor Deposition and Characterization of Metal Oxide Thin Films for Electronic Applications, Dec., p. 728